Equilibrium bays

A numerical study after the behaviour of equilibrium bays

K.B. Sweers

M.Sc. Thesis

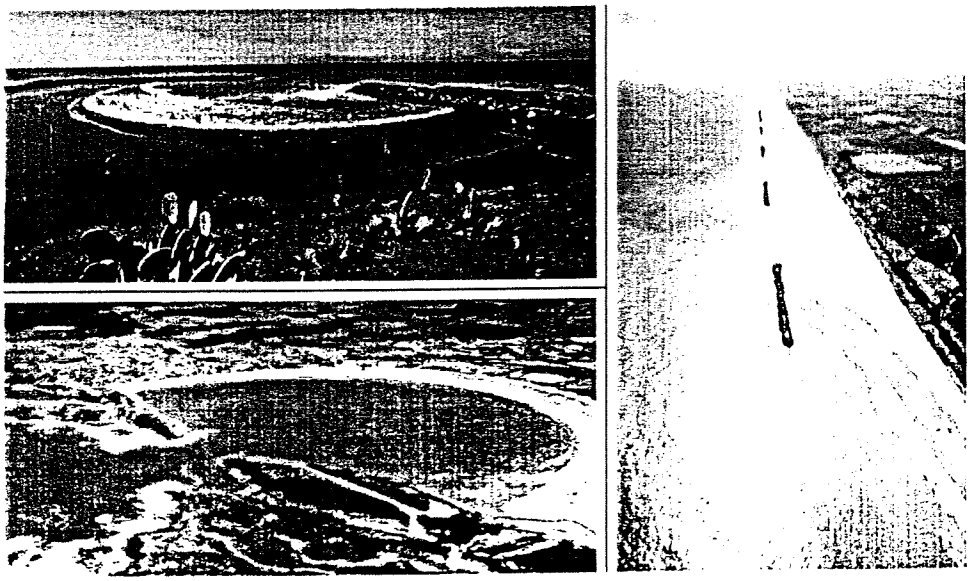

Delft, November 1999

Subfaculty of Civil Engineering
Hydraulic Engineering Section

TUDelft
Delft University of Technology

MaST III
SASME

Equilibrium bays

A numerical study after the behaviour of equilibrium bays

K.B. Sweers

M.Sc. Thesis

Professor:	Prof. ir. K. d'Angremond
Mentors:	Dr. ir. J. van de Graaff
	Dr. ir. J.A. Roelvink
Graduation Committee:	Prof. ir. K. d'Angremond
	Dr. ir. A. van Dongeren
	Dr. ir. J. van de Graaff
	Dr. ir. J.A. Roelvink

Hydraulic Engineering Section
Department of Civil Engineering
Delft University of Technology

Delft, November 1999

Abstract

At the present day, the far field impact of coastal structures can be simulated beforehand with the aid of numerical models. The consequences of new coastal defence schemes can be visualised before they are applied in reality. Therefore, the objective of this study is on the one hand, to investigate the capabilities of the numerical model Delft2D-MOR to predict the coastline evolution behind a series of emerged breakwaters and on the other hand, to increase our understanding of the hydraulic and morphological behaviour of bays in order to make deliberate decisions about the application of headland control in future.

Since the work described this thesis is a continuation of the work done by Blankers (1999), morphological simulations are executed and the effect of the wave height on the suspended sediment transport in the surf zone is examined. Although a reversal in longshore transport direction is observed (indicating a certain bay shape with a zero transport rate), bay shapes which are stable in the long run have still not been found. Local longshore (and cross-shore) transport gradients alter the bathymetries, which in their turn influence the overall longshore sediment transport. The result is a change in geometry. Since with the present models it is not yet possible to calculate the equilibrium bathymetry via a long simulation, new geometries and bathymetries are suggested.

Rewriting an empirical formula leads to two geometrical requirements which describe the shape of a bay in a simplified manner. However, this logarithmic spiral is based on aerial photos and hence do not include important aspects such as wave height, bottom material and bottom slopes. Analysing bottom maps of existing stable bays showed that the slope behind the headland (or breakwater) is flatter than the slope in the centre. Combining the geometrical requirements (which define the plan view of the bay) with slope information results in bathymetries which are rather different from the bathymetries used so far in the simulations. This explains partly why equilibrium has yet not been found. An advantage of creating bathymetries via the elliptical approach used so far, is that ellipses can be mathematically expressed and hence, many bays can be used in the simulations in relatively short time. However, in order to find equilibrium further research should be done with different bathymetries. Some simulations already executed show promising results.

Samenvatting

Tegenwoordig is het mogelijk om met behulp van numerieke modellen de gevolgen van het toepassen van kustwerken te simuleren. De consequenties van nieuwe kustverdedigingswerken kunnen gevisualiseerd worden voor toepassing in de praktijk plaatsvindt. Aan de ene kant is het doel van deze studie de mogelijkheden te onderzoeken van het numerieke model Delft2D-MOR om de kustlijnveranderingen achter een serie golfbrekers te voorspellen. Daarnaast wordt de kennis vergroot van het hydraulische en morfologische gedrag van baaien om zodoende de juiste keuze te kunnen maken omtrent de toepassing van offshore golfbrekers in de toekomst.

Dit werk is een vervolg van het afstudeerwerk van Blankers (1999) en er zijn morfologische simulaties uitgevoerd. Het effect van de golfhoogte op het suspensie transport in de brandingszone is onder-zocht. Ondanks dat er een omslag in de langstransportrichting geconstateerd is (en dus is er baai zonder langstransport), is een baai die ook op lange termijn stabiel is, nog niet gevonden. Lokale gradiënten in langs- (en dwars) transport veranderen de bodemprofielen, welke op hun beurt het langstransport in de gehele baai beïnvloeden. Het gevolg is een verandering van de geometrie. Het is met de huidige nog modellen niet mogelijk om middels een lange simulatie een stabiele bodemgeometrie te berekenen. Nieuwe geometrieën en bodemprofielen zijn daarom bepaald.

Het herschrijven van een empirische formule leidt tot twee geometrische eisen waaraan een baai moet voldoen wil deze stabiel zijn. Deze logaritmische spiraal is gebaseerd op de analyse van luchtfoto's en dus zijn belangrijke aspecten zoals golfhoogte, bodemmateriaal en bodemsteilheid niet meegenomen. Analyse van bodemkaarten van bestaande baaien toont aan dat de helling achter de golfbreker flauwer is dan in het centrum. Het combineren van de geometrische eisen met hellinginformatie resulteert in bodemprofielen die aanzienlijk verschillen van de profielen die tot dusver zijn toegepast in de simulaties. Dit verklaart voor een deel waarom evenwicht nog niet is gevonden. Het voordeel van het creeëren van bodemprofielen middels de elliptisch aanpak, is dat ellipsen mathematisch uitgedrukt kunnen worden. Veel baaien kunnen dan in een relatief korte tijd doorgerekend worden. Om echter evenwicht te vinden moet verder onderzoek gedaan worden met andere bodemprofielen. Enkele simulaties reeds gedaan met de nieuwe profielen geven hoopgevende resultaten.

Acknowledgements

This research was conducted at the University of Technology Delft as a graduation research project to complete my studies in Civil Engineering. The work has been supported by the Commission of the European Union, Directorate General for Science, Research and Development, in the SASME project under contract No. MAS3 CT97-0081.

The research after the behaviour of equilibrium bays significantly increased my understanding of the complex hydrodynamic and morphodynamic processes which take place in the surfzone. Moreover, my enthusiasm for coastal engineering has increased likewise. Therefore, I would like to thank Jan van de Graaff for giving me the opportunity to graduate on this topic. His valuable ideas and constructive criticism, combined with interesting discussions about coastal engineering were the basis for this report.

Problems encountered when using the numerical model Delft2D-MOR were tackled with the aid of Dano Roelvink. I would like to thank him for spending time with me behind the computer in order to help me solve these problems. His useful tips also attributed to the contents of this thesis.

Further, I want to thank Prof. Kees d'Angremond and Ap van Dongeren as members in my graduation committee. The advice Ap gave during my preliminary presentation turned out to be very valuable.

In the first two months Grard Blankers taught me the basics of Delft2D-MOR which saved me a lot of time. And before the final version of this report was ready, Gert-Jan Liek and Daan Franssen sacrificed their spare time to proof-read this thesis and I appreciate this very much. Colleagues and fellow-student at the Hydraulic Engineering section contributed to the cosiness of the last months. I would also like to thank my friends for the discussions which sometimes had, but mostly did not have anything to do with this thesis. Especially, the questionable habit of a "bin session" after lunch and diner is something I will definitely miss.

But without the support my parents gave me during (and before) my whole study, the example role my elderly brothers have played all through the years and the support and patience Minke gave me, the goal of finishing Civil Engineering would probably not have been achieved.

Table of contents

Figures and tables

Figures:

Tables:

List of symbols

Roman symbols:

C	Chezy coefficient	($m^{1/2}/s$)
C_{max}	maximum Courant number	(-)
G	gap between two successive breakwaters	(m)
H	total water depth ($h + \eta$)	(m)
H_b	breaker height	(m)
H_d	diffracted wave height	(m)
H_i	incoming wave height	(m)
H_o	deep water wave height	(m)
H_r	refracted wave height	(m)
H_{rms}	root mean-square wave height	(m)
I	bay indentation	(m)
K_d	diffraction coefficient	(-)
K_r	refraction coefficient	(-)
K_s	shoaling coefficient	(-)
R	radius from the point of diffraction to the coastline	(m)
R_e	component of R directed perpendicular to wave crests	(m)
R_0	length of control line	(m)
T	simulation time	(s)
T_d	return time of the wave in the computational area	(s)
T_p	peak period	(s)
T_s	significant wave period	(s)
W	bay width	(m)
W_o	overall bay width	(m)
Y_B	offshore distance of the breakwater	(m)
c_{fc}	friction coefficient induced by waves	(-)
c_{fw}	friction coefficient induced by currents	(-)
c_o	propagation speed of waves in deep water	(m/s)
d_{50}	median particle size (50% by weight smaller in size)	(m)
d_{90}	particle size (90% by weight smaller in size)	(m)
g	gravity of acceleration	(m/s^2)
h	local water depth	(m)
h_b	breaker depth	(m)
h_G	water depth in the gap	(m)
k	wave number	(m^{-1})
m	slope of the bay behind the breakwaters	(-)

n	slope of the bay in the centre	(-)
t	time	(s)
w	fall velocity of the grains	(m/s)

Greek symbols:

α	boundary reflection coefficient	(s^2)
α	constant angle between the Radii R2 and R1	(°)
α	curvature of coastline at tip of downcoast headland	(°)
β	angle between wave crests and control line	(°)
γ_b	breaker index	(-)
γ_d	deep water breaking coefficient	(-)
γ_s	shallow water breaking coefficient	(-)
Δt	time step	(s)
Δx	mesh size in x-direction	(m)
Δy	mesh size in y-direction	(m)
η	surface elevation relative to still water	(m)
θ	angle between the radii R2 and R1 (logarithmic spiral)	(°)
θ	angle between wave crests and the radius (parabolic)	(°)
θ_e	angle between control line and parallel coastline	(°)
θ_l	angle between control line and perpendicular coastline	(°)
λ	wave length	(m)
μ	bottom roughness	(m)
υ	kinematic viscosity	(m^2/s)
ε	sediment porosity	(-)
ρ_s	sediment density	(kg/m^3)
ρ_w	water density	(kg/m^3)
ϕ	wave direction	(°)

CHAPTER 1

Introduction

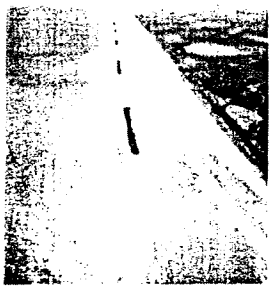

Considering the global developments in coastal management practices it can be stated that there is a shift of stress from defending land against the sea to attacking the sea in order to gain land. The latter has two main advantages. The first one is straightforward: the reclamation of land. The second one is less obvious. Many natural coasts have become a rigid system which is very narrow in certain places and has little buffer capacity landwards. By gaining land seawards it is possible to create a resilient coast, a coast that can 'survive' such events as extreme storm surges and sea level rise.

1.1 Embayed coasts

To become resilient a coast needs space for dynamic morphological and ecological processes to occur. Moreover, given the high population density in most coastal areas more space can only be realized by a seaward expansion. Constructing sand buffers and increasing and/or allowing the natural dynamics to take place also offers possibilities for nature to develop, by broadening the land-sea transition zone among other things. Possible uses (e.g., recreation) of the coast could also increase. One possibility to extract land from the sea is by making use of equilibrium crenulate shaped bays. This option not only may be more economical in the long run, it also creates a beach configuration which is attractive for recreational use. Embayed coasts (embayments larger than 50 to 100 km are known as gulfs) consist of a series of more or less regular embayments separated by cliff-type headlands or capes and are in most cases formed as a result of submergence (sea level rise) in combination with abrasive (wearing) and marine processes, but they may also have been formed by wave attack alone on cliffs of varying height and resistance. Embayed coasts can be subdivided into:

- open exposed embayed coasts - waves penetrate into the bay and reach the bay head affecting the beach there;
- sheltered embayed coasts - situated in the lee of islands or offshore shoals preventing the penetration of waves into the bay.

A sandy coast between two erosion-resistant points (headlands) will re-adjust its orientation to result in a beachface more or less perpendicular to the main wave direction. In a bay, where diffraction and refraction play an important role, wave rays show a fan-like pattern. For this reason bays also have a fan like shape (Figure 1.1). Sand will be eroded at the updrift end of the beach and carried to the downdrift end of the beach. This process is known as bay development and is quite common on swell-dominated sandy coasts between rocky outcrops (headlands, cliffs, reefs, beach rocks), where sediment supply by rivers and other sources is minimum.

A crenulate-shaped bay formed under oblique incident waves is in a stable condition, if the littoral transport is zero or constant everywhere along the beach (static or dynamic equilibrium). Storm waves or swell waves from one dominant direction are the most effective agents in bay formation. Storm waves arriving from a wide spectrum of directions have less influence on the static bay equilibrium. The planform of static (zero transport) and dynamic equilibrium (constant transport) bays may be different. Generally, the dynamic beach line is laying seaward of the static beach line; it will migrate landward if sediment supply from upcoast ceases. The shore in the lee of the headland is attacked by diffracted waves. Littoral transport may be constant, if there is a continuous supply of sand around the updrift headland. The indentation of the bay is then dictated by the amount of sediment passing through it from upcoast or by sediment input of a river outlet in the bay. The time scale of reaching equilibrium depends on the wave climate. Many existing bays may not be in a static state of equilibrium; they are rather in a dynamic state of equilibrium with constant supply of sediment from upcoast. Static equilibrium is characterized by:

- the presence of storm and/or swell waves from a dominant direction (oceanic coasts) - no further beach changes;
- (almost) simultaneous wave breaking at every location along the beach - zero longshore velocity and sand transport.

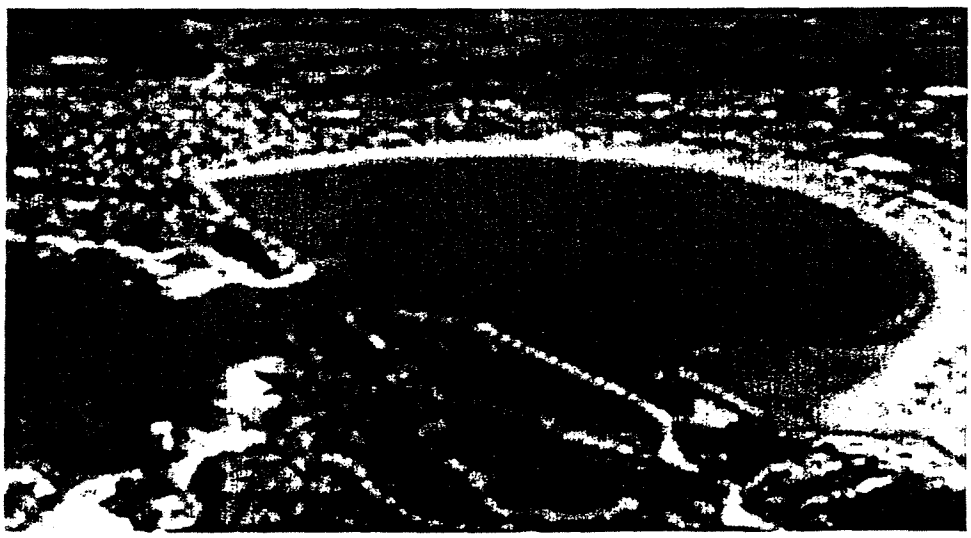

Figure 1.1

Natural equilibrium bay

(San Martinho do Porto - Portúgal)

These crenulate shaped bays are ubiquitous, not only on oceanic margins but also along coasts of enclosed seas, lakes, and river shorelines. They indicate nature's method of balancing wave energy and load of sediment transport. In this manner coasts have been kept in position for hundreds of years. It is essential to know why and how they are formed and to determine their stability, for they are a pointer to how man can stabilize a shoreline.

1.2 History

Geologists and geographers were the first to be interested in the existence of such bay shapes (Halligan, 1906), but the shape as a stable physiographic feature was first recognized by Jennings (1955), without full knowledge of the waves involved. Davies (1958) realized the importance of wave refraction. The sculpturing process was later included in a textbook (Greswell, 1957). The unique zeta-shaped beaches along the New South Wales coastline in Australia were noted by Langford-Smith and Thom (1969) without scientific analysis of their shapes. Yasso (1965) measured the planforms of a number of prototype bays in the United States of America and showed that they were equivalent to a logarithmic spiral. This empirical relationship has been accepted for almost 25 years until Hsu and Evans (1989) developed a more universal relationship.

Although the dynamic processes of this geomorphic feature have been studied by many researchers, their state of stability, that is, "how permanent they are," has only been examined by coastal engineers. It is generally believed that they have been formed over some thousands of years, at least, but have been eroded, or more greatly indented, in the past hundred years or so due to reduction in sediment supply or flood mitigation, which impedes the transport of sand and stone to their gaps, from where it is spread alongshore by wave action.

1.3 Future

In some cases a coastal defence system is required yielding a zero longshore transport. Therefore, a situation is strived after where the shoreline is reoriented parallel to the crests of the incoming waves, thus minimizing or eliminating totally the sediment transport alongshore. This condition is seen to be provided by nature in her ability to sculpture crenulate or zeta-shaped bays between headlands. Refraction and diffraction causes wave

crests to curve landward. If a structure is located offshore, but close enough to create a tombolo to it, a shoreline will be formed almost parallel to the incoming waves. On the downcoast side of the structure, waves will diffract and refract to form a curved beach nearly parallel to these curving crests. With successive headlands a bay is formed through which continuing littoral drift might pass while maintaining its crenulate shape. In such event the waves will not break parallel to these waterlines because sediment must still be transmitted through the system. However, if this supply ceases the bay will erode back until static equilibrium is reached. With the empirical formulae of Hsu and Silvester (1997) it may be possible to predict the shape of a bay in static equilibrium. When one can adequately simulate the natural headland (or enclosed beach) in the laboratory or with the computer one will be able to predict the possible success of an artificial headland structure.

The application of headland control can serve two main purposes. It can be a useful concept if one wants to defend the land against the sea. A high failure rate can be found on several places around the world when dealing with construction projects in the surf zone and on the beaches in order to defend the land. The destruction of beaches by breakwaters designed to extend the beaches, the silting of harbours and marinas as a result of structures designed to provide shelter, the re-nourishment of the beach in front of a seawall and the enhancement of wave accretion by building jetties supposed to lessen wave erosion are but a few examples of the inadequacy of our knowledge and practice in coastal engineering. If, in future, it is possible to predict the stable shape of a bay, this feature can be used to serve as a protective means against the everlasting wave attack from the sea. The property of stability is essential because it might effect great savings in investments on the coast in the long run.

On the other hand, headland control can be used in order to gain land from the sea. This can lead to a much cheaper construction because less material is needed, as can be seen in Figure 1.2. Another advantage of this kind of protection of reclaimed land is that it offers attractive beaches for recreation purposes. At this particular moment the possibilities for extending the Maasvlakte near Rotterdam harbour in the Netherlands using equilibrium bays is being investigated.

1.4 The objectives

Previously, the numerical model Delft2D-MOR has been used to predict coastline evolution behind submerged and emerged offshore breakwaters, in tidal inlets and many other cases. The development of tombolo's behind emerged offshore breakwaters has also been studied. In these simulations a

Figure 1.2

Application of headland control

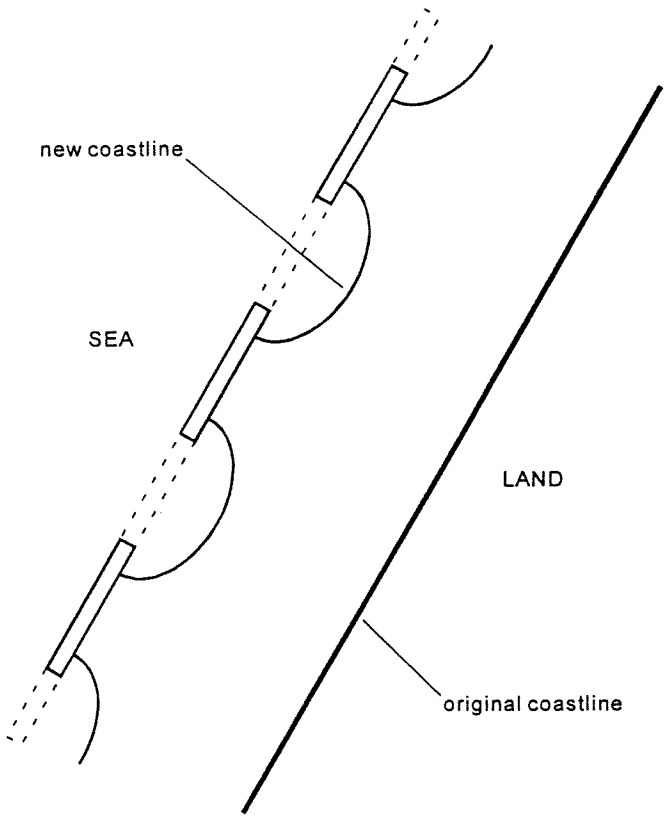

salient developed, but never a fully developed tombolo. The present study deals with a comparable situation. In fact, the shape of a bay can be seen as two fully developed tombolo's (see Figure 1.3). However, instead of starting with a straight coastline, a symmetrical bay shape is chosen as an initial shape in order to reduce calculation time considerably. Therefore, the objective of this study is on the one hand to investigate the capabilities of the numerical model Delft2D-MOR to predict the coastline evolution behind a series of emerged breakwaters and on the other hand to increase our understanding of the hydraulic and morphological behaviour of bays in order to make deliberate decisions about the application of headland control in future.

Since this study is a continuation of the work done by Blankers (1999), reference will often be made to his report. Contrary to Blankers' simulations (Blankers, 1999) which were mostly hydrodynamical, all simulations carried out during this research and described in this report are mainly sediment transport and morphological related. Morphological simulations are used to study the response of the seabed on the hydrodynamic forces which act upon it. This interaction changes the bathymetry until a new equilibrium is reached. Unless the short and long term morphological consequences of a man-made structure are known, it is difficult to intervene in nature in a justified manner. This explains the importance of morphological simulations.

1.5 Outline of the report

The necessary theoretical background considering the hydrodynamics is given in Chapter 2. In Chapter 3 the most important aspects of sediment

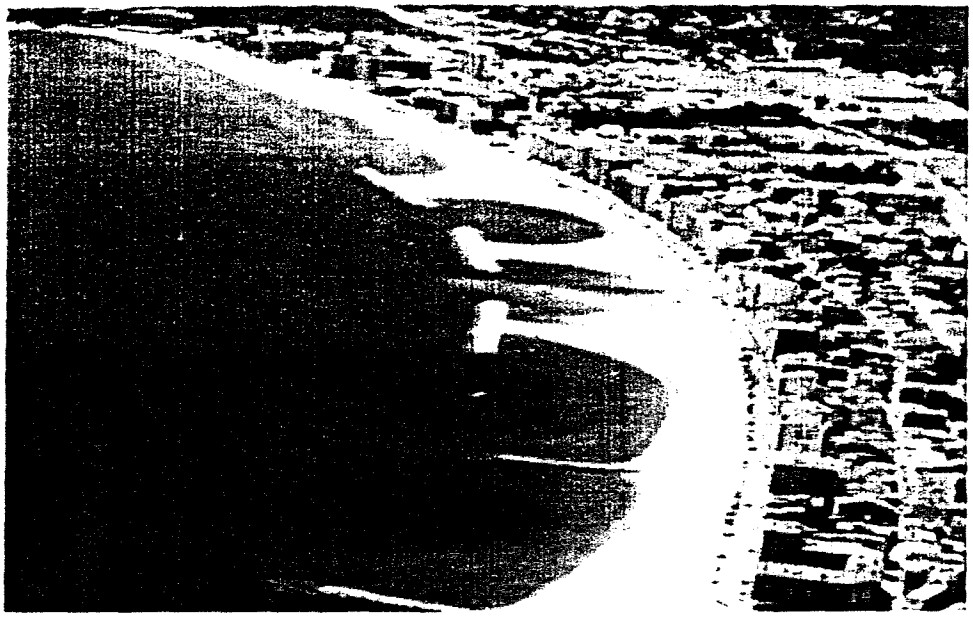

Figure 1.3

Three tombolo's or two bays...?

(San Antonio de Calonge - Spain)

transport are described. The settings used in the model are then given in Chapter 4. In order to predict the shape of a bay beforehand, new bathymetry predictors are constructed, based on the suspended sediment transport in the breakerzone. This, and the morphological changes which occur during a long simulation run, are discussed in Chapter 5. With the aid of numerical simulations the influence of the wave height, the gap width and the bay width on the morphology in bays is described in Chapter 6. Rewriting existing empirical formulae in a different form yield congruent bay bathymetries which may be in static equilibrium. These formulae, and a detailed description of the new bay lay-out are mentioned in Chapter 7. Some simulations with these new bathymetries have been carried out as well. Finally, in Chapter 8 the conclusions regarding this research and recommendations for future investigations can be found.

CHAPTER 2

Hydrodynamics

Hydrodynamics is a very essential aspect when dealing with coastal engineering. The effects of water waves are of paramount importance in the field of coastal engineering. Waves are the major factor in determining the geometry and composition of beaches and significantly influence the planning and design of coastal structures. Surface waves generally derive their energy from the winds. A significant amount of this wave energy is finally dissipated in the nearshore region and on the beaches.

2.1 Waves

Waves provide an important energy source for forming beaches: sorting bottom sediments on the shoreface, transporting bottom materials onshore, offshore and alongshore and for causing many of the forces to which coastal structures are subjected. An adequate understanding of the fundamental physical processes in surface wave generation and propagation must precede any attempt to understand complex water motion in the nearshore areas of large bodies of water. Consequently, understanding the mechanics of wave motion is essential in the planning and design of coastal works.

Waves that reach coastal regions expend a large part of their energy in the nearshore region. As the wave nears the shore, the wave energy may be dissipated as bottom friction, percolation, sound and heat through turbulent fluid motion induced by breaking. While the heat is of little concern when dealing with bay development, breaking is important because it affects both beaches and man-made shore structures. Thus, shore protection measures and coastal structure designs are dependent on the ability to predict waveforms and fluid motion beneath waves, and on the reliability of such predictions. In general, actual water-wave phenomena are complex and difficult to describe mathematically because of non-linearities, three-dimensional characteristics and apparent random behaviour. However, nowadays the computer is able to deal with these complex calculations and

reasonable results can be obtained which can be interpreted by the coastal engineer.

2.1.1 Refraction

An expression relating the wave celerity (C in m/s) to the wave length (L in m) and water depth (d in m) is given by:

$$C = \sqrt{\frac{gL}{2\pi}} \tanh\left(\frac{2\pi d}{L}\right) \qquad \text{Equation 2.1}$$

in which g is the acceleration of gravity (m/s²). This equation shows that wave celerity depends on the water depth in which the wave propagates. If the wave celerity decreases with depth, wave length must also decrease proportionally. Variation in wave velocity occurs along the crest of a wave moving at an angle to underwater contours because the part of the wave in deeper water is moving faster than the part in shallower water. This variation causes the wave crest to bend toward alignment with the depth contours. This bending effect is called refraction and depends on the relation of water depth to wave length. Refraction is important for several reasons:

- refraction, coupled with shoaling, determines the wave height in any particular water depth for a given set of incident deep water wave conditions; refraction therefore has significant influence on the wave height and distribution of wave energy along the coast in the bay;
- the change in wave direction of different parts of the wave results in convergence or divergence of wave energy and hence affects the forces exerted by waves on the coast;
- refraction contributes to the alteration of bottom topography by its effect on the erosion and deposition of beach sediments.

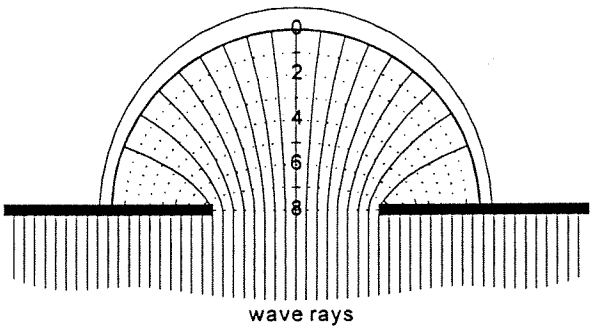

Figure 2.1

Wave refraction in a bay

(Blankers, 1999)

In addition to refraction caused by variations in bathymetry, waves may be refracted by currents. Refraction by a current occurs when waves intersect

the current at an angle. The extent to which the current will refract incident waves depends on the initial angle between the wave crests and the direction of current flow, the characteristics of the incident waves, and the strength of the current. Due to the strongly curved depth contours in bays it is obvious that the phenomenon of refraction is of great importance in understanding bay behaviour, as can be seen in Figure 2.1. Besides refraction another important phenomenon occurring in bays is diffraction.

2.1.2 Diffraction

Diffraction of water is a phenomenon in which energy is transferred laterally along a wave crest. It is often noticed in an area where an otherwise regular train of waves is interrupted by a breakwater. If the lateral transfer of wave energy along a wave crest and across orthogonals did not occur, straight, long-crested waves passing the tip of a structure would leave a region of perfect calm in the lee of the barrier, while beyond the edge of the structure the waves would pass unchanged in form and height. The line separating the two regions would be a discontinuity. Since this is not possible, energy flows across the discontinuity.

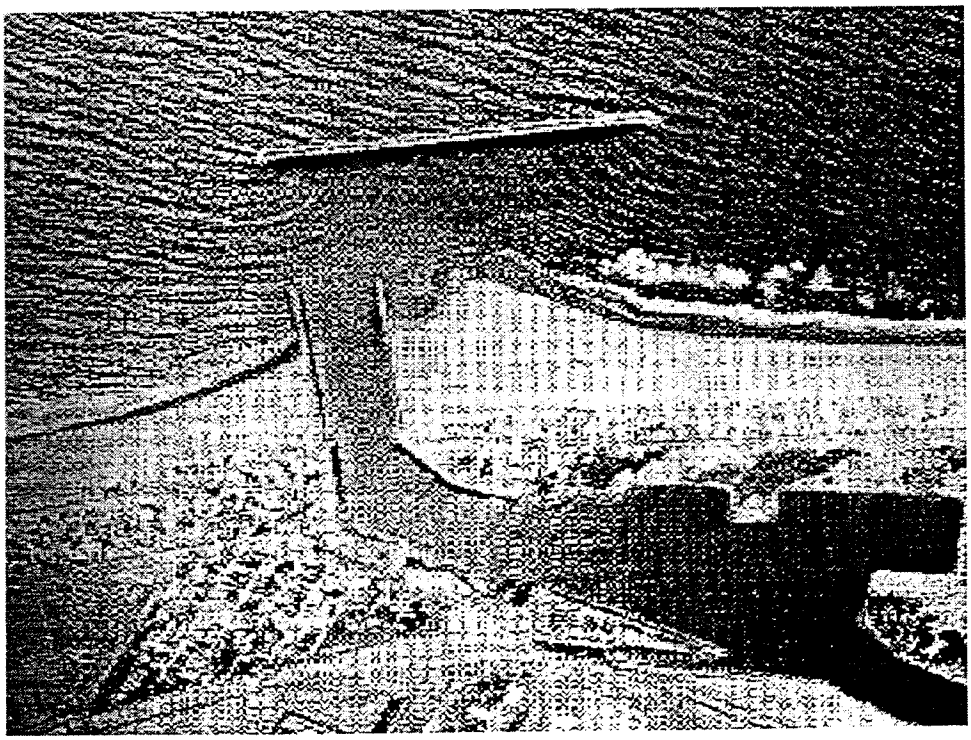

Figure 2.2

Wave diffraction at Channel Islands Harbour breakwater, California

(Shore Protection Manual, 1984)

Calculation of diffraction effects is important for several reasons. Wave height distribution in a sheltered bay is determined to some degree by the diffraction characteristics of both the natural and man-made structures affording protection from incident waves. Therefore, knowledge of the diffraction process is essential in planning such facilities. The prediction of wave heights near the shore is affected by diffraction caused by naturally

occurring changes in hydrography. An aerial photograph illustrating the diffraction of waves by an offshore breakwater is shown in Figure 2.2.

Since nearly all the waves used in the numerical simulations have wave lengths less than one-fifth the width of the gap and arrive at normal incidence, the diffraction effects of each wing are nearly independent. Hence, the diffraction patterns in the lee of both breakwaters can be drawn easily as shown in Figure 2.3(a). This sketch is based on the assumption that the depth shoreward of the breakwaters is constant. However, this is not the case. Therefore, refraction occurs in addition to diffraction. Although a general unified theory of the two has only been developed for a few special cases, an approximate picture of wave changes may be obtained by:

1. at this point, constructing a diffraction diagram carrying successive crests three or four wave lengths shoreward, if possible;
2. and with the wave crest and wave direction indicated by the last shoreward wave crest determined from the diffraction diagram, constructing a new refraction diagram to the breaker line.

It is mentioned that in Figure 2.3 shoreward of the breakwater an uniform bottom depth is assumed for some distance before refraction takes place. It is further mentioned that the method presented here is suitable for medium-period waves. For long-period waves the effect of shoaling should also be considered. But since the tide (and other long-period waves such as seiches) are not included in the simulations, a refraction-diffraction pattern as shown in Figure 2.3(b) can be expected in a bay.

2.1.3 Wave set-down/set-up

Field observations indicate that part of the variation in mean nearshore water level is a function of the incoming wave field. Waves breaking on a slope cause a decrease in the mean water level relative to the still water level just prior to breaking, with a maximum depression or set-down at about the breaking point. This is due to an increase of the momentum flux in onshore direction which results in compensating forces on the water column.

From the breaking point the mean water surface slopes upward to the point of intersection with the shore. The mean water surface displacement increases as the shore is approached. This water surface slope provides a hydrostatic pressure gradient directed offshore to counter the change of wave momentum by breaking across the surfzone. Hence, wave set-up is defined as the superelevation of the water surface due to wave action alone (see Figure 2.4).

Figure 2.3

Diffraction for breakwater gap of width > 5L (a) and combined refraction-diffraction pattern (b)

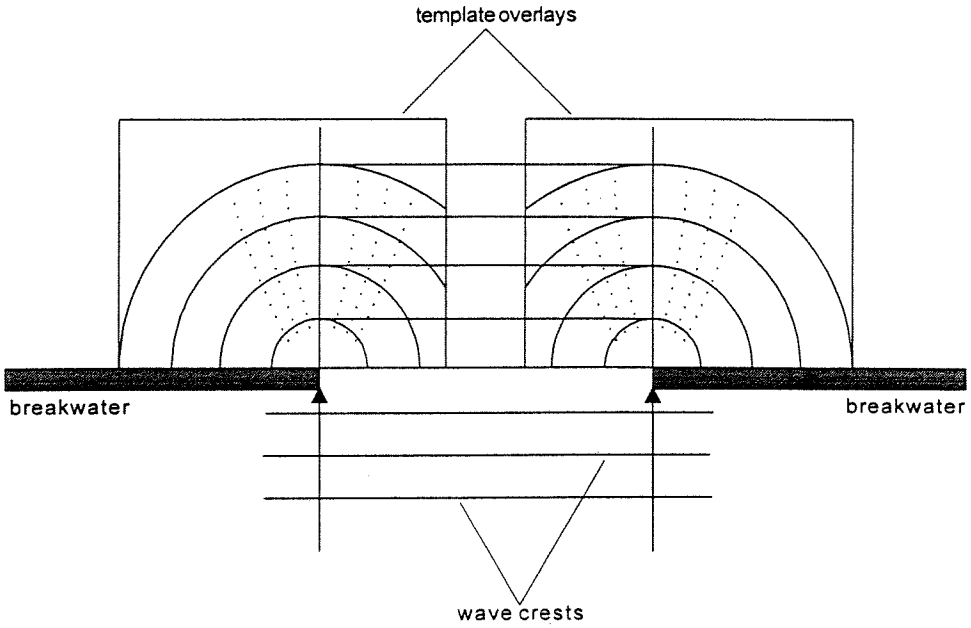

(a)

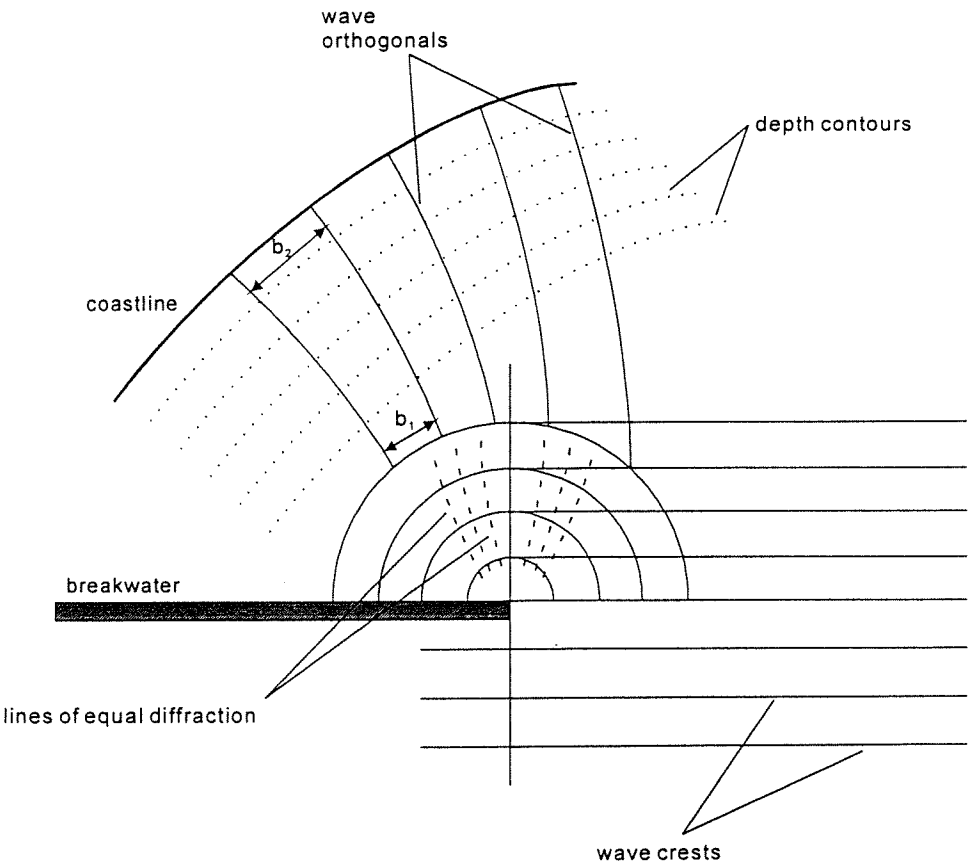

(b)

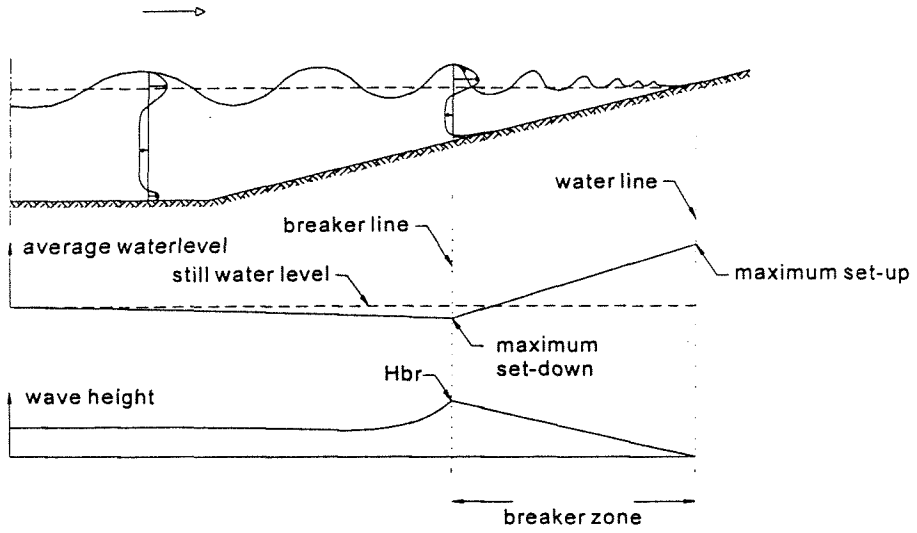

Figure 2.4

Wave set-down and set-up

(Blankers, 1999)

The theory for set-down at the breaking zone indicates that (Shore Protection Manual, 1984):

$$s_b = -\frac{g^{1/2} H_0^2 T}{64\pi d_b^{3/2}} \qquad \text{Equation 2.2}$$

where:

s_b = the set-down at the breaking zone [m]
T = the wave period [s]
H_0 = equivalent unrefracted deepwater significant wave height [m]
d_b = the depth of water at the breaker point [m]
g = the acceleration of gravity [m/s²]

The water depth at the breakerpoint can be calculated using:

$$d_b = \frac{H_b}{\gamma} = \frac{K_s \cdot H_0}{\gamma} \qquad \text{Equation 2.3}$$

in which:

H_b = height of the breaking waves [m]
H_0 = deep water wave height [m]
K_s = shoaling coefficient [-]
γ = breaking coefficient [-]

The shoaling coefficient can be determined iteratively. For a deep water significant wave height H_s = 2 m with a peak period T_p = 7 s, the shoaling coefficient yields K_s = 1.2. A general accepted value for the breaking coefficient is 0.8. Substituting all this in Equation 2.3 yields a breaking depth of

3 m. Now that the depth of water at the breaker point is known, it is possible to calculate the wave set-down for a significant wave height H_s = 2 m:

$$s_b = -\frac{\sqrt{9.81} \cdot 2^2 \cdot 7}{64 \cdot \pi \cdot 3^{3/2}} = -0.084m$$

The net wave set-up (s_w) at the shore is:

$$s_w = \Delta s - s_b \qquad \text{Equation 2.4}$$

Longuet-Higgins and Stewart (1963) have shown from an analysis of Saville's data (1961) that:

$$\Delta s = 0.15 d_b \qquad \text{Equation 2.5}$$

Combining Equation 2.2, Equation 2.4 and Equation 2.5 gives:

$$s_w = 0.15 d_b - s_b \qquad \text{Equation 2.6}$$

Therefore, the wave set-up for H_s = 2 m and T_p = 7 s is about 0.37 m. It may be obvious that in a bay significant differences occur in wave height. This results in differences in wave set-up and set-down along the pheriphery and hence longshore currents develop driven by the differences in wave set-up/ set-down. The current is directed from locations with a high set-up to places with a low-set-up.

It is mentioned that wave set-up is a phenomenon involving the action of a train of many waves over a sufficient period of time to establish an equilibrium water level condition. The exact amount of time for equilibrium to be established is unknown, but a duration of 1 hour is considered an appropriate minimum value. The very high waves in the spectrum are too infrequent to make a significant contribution in establishing wave set-up. The root mean square wave height H_{rms} represents the wave condition most suitable for design purposes.

2.2 Currents

In this study, the hydraulic and morphological phenomena which occur in a bay are simulated with the numerical model Delft2D-MOR. Since in the initial input in the numerical model the current velocities are set to zero along the boundaries of the model, the first calculated flow field is completely wave-induced. However, in its turn this calculated flow field affects

the waves and wave-current interaction has to be taken into account. The phenomenon of wave-current interaction is a consequence of among other things the next mechanisms:

- refraction by the waves by horizontal currents,
- generation of longshore currents by breaking waves,
- modification of the wave kinematics by the currents.

In order to increase the knowledge of the complex current patterns which develop in a bay a distinction is made between longshore currents and cross-shore currents.

2.2.1 *Longshore current forces*

The water in the bay moves to some direction or the other along the coast. But it does not move on its own accord. If a total water column is considered there will be driving forces which initiate the water movement. On the other hand there are also forces which try to resist the driving forces. The equilibrium of these forces in the longshore direction results in a constant current along the coast. The main driving forces for the development of longshore currents which should be mentioned with regard to bays are the radiation shear stress component parallel to the coast and the radiation stress component (see Figure 2.5).

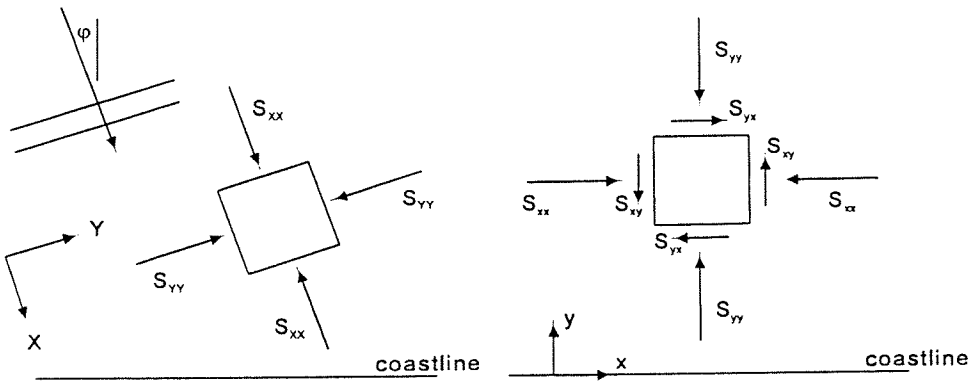

Figure 2.5

Components of radiation stress

Changes in the radiation shear stress produce the force component which acts parallel to the coast and, as such, contributes to the forces on a water mass moving along the coast. Radiation shear stresses originate when waves approach the coast at an angle. It can be demonstrated that outside the breaker zone the changes in radiation shear stress are zero and hence, there is no driving force for longshore currents there (Bowen, 1969). However, within the breaker zone along a straight coastline with constant wave height along the coast, the changes in radiation shear stress (S_{yx}) varies with distance towards the shore (y) and as a result a longshore current is present, see also Equation 2.7:

$$\frac{dS_{yx}}{dy} = \frac{5}{16}\rho\gamma^2(gh)^{3/2}\frac{\sin(\varphi_o)}{c_o}m \qquad \text{Equation 2.7}$$

in which c_o is the wave velocity in deep water, g is the acceleration due to gravity, h is the water depth, m is the beach slope, γ is the breaker index, ρ is the mass density of water and φ_o is the angle of wave approach in deep water.

Figure 2.6

Principal of radiation stresses

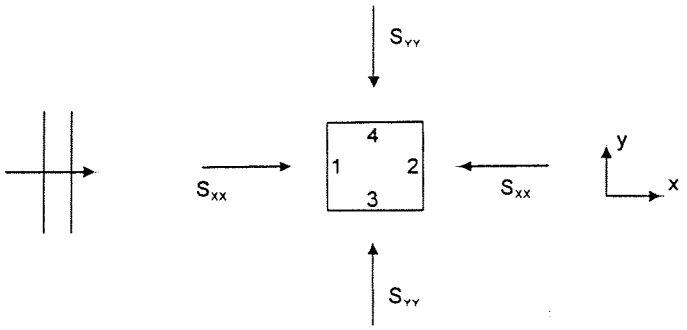

In order to explain the principal of radiation stresses, a square column of water is considered (see Figure 2.6). This column of water is enclosed by four vertical principal planes: 1, 2, 3 and 4. Then, if the wave conditions and depth at all four planes are identical, the radiation stress component on opposite sides of the column shown in the figure are identical and there is no resulting force. Only if the wave conditions vary between planes 1 and 2 or 3 and 4, will there be a resultant force. Thus, the radiation stress influences physical processes only in areas where wave conditions change. Such areas would, therefore, be at locations where wave refraction, diffraction, shoaling, and/or breaking occurs. Obviously, in a bay all these phenomena are present.

Therefore, the direction of the longshore current depends on which phenomenon dominates. Blankers (1999) found that this is determined by the geometry of the bay and the gap width between the offshore breakwaters. As can be seen in Figure 2.7 two different circulation pattern can occur in a bay. Apparently, in the case of Figure 2.7(a) the differences in wave set-up are the most dominant factor: nearshore currents are directed from the centre of the bay toward the edges. Because of continuity circulation patterns

Figure 2.7

Circulation currents in a bay

(Blankers, 1999)

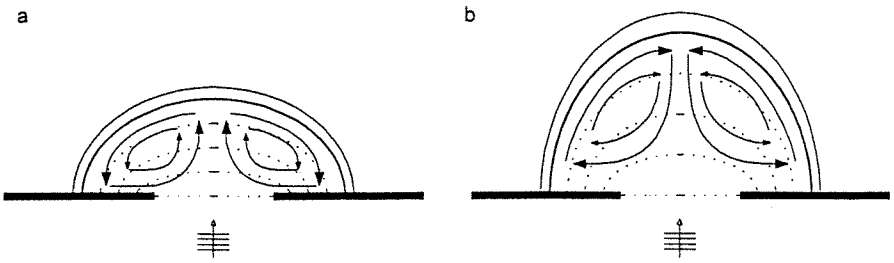

will develop yielding depth averaged onshore currents in the centre of the bay. In the case of Figure 2.7(b) the oblique approach of the waves dominates the current pattern: a nearshore longshore current pattern develops from the edges towards the centre. In this case, continuity yields offshore currents in the centre of the bay.

2.2.2 *Cross-shore current forces*

In addition to wave set-up, propagating waves initiate a cross-shore circulation current in the breaker zone. This phenomenon is understood by examining the distribution of the momentum flux over the depth which yields the radiation stress distribution over the vertical. Since the orbital motion of waves has a maximum at the surface, the momentum flux there will be greater than at the bottom. On the other hand the resisting hydrostatic pressure is evenly distributed over the depth. This yields a net shoreward force at the surface and a net seaward force near the bottom. The resulting circulation is shown in Figure 2.8.

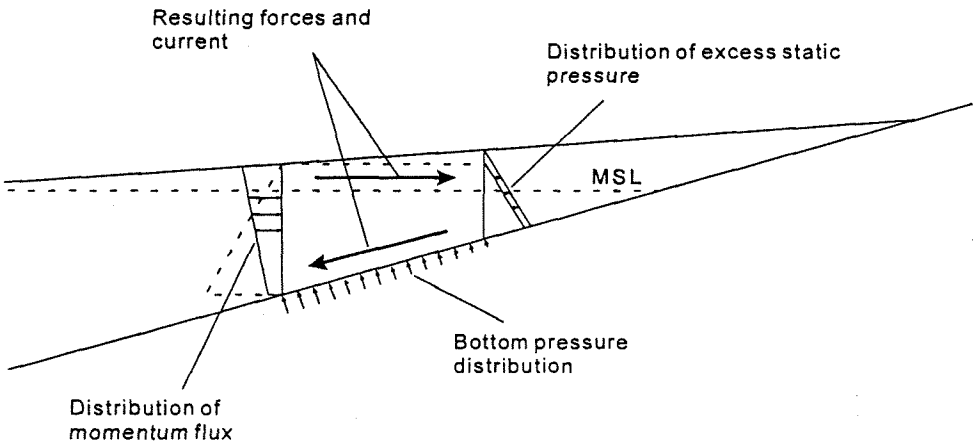

Figure 2.8

Circulation current in the breaker zone

Furthermore, the bore-like feature on top of a breaking wave transports large amounts of water landwards. Since in a 2D case in a vertical cross-section conservation of mass occurs, in the lower part a volume of water is transported seawards (see Figure 2.9).

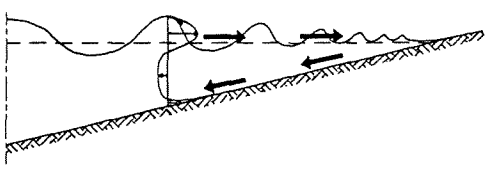

Figure 2.9

Cross-shore current due to breaking waves

In plan view (Figure 2.7) it can be seen that the cross-shore (depth averaged) currents develop where the longshore currents meet an obstacle like a breakwater or a current. The direction of the cross-shore current in the centre of the bay is caused by continuity.

2.3 Hydrodynamics in Delft2D-MOR

As mentioned before, the behaviour of bays is simulated with the aid of the numerical model Delft2D-MOR. Therefore, the computed current velocities are depth-averaged and the current patterns are calculated in a horizontal plane. However, not all the hydraulic phenomena described in this chapter are accounted for in Delft2D-MOR. It is necessary to be aware of this fact and to know precisely which phenomena are implemented in the model and which are not.

Refraction

In the wave module HISWA the refraction process is accounted for as follows. A curving wave ray implies that the direction of wave propagation changes while travelling along the ray. In other words, the energy transport continuously changes direction while travelling through the area of interest. This can be conceived as the energy travelling not only through the geographic area but also (and simultaneously) from one direction to another. This permits the Eulerian approach that has been taken in HISWA: the energy propagates not along rays but across a grid covering the area, while refraction is accounted for by shifting energy from one direction to another during propagation.

Diffraction

Diffraction is not taken into account in the wave module. This is an important limitation because the diffraction process is one of the main creating forces of equilibrium bays. However, the effect of diffraction can be simulated by a coefficient for the directional spreading. Tests executed by Ahmed (1997) show that the wave pattern around offshore breakwaters shows little deviation from a specialised diffraction model (DIFFRAC) if the value for the coefficient of directional spreading is set to 4. Differences at greater distance from the breakwaters appear to be small, while the greatest errors are expected in the shadow zone just around the head of the breakwaters. Here, the wave module HISWA will probably predict a wave height of zero, which will not occur in practice.

Wave set-up/set-down

Depth and current information (if present) forms input to the HISWA model before the computations are carried out. So wave set-up cannot be taken into account by HISWA in a dynamic manner (i.e. wave induced set-up or currents cannot be computed simultaneously with waves in HISWA). In principle however, an iterative procedure is employed in which set-up and currents are computed alternatingly with waves. Depths and currents should then be computed with a 2-dimensional flow model (TRISULA) using the radiation stresses determined with HISWA.

Cross-shore routine

Although in the present version of Delft2D-MOR a cross-shore sediment transport routine is accounted for, the version used in this report did not take into account cross-shore transport due to:

- asymmetry of waves
- undertow
- a sloping bottom

CHAPTER 3

Sediment transport

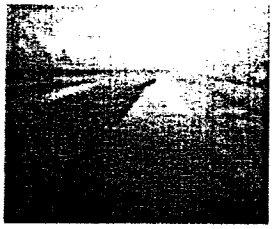

In order to predict the equilibrium shape of a bay and to understand its behaviour one must have a thorough understanding of the sediment transport processes which occur when the forces of nature act upon it. Although some of the forces which cause the sediment to move are "switched off" during the simulations they are briefly mentioned in this chapter because for the sake of completeness.

3.1 Bedload and suspended transport

Sediment transport occurs in two modes: *bedload transport*, the motion of grains rolled over the bottom by the shear of water moving above the bed and *suspended-load transport*, the transport of grains by currents after the grains have been lifted from the bed by turbulence. Both modes of transport are usually present at the same time, but it is hard to distinguish where bedload transport ends and suspended-load transport begins. However, a bedload layer thickness of about 0.05 m is often assumed.

In deeper water outside the breaker zone the transport is generally concentrated in a layer close to the sea bed and mainly takes place as bedload transport in close interaction with small bed forms (ripples) and larger bed structures (dunes, bars). In order to determine the bedload transport it is important to know the velocity just above the bedload layer, the (decreasing) velocity distribution in the direction of the bottom (shear stress) and the water pressure of the overlying water column (internal friction). It is further mentioned that the bottom slope also influences the bedload transport via the gravity. The distribution of the velocity in a water column is determined by:

- the forces acting on the water column,
- and the presence and size of possible bottom features (like ripples).

Until the present day, the bedload transport is calculated using formulas based on a combination of theoretical and empirical knowledge.

Because it is more readily measured than the bedload transport, suspended load transport has been the subject of considerable study. It has been demonstrated by many researchers that suspension concentrations decrease with height above the bottom (e.g. Kraus, et al. 1988 and 1989). The highest concentrations typically are found in the breaker and swash zones, with lower concentrations at midsurf positions.

In the executed simulations sand is only transported by currents (current related transport). In the surf zone of sandy beaches the transport generally is dominated by the waves through wave breaking and wave-induced currents in longshore and cross-shore direction. Suspended load transport will become increasingly important with increasing strength of the mean currents due to the turbulence-related mixing capacity of the mean current (shearing in boundary layer). By this mechanism the sediments are mixed up from the bedload layer to the upper layers of the flow. The above mentioned processes are summarised in Figure 3.2.

In the suspended transport mode the material is transported in suspension in the watercolumn between the bedload layer and the water surface (see also Figure 3.1). Obviously, for a grain to stay in suspension, an equilibrium has to be reached between the turbulent upward directed motion and the downward directed gravity. The extent to which turbulence is present in the water column determines the suspension rate. Near the water surface turbulence is caused by breaking waves and, in a lesser extent, to wind rubbing against the water surface. Throughout the water column and near the bottom turbulence is caused by the velocity of the current over a rough bottom.

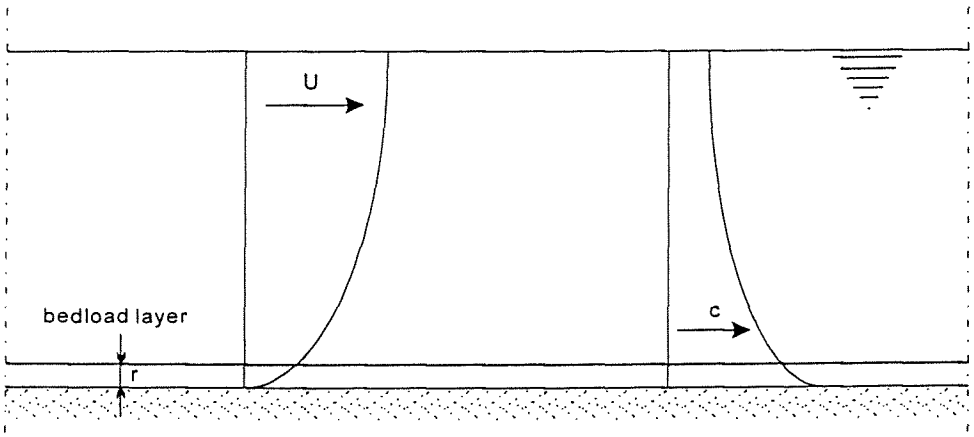

Figure 3.1

Suspended sediment transport

Writing the suspended sediment transport as the product of a sedimentconcentration (c) and a velocity (U) which is integrated over the depth (h) above the bedload layer (r) yields:

$$S_s = \int_r^h c(z)U(z)dz \qquad \text{Equation 3.1}$$

With respect to the near shore sediment transport a distinction is often made between longshore sediment transport (which is directed parallel to the coastline) and cross-shore sediment transport (which is directed perpendicular to the coastline).

Figure 3.2

Sand transport mechanisms along cross-shore profile

(Van Rijn, 1998)

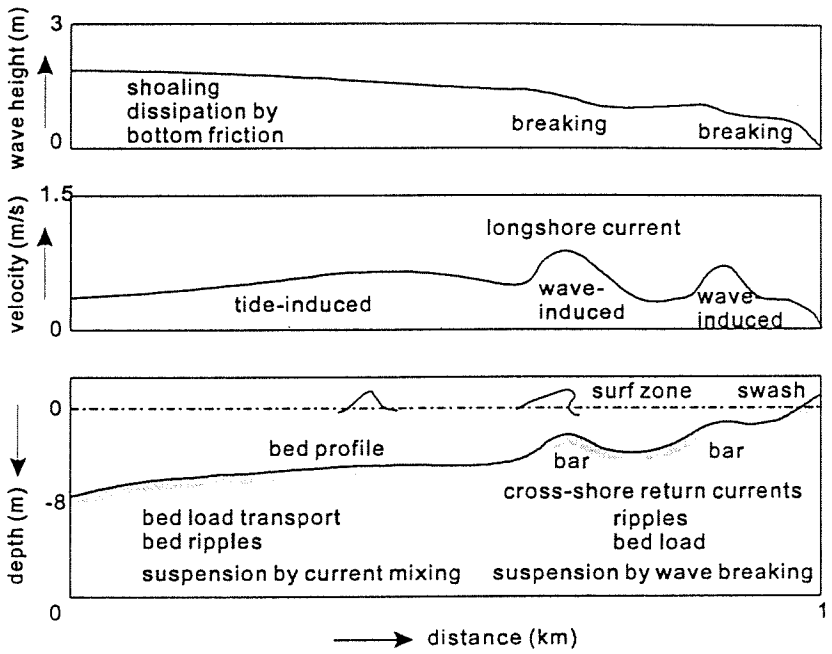

3.2 *Longshore sediment transport*

The longshore sediment transport rate is defined to occur primarily within the surf zone and is directed parallel to the coast. This transport is among the most important nearshore processes that controls the beach morphology and determines in large part whether the shores of the bay erode, accrete, or remain stable. Therefore, understanding the longshore sediment transport is essential.

Currents associated with nearshore cell circulation generally act to produce only a local rearrangement of beach sediments. The rip currents of the circulation can be important in the cross-shore transport of sand, but there is minimal net displacement of beach sediments along the coast. More important to the longshore movement of sediments are waves breaking obliquely to the coast and the longshore currents they generate. The resulting movement of beach sediment along the coast is referred to as longshore sediment transport. This transport can also result from the currents generated by alongshore gradients in breaking wave height, commonly called diffraction currents. This transport is manifest as a movement of beach sediments toward the structures which create these diffraction currents (such as head-

lands and offshore breakwaters). The result is transport in the "upwave" direction on the downdrift side of the structure. This, in turn, can create a build-up of sediment on the immediate downdrift side of the structure or contribute to the creation of a crenulate-shaped shoreline on the downdrift side of a headland.

For a detailed description of the numerical method used to calculate the sediment transport in the numerical model Delft2D-MOR reference is made to Appendix B.

3.3 *Cross-shore sediment transport*

Quantitative engineering guidance has been more firmly established for rates of longshore transport than for rates of cross-shore transport. This seems mainly due to the complexity involved in the respective processes and in adequate analyses: simple considerations using small-amplitude wave theory are applicable to longshore transport, while the need for higher order treatment in considering cross-shore transport is well established but still problematical (Wells, 1977; Van de Graaff and Tilmans, 1980). With nearshore waves propagating usually at only a slight angle with respect to a shore normal line, an appreciable unidirectional longshore current and net sediment transport are driven by fairly steady longshore wave thrust. In contrast, net cross-shore transport results from usually small differences between oscillating sediment movements in the wave direction and opposite to the wave direction.

Cross-shore transport is sensitive to the detailed structure of the reversing flow within the wave cycle and to any net flow. Also, besides the intensely agitated surf zone, relatively gentle processes out to the seaward limit of sediment motion must be considered. The integrated effect of complex cross-shore transport processes, continuously varying along the active profile, determines erosion and accretion along the profile and at the shoreline (in regions of steady longshore sediment transport).

It may be obvious that several processes cause cross-shore transport to occur. These processes are outlined in Figure 3.3.

However, since the calculation of cross-shore sediment transport is not implemented in the numerical model version used for the simulations in this report it is not taken into account. Blankers (1999) showed via simulations in which (a crude approximation) of the cross-shore option is switched on that for bay configurations the results obtained with the numerical model differ much from the results obtained when the cross-shore

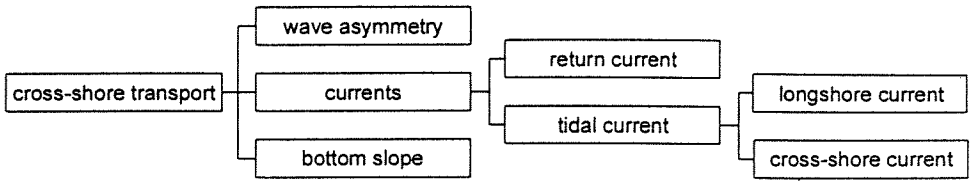

Figure 3.3

Cross-shore transport

(Nipius, 1998)

option is switched off. It is therefore recommended for further research to switch on this option and compare the results.

3.4 *Sediment transport in Delft2D-MOR*

As mentioned earlier, the simulations are done with the numerical model Delft2D-MOR (see Appendix B). Within this model three different types of transport modules can be used:

- TRSTOT
- TRSSUS
- TRSSUS+

The difference between the module with TRSTOT and TRSSUS is that in the latter a differentiation is made between bedload transport and suspended transport. Settling of sediment occurs slower with the module of the suspended transport, which results in more smooth bathymetries. The TRSSUS+ module takes cross-shore transport into account. This cross-shore routine describes the cross-shore transport with a Bailard sediment transport formula. With this formula not only the sediment by currents is modelled, but also the wave-effect and the slope effect. The sediment transport computed with the Bailard formula is added to the bedload transport of the suspended sediment transport module (TRSSUS). This is not completely correct, but has proven to yield reasonable results (Nipius, 1998).

For the simulations described in this report the module TRSSUS is used. The module with the cross-shore routine would probably give more reliable results, but the TRSSUS+ module is not yet installed in the UNIX version of Delft2D-MOR.

The transport module determines the sediment transport using the time-dependent flow and wave field. The magnitude of the sediment transport will be computed using a (to be selected) sediment transport relation. In this study the Bijker formula is used. Bijker extended the existing bed- and suspended transport formulae for current only, to formulae including wave

effects. He used the Kalinske-Frijlink formula for the bed transport and the Einstein formula for the suspended transport.

The magnitude of the sediment transport computed by the Bijker formula must be corrected for different effects which are not included in the formula itself. These effects are:

- bed level gradient effect,
- non erodible layer effect,
- numerical stability.

CHAPTER 4

Model settings

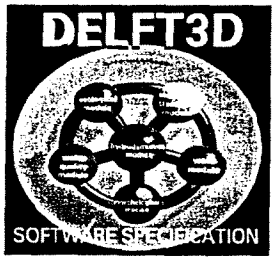

This chapter describes the settings as they are used in the model. Time step, simulations time, physical parameters and numerical parameters among other things form the input of the model. Further numerical research on equilibrium bays needs this information since different settings inevitably yields different results. Moreover, validation of results of simulations described in this report can only be done if the settings are known.

4.1 Introduction

The morphological development of an arbitrary bay shape towards an equilibrium bay between two offshore breakwaters has been investigated with the numerical model Delft2D-MOR. The set-up of this model is described in this chapter.

In order to predict the morphological changes in a coastal area it is necessary that waves, currents and their mutual interference are modelled in an integrated way. It is also necessary to involve bottom changes in the wave-current computations. All these different quantities are strongly correlated and influence each other.

Therefore WL | Delft Hydraulics has developed a flexible model system existing of separate modules for the physical processes:

- waves (HISWA),
- flow (TRISULA),
- sediment transports (TRSSUS),
- bed level variations (BOTTOM).

This modular structure of the program Delft2D-MOR ensures maximum flexibility since various combinations of the different modules are possible. The module MAIN controls the interaction between the separate modules.

In the next paragraphs the settings of the control module as well as the separate modules are described. For a extensive description of the model Delft2D-MOR reference is made to Appendix B.

4.2 The control module MAIN

The process tree used in the morphological simulations is illustrated in Figure 4.1. The main process to be simulated here (node 6) exists of one execution of subprocess 5. Within this subprocess the main simulation runs under node 4. Node 1 executes one run of the flow module and is only here to create a flow field for the first HISWA calculation. Flow fields from this calculation have a speed of approximately 0m/s, because of the absence of driving forces. After one execution of node 1 the main simulation starts. Node 2 runs in sequence the wave and the flow module. To take wave current interaction into account this node is run twice.

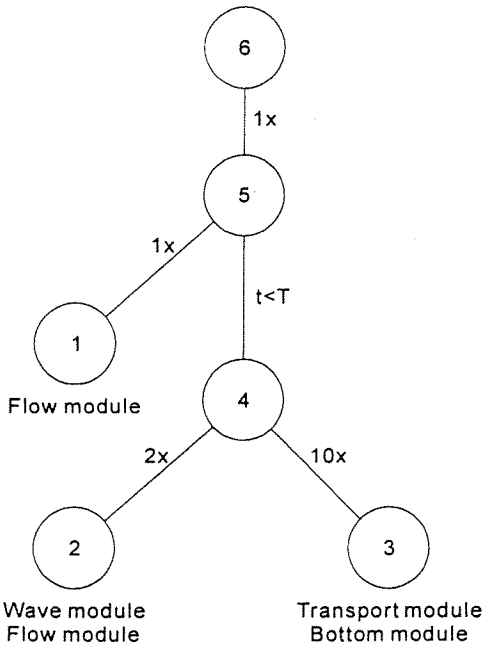

Figure 4.1

Process tree for morphological simulations

Now that the wave and the current field are known, the other two modules are started (node 3). The wave and flow data are used by the sediment transport module to compute the sediment transport rate, which in its turn is used to update the bed level in the bottom module. If the total simulation time (T) has not yet been reached and the maximum number of loops (using the continuity correction) of node 3 have been carried out, a new execution of node 2 takes place. The simulation time of the wave module is set to 0 because the wave module has no adaption time. For the flow module the

simulation time is set to 20 minutes. This is necessary because the module needs time to develop a stable current system.

The bottom module is executed with the automatic time step procedure, with a maximum Courant number of 0.8. When the horizontal bed celerity gets bigger the time step gets smaller with a minimum of the time step from the transport module (1min). This process continues until the specified end time (T) is reached. Times and number of iterations in this simulation are summarised in Table 4.1. How these simulation times are determined can be found in Blankers (1999).

Node	Iterations	Modules	Simulation time
1	1	TRISULA	20 minutes
2	2	HISWA TRISULA	0 minutes 20 minutes
3	10	TRSSUS BOTTOM	5 minutes automatic
4	1	MAIN	7 days / 30 days
5	1	-	-
6	1	-	-

Table 4.1 Simulation time

An overall simulations time of 7 days is chosen because it clearly shows the tendency to which a bay develops. Simulations longer than 7 days needs more calculations time and more computer memory. However, some simulations with interesting bay shapes are executed for a period of 30 days. Simulations longer than 30 days result in unreliable results, because the depth gradients will get too large.

4.3 The wave module HISWA

4.3.1 The bottom grid

The bottom input is provided to HISWA on a two dimensional grid. The dimensions of the input grid are chosen such that the grid covers the whole area of interest. The input grid for the wave module consists of a rectangular grid of 1100 by 1100 m, with the origin in (1250,150) and rotated over 90° (see Figure 4.2). The mesh size (Δx by Δy) is 10 by 10 m, just like the mesh size of the flow module. A smaller grid size improves the accuracy of the calculations, but also increases the computational time considerably. The grid size of 10 by 10 m is a compromise between accuracy and calcula-

tion speed. A square grid is chosen because it is easy to generate. The initial bottom position is described in the bottom depth file. This file contains depth values (positive downwards) for every grid point with its zero point at the still water level.

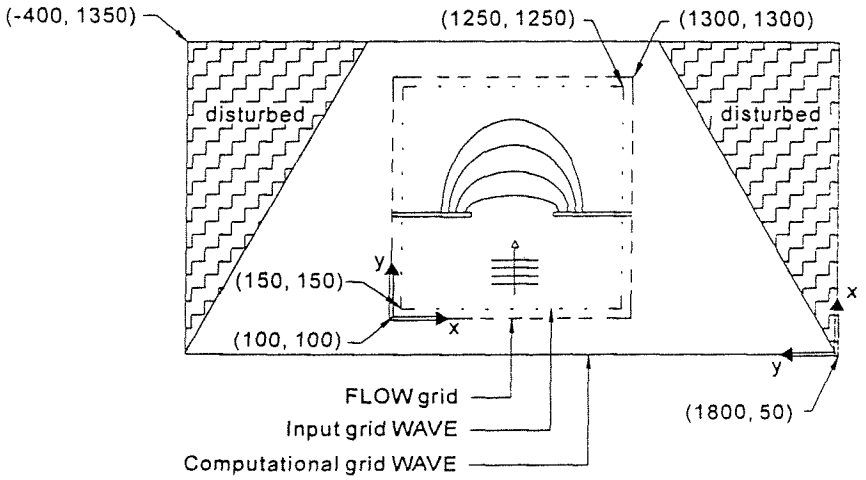

Figure 4.2

HISWA and TRISULA grids

4.3.2 *The computational grid*

Because the implementation of HISWA in Delft2D-MOR does not allow reflecting boundaries it is necessary to make the computational area for HISWA larger than the computational area for TRISULA. This is because at the side boundaries wave energy is disappearing, but no wave energy is entering. Therefore, the computational grid is in y-direction longer than the area of interest (the input grid). Outside the input grid HISWA assumes the bottom level to be identical to the nearest boundary of the input grid.

On each lateral side the computational grid is taken 550 m larger than the input grid. In y-direction the mesh size is taken equal to the Δx of the input grid (10 m). In x-direction the mesh size is now determined by HISWA's conditions of numerical stability:

$$\frac{\Delta y}{\Delta x} \geq \tan\frac{\theta}{2} \qquad \text{Equation 4.1}$$

$$\Delta x \leq \frac{10}{\tan(60)} = 5.77m \qquad \text{Equation 4.2}$$

in which θ represents half the sector of wave energy distribution (here $120^o/2 = 60^o$).

4.3.3 Boundaries

The upwave boundary is drawn parallel to the y-axis of the computational area. The position of this boundary has been set in the flow module. Along this boundary the incoming waves are described. The wave height and period are given as the significant wave height (H_s) and the peak wave period (T_p). Irregular waves are assumed with a Jonswap wave spectrum. A standard Jonswap spectrum is applied with a spectral peak enhancement factor of 3.30. This peak enhancement factor is a factor that reshapes a standard spectrum to a more realistic spectrum. Because the waves are approaching perpendicular, the wave direction in HISWA is 180° (nautical conventions: clockwise from the North).

Diffraction is not taken into account in HISWA. This is an important limitation because diffraction is one of the main creating forces of equilibrium bays. In HISWA the effect of diffraction can be simulated by a constant for directional spreading. Tests executed by Ahmed (1997) show that the wave pattern around offshore breakwaters shows little deviation from a specialised diffraction model (DIFFRAC) if the value for the constant of directional spreading is set to 4. Differences at a greater distance from the breakwaters appear to be small, while the greatest errors are expected in the shadow zone just around the heads of the breakwaters. Here, the wave module HISWA will probably predict a wave height of zero, which will not occur in practice.

Both left and right boundaries are set open. This means that energy is allowed to pass the boundaries. Because no wave energy is coming in through these boundaries, a lack of energy occurs. Therefore the left and right boundaries are placed well outside the area of interest.

4.3.4 Physical parameters

The physical constants needed for a wave calculations are:

g = acceleration due to gravity (default: 9.81 m/s^2)
ρ_w = water density (default: 1025 kg/m^3)
c_{fw} = friction coefficient induced by waves (default: 0.0100)
c_{fc} = friction coefficient induced by current (default: 0.0050)

The maximum wave height of a wave in shallow water is expressed by $\gamma_s \times h_b$, where h_b is the water depth where breaking occurs. The default value for white capping (breaking in deep water) is determined by the wave steepness $\gamma_d = H/\lambda$. This is important for breaking in deep water, which will not occur in the bay. The coefficient α is used as a switch to adjust the magnitude of dissipation for different circumstances. Together with γ_s they determine the wave height development from the sea towards the shore. The dissipation of waves in shallow water due to bottom and current friction

can be accounted for with c_{fw} and c_{fc}. The effect of the wave and bottom friction on the wave frequency is taken into account.

4.4 *The flow module TRISULA*

4.4.1 *The input grid*

The TRISULA input grid (see also Figure 4.2) has dimensions of 1200 m by 1200 m with its origin in (100,100) for numerical reasons: TRISULA does not accept an origin with coordinates (0,0). The mesh size in TRISULA's input grid is equal to HISWA's input grid: 10 m by 10 m. The grid enclosure on the water level points of the staggered grid cells defines the computational area and ranges from cell 1 to 119 in x and y-direction.

4.4.2 *The bathymetry and the breakwaters*

The bathymetry of the bay is imported in the flow module as a file. This file has been created with a MathCAD worksheet. This file describes the initial depth at every grid point. The breakwaters are replaced in the simulation by two rows of dry points, so the width of the breakwater is 20 m (2 cells wide). The coordinates of the dry points are imported in the flow module as a file, with the begin and end coordinates of the rows of dry points. Dry points can be seen as impermeable vertical columns of an infinite height. This does not really look like a breakwater, but since local effects (like scour) are not the main subject of this study, this is accepted.

4.4.3 *Initial and boundary conditions*

At the start of the simulation the water velocities and levels are set to zero in the whole area. Open boundaries are used to keep a limited computational area. At the seaward side an open boundary is chosen characterized by a constant water level. This boundary is also used in the waves module as the upwave boundary. In nature waves pass the open boundaries undisturbed and without reflections. A weakly reflecting boundary is chosen (α = 100) to reduce the spin-up time of the model. The spin-up time is the time the model needs to develop a stationary situation.

4.4.4 *Physical constants*

The physical constants needed for a flow calculation are:

g = acceleration due to gravity (default: 9.81 m/s^2)
ρ_w = water density (default: 1025 kg/m^3)

Bottom roughness and viscosity effects are taken into account by the parameters:

C = Chezy coefficient (m$^{1/2}$/s)
Visc = eddy viscosity (m^2/s)

C is taken equal to 65 m$^{1/2}$/s (which means a roughness height of about 0.024 m, for a depth of 8 m) in order to take bed forms into account. Experience has learned that this is a reasonable value for true scale models on a sandy coast.

The horizontal eddy viscosity describes the turbulence in the simulation. Since a 2DH version of the model is used the vertical eddy viscosity is not important. Calibration of velocity fields with measured values from physical tests is often done by varying the eddy viscosity. Since no practical velocities are known a uniform eddy viscosity equal to 1.00 m^2/s is applied in this model. An increase of the viscosity resulted in a more uniform current pattern without small eddies, while decreasing viscosity values led to a highly unstable current pattern. A value of 1.00 m^2/s is considered 'normal' for a true scale simulation.

4.4.5 Numerical stability

For numerical stability TRISULA requires the Courant number to be smaller than 10. The Courant number for two-dimensional problems is defined as (Stelling, 1984):

$$C_{max} = \Delta t \sqrt{gh\left(\frac{1}{\Delta x^2} + \frac{1}{\Delta y^2}\right)} \leq 10 \qquad \text{Equation 4.3}$$

in which:

Δt = time step (s)
g = acceleration due to gravity (m/s^2)
h = local water depth (m)
Δx = grid mesh size in x-direction (m)
Δy = grids mesh size in y-direction (m)

With a mesh size in x-direction of 10m and a depth of 8m a time step of 6s is numerically stable:

$$C_{max} = 6\sqrt{9.81 \cdot 8\left(\frac{1}{100} + \frac{1}{100}\right)} \approx 7.5 \leq 10 \qquad \text{Equation 4.4}$$

Since nowhere in the bay a water depth greater than 8 m is found, the Courant number is always less than 7.5. A time step of 6s seems small for a simulation that sometimes takes some weeks, but it is necessary because of the mesh size of 10m. Since a reasonable accuracy has to be reached the mesh sizes can not be taken larger.

4.5 *The sediment transport module TRSSUS*

4.5.1 The transport formula

Because the TRSSUS module keeps the sediment longer in suspension, smoother results are expected with this module. To calculate the sediment transports the Bijker formula for waves and currents is used. The physical constants needed for a transport calculation are:

- grain size d50 = 200 μm
  d90 = 300 μm
- fall velocity w = 0.023 m/s
- sediment density ρs = 2650 kg/m^3
- water density ρw = 1025 kg/m^3
- bottom roughness μ = 0.05 m
- sediment porosity ε = 0.4
- kinematic viscosity ν = 1 10^{-6} m^2/s

When the values for the bottom roughness between the flow module and the transport module are compared, it can be seen that the bottom roughness used in the transport calculations is about twice as large as in the flow calculations. This seems like a contradiction, but it is justified because these values are not just physical values but are also a tool to tune a simulation to acquire more reliable results. For a true scale transport simulation on a sandy beach μ = 0.05 m is a reasonable value.

4.5.2 Sediment transport rate correction

A multiplication factor depending on the bed level gradient is included because the Bijker formula does not take into account the effect of a bed-level gradient. The standard value is used: 1.0. This means that the effect of the bed level gradient is taken into account, but is not extra enlarged. The

sediment transport rates are calculated at each grid point of the flow module. The automatic time step regulates the time step of the bottom module dependent on the bed celerity. If the celerity increases the time step decreases. This is done to avoid large errors for a rapidly changing morphology.

4.6 The bottom module BOTTOM

The input of the bottom module mainly prescribes the output of data and the conditions at the boundaries. In the simulations only one boundary is created: the upwave boundary at the seaside. The condition of this boundary is set to a stationary bottom depth. Because the distance from the boundary and the area of interest is large, this seems acceptable.

CHAPTER 5

Predicting bay shapes

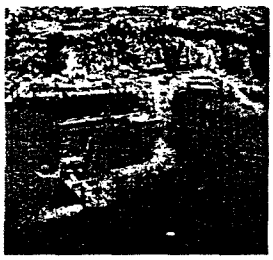

The application of headland control schemes depends strongly on the capability of man to predict the shape of a bay beforehand. Knowing the equilibrium position of the bay in relation to the position of the offshore breakwaters can yield financial benefit. With the aid of computers one is able to imitate the consequences of applying coastal structures and as a result, guidelines for coastal engineering practices can be drawn up.

5.1 Introduction

Blankers (1999) based the Blankers Bay Bathymetry-predictor (see Figure 5.1) on the average of the maximum of the longshore current of three cross-sections. These cross-sections are directed perpendicular to the coast and evenly divided over half the bay (see Figure 5.4). In order to gain enough data Blankers (1999) executed simulation runs with 40 different bay geometries. The goal of these hydraulic simulations was to find out for what kind of bay shape low current velocities can be found. Blankers (1999) assumption was that the longshore flow velocities must be small along the whole shoreline for a bay to be close to an equilibrium shape.

A disadvantage of the parameter 'average of the maximum longshore velocity over the three cross-sections' is that in some bays the average velocity is close to zero, but the absolute values of the maximum velocities in the cross-sections can still be different from zero. This might yield a wrong conclusion since significant morphological changes occur while this bay is expected to be in equilibrium.

The BBB-predictor is a contour plot with the average maximum longshore velocity as a function of the gap-width ratio (G/W) and the indentation-with ratio (I/W). The flow velocities in the BBB-predictor are absolute; the flow direction can be found by checking at which side of the blue low-velocity belt the bay is situated in the graph. Bays situated left or under this belt have negative current patterns (from the centre to the edges, see Figure

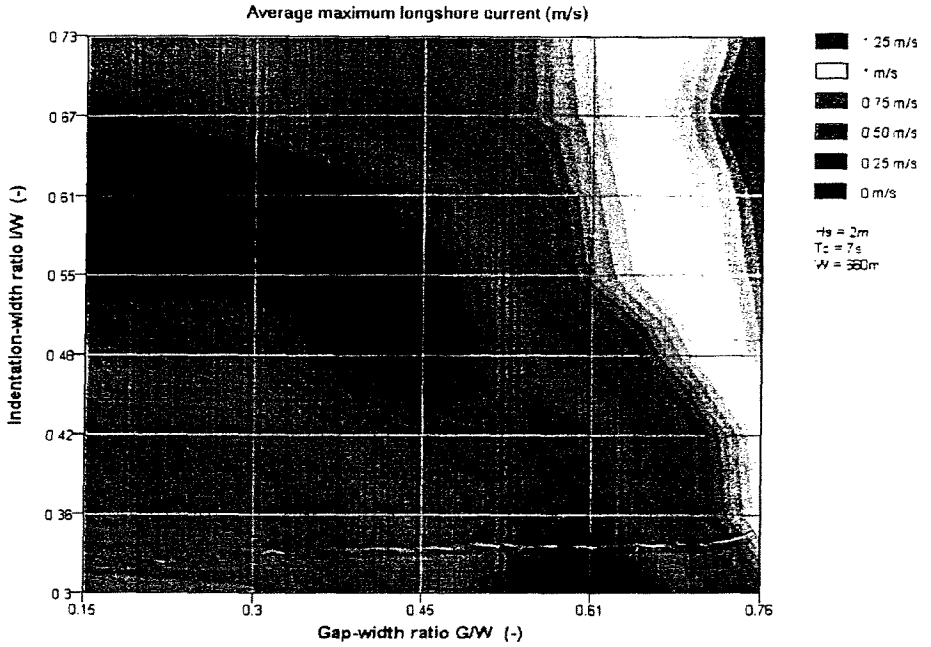

Figure 5.1

BBB-predictor

(Blankers, 1999)

2.7a) and hence, the currents in these bays are apparently dominated by the differences in wave set-up. Bays right or above the belt have a positive current pattern (from the edges to the centre, see Figure 2.7b) and the currents in these bays are dominated by the oblique approach of the waves. Bays situated in the blue belt have low velocities and are expected to be close to equilibrium.

In order to confirm that bays situated in the blue belt are stable, Blankers (1999) executed morphological simulations with bay shapes which should be stable according to the BBB-predictor. Unfortunately, it turned out that these bays were not in an equilibrium state.

5.2 *Equilibrium parameter*

The average of the largest values of the longshore velocity in three cross-sections is probably a too simple parameter to judge the stability of a bay. The turbulence caused by the waves is enough to stir up a lot of sediment and consequently large flow velocities are not required to erode the sediment from the bottom. Moreover, large discharges (even if the flow-velocity is low) are able to transport large volumes of sediment, resulting in large morphological developments. A better parameter to define equilibrium might be the average longshore sediment transport. It can be seen in Figure 5.2 that in the breaker zone the bedload transport is considerably smaller than the suspended load transport. Although this graph only shows the

Figure 5.2

Suspended load versus bedload transport in cross-sections 2, 5 and 8

(the location of the cross-sections is given in Figure 5.4)

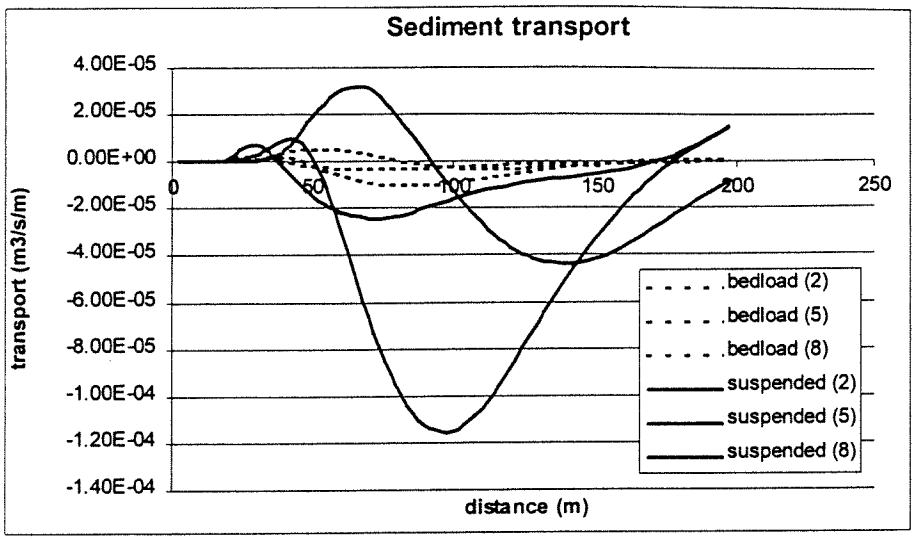

results for bay 4c (see Appendix E.1) and a $H_s = 2$ m, the results of simulations done with other bays and different wave heights also show that the bedload is significantly smaller than the suspended load.

In Figure 5.3 the longshore current velocities for bay 4c are plotted. It can be seen that the suspended sediment transport is related to the current velocities. The fact that in cross-section 2 this relation is less visible is because this cross-section is in the shadow zone behind the breakwaters and there is less sediment in suspension. So, in order to simplify the calculations the bed load term is neglected. Consequently, the parameter on which the Sweers Bay Bathymetry-predictor (SBB-predictor) is based is the average of the integrated suspended sediment transport through three cross-sections perpendicular to the coast. The difficulty with this parameter is the determination of the length of the cross-sections.

Figure 5.3

Longshore velocity in cross-sections 2, 5 and 8

(velocity component perpendicular to the cross-section; the location of the cross-sections is given in Figure 5.4)

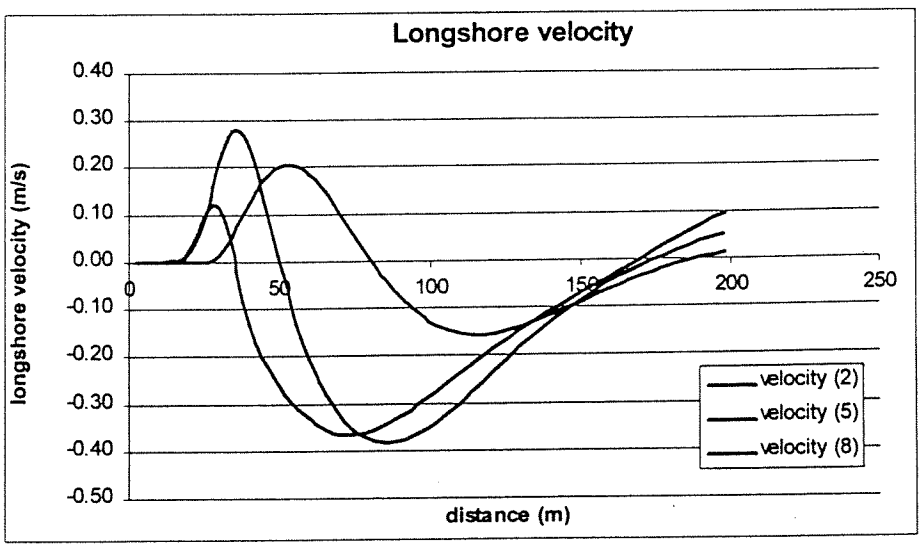

5.2.1 *Defining the breaker zone*

Since nearly all suspended sediment transport occurs within the breaker zone, the amount of sediment passing the coast on a certain location is calculated via an integration of the sediment transport rates over the breaker zone. Due to the directional spreading and refraction of incoming waves, the waves break at different distances from the coast at different locations, resulting in different lengths of the cross-sections at different locations. In order to get a consistent and reliable SBB-predictor the seaward boundary of the breaker zone must be defined accordingly.

Determining the seaward boundary of the breaker zone is very arbitrary. There are several possibilities to define this boundary and a few are examined in order to determine a feasible one. As long as one uses the same boundary definition for all cross-sections to determine the integrated suspended sediment transport, it is possible to make sound qualitative statements about the amount and direction of this transport.

First, it is important to determine a suitable quantity which clearly visualizes the seaward boundary of the breaker zone. Therefore several quantities are examined. These quantities are:

- the significant wave height H_s
- the energy dissipation
- the fraction of breaking waves
- the suspended sediment transport

These quantities are plotted over three cross-sections 2, 5, and 8 (see Figure 5.4). The cross-sections have the same length of 200 m. The origin is located at MSL +1 m in order to take run-up effects into account. The distance of 200 m is chosen because this distance is longer than the width of the breaker zone for all bays used in the simulations and hence, the seaward boundary of the breaker zone is located somewhere along the cross-section. It is mentioned that bay 4c is used in this report as an example to illustrate one thing and another, but simulations done with bays with different geometries showed the same tendency.

Significant wave height

Since in the breaker zone most of the incoming waves break, the significant wave height (H_s) may be a good quantity to determine the boundary of the breaker zone. A sudden decrease in significant wave height along the cross-section would indicate breaking waves. But as it can be seen in Figure 5.5 this sudden decrease in wave height only occurs in cross-section 2 (it is again mentioned that the results of only one bay geometry are plotted, namely bay 4c, but that other bay geometries give similar graphs). The sea-

Figure 5.4

Location of cross-section 2, 5 and 8

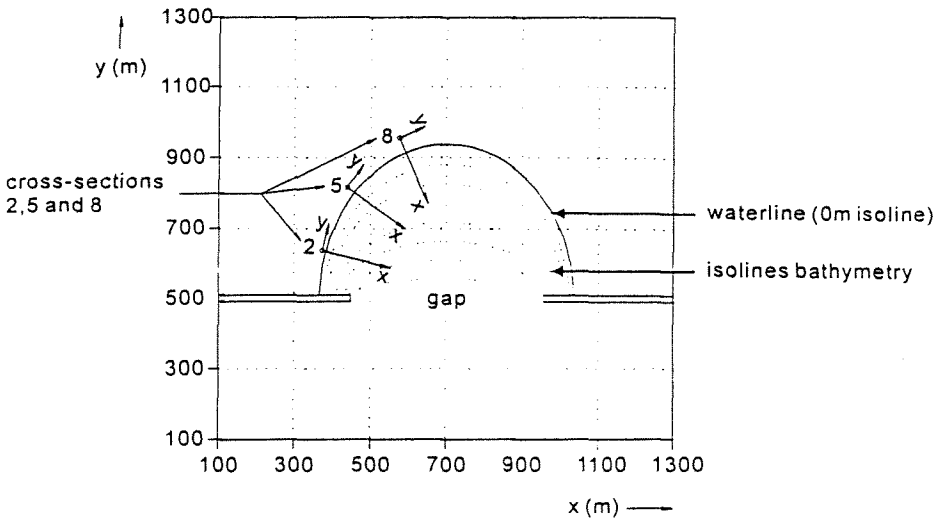

ward boundary of the breaker zone is very well visible for cross-section 2, as can be seen in the sudden decrease in wave height at a distance of about 40 m. However, this is certainly not the case for cross-sections 5 and 8. The wave height decreases gradually and this makes it complicated to define the breaker zone. Therefore, the significant wave height is not suitable for determining the breaker zone.

Figure 5.5

Significant wave height as function of the offshore distance

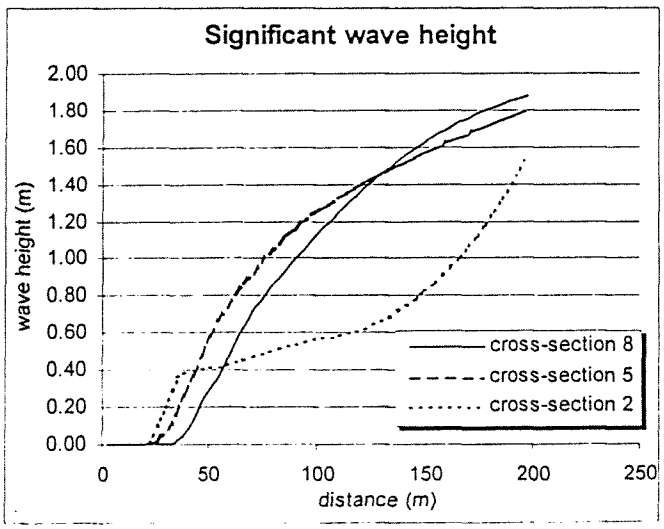

Energy dissipation

In the breaker zone waves lose their propagated energy via breaking due to (among other things) turbulence, bottom friction, sound and heat. This energy, which has been generated by e.g. wind shear against the water surface, has travelled within a wave train for hundreds of miles and eventually gets totally lost in the breaker zone. Thus, it may be that the wave energy dissipation is a good quantity to use for the above described goal. In Figure 5.6 the wave energy dissipation is plotted for the cross-sections 2, 5 and 8.

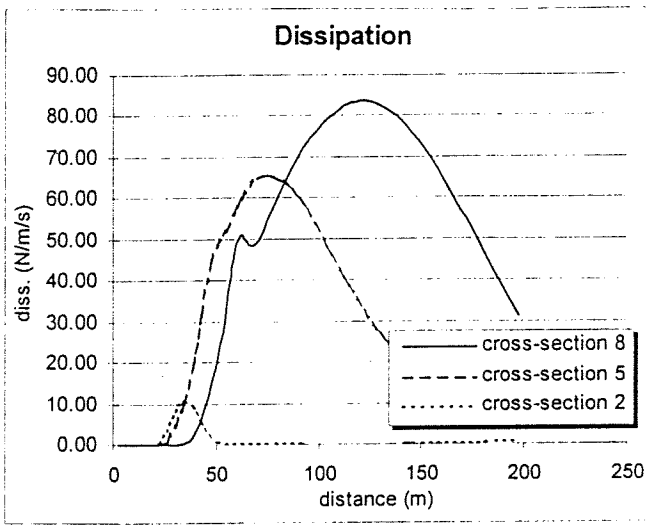

Figure 5.6

Energy dissipation as function of the offshore distance

As it can be seen in this graph, the energy dissipation shows a maximum value for all cross-sections. Since the most energy gets dissipated at that location, this maximum probably indicates the position at which most of the incoming waves break. Therefore, this quantity may be a good quantity to define the seaward boundary of the breaker zone. However, to make sure that the locations indicated by the maximum energy dissipation coincide with the seaward boundary of the breaker zone (and to examine whether another quantity is even more suitable), other quantities are examined as well and compared with Figure 5.6.

Fraction of breaking waves

Another quantity which can be analysed is the fraction of breaking waves. The value of this fraction describes the extent to which waves break: the higher this fraction, the more waves break (multiplying this fraction with 100 yields the percentage of breaking waves). As can be seen in Figure 5.7

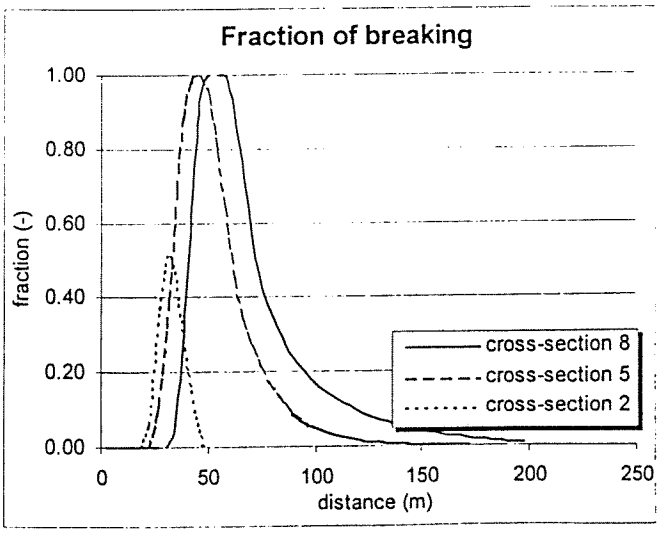

Figure 5.7

Fraction of breaking waves as function of the offshore distance

at a certain location in cross-section 5 and 8, all the incoming waves break (value of the fraction is 1). This is not the case for cross-section 2 in which about 50% of the incoming waves break at the peak location. However, this quantity may be a good quantity to define the breaker zone for it is possible to determine a concrete, non-arbitrary value for the fraction of breaking waves. If Figure 5.7 is compared with Figure 5.6, it can be seen that the locations indicated by 10% breaking of the incoming waves, more or less coincide with the locations of maximum energy dissipation. The higher waves break further in sea than at the peak location (100% breaking), but they also contribute to the suspended sediment transport in the breaker zone. Hence, the seaward boundary of the breaker zone is set at the location where 10% of the incoming waves break. From that point (see graph) the percentage of breaking waves increases drastically. So, this quantity may also be a good quantity to define the breaker zone.

Suspended sediment transport

The last quantity which can be useful is the suspended sediment transport. As mentioned before, suspended sediment transport mainly takes place within the breaker zone. Outside the breaker zone this transport decreases rapidly and becomes almost zero. Thus, plotting the suspended sediment rate along the cross-section might indicate the width of the breaker zone. Unfortunately, as can be seen in Figure 5.8, outside the breaker zone the transport rate is not zero. This can be explained as follows. Due to the cir-

Figure 5.8

Suspended sediment transport as function of the offshore distance

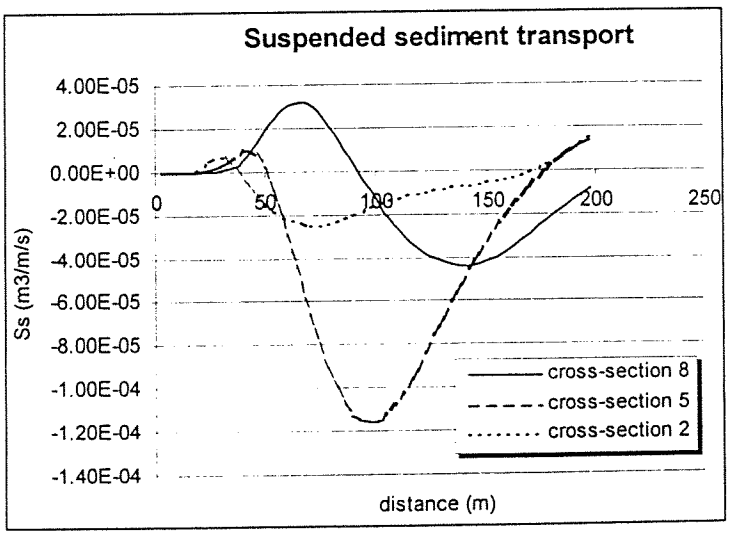

culation patterns which are present in the bay a distinction has to be made between the breaker zone and the offshore zone. In the breaker zone, which is narrow with respect to the offshore zone, the flow direction (and thus the sediment transport direction) is controlled by the angle to which the waves break on the beach and by differences in wave set-up. As a consequence of continuity (and the presence of the breakwater) the flow direction in the

offshore zone is opposite to the flow direction in the breaker zone. It has already been shown that the suspended sediment transport and the current velocity are strongly related (see Figure 5.2 and Figure 5.3). Since the distinction between the breaker zone and the offshore zone can be clearly made (via a suspended sediment transport rate of zero) a concrete, non-arbitrary parameter can be defined.

5.2.2 *Defining equilibrium*

As described in the previous section, it turned out that three quantities may define the seaward boundary of the breaker zone on a non-arbitrary manner. This section will deal with the choice eventually made. In Figure 5.9 the seaward boundary of the breakerzone is plotted for the cross-sections 2, 5 and 8 for the three quantities: dissipation (green), fraction of breaking waves (blue), suspended sediment transport (red). It can be seen that the

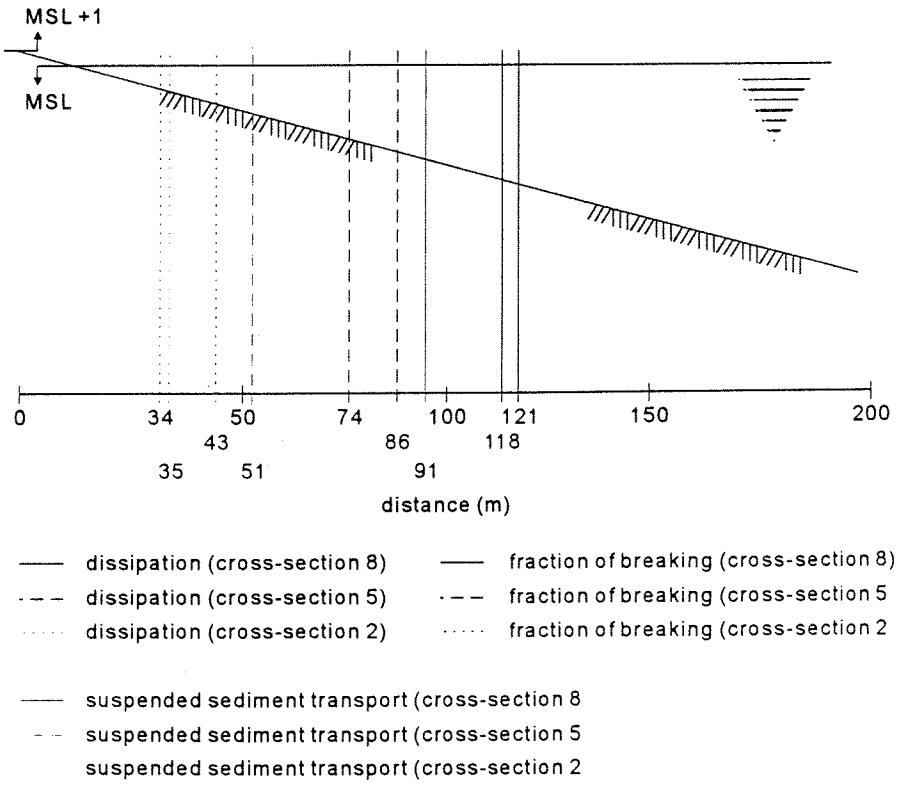

Figure 5.9

Definition of the breaker zone according to three quantities

quantity 'suspended sediment transport' yields a breaker zone which is significantly smaller than when using the other quantities. This is due to the circulation patterns in the bay. The suspended sediment transport is strongly related with the current velocities. Due to the offshore return current which is directed in the opposite direction as the current in the breaker zone, the location where the longshore velocity reverses direction (and thus is 0 m/s) is moved shoreward. Hence, the zero-crossing point of the suspended sediment transport is moved shoreward as well. Using this quantity

to define the breaker zone will therefore result in smaller suspended sediment transport rates.

According to Figure 5.9, in most cases the quantity 'dissipation' yields a shorter breaker zone than when using the fraction of breaking waves. This is due to the fact that the maximum dissipation is used. However, some high waves will break before they reach the location of maximum dissipation. These waves also contribute to the sediment transport in the breaker zone. By choosing a fraction of breaking waves of 0.1, these waves are taken into account and hence, this will probably yield the most accurate results. Therefore, the fraction of breaking waves is chosen to define the seaward boundary of the breaker zone.

It is mentioned that all three quantities will eventually lead to similar SBB-predictors and hence, they can all be used to draw qualitative conclusions. However, the amount of suspended sediment transported differs significantly for each quantity.

The SBB-predictor will now be based on the integrated suspended sediment transport within the breaker zone in the initial situation. Thus an integration takes place from the shoreline to the seaward boundary of the breaker zone, defined by the fraction of breaking waves.

5.3 *The SBB-predictors*

New contour plots are created, the SBB-predictors, which are based on the results of computations for 40 different bay geometries. These bay geometries are identical to the bay geometries on which the BBB-predictor is based (Blankers, 1999) and are shown in Appendix E.1. For each bay, the seaward boundary of the breaker zone is determined using the fraction of breaking waves. Determining the sum of the three cross-sections of the integrated suspension transport over the breaker zone results in a predictor which is direction dependent: negative values indicate overall sediment transport from the centre of the bay to the sides, positive values indicate transport in the opposite direction. The advantage of this approach is that it is easy to see whether a bay tends to increase its indentation (negative values) or whether it tends to decrease its indentation (positive values). For a bay to be initially stable no transport should occur in all cross-sections. Summarizing the transports in the three cross-sections may yield a zero transport value, even if the transports in each cross-section are not zero (a positive value in cross-section 2 may compensate the negative value in cross-section 8, for instance). Therefore, predictors have also been constructed, based on the sum of the absolute values of the suspended sediment transport in the breaker zone. Since no negative values are present in this

graph, no information is available about the direction in which the overall transport takes place. Bay geometries with (almost) zero-values are assumed to be initially stable in all cross-sections.

5.3.1 *Direction dependent sediment transport*

The obtained data is plotted in a contour plot (see Figure 5.10). At the crossings of the vertical and horizontal lines the sediment transport is actually calculated; this is elucidated by the upper and right axes which identify the bay nr. and the bay letter as defined in Appendix E.1. By interpolation the whole contour plot is filled. Comparing Figure 5.10 with Figure 5.1, it

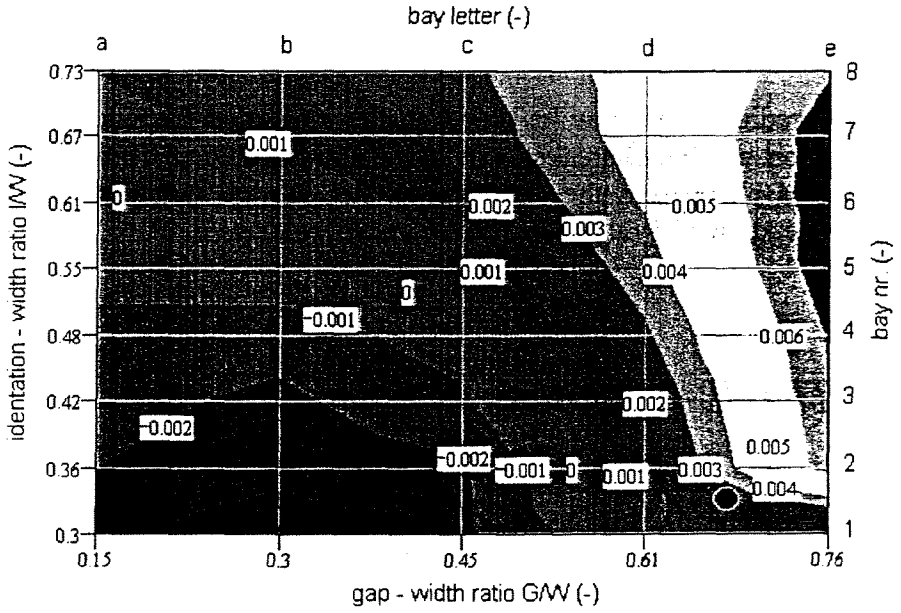

Figure 5.10

SBB-predictor based on a fraction of breaking waves of 0.1

Hs = 2 m
Tp = 7 s
W = 660 m

can be clearly seen that the a similar conclusion can be drawn with respect to the geometry of a bay which is expected to be in a equilibrium state. Although less contour classes are used in Figure 5.10 (in order to get a clear plot) it is obvious that the blue belt of the BBB-predictor more or less coincides with the zero-line in the SBB-predictor. This is an unexpected result since Blankers (1999) showed that bays having geometries according to this blue belt were not in an equilibrium state.

A similar contourplot is constructed for a significant wave height of 1 m and a peak period of 5 s (yielding the same wave steepness as a wave height of 2 m and a peak period of 7 s). This is done in order to examine how the contour plot changes as the wave height changes. The results of these simulations are plotted in Figure 5.11. Due to a significant decrease in wave energy entering the bay, the amount of suspended sediment transport

Figure 5.11

SBB-predictor based on a fraction of breaking waves of 0.1

Hs = 1 m
Tp = 5 s
W = 660 m

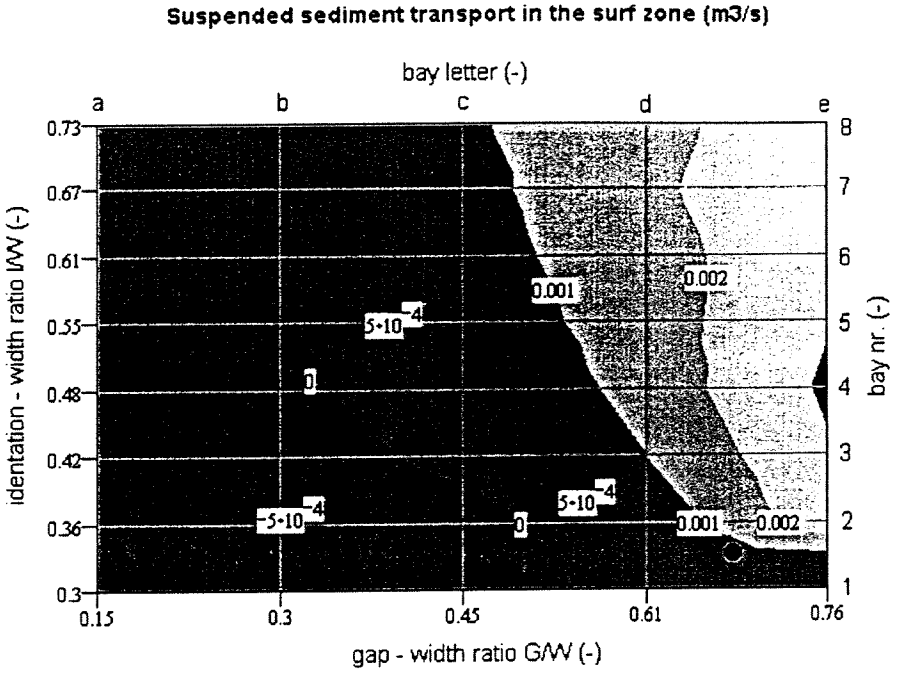

is much smaller for a 1 m wave height compared to a 2 m wave height. It can also be seen that the line indicating a zero suspended sediment transport is shifted to the lower left corner of the graph. So, according to the SBB-predictor, a smaller wave height results in a flatter bay with a smaller gap between the breakwaters. In a situation with a given gap width (the gap width is fixed), a smaller wave height results in a bay with a smaller indentation.

5.3.2 *Direction independent sediment transport*

In this section the SBB-predictors are based on the absolute values of the longshore suspended sediment transports in the breaker zone in three cross-sections. This enables a quick insight into the stability of the bay: (almost) zero values would indicate initial stability, non-zero values indicate initial instability.

As can be seen in Figure 5.12 and Figure 5.13, zero values do not occur in the given ranges. Comparing Figure 5.10 and Figure 5.12 (H_s = 2 m) shows basically the same tendencies for large parts of the plots. Especially near the right lower parts of the plots serious differences occur. Apparently positive and negative transport do occur for the various cross-sections, yielding a zero-averaged transport in Figure 5.10. For Figure 5.11 and Figure 5.13 (H_s = 1 m) similar tendencies might be observed. Moreover, the consequence of reducing the wave height is a reduction in the amount of sediment moving along the coast.

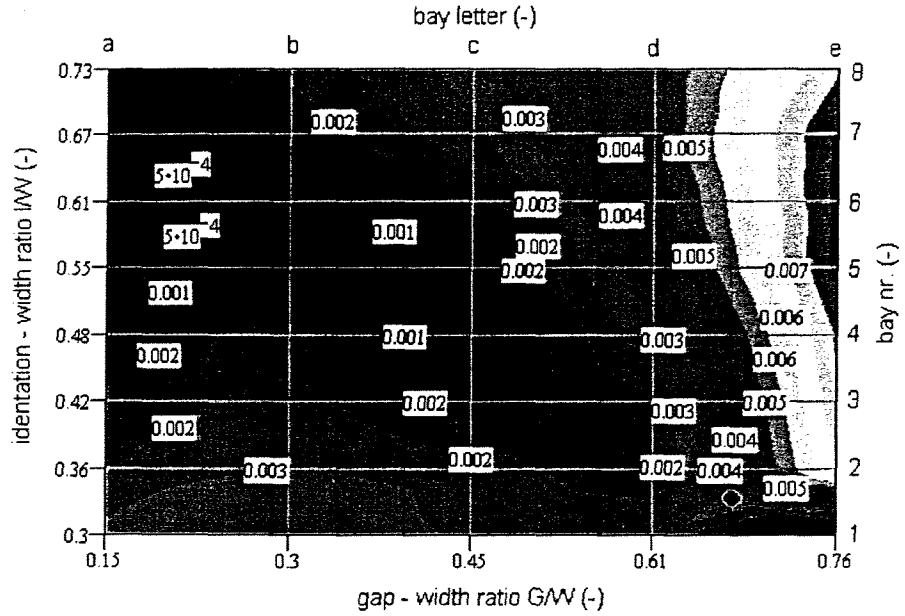

Figure 5.12

Absolute SBB-predictor based on a fraction of breaking waves of 0.1

Hs = 2 m
Tp = 7 s
W = 660 m

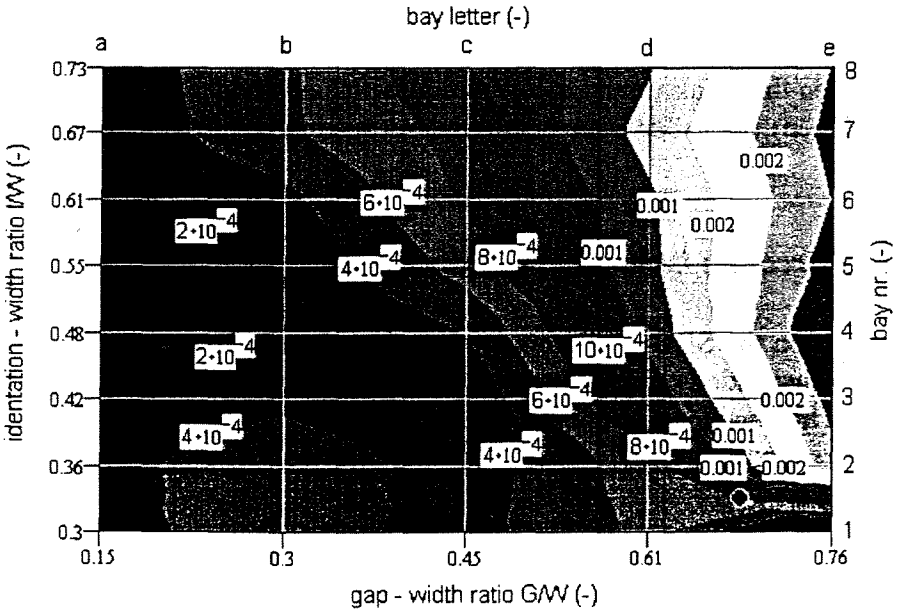

Figure 5.13

Absolute SBB-predictor based on a fraction of breaking waves of 0.1

Hs = 1 m
Tp = 5 s
W = 660 m

5.4 *Summary*

In order to check whether a different parameter than the parameter used for the BBB-predictor (which is the average of the maximum of the longshore

velocities through three cross-sections) is better able to predict the equilibrium shape of a bay, the SBB-predictor is constructed. The SBB-predictor is based on the integrated longshore suspended sediment transport in the breaker zone in three cross-sections. An additional difficulty when using this parameter is the definition of the seaward boundary of the breaker zone. Therefore, several quantities are examined:

- the significant wave height
- the wave energy dissipation
- the fraction of breaking waves
- suspended sediment transport

It turned out that all these quantities determine a different location of the seaward boundary of the breaker zone. However, this will eventually lead to predictors which show the same tendency and hence, qualitative conclusions can be made with all four quantities. For a quantitative analysis, it is expected that a fraction of breaking waves of 0.1 yields the most accurate results and the SBB-predictors are therefore based on this quantity.

Two different kinds of SBB-predictors are constructed: direction dependent and direction independent. In the former a zero-transport value might occur due to the counterbalancing effect of positive and negative transport values in different cross-sections. The bay may be global stable, but locally morphological changes can occur. Zero-transport values in the direction independent SBB-predictors would indicate both local and global stability, but these values have yet not been found in the simulations. The SBB-predictors show the same tendency as the BBB-predictors. According to the SBB-predictor, a smaller wave height results in a flatter bay with a smaller gap between the breakwaters. In a situation with a given gap width (the gap width is fixed), a smaller wave height results in a bay with a smaller indentation.

CHAPTER 6

Wave height effects

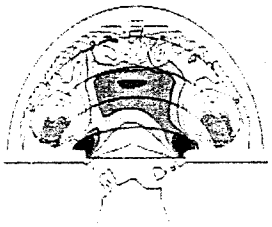

In nature, waves of varying heights approach the shore. Periods with high (storm) waves alternate with calm weather conditions. If the consequences of various wave heights are known, it may be possible to interpret the outcome of model tests with a random wave climate better. Hence, this research should be considered as a first step to model a bay with a certain wave climate including periods of high waves and periods of low waves.

6.1 Introduction

Blankers (1999) investigated the current patterns which are present in a bay subjected to constant waves H_s = 2 m and T_p = 7 s. He simulated several bathymetries (see Appendix E.1 in which each bay shape is identified by a number and a letter) and concluded that two different current patterns developed, dependent on the bathymetry. He then recommended to examine the consequences of a varying wave height. In this chapter the results are shown for waves with different heights. Furthermore, instead of

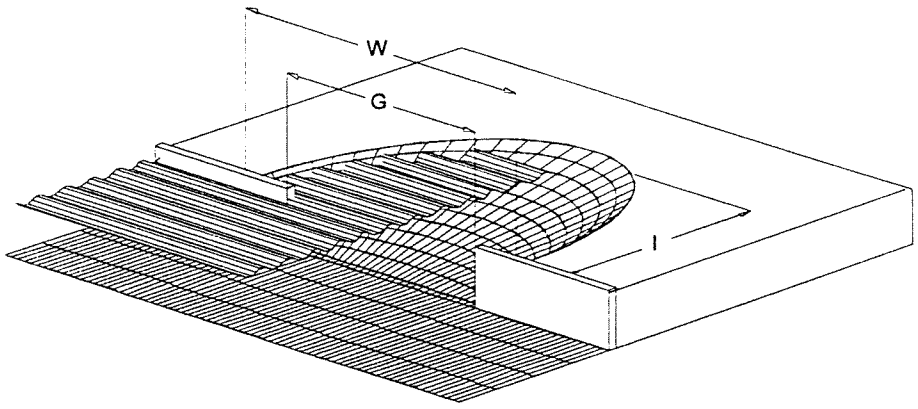

Figure 6.1

Bay dimensions

(Blankers, 1999)

hydraulic simulations as executed by Blankers (1999), simulations described in this chapter are morphological and both the current velocities and the sediment transport rates are examined. In Section 4.2, the effect of

the wave height on the longshore current velocities are examined for bays with varying indentation or gap width (Figure 6.1). Then, in Section 4.3 the effect of the wave height on the sediment transport through the gap is analysed. In Section 4.4, simulations are executed in which several bay shapes are subjected to wave heights of 1 m, 2 m or 3 m for 7 days and the morphological changes are visualised.

6.2 *Longshore current velocities*

In order to make sound statements about the influence of the wave height on the longshore current velocities, simulations are executed with a different wave height for different bay shapes. First the influence of different waves for a varying indentation is examined. Then the influence is examined for a varying gap width. However, not all forty bays as shown in Appendix E.1 are used. As can be seen in the BBB-predictor (Figure 5.1), a blue belt with low velocities is present. In Figure 6.2 this belt is simplified

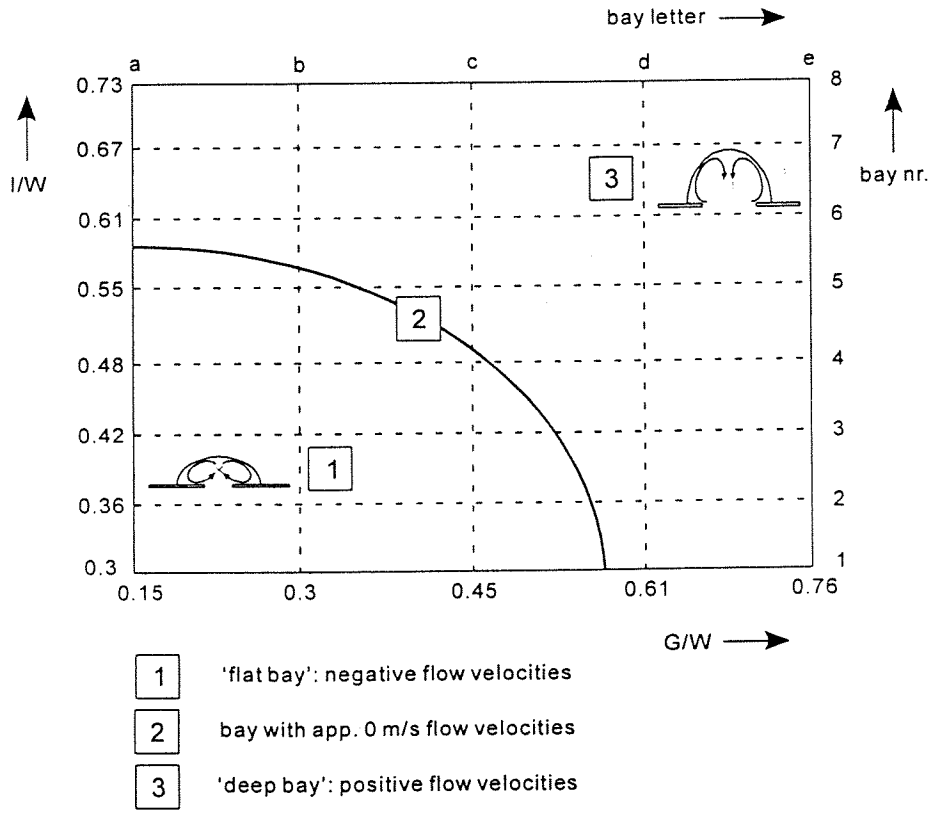

Figure 6.2

Outline of the BBB-predictor

with a line. Three areas can now be identified: area 1 represents bays with negative circulation patterns (from the centre to the sides), area 3 represents bays with positive circulation patterns (from the sides to the centre) and area 2 (the solid line) indicates bay shapes which have low longshore cur-

rent velocities. It can also be seen in this figure that bay 4c is a bay with small flow velocities and is located almost in the centre of the predictor. By choosing bay 2c, 3c, 4c, 5c and 6c it is possible to examine the influence of different wave heights on bays with varying indentation, but the same gap width. Moreover, the influence can be examined on two different current circulation patterns (a positive and a negative current pattern). On the other hand, by choosing bay 4b, 4c and 4d it is possible to examine the influence of different wave heights on bays with varying gap width, but the same indentation. And again, this choice of bay shape makes it possible to examine the influence of two different current circulation patterns.

6.2.1 Effects on bays with a varying indentation

As mentioned previous simulations were executed with bays with varying indentation. Bay 2c and 3c have a negative circulation pattern, bay 5c and 6c have a positive circulation pattern and bay 4c has very low velocities. They all have a gap width of 300 m and an overall width of 660 m (see also Appendix E.1). The indentation for bay 2c, 3c, 4c, 5c and 6c is respectively 240 m, 280 m, 320 m, 360 m and 400 m.

For these five bays simulations are done with a significant wave height of H_s = 1 m, H_s = 2 m and H_s = 3 m (Blankers only used H_s = 2 m). The peak period is respectively T_p = 5 s, T_p = 7 s and T_p = 8.5 s. These properties describe waves with the same wave steepness. The longshore current velocities in the three cross-sections 2, 5 and 8 are plotted in Appendix E.2.

Cross-section 2

Cross-section 2 is situated in the shadow zone directly behind the breakwater (see also Figure 5.4, Chapter 5). From the results plotted in Appendix E.2 it can be seen that (compare the upper three graphs):

- the negative velocity component of the (return) current dominates independent of the wave height;
- for bays with a positive circulation pattern (bay 5c and 6c, represented by respectively a yellow line and a red line), increasing the wave height results in higher offshore return current velocities;
- for bays with a negative circulation pattern (bay 2c and 3c: light blue line and a dark blue line), increasing the wave height results in significantly higher current velocities;
- increasing the wave height yields larger velocity gradients in the cross-sections for all bay shapes (in other words, the difference between the maximum longshore current velocity in the surf zone and the maximum longshore current velocity offshore gets larger while the distance between the locations of these maximum velocities gets smaller).

Cross-section 5

This cross-section is located halfway the centre and the side of the bay and hence, is subjected to higher waves. The consequences of this are also plotted in Appendix E.2 and it can be stated that (compare the middle three graphs):

- as the wave height increases the dominance of the negative velocity component increases;
- for bays with a positive circulation pattern (yellow line and red line), increasing the wave height results in higher offshore return current velocities;
- for bays with a negative circulation pattern (light blue line and a dark blue line), increasing the wave height results in significantly higher current velocities;
- increasing the wave height yields the same velocity gradients for all bay shapes.

Cross-section 8

Cross-section 8 is situated almost in the centre of the bay. Waves arrive at this location almost unhampered and hence, are higher than in the previous two cross-sections. Considering the lowest three graphs of Appendix E.2, it can be seen that:

- the positive velocity component of the current dominates for wave heights of H_s = 1 m and H_s = 2 m, while for H_s = 3 m, the positive and negative current component quite balance each other;
- for a bay with an indentation I = 360 m (positive circulation pattern, yellow line) and an indentation I = 320 m (low velocity bay, green line), the magnitude of the near shore current velocity is independent of the wave height;

In all graphs of Appendix E.2 it can be seen that the effect of increasing the wave height has most influence on the negative velocity component of the current. Although the positive velocity component does increase with increasing wave height, this increase is just small compared to the increase of the negative velocity component.

6.2.2 Effects on bays with varying a gap width

In this section the results are described of simulations done with bays with a varying gap width, but the same indentation. In the BBB-predictor these bay shapes are located at horizontal lines (I/W is constant). In order to examine the effect of different waves, three types of bay shapes are sub-

jected to significant wave heights of H_s = 1 m, H_s = 2 m and H_s = 3 m. All bays have an overall width W = 660 m and an indentation I = 320 m. Bay 4b has a gap width G = 200 m and a negative circulation pattern. Bay 4c has a gap width G = 300 m and is situated in the low velocity region according to the BBB-predictor. Bay 4d has a gap width G = 400 m and a positive circulation pattern. For information about the bottom slopes, reference is made to Appendix E.1. Again, the longshore current velocities in the three cross-sections 2, 5 and 8 are plotted (see Appendix E.3).

Cross-section 2

With respect to the consequences of a increasing wave height in cross-section 2, the following conclusions can be made (compare upper three graphs in Appendix E.3):

- for a bay with a positive circulation pattern (bay 4b, represented by a red line), increasing the wave height results in higher offshore return current velocities (the near shore current velocity stays more or less the same);
- for bays with a negative circulation pattern (bay 4d, represented by a blue line), increasing the wave height results in significantly higher current velocities;
- increasing the wave height yields larger velocity gradients for all bay shapes;

Cross-section 5

When the middle three graphs of Appendix E.3 are compared, it can be seen that:

- bay 4b (positive circulation pattern) does not have a negative velocity component for wave heights varying from H_s = 1m up to H_s = 3m and the magnitude of the velocity increases with increasing wave height;
- bay 4c (small velocity bay according to BBB-predictor) develops an increasing velocity gradient in the cross-section for increasing wave height;
- bay 4d (negative circulation pattern) does not have a positive velocity component for wave heights varying from H_s = 1m up to H_s = 3m;

Cross-section 8

The results of increasing the wave height on cross-section 8 (which is most exposed to the incoming waves) are plotted in the lower three graphs of Appendix E.3. From these graphs it can be concluded that:

- the increase of the magnitude of the current velocity is not very significant for increasing wave height in all bays;

- bay 4d (negative circulation pattern) does not have a positive velocity component for wave heights varying from H_s = 1m up to H_s = 3m;
- bay 4c (low velocity bay according to the BBB-predictor) develops a negative velocity component which gets closer to the shore as the waves get higher.

6.2.3 Remarks

It can be seen in both Appendix E.2 as Appendix E.3 that the currents are wave-induced, because higher waves yield higher longshore current velocities. This is a consequence of the fact that in the input in the model all other current driving forces are switched off (e.g. the tide, wind).

In general it can be said that a bay develops a positive (from the sides to the centre) or a negative circulation pattern, dependent on its shape. If this distinction is made it can further be said that the height of the waves does not influence this circulation pattern. In other words, if a bay with for instance a wave height of H_s = 1 m develops a positive circulation pattern, it will develop a similar circulation pattern for waves of a different height. The magnitude of the velocity, however, does change. Higher waves yields higher current velocities.

6.3 Sediment transport through the gap

6.3.1 Introduction

Three different situations can be distinguished when dealing with sediment transport in a bay.

1. Morphological changes occur within the bay while no sediment is actually leaving or entering the bay through the gap. Redistribution of the sand in the bay causes a retreat (or advance) of depth contours at a certain place. This retreat (or advance) is undoubtedly accompanied with an advance (or retreat) at another location in the bay, since conservation of mass occurs (no sediment entering or leaving the bay through the gap).

2. Due to a loss (or gain) of sediment through the gap the depth contours within the bay retreat (or advance). In other words, the bay erodes (gets larger) or accretes (gets smaller).

3. It is most likely that a combination of the two above mentioned situations occurs.

Figure 6.3

Triggers the bay shape the sediment transport through the gap?

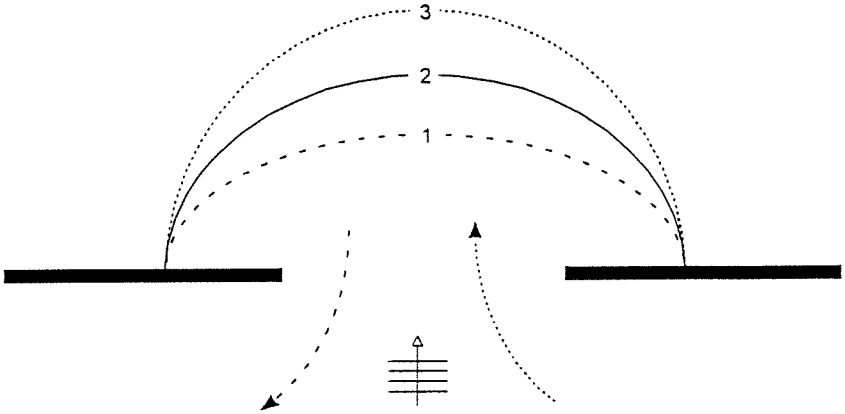

If, under given wave conditions bay nr. 2 in Figure 6.3 is in an equilibrium state, it might be that a bay with an initial shape as bay nr. 1 in Figure 6.3 erodes. Hence, sediment must leave the bay in order to achieve the equilibrium state bay nr. 2. On the other hand, in the case of a bay with an initial shape as bay nr. 3 in Figure 6.3, sediment will probably enter the bay through the gap and the bay will accrete until it reaches the equilibrium shape (bay nr. 2). By examining the sediment transport through the gap, it may be possible to find a relationship between the sediment transport through the gap and the shape of the bay, indicated by for instance its indentation (see Figure 6.4). In this figure the relationship is drawn linear. However, this is still schematic.

Figure 6.4

Sediment transport through the gap

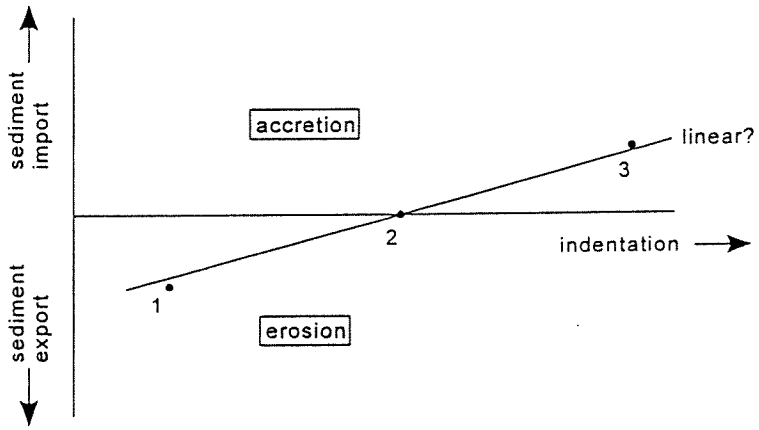

It is mentioned that sediment entering or leaving the bay through the gap is not so logical as it may seem at first sight. Due to continuity the amount of water entering or leaving the bay is zero (no tide). In the case of a positive circulation pattern the flow velocities over the gap show a pattern as shown in Figure 6.5. It can be seen that in the centre of the gap water is actually leaving the bay, while at the sides this loss of water is compensated by an amount of water entering the bay. The suspended sediment shows the same

tendency. However, due to differences in suspended sediment concentrations over the gap width it is possible that sediment leaves or enters the bay. (In the present simulations, however, no importing cases have been found.) Moreover, in the simulations depth averaged velocities have been calculated (2D calculation). And hence, it might be interesting to perform 3D simulations in future.

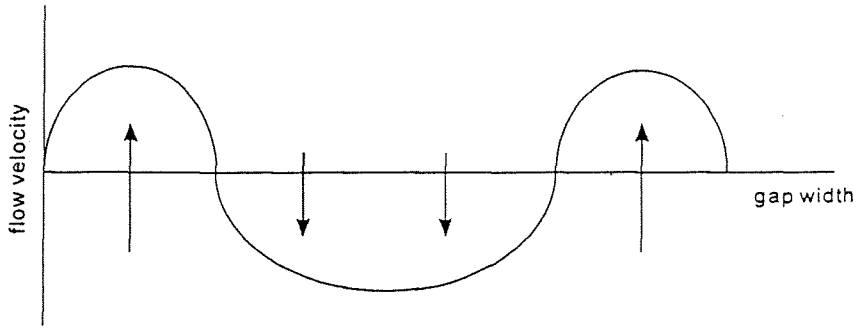

Figure 6.5

Sketch of flow velocity distribution through the gap width

It may very well be possible that higher waves yield bay shapes with larger indentations. If for a given wave condition bay nr. 2 from Figure 6.3 is stable, it may be possible that bay nr. 3 is stable for higher waves. And vice versa, bay nr. 1 may be stable for smaller waves. In order to examine whether this is true or not, the sediment transport through the gap is examined for different wave heights. The executed simulations are described in the next section.

6.3.2 Results of the simulations

In order to check the resulting sediment transport through the gap of a bay, calculations are executed with bays with varying indentation. The bay shapes which are used for these simulations are bay 2c, 4c, 6c and 8c, because in this manner the effect of both a negative circulation pattern (bay 2c) and a positive circulation pattern (bay 6c and 8c) on the import or export of sediment through the gap can be examined. Since bay 4c is a bay with low longshore current velocities according to the BBB-predictor it is interesting to investigate the resulting sediment transport for this bay shape as well. Other dimensions of the bay are summarized in Table 6.1. Both the gap width G as the overall width W are constant.

As it can be seen in Table 6.1 simulations are also executed for bays which have the same horizontal dimensions, but steeper slopes. Since the sediment transport also depends on the near bed current velocity, it is very interesting to examine bays which have smaller depths (6 m instead of 8 m). Due to the orbital motion of the waves, this smaller depth should result in more sediment transport. The eight above mentioned bay shapes are successively subjected to significant waves of H_s = 1 m, H_s = 2 m and H_s = 3 m. The wave steepness is taken to be constant.

nr.	G (m)	W (m)	I (m)	m (-)	n (-)	
2c	300	660	240	22.5	30	*G = gap width*
4c	300	660	320	22.5	40	*W = overall width*
6c	300	660	400	22.5	50	*I = indentation*
8c	300	660	480	22.5	60	*m = slope at sides*
2c*	300	660	240	30	40	*n = slope in centre*
4c*	300	660	320	30	53	*All bays successively subjected to waves:*
6c*	300	660	400	30	67	*Hs = 1 m; Tp = 5 s*
8c*	300	660	480	30	80	*Hs = 2 m; Tp = 7 s*
						Hs = 3 m; Tp = 8.5 s

* *depth in gap is 6 m*

Table 6.1 Bay shape properties

The suspended sediment transport through the gap for the initial bay geometry is computed and plotted in a graph as a function of the indentation. The computed sediment transport is the transport which takes place initially. The results are shown in Figure 6.6. The upper graph shows the results obtained for bays with a depth in the gap (and the area seaward of the breakwaters) of 8 m; the lower graph shows the results obtained with a depth in the gap of 6 m. According to these graphs the following conclusions can be made with respect to a varying wave height (negative values export of suspended sediment transport, positive values indicate import directed suspended sediment transport):

- Higher waves yield higher suspended sediment transport through the gap, independent of the shape of the bay.
- In the case of a depth between the breakwaters of 8 m (upper graph in Figure 6.6) the difference in the suspended sediment transport through the gap between H_s = 2 m and H_s = 1 m is smaller than the difference between H_s = 3 m and H_s = 2 m, independent of the indentation of the bay.
- In the case of a depth between the breakwaters of 6 m (lower graph in Figure 6.6) the difference in the suspended sediment transport through the gap between H_s = 2 m and H_s = 1 m is larger than the difference between H_s = 3 m and H_s = 2 m, independent of the indentation of the bay.
- All bays shapes erode independent of the wave height. Although the sediment export through the gap decreases with increasing indentation, a bay shape with zero sediment transport through the gap is not found. It seems if the erosion rate decreases asymptotically to zero with increasing indentation. An import of sediment is not found.

With respect to a varying depth between the breakwaters (and at sea) it can be stated that:

- a smaller depth in front of the breakwater results in more suspended sediment loses through the gap.

This might be expected due to the fact that the orbital velocities near the bottom are relatively higher and hence, more sediment gets stirred in the breakerzone and transported by these higher velocities.

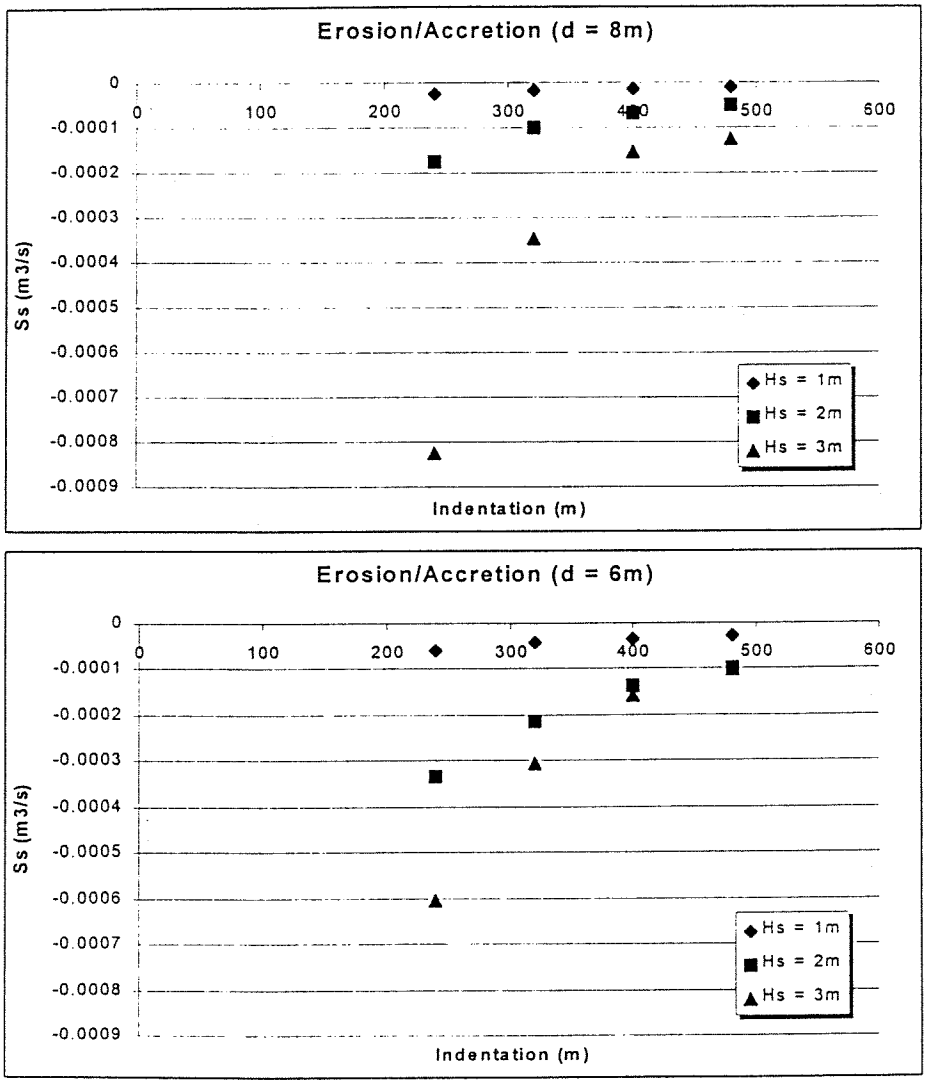

Figure 6.6

Sediment transport through the gap as function of the indentation

It is further mentioned that the annual loses through the gaps in the present simulations are in the order of 10000 m^3 per year. For instance, a transport rate through the gap of 0.0003 m^3/s results in a loss of sand of 0.0003 x 365 x 24 x 3600 = 9500 m^3 per year. Consequently, a bay with a circumference of about 1000 m retreats about 1 m a year (this is a crude approximation).

6.4 Morphological changes

As shown in the previous section no bay shape developed a zero suspended sediment transport through the gap in the initial situation. However, it may be interesting to find out how the bay shapes changes in time as a result of this loss of sediment. It may be that the bay changes in such a manner that after a while the direction of the integrated suspended sediment transport through the gap reverses. Moreover, as describes in Chapter 1, one of the objectives of this study is to investigate the capabilities of the numerical model Delft2D-MOR to predict the evolution of the coastline behind a series of emerged breakwaters. With this respect, simulations are executed with the bay shapes and wave heights mentioned in Table 6.1 for a period of 7 days. It is chosen to simulate for 7 days because calculation time remains relatively short, while the tendency to which the bay wants to develop is clearly visible after a week.

In Appendix E.4 up to Appendix E.15 the results are shown. Results are shown for a bay with a small indentation (2c) and for a bay with a large indentation (8c). Results for intermediate bays are not shown in the appendix, but through interpolation one can get a pretty good image of the behaviour of these bays. In the upper graphs of these appendices the sedimentation and erosion pattern are plotted. The amount of sedimentation and erosion is expressed in meters relative to the initial bottom profile. If, for instance, Appendix E.6 is examined, the upper plot shows that a redistribution of sand occurs: from the centre of the bay to the sides behind the breakwaters. Also, scour holes develop near the breakwater heads. The morphological changes which occur seaward of the breakwater heads are disturbances in the computation. The fact that the results are not perfectly symmetrical is due to the numerical procedure carried out by the model. The propagation of the truncation error in combination with a random rounding off introduces the asymmetrical pattern. For a detailed description, reference is made to Appendix C.

The lower graphs of the appendices shows the retreat or advance of the depth contours after 7 days. The smooth curves lines indicate the depth contours in the initial situation, while the erratic line indicates the depth contours after 7 days. If, again Appendix E.6 is examined, it can be seen that in the centre the depth contours retreat and hence the slope gets steeper. On the other hand, at the side the depth contours advance and therefore the bottom slopes become milder.

After examining all simulations it can be concluded that most bays show the tendency to create milder slopes behind the breakwaters and steeper slopes in the centre of the bay (and thus creating a certain shoal of uniform depth in the middle). This phenomenon will be further discussed in Chapter 7.

6.5 Critical evaluation

The research done so far with respect to the effect of waves is far from complete. Although the wave height is probably one of the most important characteristics when considering the effect of waves on the beach profile, several other parameters are also of interest. The wave steepness is kept constant during the simulations, but it surely effects the morphology. Steep waves tend to break at an earlier stage, while very long waves do not break at all.

Once a stable situation is found for waves arriving perpendicular to the off-shore breakwaters (and gap), it is very interesting to know how waves arriving at a certain angle, effect the bathymetry of the bay. Varying the obliquity of the waves and examining its influence on the morphology of the bay increases the knowledge of bays which are in a dynamic equilibrium rather than in a static equilibrium.

Another aspect which must be investigated in a latter stadium is the effect of a varying wave climate. The alternate effect of storms and calms results in an instationary equilibrium and the retreat of the coast during storm is of great importance.

CHAPTER 7

Empirical Relations

In pursuance of the visit to Delft of J.R.C. Hsu, who has accumulated more than 13 years experience researching into stable bay shapes and its engineering applications, renewed attention was given to existing empirical formulae. Rewriting these formulae lead to the derivation of two geometrical requirements. This different approach may eventually result in a better understanding of the behaviour of symmetrical bays.

7.1 Introduction

Through the years several researchers have examined the equilibrium geometry of crenulate shaped bays. For a long time, a logarithmic spiral has been the only design formula, until recently the possibilities of a parabolic formula have been investigated (Hsu et al, 1987). This new approach is based on empirical relations only and it is suggested to test the parabolic formula with a numerical model. Eventually, this may lead to an implementation of additional parameters in the existing formula and maybe, to an improved formula.

A stable bay consists of three parts: an almost circular section behind the upcoast headland, a logarithmic-spiral curve and a nearly tangential straight beach segment at the downcoast end. The upcoast headland is the point at which diffraction takes place. In static equilibrium bays with a downcoast straight section, the local shoreline is parallel to the incident wave crests. A wave propagating to the downcoast section of an equilibrium bay will shoal and arrive almost normal to the downcoast beach and break. A wave at the upcoast section will first diffract and then refract as it propagates across the lee zone toward the beach; it will also arrive at the beach at almost right angles and break at the same time as the wave in the downcoast segment. Thus, breaking will occur simultaneously in static equilibrium bays (see also Figure 7.1 and Silvester and Ho, 1972). This, in turn, would mean no longshore component of breaking wave energy and hence no littoral drift within the embayment. At present, bays in dynamic

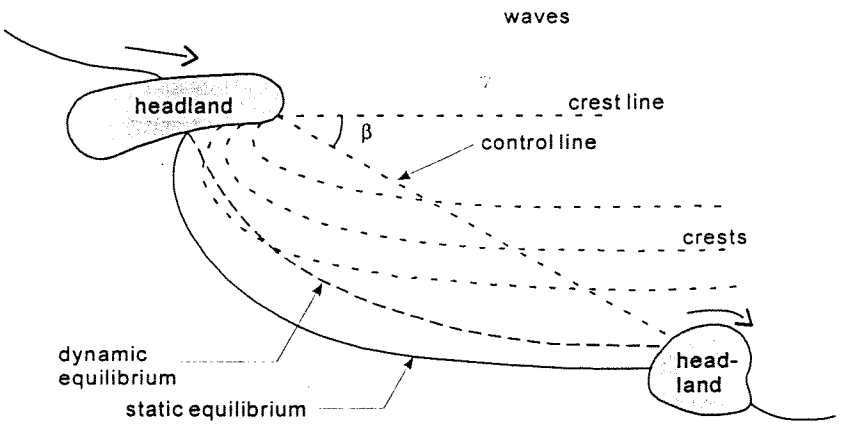

Figure 7.1

Static and dynamic equilibrium beach lines in bays

(Van Rijn, 1998)

equilibrium can not be predicted, mainly because the littoral drift that is still occurring is difficult to assess. However, if the upcoast supply of material is cut off the bay will become more indented until littoral drift ceases. The plan shape is then in static equilibrium and it is for this condition that it can be related to the wave obliquity. At this stage all waves arrive normal to the beach. Obliquity is measured by the angle of wave crests at the upcoast headland to a control line joining the point of diffraction with the downcoast limit of the bay. This is the same angle as between the control line and the downcoast tangent to the bay. Two empirical equations have been proposed in deriving bay shaped beaches in the past 30 years, these being referred to as logarithmic spiral and parabolic bay shape.

7.2 *Logarithmic spiral bay shape*

The logarithmic spiral has been applied extensively by geographers and coastal engineers alike since its introduction. Several natural headland bay beaches were investigated by Yasso (1965) and they approximated the same form. A definition sketch of such spirals is given in Figure 7.2 (left) of which the equation is:

$$\frac{R_2}{R_1} = \exp(\theta \cot \alpha) \qquad \text{Equation 7.1}$$

where θ is the angle (°) between radii R_2 (m) and R_1 (m) (where $R_2 > R_1$) and α is the constant angle (°) between either radius and its tangent to the curve. A disadvantage of the log spiral is that the spiral applies only to the curved section of the beach in the shadow zone of the upcoast headland, and its centre does not match the point at which diffraction takes place. It is mentioned that bays can have this crenulate shape even before stability is reached and hence are sometimes (wrongly) assumed to be in equilibrium.

Figure 7.2

Definition sketch of logarithmic spiral (left) and comparison with actual bays (right)

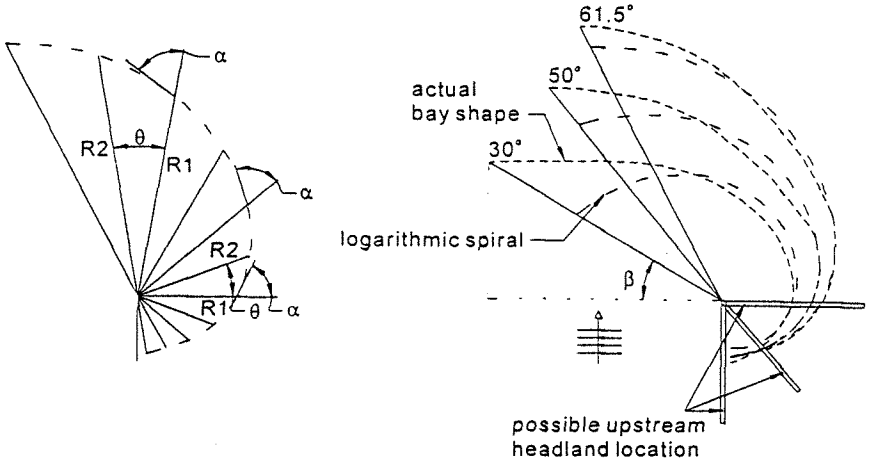

For this reason, and maybe others, it was difficult for engineers to apply this criterion of stability. It was found later (Hsu et al. 1987) that the spirals did not apply to the downcoast periphery of the bays if their centres are fixed at the upcoast control point, at which diffraction takes place (see Figure 7.2, right). This difference is accentuated more for smaller values of β, which usually apply.

7.3 *Parabolic bay shape*

The term parabolic was first mentioned by Mashima (1961). He derived a parabola. An expression for this parabola is given in Equation 7.2:

$$y = px^2 - b \qquad \text{Equation 7.2}$$

where p is a coefficient, b is the maximum indentation (m) and y and x are coordinates in an orthogonal coordinate system (m) as seen in Figure 7.3. The bay shape can be constructed with a parabolic part (BD) and a straight part (AD). The most indented part of the bay (b) can be found at the cross-section of the parabola with the y-axis. Point D is the intersection between the parabola and a line drawn perpendicular to the x-axis through C, which is the midpoint of the line between the upcoast (B) and the downcoast (A) limitation of the bay. There were complications however, such as centering the parabola for any particular bay, not taking diffraction into account, nor the wave obliquity. Only the curved waterlines were shown and not the headlands, nor their points of diffraction upcoast. Reanalysis of model data, together with those from prototype bays known to be in static equilibrium from sediment source conditions, suggested a new approach (Hsu et al. 1987). This is illustrated in Figure 7.4, where radii (R) are drawn from the point of diffraction to the beach at angle θ to the wave-crest line. One such

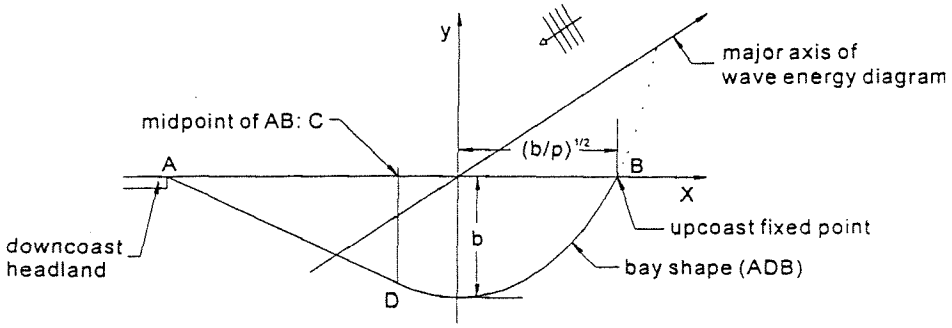

Figure 7.3

Coordinates of a parabola defined by Mashima (1961)

radius is R_0 or the control line at angle β to the same wave-crest line. For a bay in static equilibrium this angle is the same between R_0 and the tangent to the downcoast beach line. Even though the bay may not be completely stable, this tangent alignment is likely to be reached prior to the bay eroding back to its limiting shape (Silvester and Ho, 1972). The subsequent erosion takes place at the deepest indentation zone (Everts, 1983). It is

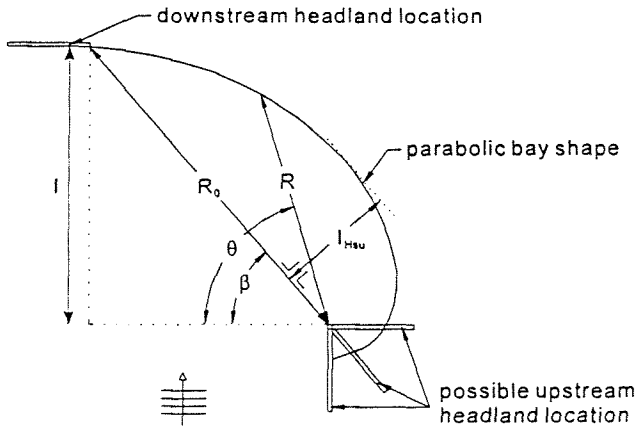

Figure 7.4

Definition sketch of a parabolic bay shape

(Hsu et al, 1987)

emphasized here that Hsu's definition of the indentation differs from the definition used in this report. Hsu defines the indentation as the maximum distance between the control line and the coastline. The 'I' used to define equilibrium bays in this report is the component of R_0 directed parallel to the direction of wave propagation (or $I = R_0 \sin \beta$). Moreover, the indentation 'I' cuts the coastline at the location where the shore becomes directed perpendicular to the incoming wave direction. This is because in this report the behaviour of symmetrical bays is investigated and now 'I' coincides with the symmetry axis of the bay. Mirroring in this axis yields the whole bay pheriphery.

For engineering applications, nondimensional parameters are preferred. The value of R (m) at any angle θ (°) has to be normalized by taking its

ratio to R_0 (m). For specific angles θ, log (R/R_0) was then plotted against logβ which resulted in a series of nearly parallel straight lines. This enabled θ to be plotted against R/R_0 for constant values of β (°) and the values to be smoothed. This then gave an equation (Hsu et al, 1987; Silvester and Hsu, 1997):

$$\frac{R}{R_0} = \frac{0.81\beta^{0.83}}{\theta^{0.77}} \qquad \text{Equation 7.3}$$

This formula predicts the shape of a bay very closely for $\theta = 45°$ to $90°$. But for $\theta = 120°$ to $180°$ the accuracy is less. It is likely that the prototype bays in this zone may differ slightly from the predicted stable condition (i.e., be more seaward than the predicted stable condition) because the removal of material in these areas is very slow due to the small height of waves in this greatly diffracted condition. Storm waves oblique to the bayed shoreline may transport material into the leeward area which may not spread evenly to the correct stable shape readily. In other words, close to the breakwater (in the shadow zone) the predicted bay shapes differ from the observed bay shapes, but the other parts of the waterline are predicted very well with Equation 7.3.

In order to predict the complete periphery in an accurate manner, Hsu and Evans (1989) derived a polynomial of the form:

$$\frac{R}{R_0} = C_0 + C_1\left(\frac{\beta}{\theta}\right) + C_2\left(\frac{\beta}{\theta}\right)^2 \qquad \text{Equation 7.4}$$

Although this formula represents the actual bay shape more accurate, it also introduces three coefficients which vary uniformly with β. This makes this formula less suitable for numerical computation, since the generation of a lot of different bay bathymetries (necessary for the simulations) is much more complicated. Since the elliptical approach initiated by Blankers (1999) shows the same deviation close to the breakwaters (no seaward curvature close to the breakwaters), Equation 7.3 is used to describe the shape of a bay in static equilibrium. However, in Section 7.4.2 Equation 7.4 will be examined in more detail. The consequences of choosing Equation 7.3 instead of Equation 7.4 to describe the shape of a stable bay are pointed out.

7.4 Geometrical requirements

7.4.1 Analysing the logarithmic spiral

The simulations shown so far are executed with (probably) unstable geometries. These geometries are generated by Blankers' method and seem to satisfy Hsu's formula. However, Blankers approached only one stable geometry with ellipticals (Blankers, 1999). He then stretched this geometry (by increasing or decreasing the indentation and/or the gap width). The result is that these bay shapes do not satisfy the empirical formulae any longer. Hsu's visit to the Delft University of Technology in April 1999 inspired to re-investigate the bay geometries. Therefore, a closer look is taken at Equation 7.3.

Rewriting this equation in a different form yields:

$$R \cdot \theta^{0.77} = R_0 \cdot 0.81 \cdot \beta^{0.83} \qquad \text{Equation 7.5}$$

In order to determine the point of maximum indentation (and hence the symmetry-axis of the bay), the component of R parallel to the propagation direction of the waves is examined. This component is defined as:

$$R_e = R \cdot \sin\theta \qquad \text{Equation 7.6}$$

Substituting Equation 7.6 in Equation 7.5 and rewriting the latter in a different form yields:

$$R_e = \frac{R_0 \cdot 0.81 \cdot \beta^{0.83} \cdot \sin\theta}{\theta^{0.77}} \qquad \text{Equation 7.7}$$

or expressing the θ value in the sine function in radians:

$$R_e = \frac{R_0 \cdot 0.81 \cdot \beta^{0.83} \cdot \sin\left(\frac{\theta \cdot \pi}{180}\right)}{\theta^{0.77}} \qquad \text{Equation 7.8}$$

The location where the coastline is perpendicular to the incoming wave crests coincides with a local maximum (or minimum) of Equation 7.8 and this is determined by the first derivative:

$$\frac{dR_e}{d\theta} = \frac{\theta^{0.77} \cdot R_0 \cdot 0.81 \cdot \beta^{0.83} \cdot \frac{\pi}{180} \cdot \left(\cos\frac{\theta\pi}{180}\right)}{\theta^{1.54}}$$

$$- \frac{\left\{R_0 0.81 \beta^{0.83}\left(\sin\frac{\theta\pi}{180}\right) 0.77\theta^{-0.23}\right\}}{\theta^{1.54}} \qquad \text{Equation 7.9}$$

This derivative should have a value of zero. This is only true when the numerator is zero and the denominator is non-zero (which is always the case). The consequence is that both R_0 as β are eliminated and hence, the angle between the wave crests and the line joining the breakwaterhead and the point of maximum indentation (or the point where the coast becomes parallel to the incoming wave crests) is constant (and independent of the incoming wave direction)!

$$\left\{\theta^{0.77} \cdot \frac{\pi}{180} \cdot \left(\cos\frac{\theta \cdot \pi}{180}\right)\right\} - \left\{\left(\sin\frac{\theta \cdot \pi}{180}\right) \cdot 0.77 \cdot \theta^{-0.23}\right\} = 0 \qquad \text{Eq. 7.10}$$

Solving Equation 7.10 iteratively yields:

$$\theta = 46.5^o \qquad \text{Equation 7.11}$$

Taking the tangens of this angle finally yields:

$$\tan 46.5^o = \frac{I}{(G/2)} = 1.054 \qquad \text{Equation 7.12}$$

A first geometrical requirement is now analytically proven, and reads:

$$I = 0.53 \cdot G \approx \frac{1}{2}G \qquad \text{Equation 7.13}$$

The approximation of the coefficient by 0.5 significantly simplifies one thing and another. The error of 5% which is introduced by this approximation is quite acceptable.

Besides the indentation of a symmetrical bay, the shadow zone directly behind the breakwater is also an important parameter which defines the geometry of a bay. This shadow zone (k) can be defined as:

$$k = \frac{W - G}{2}$$ Equation 7.14

This distance can be expressed in terms of R, because k equals R when θ = 180°. It is already shown that the line joining the tip of the breakwater and the downcoast (soft) control point (the control line R_o) has a constant angle (β = 46.5°). At the control point the coastline is perpendicular to the incoming wave crests (and R_e is maximum) and I is defined there. Substituting all this in Equation 7.3:

$$\frac{R_{\theta = 180^0}}{R_0} = \frac{0.81 \cdot 46.5^{0.83}}{180^{0.77}} = 0.36$$ Equation 7.15

$$\frac{k \cdot \sin(46.5^0)}{R_{e,max}} = \frac{k \cdot \sin(46.5^0)}{I} = 0.36$$ Equation 7.16

The latter formula yields:

$$\frac{k}{I} = 0.496 \approx 0.5$$ Equation 7.17

Again, the approximation introduces a minor error which is acceptable. A second geometrical requirement is now analytically proven. Summarizing:

Geometrical requirement I: $I = \frac{1}{2}G$

Geometrical requirement II: $\frac{I}{W} + \frac{G}{W} = 1$

According to this reanalysis of this empirical formula (Equation 7.3), a symmetrical bay geometry is completely determined as soon as one of the parameters G, W, or I is (randomly) chosen. For instance, if the gap width is chosen G, then the indentation I = 0.5G and the overall width W = 1.5G. The difference in approach between the method described in Silvester and Hsu (1993, 1997) and the method described in this report is that the former approximates the location of the control point (the point on the coast which determines the control line) by determining the position where the coastline becomes straight (and then determines the direction at which the deepwater waves approach the shore), while the latter assumes that the direction of wave propagation is known. It is obvious that the latter has more practical purposes.

Further, these requirements define a gap-width ratio (G/W) of 0.67 and a indentation-width ratio (I/W) of 0.33. In the SBB-predictors in Chapter 5,

this combination of both ratios is visualized as a black dot. Unfortunately, this dot does not coincide with the lowest suspended longshore transport. But one must keep in mind that the bottom slopes are not defined in Hsu's formula, nor bottom material or wave heights.

7.4.2 An evaluation on the parabolic bay shape

The parabolic formula as derived by Hsu and Evans (1989) is given in Equation 7.4. The same derivation as used to derive the geometrical requirements from the logarithmic spiral can be applied to the parabolic formula. This means that an expression has to be found which determines the location where the coast becomes parallel to the incoming wave crests. Again, the radius R is expressed in terms of R_e, which is the component of R directed parallel to the wave propagation direction:

$$R_e = R \cdot \sin\theta \qquad \text{Equation 7.18}$$

The location where the coastline is parallel to the incoming wave crests coincides with a local maximum (or minimum) of Equation 7.4. This maximum (or minimum) is determined by the first derivative with respect to θ. After substituting Equation 7.18 into Equation 7.4 this yields:

$$\frac{dR_e}{d\theta} = R_0 \sin\theta \cdot \left(-\frac{C_1\beta}{\theta^2} - \frac{2C_2\beta^2}{\theta^3} \right) +$$

$$R_0 \cos\theta \cdot \left\{ C_0 + C_1\left(\frac{\beta}{\theta}\right) + C_2\left(\frac{\beta}{\theta}\right)^2 \right\} \qquad \text{Equation 7.19}$$

In order to find the maximum this derivative should have a value of zero. The consequence is that R_0 is eliminated. However, due to the presence of the dimensionless coefficients (which are a function of β) both β and θ remain in the equation. As a result, the location where the coast becomes parallel to the incoming wave crests is a function of the angle β, which can be chosen at random.

Further analysis can only be done numerically, since analytical expressions which describe the relations between the coefficients C_0, C_1, C_2 and β are not yet known. In order to do so, some important parameters are defined as illustrated in Figure 7.5. The control line R_0 and the control angle β define the position of the downcoast headland. These parameters can be chosen randomly, but once chosen they become constants. With the aid of Equation 7.4 it is now possible to determine the shape of the coastline, for a range of randomly chosen combinations of R_0 and β. Since this report deals with symmetrical bay shapes, the location where the coast becomes parallel

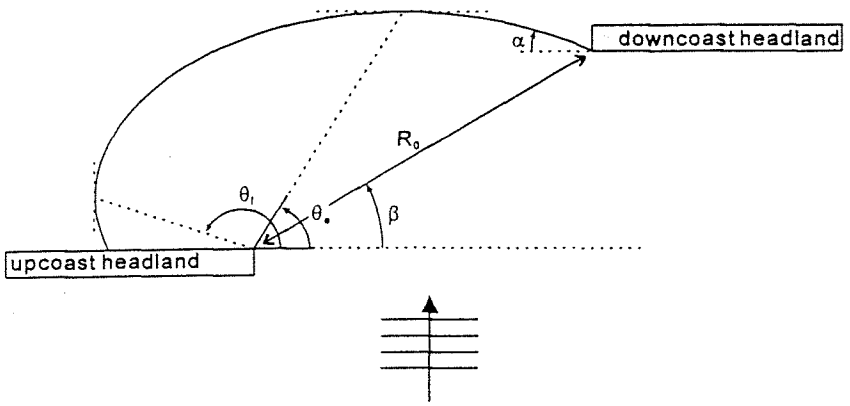

Figure 7.5

Parameter definitions

to the incoming wave crests is of interest. Therefore, the angle between this location and the wave crests is defined as θ_e. The angle α defines the curvature of the coastline at the tip of the downcoast breakwater. Other parameters are the indentation (I), the width directly behind the breakwaters (W) and the gap width (G). The results of the calculations are shown in Table 7.1.

R_0	β	θ_e	$\lvert\theta_e-\beta\rvert$	α	I/G	I/W	G/W
100	20	36	16	1.56	0.36	0.27	0.75
	30	42	12	2.37	0.45	0.32	0.71
	40	49	9	3.17	0.57	0.38	0.67
	50	56	6	3.31	0.74	0.46	0.62
	60	63	3	1.61	0.98	0.56	0.57
	70	68	2	-2.28	1.24	0.65	0.52
	80	70	10	-8.98	1.37	0.72	0.53
	64	65	1	0.54	1.07	0.60	0.56
	66	*66*	*0*	*0*	*1.12*	*0.61*	*0.54*
200	20	36	16	1.56	0.36	0.27	0.75
	30	42	12	2.37	0.45	0.32	0.71
	40	49	9	3.17	0.57	0.38	0.67
	66	*66*	*0*	*0*	*1.12*	*0.61*	*0.54*
300	20	36	16	1.56	0.36	0.27	0.75
	30	42	12	2.37	0.45	0.32	0.71
	40	49	9	3.17	0.57	0.38	0.67
	66	*66*	*0*	*0*	*1.12*	*0.61*	*0.54*

Table 7.1 Results of calculations using the parabolic formula

In Figure 7.6 the absolute value of the difference between θ_e and β is plotted as a function of the control angle β. It can be seen that for $\beta = 66^o$ the coastline becomes parallel to the wave crest for the same value of θ_e. For values of $\beta < 66^o$ the coastline intersects the downcoast headland with a positive curvature ($\alpha > 0$, measured clockwise as shown in Figure 7.5). And

Figure 7.6

Angle between the control line and the line connecting the upcoast headland and the location where the coast becomes parallel to the incoming wave crests.

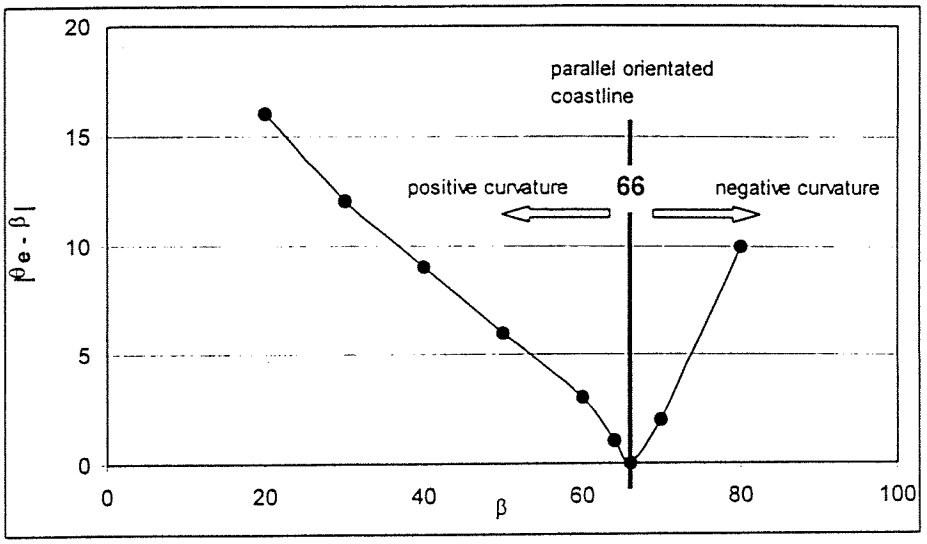

For values of $\beta < 66^o$ the coastline intersects the downcoast headland with a negative curvature ($\alpha < 0$). This graph is independent of the length of the control line R_0, as already shown analytically. As it can be seen in Figure 7.7, the angle at which the coastline intersects the downcoast headland has a positive maximum of $\alpha = 3.4^o$. It then decreases gradually as β increases until the coastline intersects the downcoast headland parallel to the wave crests. Increasing β even more yields a rapid decrease of α. The conse-

Figure 7.7

Orientation of the coastline at the downcoast headland

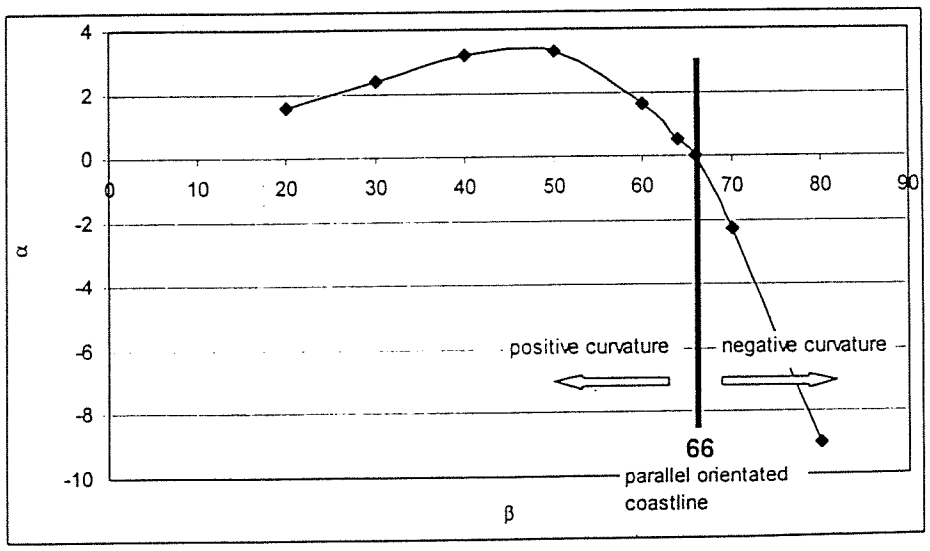

quences of these results can be made clear if the dimensionless parameters I/G, I/W and G/W are considered (see Table 7.1). These parameters remain constant as long as β remains constant and hence, the length of the control line R_0 acts as a scaling factor; by changing this length, congruent bay shapes develop of different sizes. However, as R_0 remains constant and the control angle β increases, both the indentation-gap ratio (I/G) and the indentation-width ratio (I/) increase while the gap-width ratio (G/W)

decreases. In other words, increasing β yields a relatively deeper bay with a smaller gap with respect to the bay width.

The logarithmic spiral describes the shape of a bay in static equilibrium and hence, no longshore sediment transport is present. Therefore, the angle α must be zero which is not the case according to Table 7.1 (except when the control angle $\beta = 66^{o}$). However, the angle α is relatively small and the orientation of the coastline at the tip of the downcoast headland is more or less parallel to the incoming wave crests. As a result, when using the logarithmic spiral the geometrical requirements are not valid; bays can develop with random sizes dependent on the location of the upcoast and downcoast headland.

According to the analysis described in this Section it can be concluded that one must be careful when applying the geometrical requirements as derived in Section 7.4.1. These requirements are solely based on the logarithmic spiral and as such are limited in their use. Apparently, bays can also have shapes which are different as defined by the geometrical requirements. However, the logarithmic spiral does predict the coastline accurately in the centre of the bay and it provides a quick and easy manner to draw a draft version of the shape of the bay.

7.4.3 Graphical interpretation

It is mentioned that if the angle at which the incoming waves approach the breakwater changes, the geometrical requirements as derived in Section 7.4.1 can still be applied when using the logarithmic spiral. The angle between the incoming wave crests and the line joining the tip of the breakwater and the location where the coast becomes parallel to these wave crests remains about 45^{o}. This makes it possible to construct a bay shape as shown in Figure 7.8. Assuming that the position of the breakwaters and the direction from which the waves approach the breakwaters is known, the graphical procedure is as follows:

- draw a line which intersects point A and is directed parallel to the incoming wave crests;
- draw another line, sufficiently long, which intersects point A, but now under an angle of 45^{o} with the previous line;
- draw a line which intersects point B and is directed parallel to the incoming wave crests;
- draw another line, sufficiently long, which intersects point B, but now under an angle of 45^{o} with the previous line. Point C is now determined. This is the location where the orientation of the coast becomes parallel to the incoming wave crests. The value of R_0 is to be determined;

- extend line DB with half its length to determine the location where the coastline intersects the downcoast breakwater;
- extent line EA with half its length to determine the location where the coastline intersects the upcoast breakwater;
- draw the curves between points C and F and between C and G.

Figure 7.8

Geometrical requirements (oblique approaching waves)

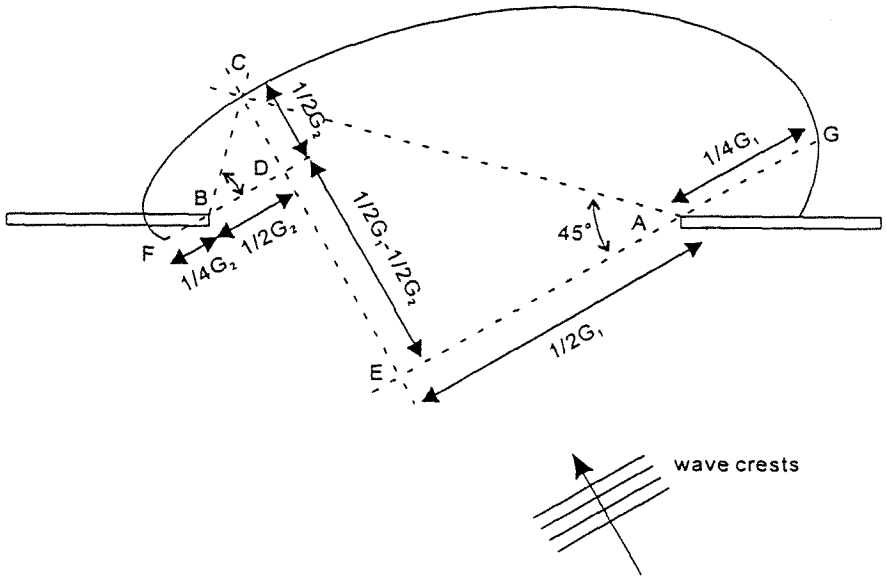

Since both G_1 and G_2 are components of the gap width between the two offshore breakwaters, they can be calculated once the direction of wave propagation is known. It is mentioned that the above described graphical procedure is speculative and that no numerical simulations are done to verify whether the obtained bay shapes are stable. However, it might be interesting to do so in future.

Critical note

The geometrical requirements are derived via adapting an empirical formula to symmetrical bay shapes. These requirements describe congruent bay shapes. In other words, if the wave climate changes, the indentation (I) as well as the gap width (G) as the overall width (W) should change. However, in most situations the gap width is fixed (e.g. by offshore breakwaters) and it remains questionable what the natural response of the bay might be to a change in wave climate when the gap width is fixed. It is very well possible that the indentation and the overall width change. Hence, the geometrical requirements do not apply any longer. This might explain why there are also bays present in nature which do not satisfy the geometrical requirements. Further research is necessary on this topic.

7.4.4 *Executed simulations*

Simulations are executed with a bay shape which satisfies the geometrical requirements. Since the size of the (congruent) bay shape may depend (among other things) on the wave height, simulations are executed with varying wave height. The waves entering the bay vary from 0.5 m to 2 m, with steps of 0.5 m. The horizontal dimensions of the bay are as follows: it has a gap width G = 600 m, resulting in an indentation I = 300 m and a overall width W = 900 m. The depth at the seaward side of the breakwaters is 8 m.

In Appendix E.16 the average suspended sediment transport in the initial situation is plotted for the wave heights mentioned above. It can be seen in these plots that for wave heights up to H_s = 1 m no suspended sediment is actually leaving the bay through the gap. But wave heights higher than H_s = 1 m result in a initial loss of sediment through the gap. In order to examine especially the redistribution of sand within the bay (and thus almost no sediment should leave or enter the bay through the gap), a simulation run of 30 days is done for a significant wave height H_s = 1 m. A period of 30 days is chosen because the results get less reliable after 30 days (the fact that cross-shore transport is not accounted for might be a reason). As can be seen in the upper graph of Appendix E.17, sedimentation occurs in the centre of the bay after a simulation period of one week. The bottom material gets stirred in the breaker zone by the waves and is being transported in suspension by the offshore current in the centre of the bay. As the flow velocities decrease, the suspended sediment settles and the depth contour advance in seaward direction. However, if the lower graph of Appendix E.17 is examined, it can be seen that after 30 days the bathymetry has almost restored itself to the original situation. Moreover, the flow velocities have significantly decreased in magnitude and the offshore rip-current in the centre of the bay has disappeared. This result is quite promising and it might be that this bay shape is stable in the long run. However, it must be kept in mind that the depth contours are still based on elliptical shapes and that the cross-shore profile is linear (in nature a concave profile is more common). Therefore, a more detailed research is done after the cross-shore profile of the bay. Moreover, simulations executed with different wave height show also show the tendency to restore the bathymetry to the initial situation after a certain simulation time. Apparently, the model needs some time to reach a more or less stationary situation and in future further research may indicate whether or not this assumption is correct.

7.5 Bottom topography

7.5.1 Grain size variations

In nature, longshore variations of sediment shape, size, density and composition have been observed along many crenulate shaped beaches. The factors leading to longshore sorting/grading of sediment can be described as:

- shoreline configuration: the presence of cliffs and headlands;
- the presence of heterogeneous sediments in abundant quantities: each fraction of sediment may follow its own transport pathway (the coarsest and the most dense grains are the least mobile;
- longshore gradients in wave energy: the coarsest sand grains tend to accumulate in the zones of greatest energy; even under nearly normal wave attack there may be longshore drifting from regions of higher breakers and higher set-up to regions of lower breaker and lower set-up depending on the degree of wave exposure and profile steepness;
- a variable wave climate causing alternating longshore currents throughout the year;
- longshore gradients in topography (profile shape and bottom slope) and wave exposure: in an embayment the most exposed section generally is steepest and contains the coarsest sediment;
- mechanical and chemical disintegration of sediment material.

Beaches between headlands and rocky or bouldery shore protrusions often show longshore grading with poorly sorted sand and gravel on the more sheltered section (behind the breakwaters) and better sorted coarser gravel/ shingle on the more exposed section (in the centre of a bay). This is a result of the phenomenon that the higher waves in the exposed section transport the coarser material (and the smaller as well), while the lower waves are only able to transport the smaller material. Moreover, coarser material yields steeper bottom slopes than smaller material. This explains why in the centre of the bay the bottom should be modelled steeper than at the sides behind the breakwaters.

7.5.2 Overall layout

If the consequences of the geometrical requirements based on the logarithmic spiral are combined with the bottom slope information resulting from grain size variations, it can be found that the bottom topography should change considerably. According to the geometrical requirements, equilibrium bays are much wider than the bays used so far in the simulations (see

Figure 7.7). Due to grain size variations in nature the bottom slope in the centre of the bay is probably steeper than the slope behind the breakwaters. This is a major difference compared to the previous used bathymetries in which the opposite is the case: the slope in the centre is flatter than the slope at the sides of the bay. Most simulations so far show erosion patterns in the centre of the bay and sedimentation behind the breakwaters. This confirms the idea that the bathymetry should change. Another aspect which immediately draws attention is the shoal in the centre of the bay. Higher waves are now able to approach the shore and effect the shape of the bay.

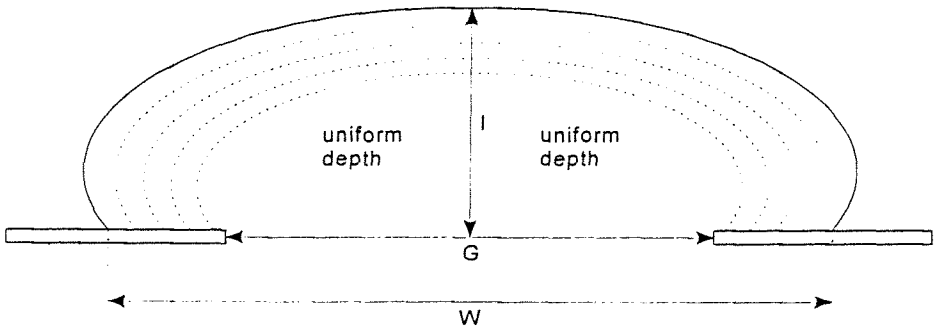

Figure 7.9

New topography

7.5.3 *Equilibrium cross-shore profile*

Ideally, an equilibrium profile represents a bed profile generated under constant wave energy conditions with a constant water level in the absence of longshore transport gradients for such a long time that a stable profile is obtained. Basically, the cross-shore profile is described by the sediment continuity equation, as follows (neglecting longshore transport gradients):

$$\frac{\Delta z_b}{\Delta t} + \frac{\Delta q_t}{\Delta y} = 0 \qquad \text{Equation 7.20}$$

in which z_b is the bed level to datum expressed in meters, q_t the net cross-shore sand transport (bedload plus suspended load transport) expressed in m^2/s, y the cross-shore coordinate (m) and t is the time (s). Equilibrium conditions implies that the spatial gradient of the cross-shore transport is zero everywhere along the profile (constant profile). Contrary to the profile used in the simulations, equilibrium profiles generally show a concave upward profile, which can be explained by the fact that the onshore wave-induced forces on a sand grain increase in landward direction and that this onshore-directed force can only be balanced by an equivalent landward increase in the downslope component of gravity, requiring steeper slopes in landward direction. The cross-shore profiles used in this study exhibit a monotonically sloping bed surface.

However, the cross-shore transport due to wave-asymmetry is not modelled in the Delft2D-MOR version used for this study. The cross-shore sediment

transport which occurs as observed in the simulations is the result of the settling of suspended sediment which is transported offshore with the offshore currents. As the flow velocity decreases, more sediment settles. Moreover, in the present version of the model, variations in bottom material are not taken into account. The model uses a constant grain size all over the modelled area. This introduces a problem, because the difference in slopes between the centre and the sides is probably determined by differences in grain size. The reason why both phenomena are mentioned here is because it indicates that the used bathymetry in the simulations should be changed into a more concave profile with steeper slopes in the centre and milder slopes at the sides. This kind of bathymetries are more likely to be found in nature. Future simulations should indicate whether the proposed bay bathymetry better coincides with stable bay shapes.

7.6 Summary

Validation of bay shapes developed by Blankers (1999) with the logarithmic spiral showed that only few bays satisfied the geometrical requirements resulting from this formula. Re-writing the logarithmic spiral resulted in two geometrical requirements which describe the shape of the bay in a simplified manner:

- $I = \frac{1}{2}G$
- $\frac{I}{W} + \frac{G}{W} = 1$

in which I is the indentation (m), G is the gap width (m) and W is the overall width of the bay just behind the breakwaters (m). A graphical interpretation of the geometrical requirements is given in the case of oblique approaching waves (resulting in asymmetrical bay shapes). Simulations with symmetrical bay shapes satisfying these geometrical requirements showed promising results, especially for H_s = 1m. Although initially sedimentation occurs in the centre of the bay, the bathymetry restores itself and a more or less stable situation is present after 30 days.

The next step was to combine the geometrical requirements with the bottom slope information resulting from grain size variations. This resulted in bay shapes with steeper slopes in the centre and milder slopes at the sides. Further research into these shapes is necessary to verify whether these proposed shapes are stable.

CHAPTER 8

Discussion

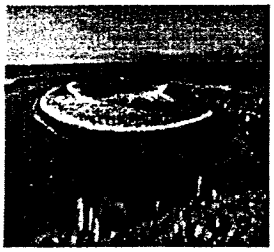

In this chapter the most important conclusions and recommendations are described. Since this report is the second report in a series of probably three, further research will follow and therefore, this report must be seen as a part of a bigger picture. Advantages and disadvantages encountered as a result of taking over somebody else his work are described in the critical note, for they highly influenced the research done by the author.

8.1 Critical note

The phenomena taking place in a bay are complex due to an excessive interaction between diffraction, refraction, wave set-up and set-down and wave-current interaction. Due to a lack of knowledge and field data it is difficult to correctly model and validate the processes taking place in a bay. Conclusions presented are therefore mostly qualitative and further research is necessary.

Continuing somebody else his research has the main advantage of the possibility of making a flying start. Especially when working with numerical models earlier research enables it to reap the fruits of the modelling work of the predecessor. Most problems concerning the modelling of bays have already been overcome and moreover, when starting this research the assumption is made that simulations could be executed without adapting the numerical parameters of the model.

However, some disadvantages have been encountered as well. Minor errors introduced into the model in a former phase of the project may influence the present outcome as well, without the full awareness of the cause and/or location of the problem. This may sometimes slow down the research, because it is necessary to gain detailed insight into the build up of the model.

8.2 Conclusions

The aim of this research is on the one hand to investigate the capabilities of the numerical model Delft2D-MOR to predict the coastline evolution behind a series of emerged breakwaters and on the other hand to increase our understanding of the hydraulic and morphological behaviour of bays in order to make deliberate decisions about the application of headland control in future. In this thesis simulations are executed which clearly show the applicability of the model Delft2D-MOR to compute complex situations such as bays. Some shortcomings are found, but there are manners to overcome these problems. Although field data is not present, qualitative statements can be made and the knowledge of the behaviour of bays has definitely increased. However, further research is necessary since initial full equilibrium has yet not been found and a relation between wave conditions and the equilibrium shape of a bay still has to be determined. Moreover, more processes such as a varying wave climate, the tide and longshore sediment transport must be added to the model and their influence still has to be investigated.

The following conclusions can be drawn regarding the applicability of the numerical model Delft2D-MOR to predict the coastline evolution behind a series of emerged breakwaters:

- Flow field, wave field and sediment transport calculations are very well possible and, although calibration with field data is not possible, hand calculations show that the obtained results are satisfying.
- Diffraction is not taken into account in the wave module. This is an important limitation because the diffraction process is one of the main creating forces of equilibrium bays. However, the effect of diffraction can be simulated by a coefficient for the directional spreading. Tests executed by Ahmed (1997) show that the wave pattern around offshore breakwaters shows little deviation from a specialised diffraction model (DIFFRAC) if the value for the coefficient of directional spreading is set to 4. Differences at greater distance from the breakwaters appear to be small, while the greatest errors are expected in the shadow zone just around the head of the breakwaters. Here, the wave module HISWA will probably predict a wave height of zero, which will not occur in practice.
- Since the position of the waterline is fixed in the present release of Delft2D-MOR it is impossible to compute the development of an equilibrium bay via a long simulation run. Simulations executed show that for simulations longer than approximately 30 days the depth gradients near an erosive shore get too large and hence, the results are not reliable. Adapting the bathymetry of the bay and executing a new simulation overcomes this problem.

- Due to the discretization of nature (which is always necessary when working with numerical models) and the used numerical procedure, an asymmetric propagation of the truncation error is introduced, resulting in asymmetric results. However, this truncation error is very small. Moreover, it is likely that other numerical models have the same problem.
- The transport module used in the research described in this report does not take the cross-shore transport into account. This routine is not yet installed at the computer of the Hydraulic Engineering Group. However, by the time this report was nearly finished, newer versions of the transport module were installed and further research should therefore be done with the cross-shore transport routine switched on.
- Sedimentation and erosion patterns can be visualised in a clear way and movies showing the morphological development in time elucidate the erosion/sedimentation process significantly.

Regarding the hydraulic and morphological behaviour of bays the following conclusions can be made:

- The suspended sediment transport in the breaker zone is much higher than the bed load transport in the breaker zone and hence, the latter may be neglected if the sediment transport in the breaker zone is examined.
- The generated currents are wave-induced. As a result the direction of the large scale circulation patterns in a bay (positive or negative circulation pattern) are not influenced by the wave height. However, the current velocities increase with increasing wave height.
- Decreasing the gap width results in smaller longshore velocities.
- The SBB-predictors show the same tendency as the BBB-predictor and hence, a strong correlation is present between the longshore velocities and the longshore suspended sediment transport. The location of bays satisfying the logarithmic spiral in the predictors triggered a more detailed research after the shape of equilibrium bays.
- Re-writing the logarithmic spiral resulted in two geometrical requirements which describe the shape of the bay in a simplified manner:

$$I = \frac{1}{2}G$$

$$\frac{I}{W} + \frac{G}{W} = 1$$

in which I is the indentation (m), G is the gap width (m) and W is the overall width of the bay just behind the breakwaters (m).

- Simulations executed with H_s = 1 m, T_p = 5 s and with bays satisfying the geometrical requirements showed promising results. Although the bay shape changed initially, it restored itself to the original shape after approximately 30 days. Moreover, current velocities significantly decreased after this period.
- Combining bottom slope information resulting from grain size variations with the geometrical requirements results in bay shapes with steeper slopes in the centre and milder slopes at the sides. As a result a shoal with constant depth is present in the bay.

8.3 *Recommendations*

The hydraulic and morphological research after the behaviour of bays is still young and further research is definitely necessary. Recommendations for further research are:

- Validate the model with field data of existing bays. The phenomena which occur in bays according to the simulations are probably right, but using field data would prove this and moreover, quantitative statements can then be made as well.
- The reason why equilibrium has yet not been found is probably the result of using unrealistic bottom profiles. Using bathymetries which satisfy the geometrical requirements and which have steeper slopes in the centre and milder slopes at the sides probably yield better results. Moreover, it is recommended to use concave bottom slopes rather than linear bottom slopes.
- Now and then execute simulations over a longer period (e.g. 30 days) to gain insight into the adaption time of the model to reach a stationary situation during a morphological computation. This results in a better understanding of the long-term performance of the model.
- With a view to present developments in coastal engineering (Maasvlakte 2), it might be interesting to investigate a bay shapes with a straight section of coast inserted in the centre.
- It would further be interesting to check the computed current patterns and erosion and sedimentation patterns with results obtained via a physical model test.
- Diffraction is not taken into account in the wave module, but it is accounted for by means of extra directional spreading. Sensitivity analysis for the value of directional spreading is an interesting topic for further research.

- Using the transport module version which takes cross-shore sediment transport into account probably yields more realistic results for overall morphological developments with time. Since most versions which are yet in use have this phenomenon implemented, it is advised to switch this option on.
- Once equilibrium is found for waves arriving perpendicular at the breakwaters, it may be interesting to find out in what manner this equilibrium changes when waves arrive obliquely.
- It is further recommended to examine the effect of the tide. It is expected that for large gap-width ratios the effect of the tide is more important than for small gap-width ratios.
- The effect of a constant longshore sediment transport results in a bay which is in a dynamic state of equilibrium (rather than a static state). It is expected that the location of a dynamic coast is seaward of the location of the static coast. It would be interesting to investigate whether this assumption is right or not.

Bibliography

AHMED, A.S.M. (1997), *2D and 1D model simulations for the effect of a single detached breakwater on the shore*, Institute for Hydraulic and Environmental Engineering, Delft

BLANKERS, G. (1999), *Equilibrium bays*, Msc. thesis, Delft University of Technology

BOWEN, A.J. (1969), *The generation of Longshore Currents on a plane beach*, Journal of Marine Research, Volume 27, No. 2, pp 206-215

DAVIES, J. L. (1958), *Wave refraction and the evolution of shoreline curves*, Geogr. Stud. 5:1-14

EVERTS, C.H. (1983), *Shoreline changes downdrift of a littoral barrier*, Proc. Coastal Structures '83, ASCE 673-89

GRESWELL, R.K. (1957), *The Physical Geography of Beaches and Coastlines*, London: Hulton Ed. Publ.

HALLIGAN, G.H. (1906), *Sand movement on the New South Wales coast*, Proc. Limn. Soc. N.S.W. 31

HSU, J.R.C. and EVANS, C. (1989), *Parabolic bay shapes and applications*, Proc. Instn. Civil Engrs. 87: 557-70

HSU, J.R.C. and SILVESTER, R. (1997), *Coastal stabilization*, World Scientific Publishing Co. Pte. Ltd.

HSU, J.R.C., SILVESTER, R. and XIA, Y.M. (1987), *New characteristics of equilibrium shaped bays*, Proc. 8th Aust. Conf. Coastal and Ocean Eng., 140-44

JENNINGS, J.N. (1955), *The influence of wave action on the coastal outline in plan*, Aust. Geogr. 6: 36-44

KRAUS, N.C., GINGERICH, K.J. AND ROSATI, J.D. (1988), *Toward an improved empirical formula for longshore sand transport*, Proceedings of the

21st International Conference on Coastal Engineering, American Society of Civil Engineers, pp 1182-1196.

KRAUS, N.C., GINGERICH, K.J., AND ROSATI, J.D. (1989), *DUCK85 - surf zone sand transport experiment*, Technical Report CERC-89-5, U.S. Army Engineer Waterways Experiment Station, Vicksburg, MS.

LANGFORD-SMITH, T. and THOM, B.G. (1969), *New South Wales coastal geomorphology*, J. Geol. Soc. Aust. 16

LONGUET-HIGGINS, M.S., and STEWART, R.W. (1963), *A note on Wave Setup*, Journal of Marine Research, Vol. 21(1), pp. 4-10

MASHIMA, T. (1961), *Stable configuration of coastline*, Coastal Eng. in Japan, 4:47-59

NIPIUS, K. (1998), *Dwarstransportmodellering m.b.v. Bailard, toegepast op de Voordelta Grevelingen-monding*, Delft University of Technology

SAVILLE, T., JR. (1961), *Experimental Determination of Wave Setup*, Proceedings, Second Technical Conference on Hurricanes, National Hurricane Research Project, Report No. 50. pp. 242-252

SHORE PROTECTION MANUAL (1984), Coastal Engineering Research Centre, Department of the Army, Waterways Experiment Station, Corps of Engineers, Vicksburg, Mississippi, USA

SILVESTER, R. AND HO, S.K. (1972), *Use of crenulate shaped bays to stabilize coasts*, Proc. 13th Inter. Conf. Coastal Eng., ASCE 2: 1347-65

STELLING, G.S. (1984), *On the construction of computational methods for shallow water flow problems*, Rijkswaterstaat communications, No. 35

VAN DE GRAAFF, J. AND TILMANS, W. (1980), *Sand Transport by Waves*, Proceedings of the 17th Coastal Engineering Conference, Sydney, Australia

VAN RIJN, L.C. (1998), *Principles of coastal morphology*, Aqua Publications

WELLS, D.R. (1977), *Beach Equilibrium and Second-Order Wave Theory*, Journal of Geophysical Research, Vol. 72, No. 2, pp. 497-504.

YASSO, W.E. (1965), *Plan geometry of headland-bay beaches*, Journal of Geology, nr. 73

Subjoined references were studied to use the model Delft2D-MOR:

DELFT HYDRAULICS (1996)a, *An introduction to Delft2D-MOR*, Delft Hydraulics

DELFT HYDRAULICS (1996)b, *Delft-gpp*, Delft Hydraulics

DELFT HYDRAULICS (1996)c, *rgfgrid*, User manual, Delft Hydraulics

DELFT HYDRAULICS (1997)a, *Delft3D-FLOW*, User manual, release 3.00, version 0.1, Delft Hydraulics

DELFT HYDRAULICS (1997)b, *Delft3D-MOR*, User guide, Version 0.1, Delft Hydraulics

DELFT HYDRAULICS (1997)c, *Delft3D-WAVE*, User manual, version 1.02, Delft Hydraulics

DELFT HYDRAULICS (1997)d, *quickin*, Delft Hydraulics

Appendices

Appendix A The SASME project

Objectives of the SASME-Project

The work done for this thesis is partly sponsored by the Commission of the European Union, Directorate General for Science, Research and Development under the Marine Science and Technology (MaST) Programme. The work is part of the Surf and Swash Zone Mechanics (SASME) project under contract MAS3-CT97-0081.

The objective of the SASME project is to investigate the physical processes which take place in the surf zone on a coast with and without coastal structures. The project has to lead to a significantly improved description of the cross-shore and longshore sediment transport, which mainly occurs within the surf zone. The SASME project is divided into two interlinked parts:

1. surf and swash zone hydrodynamics and sediment transports;
2. surf and swash zone morphology.

The surf and swash zone hydrodynamics and sediment transport will concentrate on the behaviour of breaking and broken waves, their generation of small and large scale turbulence, and the resulting sediment transport. The morphological study will focus on the bed behaviour in the surf/swash zone which includes bed instabilities and the formation of bars and their behaviour (like erosion and accretion in 2 horizontal dimensions and non-uniformities in the alongshore direction due to rip currents).

The far field impact of coastal structures is investigated: the effect of the modifications of wave, current and sediment transport fields by the structures. The project will thus address important aspects of the function of the coastal structures. The project will not treat the three-dimensional near-field hydrodynamics and sediment transport around structures that are associated with local scour phenomena.

The project will comprise:

- Laboratory and field studies on wave behaviour in the surf and swash zone.
- Laboratory studies of the wave-induced turbulence, as well vertically as horizontally (like shear waves).
- Interpretation of available field data.
- Numerical and analytical analysis of the processes.
- Numerical morphological area modelling.

Participants

This project on surf and swash zone mechanics is made jointly by 13 hydraulic laboratories, advisory institutes and universities. The table lists the names of the participants, their number, code and nationality.

no.	Code	Name and location	Nat.
01	DHI	Danish Hydraulic Institute, Hoersholm	DK
02	DH	Delft Hydraulics, Delft	NL
03	LWI	Leichtweiss Institute, Braunschweig	DE
04	HR	HR Wallingford, Wallingford	GB
05	LNH	Lab. National d'Hydraulique, Chatou	FR
06	DTU	Technical University Denmark, Lyngby	DK
07	DUT	Delft University of Technology, Delft	NL
08	BrU	Bristol University, Bristol	GB
09	UPl	University of Plymouth, Plymouth	GB
10	UCa	University of Cantabria, Santander	ES
11	UPc	Univ. Polytecnica de Catalunya, Barcelona	ES
12	UFl	University of Florence, Florence	IT
13	UEDIN	University of Edinburgh, Edinburgh	GB

A major reason for including 13 participants is to bring in the full range of study methods. Some field data is to be collected and existing field data will be utilized. Laboratory studies of all components, waves, turbulence, currents and sediment, are essential companions for interpretation of field data and to guide theoretical developments. Theoretical approaches, sometimes with more than one model for a topic, are vital to develop predictive capabilities and are also useful for interpreting the laboratory and field observations.

In each topic which concentrates on particular processes, the end result will be a larger understanding leading to an improvement in the elements that go into the integrated models that are describing overall transports and topographic evolution. For the studies involving the integrated models there will be incorporation of such improvements, and also feedback as to which components are the most critical and require further study.

In terms of practical outcome, the project is expected to produce significant improvements in "medium" term modelling, which is necessary for the development of longer term prediction methods. In addition, improvements at a fundamental level will yield a basis for developments of transport and mixing models for quantities other than sediments in the surf and swash zone, plus some results of wider significance, for example in relation to

breaking waves in deep water and their significance for air-sea exchange and mixing.

Task structure of the project

As mentioned before, the project is divided into two interlinked parts, each with a small number of tasks within which details relate to specific physical subtasks.

Part 1 **Surf and swash zone hydrodynamics and sediment transport**

Task 1.1 Breaking and broken waves in the surf and swash zone.

Subtasks:

a. Breaking and broken waves.
b. Swash zone mechanics.
c. Long waves and wave reflection.
d. Sediment transport in surf beat.

Task 1.2 Vertical structure of wave- and breaker-induced motion and associated sediment transport.

Subtasks:

a. Description of a plunging breaker.
b. Wave boundary layer investigations under breaking waves.
c. Influence of breaking waves on sediment transport.
d. Wave-induced currents.

Task 1.3 Horizontal structure of wave- and breaker-induced motion.

Subtasks:

a. Shear waves.
b. Rip current systems.

Part 2 **Surf and swash zone morphology**

Task 2.1 Morphological modelling of the surf zone without structures.

Subtasks:

a. Profile development.
b. Morphological development of a complex beach topography.

Task 2.2 Impact of structures on near-shore morphology.

Subtasks:

a. Modelling of the far field morphological evolution around structures.
b. Review of the experience on implementation of coastal structures.

Since the University of Delft is in charge of the task which deals with the impact of structures on the near-shore morphology, the research after the behaviour of equilibrium bays is part of subtask 2.2a.

Methodology

The models for currents, sediment transport and morphological development in the surf zone will be applied to study the morphological impact of coastal structures. This subtask will concentrate on the far field impact. This means that local scour associated with very local three-dimensional flow phenomena (e.g. horseshoe vortices) and turbulence generated locally at the structures will not be considered. The task will involve the use of a the numerical model Delft2D-MOR (developed by Delft Hydraulics, Delft, The Netherlands) to simulate different types of structures.

Predictions of the effect of structures on the coast are often based on simulations with coastal profile and coastline models. This is quite acceptable for large-scale structures, but for small-scale groynes and offshore breakwaters these models lack essential physics, such as inertia and advection terms in the current motion, lag effects in the suspended sediment transport and cross-shore transport effects. Because of these effects entirely different behaviour of the bathymetry around such structures may result; for example, the maximum lee erosion due a groyne may occur some distance downstream of the groyne, rather than close to the downstream side.

The capability of area models to describe this kind of behaviour has greatly improved during the MaST-II. However, the 2DH approach adopted so far limits the accuracy of the results. A first step towards Q3D simulations including cross-shore wave effects have been taken, but much further research is needed on the representation of 3D effects and on the analysis of the resulting behaviour of the coast.

The morphodynamic model including these 3D effects will be run for realistic sequences of wave conditions, to assess the variability of the coastal behaviour. This will also allow field validation of the model for some well-documented cases. Finally, a large number of sensitivity computations will be carried in order to derive practical guidelines for assessing the effects of structures on the coast. The concentration will be on the morphological behaviour of coasts behind and between series of detached breakwaters.

Since the SASME project has a duration for three year, (probably) three Msc. students will succeed their predecessor's work.

Appendix B The numerical model Delft2D-MOR

Introduction

Delft2D-MOR is a flexible numerical model system for morphological studies existing of separate modules for the physical processes:

- waves
- flow
- sediment transport
- bed level variations

Each module calculates a certain part of the problem. This modular structure of the program Delft2D-MOR ensures maximum flexibility since various combinations of the different modules are possible. The general structure of the model as well as the separate modules are described in this appendix.

The control module MAIN

The general structure of the compound morphological model is illustrated in figure B.1. A user-supplied process tree must specify routes that should

Figure B.1

Structure of model Delft2D-MOR

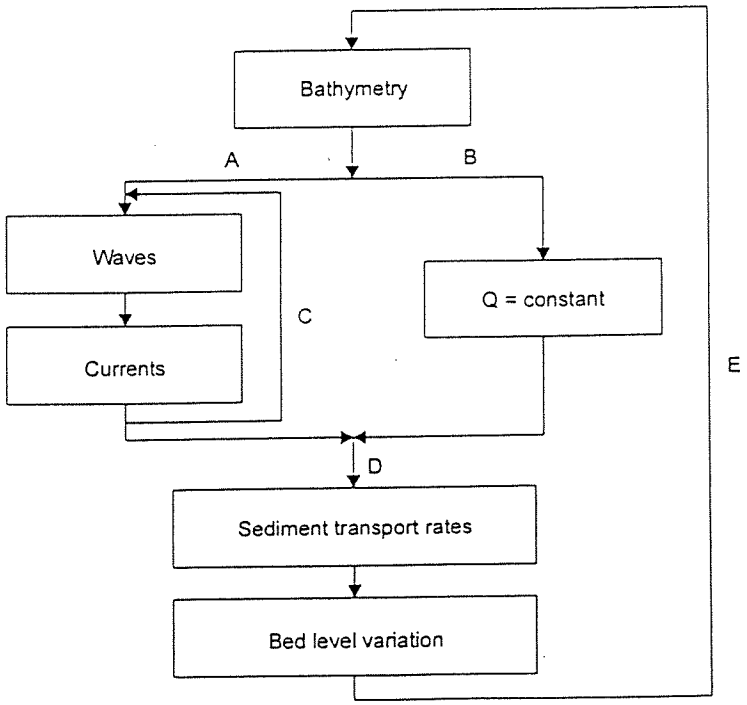

be followed in the morphological model. This tree is a scheme to describe a hierarchical system and consists of a set of nodes and branches. The graphical representation of such a tree is usually top-down. An example of a process tree is given in figure B.2.

Figure B.2

Example process tree

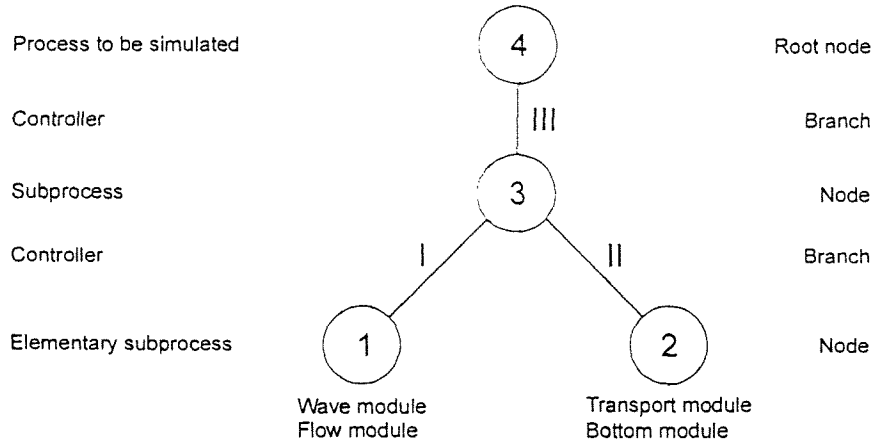

In the process tree parent and child nodes can be identified. A branch connects two nodes: a parent node and a child node. A node without a parent node is called the root node (here: node 4). Each branch of the process tree corresponds to a controller. This controller controls the execution of the elementary process or subprocess. The user should specify the control criterion of each controller.

The process starts at the root node (node 4) by activating the subprocess (node 3). This node starts the subprocesses it controls, beginning with the subprocess with the lowest number (node 1). If this one is stopped, the next child subprocess (node 2) will be activated and so on until all child subprocesses satisfy their own stop criteria. A process can be repeated as often as necessary.

An elementary subprocess represents the execution of a set of modules (waves, currents, sediment transport and bottom level variation). In this manner the process tree allows the user to construct a specific tree suitable for his specific problem.

The followed procedure for a morphological computation is as follows. In the scheme (see figure B.1) two alternative main routes (A and B) are present for the computation of the bed-level changes. If there is no information available on the waves and flow field, first a wave and flow computation has to be made on the initial topography (route A). These computations are made on the assumption that the bottom level is invariant during the wave and flow computation (quasi-stationary). The wave-induced forces resulting from the wave computation serve as input for the flow computation. The results of the flow computation can be used again for a next wave computation (loop C) if wave-current interaction must be taken into

account. The next step is the determination of the sediment transport rate (route D) which is again done at the assumption of quasi-stationary. The bottom changes are computed which will be superimposed on the original bathymetry (loop B) after which the next cycle starts. If we have wave and flow information at our disposal, we can optionally follow route B for the flow field computation. It is assumed that for small changes of the bottom level the wave height and flow pattern (rates and directions) remain constant. This results in a simple computation of the new flow velocities by dividing the constant flow rate by the new depth values. Application of this continuity correction reduces the computation time considerably.

data communication The coupling of the various modules requires a file into which relevant data used by the various modules can be stored. In Delft2D-MOR this file is called a communication file. This file has a nefis structure (Neutral FIle System). All the data relevant to the various modules will be written to and can be read from this communication file. This file can also be used for post processing of the data. Besides the communication file, extra output files are generated by the independent modules (waves, flow, trssus, bottom). Information about specific features of each subprocess can be found here.

The wave module WAVE

introduction The wave module is the physical process module, which simulates the propagation of waves and as a result predicts the distribution of wave parameters and current-driving terms. Waves play an important role in the morphological evolution of a coastal area. They stir up the bottom material and bring it into suspension. Furthermore, waves cause currents which are able to transport the bottom material. From this it is obvious that it is important, especially in a complicated situation between two breakwater, to predict the wave field correctly for assessing the morphological change.

The wave module in Delft2D-MOR makes use of the HISWA model. HISWA, which stands for Hlndcast Shallow water WAves, is a numerical model for the prediction of stationary, short crested waves in shallow water.

general structure Within the wave module the HISWA model is used. The user prescribes the input and output of the wave module by means of switches. These switches determine the way the bottom depth, water level and current velocity are taken into account by the wave module. In general the next procedure is followed.

Each time the wave module is started by the process tree, the bottom and flow data are read from a user-specified file containing this data. In general this will be the communication file. Since the flow data computed by TRISULA (model used by the flow module) is available at a staggered grid, the

data must first be interpolated onto the HISWA input grid. Next the HISWA computation can be executed after which the results must again be interpolated back onto the TRISULA grid.

physical background

In HISWA the wave propagation is determined across the grid according to the Eulerian approach of the action balance of the waves. The wave action is a function of the spatial coordinates (x, y) and of the spectral wave direction (θ). In this approach all wave information is available at the meshpoints of a regular grid.

The action density A is defined as:

$$A(\omega, \theta, x, y, t) = \frac{E(\omega, \theta, y, y, t)}{\sigma} \qquad \text{Equation B.1}$$

in which:

A	=	wave action (Js/m^2)
ω	=	wave frequency (1/s)
θ	=	spectral direction (^{0})
x, y	=	coordinate in cross-shore and longshore direction (m)
t	=	time (s)
E	=	wave energy density (J/m^2)
σ	=	relative frequency of wave and current (1/s)

$$\sigma = \omega - (\underline{K} \cdot \underline{U}_c) \qquad \text{Equation B.2}$$

in which:

$\underline{K}$	=	wave number vector (1/m)
$\underline{U}_c$	=	current velocity vector (m/s)

The action balance equation is then (without the notation for the independent variables):

$$\frac{\partial A}{\partial t} + \frac{\partial (c_x A)}{\partial x} + \frac{\partial (c_y A)}{\partial y} + \frac{\partial (c_\theta A)}{\partial \theta} + \frac{\partial (c_\omega A)}{\partial \omega} = T \qquad \text{Equation B.3}$$

in which:

c_x, c_y	=	wave group velocity in x, y direction (m/s)
c_θ, c_ω	=	wave group velocity in the θ, ω space (^{0}/s)
T	=	dissipation of action (J/m^2)

The first term in this equation represents the local rate of change of action density. The other terms on the left-hand side represent the net transport of action in the x-, y- θ -, and ω -domain respectively. The total effect of generation and dissipation of action is represented by the source term T. The energy dissipation caused by bottom friction and wave breaking are calculated in the wave module by:

$$D_b = \frac{1}{4}\alpha \rho_w g f_m Q_b (H_{max})^2$$ Equation B.4

in which:

α = coefficient (-)
f_m = mean wave frequency (1/s)
H_{max} = maximum wave height (m)
Q_b = the local fraction of breaking waves (-)

The fraction of breaking waves can be calculated by:

$$\frac{1 - Q_b}{-\ln Q_b} = \left(\frac{H_{rms}}{H_{max}}\right)^2$$ Equation B.5

H_{max} can be calculated via the following formula:

$$H_{max} = \frac{0.88}{k}\tanh\left(\frac{\gamma k h}{0.88}\right)$$ Equation B.6

in which:

k = wave number (1/m)
γ = breaker index (-)

The breaker index is a function of the wave steepness and can be calculated by:

$$\gamma = 0.50 + 0.4\tanh(33 s_0)$$ Equation B.7

in which:

s_0 = wave steepness (-)

This action balance has been simplified in the following manner. Assuming that the time scale of the wave propagation over the model area is small compared to that of the local wind or current field the time dependent parameters are neglected. This means that the first and fifth terms on the left-hand side are left out of the action balance which makes the model sta-

tionary. The second simplification consists of the parameterization of the remaining action balance. Therefore, two directional wave functions are defined: the directional action spectrum $A_0(\theta)$, resulting from the integration of the action density $A(\omega, \theta)$ over the total frequency domain, and a mean wave frequency as a function of spectral direction $\omega_0(\theta)$.

$$A_0(\theta) = m_0(\theta) \qquad \text{Equation B.8}$$

$$\omega_0(\theta) = \frac{m_1(\theta)}{m_0(\theta)} \qquad \text{Equation B.9}$$

in which:

$A_0(\theta)$ = one-dimensional directional action spectrum (J/m^2)

$\omega_0(\theta)$ = mean frequency as a function of the spectral direction (1/s)

$m_0(\theta)$ = zero-th order moment of the action density spectrum (J/m^2)

$m_1(\theta)$ = first order moment of the action density spectrum (J/sm^2)

The moment m_n of the action density spectrum are defined as:

$$m_n(\theta) = \int_0^\infty \omega^n A(\omega, \theta) d\omega \qquad \text{Equation B.10}$$

When the zero-th and first order moments of the action density spectrum are used the following two evolution equations remain of the action balance:

$$\frac{c'_{0x} m_0)}{\partial x} + \frac{\partial (c'_{0y} m_0)}{\partial y} + \frac{\partial (c'_{0\theta} m_0)}{\partial \theta} = \qquad \text{Equation B.11}$$

$$\frac{c''_{0x} m_1)}{\partial x} + \frac{\partial (c''_{0y} m_1)}{\partial y} + \frac{\partial (c''_{0\theta} m_1)}{\partial \theta} = \qquad \text{Equation B.12}$$

in which:

c'_{0x}, c'_{0y}, $c'_{0\theta}$ =propagation speed of the wave action in x, y, θ space (m/s)

c''_{0x}, c''_{0y}, $c''_{0\theta}$ =propagation speed of the mean wave frequency in x, y, θ space (m/s)

T_0, T_1 = source terms

With these final two equations HISWA computes for given x, y the propagation of the frequency-integrated energy density and the mean wave frequency for each spectral direction.

The physical phenomena, which are accounted for in HISWA, are:

- directional spreading,
- bottom refraction,
- current refraction,
- bottom dissipation,
- wave breaking,
- wave blocking,
- wave generation by wind.

Diffraction is not taken into account. Therefore, in this study the lack of wave energy penetrating into the lee of the breakwater is to some extent compensated by directional spreading. Booij et al. (1992) show that in areas where refraction occurs this will give plausible results. Since diffraction plays an important role in the development of equilibrium bays the coefficient for the directional spreading factor must be chosen carefully.

For information about the implementation of the physical phenomena in HISWA reference is made to Holthuijsen (1989).

numerical procedure

Because of the fact that the status of a point is determined by the status upwave from this point, the computation is carried out in a direction roughly parallel to the main wave propagation direction (not more than 20^0 oblique). Consequently, it follows that the program needs the wave conditions at the upwave boundary at each grid-point as the boundary conditions. For the propagation in x and y-direction an explicit scheme (leap-frog) and in θ-direction an implicit scheme (backward Euler) is used. As a consequence of the use of an explicit scheme the following numerical stability criterion has to be satisfied:

$$\frac{|c_y \Delta x|}{|c_x \Delta y|} \leq 1.0 \qquad \text{Equation B.13}$$

Which can be simplified to:

$$\frac{\Delta x}{\Delta y} \geq \tan\theta \qquad \text{Equation B.14}$$

in which:

θ = half of the directional energy distribution sector (^{0})

c_x = group velocity of the mean frequency in x-direction (m/s)

c_y = group velocity of the mean frequency in y-direction (m/s)

Δx = grid size in x-direction (m)
Δy = grid size in y-direction (m)

grid definition

HISWA uses different grids for input, computation and output (see figure B.3). The input grid has to contain the water depth and current-field. The computational grid obtains this information by interpolation (from the TRISULA grid). Outside the input grid HISWA extrapolates the water depth and current information by taking the value at the nearest boundary of the input grid.

Figure B.3

HISWA and TRISULA grids used in the simulations

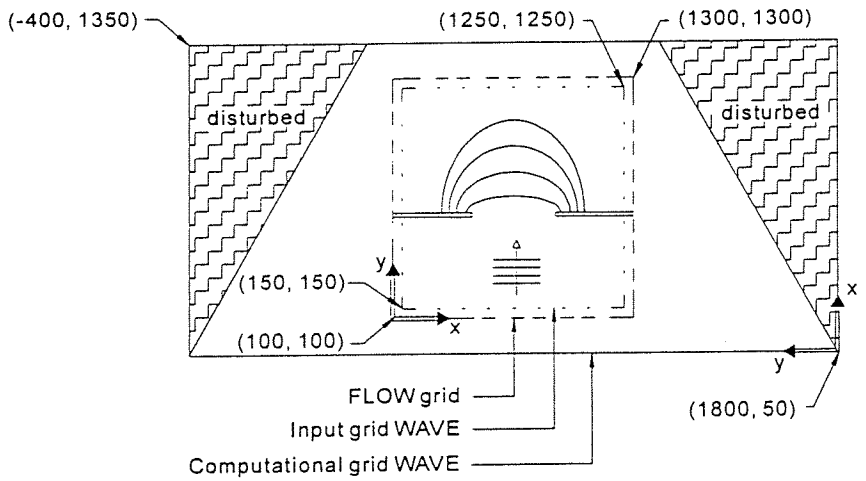

The computational grid is a grid in the dimensions x-, y- and θ. The orientation of the x-axis of this grid has to be chosen so that it is more or less equal to the main wave direction because this is the direction in which HISWA carries out the computation as explained above. The computational grid must be larger than the area of interest, especially when open boundaries are used. In that case a region exists along each lateral side of the grid where the wave field is disturbed as a consequence of the fact that no wave energy enters the model area here. So the y-direction has to be sufficiently large to prevent that these regions fall into the area of interest. The output grid within Delft2D-MOR is equal to the TRISULA grid. The information from the computational grid is interpolated onto this grid by the wave module.

The flow module TRISULA

introduction

The flow module is the physical subprocess which simulates the non-steady flow and water level variation from a tidal, a wave or meteorological forcing. The flow module in Delft2D-MOR consists of the TRISULA model

which is a program for 2DH or 3D flow computations, including the effects of waves, wind and density differences.

physical background

The 2DH version of the TRISULA model solves the unsteady shallow water equations. In this approach the vertical momentum equation is reduced to the hydrostatic pressure relation. Vertical acceleration are assumed to be small compared to the gravitational acceleration and are not taken into account. The momentum equations in x- and y-direction are:

$$\frac{\partial(hu)}{\partial t} + \frac{\partial(hu^2)}{\partial x} + \frac{\partial(huv)}{\partial y} + gh\frac{\partial(h+z_b)}{\partial x}$$

$$-{}_xh\left(\frac{\partial^2 u}{\partial x^2} + \frac{\partial^2 v}{\partial y^2}\right) - \frac{\tau_{b,x}}{\rho_w} - hfv - \sum\frac{F_x}{\rho_w} = \qquad \text{Equation B.15}$$

$$\frac{\partial(hv)}{\partial t} + \frac{\partial(hv^2)}{\partial x} + \frac{\partial(hvu)}{\partial y} + gh\frac{\partial(h+z_b)}{\partial y}$$

$$-{}_yh\left(\frac{\partial^2 v}{\partial x^2} + \frac{\partial^2 u}{\partial y^2}\right) - \frac{\tau_{b,y}}{\rho_w} - hfu - \sum\frac{F_y}{\rho_w} = \qquad \text{Equation B.16}$$

in which:

u, v	=	depth averaged water flow velocities in x, y directions (m/s)
h	=	local water depth (m)
t	=	time (s)
ρ_w	=	water density (kg/m^3)
τ_b	=	bed-shear stress (N/m^2)
F_x, F_y	=	external stresses (wind, waves) (N/m^2)
z_b	=	bed level above reference datum (m)
k_x, k_y	=	effective dispersion coefficient representing the integration effects (m)
f	=	Coriolis coefficient (1/s)

And:

$$\tau_{b,x} = \rho_w g\left(\frac{uV}{C^2}\right) \qquad \text{Equation B.17}$$

$$\tau_{b,y} = \rho_w g\left(\frac{vV}{C^2}\right) \qquad \text{Equation B.18}$$

in which C is the Chezy-coefficient ($m^{1/2}/s$) and V is the magnitude of the resultant velocity (m/s) and can be formulated is follows:

$$V = \sqrt{u^2 + v^2}$$ Equation B.19

The depth-averaged continuity equation is given by:

$$\frac{\partial h}{\partial t} + \frac{\partial (hu)}{\partial x} + \frac{\partial (hv)}{\partial y} = 0$$ Equation B.20

For the depth averaged flow the shear stress on the bed induced by a turbulent flow can be calculated with a quadratic friction equation:

$$\tau_b = \rho_w g \left(\frac{V^2}{C^2} \right)$$ Equation B.21

Where V is the magnitude of the depth-averaged horizontal velocity. The 2D-Chezy coefficient is determined to White-Colebrook's formula and is a function of the waterdepth (H) and the Nikuradse roughness length (k_s):

$$C = 18 \log \left(\frac{12H}{k_s} \right)$$ Equation B.22

The main physical phenomena which are accounted for in TRISULA are:

- tidal forcing,
- the effect of the earth's rotation (Coriolis force),
- density differences,
- wind shear stress on the water surface,
- bed shear stress on the bottom,
- influence of the waves on the bed shear stress,
- wave-induced stresses and mass fluxes.

For a complete review of the physical phenomena which are taken into account in their implementation, reference is made to the TRISULA user manual.

numerical procedure

The equations for the water levels are solved with an Alternating Direction Implicit (A.D.I) technique, Stelling (1984). This means that water levels and velocities in the x-direction are implicitly solved in the first half time step, while water levels and velocities in the y-direction are implicitly

solved in the second half-time step. For more details about this numerical method reference is made to the TRISULA manual and to Stelling (1984).

grid definition

In the horizontal plane TRISULA uses as staggered grid. Each grid cell contains a water level point, a bottom depth point, a x-direction velocity point (u) and a y-direction velocity point (v). The points in a grid cell all have the same indices (i, j). This is illustrated in figure B.4.

At the end of the computation the velocities are know at the velocity points. These values are transformed to the water level points by averaging. For the x-direction this yields:

$$u(i,j) = \frac{u(i-1,j) + u(i,j)}{2}$$ Equation B.23

Figure B.4

Staggered Flow grid

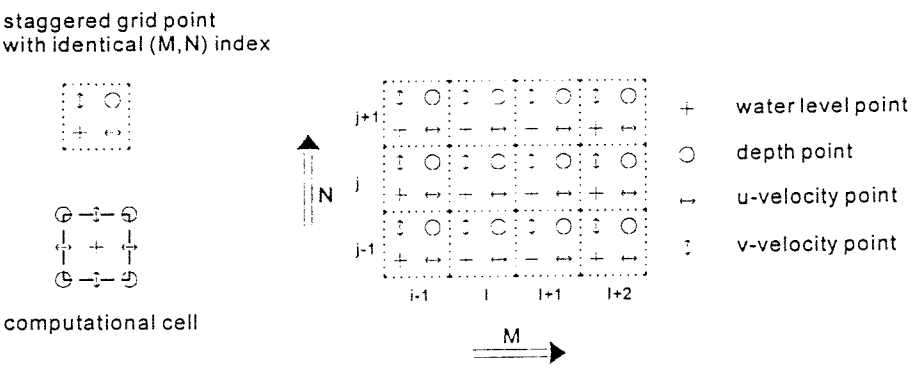

While for the y-component this yields:

$$v(i,j) = \frac{v(i,j-1) + u(i,j)}{2}$$ Equation B.24

Hence, eventually all properties except the bottom depths are known at the coordinates of the water-level points.

The transport module TRSSUS

introduction

The transport module determines the sediment transport using the time-dependent flow and wave field. The general advection-diffusion equation to be solved reads:

$$\frac{\partial c}{\partial t} + u\frac{\partial c}{\partial x} + v\frac{\partial c}{\partial y} + \frac{\partial}{\partial x}\varepsilon_x\frac{\partial c}{\partial x} + \frac{\partial}{\partial y}\varepsilon_y\frac{\partial c}{\partial y} = \frac{c_e - c}{T_s}$$ Equation B.25

in which:

$$c_e = \frac{S}{uh} \quad = \text{local equilibrium concentration}$$

The magnitude of the sediment transport (S) will be computed using a selected sediment transport relation. In this study the Bijker formula is used. This formula accounts for a bed load and a suspended load component of the total sediment transport. In this section a short description of the transport relation is given. More details can be found in Bijker (1971).

description of Bijker's formula

Bijker extended the existing bed- and suspended load transport formulae for currents only to formulae including wave effects. He used the Kalinske-Frijlink formula for the bed load and the Einstein formula for the suspended load transport.

bed load transport

The layer in which the bed load takes place is taken equal to the bottom roughness r. Waves contribute considerably to the amount of sediment transport. Bijker assumed that only the waves contribute to the stirring up of sediment rather than the transport. This stirring effect has been taken into account by a modification of the bed-shear stress. In case of waves and currents the bed-shear stress increases considerably. This increased bed-shear stress increases the bed load transport. Bijker calculated the velocities of waves and currents separately at a specified height above the bed level. After superposing these two velocity vectors the total velocity is substituted into the formula of the bottom shear stress.

$$\underline{U}_{cw} = \underline{U}_c + \underline{U}_w \qquad \text{Equation B.26}$$

in which:

$\underline{U}_{cw}$ = wave-current velocity vector (m/s)

$\underline{U}_c$ = current velocity vector (m/s)

$\underline{U}_w$ = orbital velocity vector (m/s)

The wave-current velocity is now substituted in the equation for the bottom shear stress:

$$\tau_{cw} = \rho_w \kappa^2 (U_{cw})^2 \qquad \text{Equation B.27}$$

in which:

ρ_w = water density (kg/m^3)

κ = Von Karman constant (-)

Due to the oscillating wave motion the direction of this bottom shear stress varies with time. However, the only important condition for the stirring of the bed material is the exceeding of the critical velocity regardless of its direction. So it is sufficient to know the mean shear stress. The time-averaged value of the bed-shear stress finally yields:

$$\bar{\tau}_{cw} = \tau_c + \frac{1}{2}\tau_w \qquad \text{Equation B.28}$$

in which τ_w is the maximum shear stress due to the waves and is expressed in N/m^2. This maximum shear stress can be determined using:

$$\tau_w = \frac{1}{2}\rho_w f_w (\hat{u}_0)^2 \qquad \text{Equation B.29}$$

The equation for the time averaged bed shear stress can be re-written which yields:

$$_w = \tau_c\left[1 + \frac{1}{2}\left(\xi\frac{\hat{u}_0}{U_c}\right)\right. \qquad \text{Equation B.30}$$

in which:

$$\tau_c = \rho_w g\left(\frac{U_c}{C}\right)^2 \qquad \text{Equation B.31}$$

$$\xi = C\sqrt{\frac{f_w}{2g}} \qquad \text{Equation B.32}$$

Consequently, the bed load transport of Kalinske-Frijling in terms of the mean bed-shear stress yields:

$$S_b = \frac{b d_{50} U_c \sqrt{g}}{C} \exp\left\{\frac{-0.27\Delta d_{50} C^2}{\mu (U_c)^2\left[1 + \frac{1}{2}\left(\xi\frac{\hat{u}_0}{U_c}\right)^2\right]}\right\} \qquad \text{Equation B.33}$$

in which:

b	=	constant which depends on wave height and water depth (-)
d_{50}	=	median grain size (m)
Δ	=	relative sediment density (-)
μ	=	ripple factor (-) which can be determined using:

$$\mu = \left(\frac{C}{C_{90}}\right)^{3/2}$$ Equation B.34

in which:

$$C = 18\log\left(\frac{12h}{r}\right)$$ Equation B.35

$$C_{90} = 18\log\left(\frac{12h}{d_{90}}\right)$$ Equation B.36

Bijker assumed that the bottom transport occurs in a layer with a thickness of r. If the thickness of that layer is unknown, half the height of the ripples on the bottom can be taken as approximation. As mentioned above only the waves contribute to the stirring effect. Transport by waves due to asymmetry of the orbital motion is therefore neglected in the approach of Bijker.

suspended load transport

Bijker modified the suspended transport formula of Einstein by changing the shear stress due to a current into the time averaged shear stress due to waves and currents. The concentration distribution is given by:

$$c(z) = c_a\left[\frac{r}{(h-r)}\cdot\frac{(h-z)}{z}\right]^{Z^*}$$ Equation B.37

in which:

r = bottom layer thickness (m)

h = local waterdepth (m)

Z^* = exponent of the concentration distribution with the modified bed-shear velocity (-)

c_a = bed load concentration (kg/m^3)

Bijker assumed that the concentration in the bottom layer (c_a) is constant over the entire thickness r and is given by:

$$c_a = \frac{S_b}{\int_0^r u(z)dz}$$ Equation B.38

in which u(z) is the Prandtl-Von Karman logarithmic velocity profile (m/s).

The exponential part Z^* is the Rouse number given by:

$$Z^* = \frac{w_s}{\kappa U_{cw^*}}$$ Equation B.39

in which:

κ = Von Karman constant = 0.4 (-)

w_s = fall velocity of the sediment (m/s)

The shear stress velocity can be computed from:

$$_{w^*} = \sqrt{\frac{\bar{\tau}_{cw}}{\rho_w}} = \sqrt{\frac{\tau_c}{\rho_w}\left[1 + \frac{1}{2}\left(\xi \frac{\hat{u}_0}{U_c}\right.\right.}$$ Equation B.40

The suspended load transport in the layer between the water surface and the bottom layer is determined by:

$$S_s = \int_r^h c(z)U(z)dz$$ Equation B.41

in which U(z) is the velocity profile according to Prandtl-Von Karman. The equation of S_s has been solved numerically and after using the total Einstein integral term, it can be shown that:

$$S_s = 1.83 \cdot Q \cdot S_b$$ Equation B.42

The total transport (S_{tot}) can now be calculated by adding the bed load transport to the suspended transport:

$$S_{tot} = S_b + S_s = S_b(1 + 1.83Q)$$ Equation B.43

The magnitude of the sediment transport computed by the Bijker formula must now be corrected for different effects which are not included in the formula itself. These effects are:

- bed-level gradient effect,
- non-erodible layer effect,
- numerical stability.

Because the Bijker formula does not take into account the effect of a bed-level gradient, a multiplication factor depending on the bed-level gradient is included. Also for numerical stability a correction has to be applied. Both effects are applied by adding correction terms to the computed sediment transport rate:

$$S = \alpha_s \alpha_n S' \qquad \text{Equation B.44}$$

in which:

α_s = correction term for physical slope effect (-)

α_n = correction term for numerical stability (-)

S' = computed sediment transport by Bijker's formula ($m^3/s/m$)

The correction term for the physical slope effect can be calculated by:

$$\alpha_s = 1 + \alpha_{bs} \frac{\partial z_b}{\Delta l} \qquad \text{Equation B.45}$$

in which:

α_{bs} = coefficient = 1 (-)

z_b = bed level above datum (m)

Δl = grid increment measured in the transport direction (m)

The correction term for numerical stability is slope dependent and can be calculated by:

$$\alpha_n = 1 + \alpha_{nn} \frac{\partial z_b}{\Delta l} \qquad \text{Equation B.46}$$

in which α_{nn} is the coefficient for numerical stability (-). This coefficient can be computed via:

$$\alpha_{nn} = \frac{\alpha_{st} \beta \Delta l}{2 h_{tav}} \qquad \text{Equation B.47}$$

in which:

α_{st} = coefficient = 1 (-)

β = power of the used formula = 5 (-)

h_{tav} = average water depth over the time interval used in the bottom computation (m)

More details on this subject can be found in the Delft2D-MOR manual.

The bottom module BOTTOM

introduction

The bottom module computes the bottom changes from the transport rates (S_x, S_y) following from the transport module. Next, these changes are superimposed on the original bottom which gives the new bottom.

physical background

The determination of the bottom level changes is based on the conservation of sediment mass:

$$(1-\lambda)\frac{\partial z_b}{\partial t} + \frac{\partial S_x}{\partial x} + \frac{\partial S_y}{\partial y} = 0 \qquad \text{Equation B.48}$$

in which:

z_b = the bed level (m)

λ = sediment porosity (-)

S_x, S_y = sediment transport in x and y direction (m^3/s)

numerical procedure

The above mentioned continuity equation is solved using the explicit FTCS (Forward-Time Central-Space) scheme. In fact, a Lax-like scheme is applied because the FTCS scheme generates negative diffusion. To compensate for that a Lax correction has been applied by introducing positive diffusion in the form of an artificial down slope term in the transport rates. For the transport rate in x and y direction this yields:

$$S_{x^*} = S_x\left(1 + \alpha_{nn}\frac{\partial z_b}{\partial r}\right) \qquad \text{Equation B.49}$$

$$S_{y^*} = S_y\left(1 + \alpha_{nn}\frac{\partial z_b}{\partial r}\right) \qquad \text{Equation B.50}$$

in which:

S_{x^*}, S_{y^*} = modified sediment transport rates ($m^3/s/m$)

S_x, S_y = original sediment transport rates ($m^3/s/m$)

α_{nn} = coefficient for artificial diffusion (-)

r = coordinate in transport direction (m)

Since the sediment transport rates are known at the water level points of the TRISULA grid, the bottom module computes with the FTCS scheme the bottom changes at the bottom points of the grid using the sediment transport values at the four surrounding water level points. This yields the following formula which is valid for the grid used in this study (which is orthogonal with a constant grid size):

$$\frac{Z_{bij}^{n+1} - Z_{bij}^{n}}{\Delta t} = \frac{\left(S^{*n}_{x,i+\frac{1}{2},j+\frac{1}{2}} - S^{*n}_{x,i-\frac{1}{2},j+\frac{1}{2}}\right) + \left(S^{*n}_{x,i+\frac{1}{2},j-\frac{1}{2}} - S^{*n}_{x,i-\frac{1}{2},j-\frac{1}{2}}\right)}{2\Delta x} +$$

$$\frac{\left(S^{*n}_{y,i+\frac{1}{2},j+\frac{1}{2}} - S^{*n}_{y,i+\frac{1}{2},j-\frac{1}{2}}\right) + \left(S^{*n}_{y,i-\frac{1}{2},j+\frac{1}{2}} - S^{*n}_{y,i-\frac{1}{2},j-\frac{1}{2}}\right)}{2\Delta y} \qquad \text{Equation B.51}$$

Since the FTCS scheme is an explicit scheme, the Courant number should be less than one. On the other hand, the Courant number should not be much lower than one as low Courant numbers will generally induce numerical diffusion. In order to ensure this stability criterion the time-step used in the bottom module can be determined by the module by specifying the maximum Courant number which may not be exceeded. This results in a varying time step during the simulation run. For a given Courant number the maximum allowed time step follows from the minimum value of the stability criterion:

$$\sigma = c_b \frac{\Delta t}{\Delta x} \qquad \text{Equation B.52}$$

Re-writing this equation yields:

$$\Delta t = \frac{\sigma \Delta x}{c_b} \qquad \text{Equation B.53}$$

in which:

σ = Courant number (-)
Δx = the grid spacing (m)
c_b = bed-level celerity (m/s)

The smallest value of Δt throughout the field finally determines the step for updating the bottom level. The above mentioned bed-level celerity c_b can be seen as the propagating speed of bed-level disturbances and is determined by assuming that the sediment transport relation can be written as:

$$S = \alpha U^{\beta} \qquad \text{Equation B.54}$$

in α and β are constants (-). Using some algebra it is possible to re-write the bed-level celerity as:

$$c_b = \frac{\beta S}{(1-\lambda)h} \qquad \text{Equation B.55}$$

in which:

β	=	power of the used transport formula (-)
S	=	sediment transport ($m^3/s/m$)
λ	=	sediment porosity (-)
h	=	water depth (m)

The optimal time step now follows from:

$$\Delta t = \frac{\sigma \Delta x h}{\beta S}$$ Equation B.56

The optimal timestep is determined by the BOTTOM module for every iteration, with a minimum timestep of the user defined time step used by all modules. The computational grid to be used by the BOTTOM module is equal to the computational area defined by the flow module. The boundaries are equal to the flow module boundaries too.

Appendix C The asymmetry problem

Introduction

The bathymetry of the bay, which serves as input for the numerical model, is a perfect symmetrical shape obtained via an elliptical approach (Blankers, 1999). Since the wave conditions at the upwave boundary are set in such a manner that the waves arrive perpendicular at the breakwaters, the obtained results should also be perfectly symmetrical. However, this is not the case. The asymmetrical results can be caused by a numerical phenomenon or a physical phenonemon (like the instability of a rip current). But since the asymmetry always develops in the same direction it can be concluded that it must be the result of a numerical problem rather than a physical problem.

According to Blankers (1999) all bay shapes developed an asymmetric current field after a simulation time longer than approximately 2·30 minutes. Although the orientation of this current field was always to the right side of the bay, the Coriolis effect could not have caused the disturbances because this effect was switched off during the simulations. As the simulations got longer the results got more and more asymmetrical and hence it is difficult to interpret the results. Therefore, an extensive research is done in order to determine the cause of the problem.

In order to determine whether the output of the model is perfectly symmetrical a few observation points are implemented in the model. These points are situated at equal distances at either side of the symmetry axis. Comparing the results by plotting a certain parameter (for instance the current velocities) in the same graph yields a statement about whether or not the model is symmetrical.

The approach

It is always difficult to search for (probably) minor errors in a numerical model. The fact that the input, output and the numerical computation are closely connected with each other complicates the problem significantly. Therefore, a systematical approach is needed to gain more insight into the problem.

First of all, a distinction is made between the input and the output of the model. The input in the model can further be subdivided into variable input and non-variable input. The variable input can easily be adapted by 'switching a few buttons' using the model's interface (e.g. the boundary conditions), while changing the non-variable input is labour-intensive (like

geometry, bathymetry and grids among other things). The latter consists of general files which are being used by all modules.

The aim is to obtain perfectly symmetrical output if possible and if not, to identify the source(s) which causes the error. A sound statement concerning the output can only be made if the program which visualizes the output works properly. Since, initially, it is not known if the post-processing program GPP is plotting the results in an accurate manner, this program is also considered as a source of error. Therefore, the results are always visualized by means of two post-processing programs: GPP and Excel. Obviously, only when these two programs show the same symmetrical results the conclusion can be made that the source of error must be somewhere within the numerical model.

Since the model Delft2D-MOR consists of more or less independent modules, the above described approach is applied to the model as a whole, as well as to the several modules. In a diagram the approach has a structure as shown in Figure C.1 (only the TRISULA module is shown, the approach for the other modules is identical).

Figure C.1

Problem approach

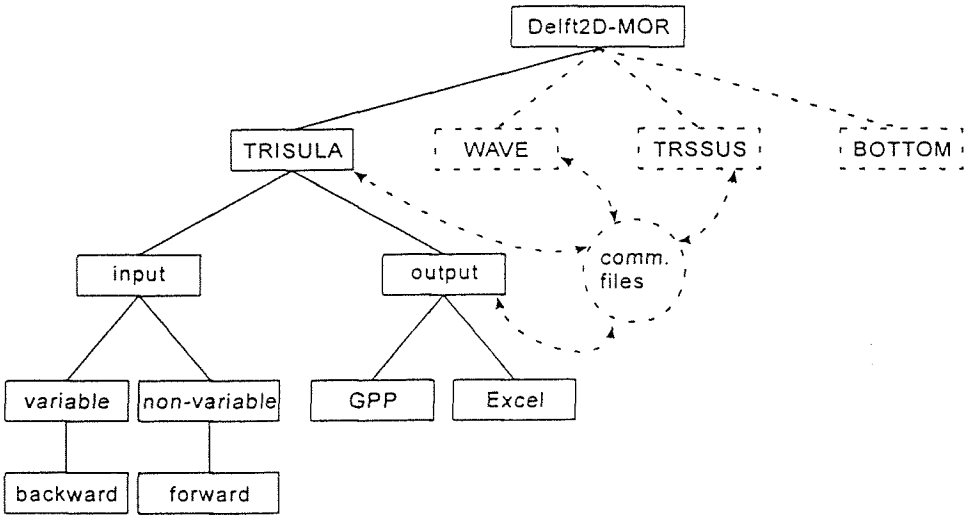

Analysing the input is done via two different methods, namely the Backward method (variable input) and the Forward method (non-variable input). In the Backward method the assumption is made that the asymmetry is the result of an error in the variable input files created by G. Blankers and hence the problem is closely related to the specific problem dealt with in this study. By means of a 'trial and error' procedure several switches, which are likely to influence the symmetrical results, are changed (one at a time) and the obtained results are examined. Since it is easy to change the variable input a lot of switches can be examined in a relatively short time. In this way the cause of the problem is located by crumbling down the model to its smallest element. In the case of the Forward analysis method the opposite happens. The model is built up by starting with the most

stripped version of the model (e.g. only the TRISULA module is present) and then adding more and more elements to the model. Assuming that the most stripped version gives symmetrical results the cause of the problem can be identified because somewhere during the Forward method the results get asymmetrical.

It is mentioned that although it may seem that no interaction takes place within the model according to Figure C.1 this is certainly not the case. The output of one module serves as input for another module. This takes place by means of communication files. A wrong flow of information between the modules and/or the post processing programs leads undoubtedly to (asymmetrical) errors.

In short, according to this approach the error which causes the problem is located within one of the four modules or within their mutual interaction. The latter may be caused by a wrong reading and/or writing to and from the communication files. A third possibility which causes the results to get asymmetrical, can be a wrong reading and/or plotting routine in the post processing program GPP.

Analysing the grids

Although G. Blankers claimed that all the input in the model was perfectly symmetrical (see Blankers, 1999) this was not the case. WAVE uses different grids for input, computation and output. In bay simulations the input grid has to contain the water depth and the current field. The computational grid obtains this information by interpolation from the TRISULA grid. Outside the input grid WAVE extrapolates the water depth and current information by taking the value at the nearest boundary of the input grid. The output grid within Delft2D-MOR is equal to the TRISULA grid. The information from the computational grid is interpolated onto this grid by the wave module. In Blankers' simulations these three grids were shifted with respect to each other (compare coordinates in Figure C.2).

Therefore, it was necessary to adapt the TRISULA grid and the WAVE grid. The new grids are shown in figure B.3 (Appendix B). An irksome consequence was that in addition the bathymetry file had to be adapted because the new TRISULA and WAVE grids have different overall sizes than Blankers' grids. This was a serious problem because all the depth files created by G. Blankers could not be used any longer (further research on equilibrium bays required a whole range of new depth files). However, the main problem in finding that the grids and the bathymetry were shifted with respect to each other was the difference in presentation of the bathymetry. The pre-processing program QUICKIN plots the depth points using dots at the corners of a grid cell. The visualization area in the flow module hatches the grid cell with a certain colour. This colour represents the average depth

Figure C.2

Grids used by G. Blankers

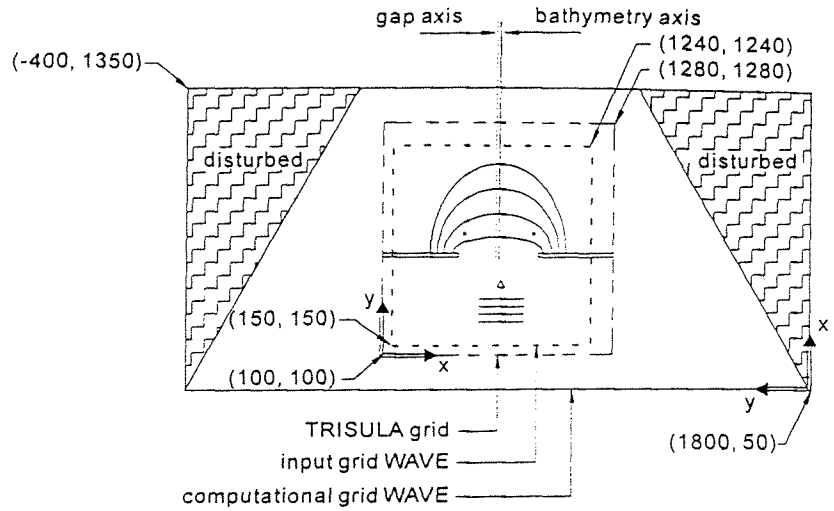

of the four surrounding depth point at the corners. First it took some time to discover that both plotting options plot the bathymetry in a different manner, secondly it took time to find out which one is the most accurate. It turned out that the visualization option in TRISULA is a very good tool to show the model quickly. However, in a staggered grid the depth points are situated at the corners of a grid cell (see also figure B.4). Thus, QUICKIN is plotting the bathymetry in the most accurate manner.

Besides these grids, another aspect of the input of the model was asymmetrical. The two breakwaters were not situated symmetrical with respect to the TRISULA grid. Consequently, the file in which the location of the breakwaters was described had to be changed. A third aspect which could have caused the results to get asymmetrical was the fact that the symmetry axis of the bathymetry did not coincide with the symmetry axis of the gap between the breakwaters. They were shifted one grid cell with respect to each other (which comes down to 10 meters).

The three aspects mentioned above must have caused subsequent errors and during long simulation runs they must have influenced the results obtained with the numerical model in a negative way.

Unfortunately, it turned out that even after all the adaptions made with respect to the grids the results were still not satisfactory. Although the symmetry had improved significantly, the expected perfect symmetry had yet not been achieved. A comparison of the results of a hydraulic simulation using Blankers' input with a simulation using the corrected input is made in Appendix D.1 and Appendix D.2. It shows that the flow pattern is more symmetrical in the latter figure. This can be clearly seen in the first figure where in the centre of the bay near the shore an exchange of flow occurs from the left side of the bay to the right side. This is not the case in the improved model in the second figure. In Appendix D.3 (Blankers' input) and D.4 (corrected input) the results are shown for a morphological simula-

tion of 7-days. Again, it can be seen that the symmetry of the model has improved significantly. It is further mentioned that the extent in which asymmetry occurs varies from one simulation to the other.

The Backward method

After examining the grids it turned out that some input files were not correct and hence the logical assumption was made that there may also be incorrect files in the variable input part and that the problem was closely related to the model under consideration. Therefore, the Backward method is applied.

As mentioned before, Blankers ascertained that all bay shapes developed an asymmetric current field during the hydraulic simulations. Apparently, the initial error is made in the flow module or in the wave module or in the interaction between these two. In TRISULA (flow module) a staggered grid is used for the discretization of the horizontal gradients (see Figure C.3). This grid is orthogonal. The water level points (pressure points) are defined in the centre of a (continuity) cell, whereas the velocity components are defined on the faces of this cell. In this way the grids for the water levels and velocities are staggered.

Figure C.3

Staggered flow grid

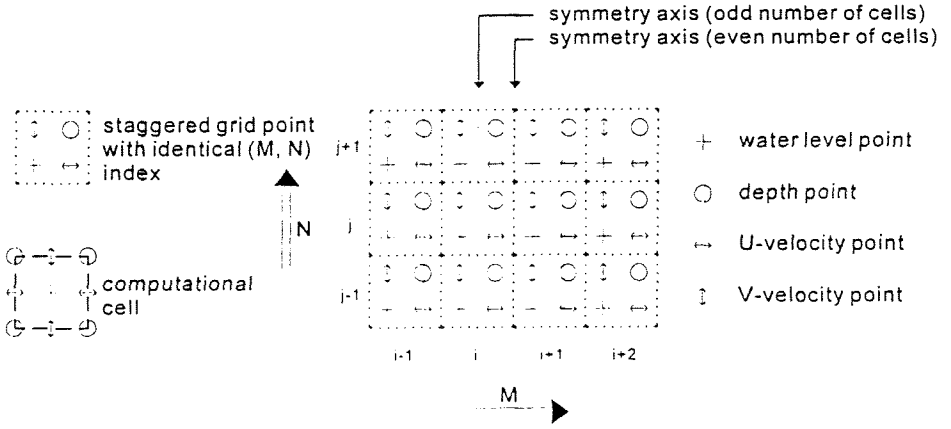

The velocities are computed using the waterlevels. Next the velocities are substituted into the depth-averaged continuity equation. The equations for the water levels are solved with an Alternating Direction Implicit (A.D.I.) technique (Stelling, 1984). The water levels are calculated implicitly along grid lines in x-direction and y-direction in an alternating way. The direction in which the integration is implicit changes each half time step. In this way for the water levels only tri-diagonal systems of equations along grid lines have to be solved. Back substitution of the calculated water levels in the momentum equations yields the horizontal velocities.

In the half time step, in which the pressure term (i.e. water level gradient) is taken explicitly, the momentum equations are solved implicitly by a Red Black Jacobi iterative scheme in the horizontal direction. With regard to the full time step the discretization is second-order accurate.

Number of cells Since the grid is staggered the first thing that was interesting to find out was what happened with the current field when the number of cells between the breakwaters is reduced by one, thereby creating an odd number of cells between the breakwaters. In this case the symmetry axis of the model is running through the centre of a computational cell instead of at the boundary of this cell (see Figure C.3). In Appendix D.5 and D.6 the results are plotted for a bay with respectively an even number of cells and an odd number of cells between the breakwaters. It can be seen in these figures that the flow pattern is almost identical and hence reducing the number of cells between the breakwaters by one does not influence the results significantly. This statement can be confirmed when examining the data obtained in the two observation points (see black dots in Figure C.2). These points are located at equal distances from either side of the symmetry axis (and have the same y-coordinate). Substracting the velocity and/or water level data should yield a straight line with a zero value, because in a perfect symmetrical case the values at these observation points should be identical. However, this is not the case and moreover the error has the same order of magnitude for both simulations (see Appendix D.7 and D.8). Since the post-processing program GPP is yet considered as source of error the data are also examined with the spreadsheet program Excel. This gives the same result and therefore the same conclusion.

Open boundaries The next step in analysing the variable input is examining the open (upwave) boundary. Usually open boundaries are introduced to limit the computational area. In nature, waves cross these boundaries unhampered and without reflections. In numerical models this can be realized by the use of weakly reflective boundary conditions in the form of incoming Riemann invariants, which have the form:

$$U \pm 2\sqrt{(gH)} = F(t) \qquad \text{Equation C.1}$$

in which U is the normal velocity component (m/s), g the acceleration due to the gravity (m/s^2) and H the deepwater wave height (m). However, the values F(t) of these incoming Riemann invariants are in general not known. Therefore, in Delft3D-FLOW the following weakly reflective form is applied for a water level boundary (Stelling, 1984):

$$\zeta + \alpha \frac{\partial}{\partial t}[U \pm 2\sqrt{(gH)}] = F(t) \qquad \text{Equation C.2}$$

in which ζ is the water level (m) and α is the reflection coefficient (-). The latter is chosen sufficiently small to dampen the short waves. Both the Riemann boundary and the water level boundary are applied in order to examine whether the type of boundary effects the (a)symmetry of the results. Moreover, for both boundary types two different uniform initial water level values are applied: a zero value and a non-zero value. By doing so it is possible to make a sound statement whether the boundary conditions influence the results and whether the numerical model can deal with uniform zero values (if the computation requires a division, a zero value can cause problems). The results are shown in Appendix D.9 through Appendix D.16. It can be clearly seen that the magnitude of the error is in the same order for both the Riemann boundary as the water level boundary and thus as expected, the type of boundary used in the model does not influence the (a)symmetrical results. It can also be seen in the figures that there is no significant difference whether the input at the boundary has a uniform zero value or not (in the executed simulations the non-uniform value was very small, namely 0.001 m). Hence, the numerical model Delft2D-MOR can deal with uniform zero-values as expected and further study is necessary to find the source of error which causes the results to get asymmetrical.

Bed slope

Since the simulations executed until now are all done with a bay bathymetry the next step was to examine the influence of the bathymetry on the results. A bay bathymetry has a depth gradient in all directions and according to the Backward method decreasing the directions in which the bed slopes is the next step. Thus, a simulation run is carried out in which a linear sloping bottom is used because a linear sloping bed has a depth gradient in only one direction. In other words, a sloping straight beach is simulated. Another advantage of this bathymetry is that no complications occur near the symmetry axis of the model with respect to the depth gradient; the depth gradient increases (or decreases) linearly parallel to the symmetry axis. However, according to the figures in Appendix D.17, which show the results of the simulations using a linear sloping bottom, perfectly symmetrical results have still not been achieved and moreover, the magnitude of the error is in the same order for both types of bathymetry. Therefore the bathymetry has no influence on the asymmetry of the results.

Forward method

As mentioned before, in the case of the Forward analysis method the model is built up by starting with the most stripped version of the model and then adding more and more elements to the model. Since the TRISULA module is the starting module for all simulations, a process tree is created in which only the flow module is present. In other words, no interaction between the modules takes place. Moreover, the most simple bathymetry is applied, namely a uniform bottom depth and the most simple geometry, namely a straight flume with a local narrowing by means of a pair of groins (see also

Figure C.4). Behind these groins the values over a certain straight cross-section are examined. These values should be perfectly symmetrical around the symmetry axis. However, in order to elucidate that the flow pattern is not perfectly symmetrical the horizontal current magnitude in the two observation points is substracted from each other. If the pattern is symmetrical the result would be a straight line with a zero value. This is not the case and hence the pattern is asymmetrical. The same conclusion can be drawn when examining the waterlevels. The results are plotted with the post-processing program GPP as well as with the spreadsheet program Excel and are given in Appendix D.18 and D.19. One must be careful when examining the Excel plot. For practical reasons it is chosen to plot the water levels and discharges over a straight cross-section. This cross-section begins at the side of the flume and ends at the symmetry axis half way the flume (see Figure C.4). The values on the other half of the symmetry axis

Figure C.4

Flume model

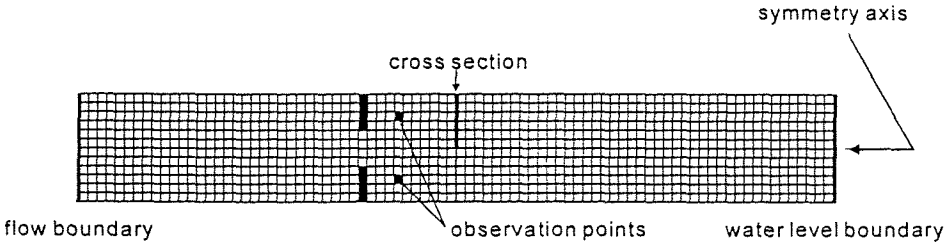

are mirrored in this axis and substracted from the values in the 'upper' half. A uniform zero value would indicate perfect symmetry; fluctuations in the value indicates asymmetry. Unfortunately, as can be seen in both the GPP plot as well as the Excel values, the results are still asymmetrical. The cause of the problem must thus be within the numerical computation.

Therefore, the error must be caused by the truncation error in combination with the applied numerical procedure used by the model. Since it is not possible to get the exact analytical solution when using a computer, the differential equations which describe the actual problem under consideration are discretizised. The price of this discretization are rounding errors. Roughly said, the order in which these rounding errors are introduced in the model are determined by the truncation error. The way in which the truncation error leads to asymmetrical results is as follows (see also Figure C.5).

Figure C.5

The computational method

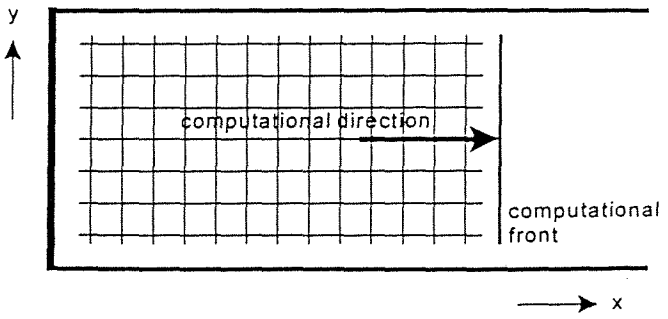

The computational front is propagating in the direction of the positive x-axis, beginning at the imposed boundary condition at x = 0. However, before this front can advance the computational molecule (a Leap-Frog molecule in this case) calculates the values at each grid point in the computational front, thus applying a 'point-sweep' in the positive y-direction, starting at y = 0. Since the value at a new point is determined using the value at the previous point, it may be obvious that the truncation error introduced at the previous point influences the truncation error computed at the next point, and so on. This not only clearifies the obtained asymmetrical results, it also explaines why the asymmetry is always directed in the same direction. Unfortunately, it is impossible to mirror the model in the x-axis in order to prove that this theory is right, for it is only possible to rotate the coordinate system. Probably, mirroring would yield results which are mirrored even so. However, it is possible to evade the problem by switching the boundaries instead of mirroring the coordinate system. Two simulations are executed in which a flume, directed parallel to the y-axis, is used with a current boundary and a waterlevel boundary. Switching the boundaries and reversing the flow direction at the flow boundary should give the same results as mirroring the coordinate system. The flow patterns are shown in Appendix D.20. Considering the substracted current magnitudes it can be seen that the results are not mirrored (Appendix D.21). This does not mean that the above mentioned theory is wrong. It may also be that a certain randomness is present in the rounding off procedure. Since the error is so small, it is very well possible that the last numerical bit sometimes 'falls right' and sometimes 'falls left'. It is not in the scope of this thesis to investigate this any further.

Using computers to describe and solve complex problems which are present in nature, irrespective of the character of the problem, inevitably introduces truncation errors via discretizations. Since the order of magnitude in which the results are asymmetrical is to the power minus seven, it can be questioned whether or not it is necessary to put much more effort and time in getting the numerical model Delft2D-MOR more accurate than it already is. Besides, one must keep in mind that in nature perfect symmetry does not exist either.

The next thing which is now interesting to know is whether this small error becomes bigger if a long simulation time is applied or if interaction between the modules takes place. Therefore, a five hour run is executed and the results are shown in Appendix D.22. It is mentioned that in order to save computer memory the computed values are written to the output files each five minutes only instead of every minute and hence this graph is smoothed somewhat. As can be seen in these figures the order of magnitude of the error does not increase significantly. Unfortunately, this is not the case in the figures in Appendix D.23 through D.26 in which interaction between the flow module and the wave module is accounted for. It can be seen that one interaction loop increases the asymmetry significantly. How-

ever, if the number of interaction loops between these modules increases the magnitude of the error remains in the same order. Hence it can be stated that, although in the ideal case the model should give perfectly symmetrical results, the results do not diverge. The fact that the asymmetry increases significantly after the first loop is probably due to the fact that the currents in the bay simulations are wave-driven and consequently the calculated flow values are much smaller when no waves-flow interaction is taken into account (and thus the difference between the computed values in the two observation points). If one consideres the obtained data carefully (a water-level difference of one millimetre over about 400 meters influences the flow pattern) and keeping the asymmetry in mind, this model is a useful tool to compute coastal engineering problems. Due to the discretization, asymmetry is inevitable and a prudent statement can be that every numerical model which is being used at the present time gives, to some extent, asymmetrical results. As long as this asymmetry does not diverge into unacceptable proportions the numerical model can be a very useful tool.

Post processing

Visualizing the obtained data is an important aspect if one wants to interpret the results in a convenient manner. As mentioned before the post processing program GPP is considered a source of error and in this section it is described whether this assumption is right or not.

In the figures in Appendix D.27 the depth contours of the bay are plotted. The difference between the solid lines and the dashed lines is that the latter are the plotted depth contours using a different output file, namely the output file of the wave module, while the solid lines are the depth contours using the communication file. Both the solid as the dashed lines should be perfectly symmetrical around the centre of the bay (which is the line x = 700m). Obviously, this is not the case. The reason why this is not the case can be because GPP is plotting these lines incorrectly or GPP is plotting the lines correctly, but the interaction between the wave output file and the communication file is not consistent (indicating a problem within the numerical model, rather than in the post processing program). The answer can be given when examining the exact data which represent these lines with the spreadsheet program Excel. It turns out (see Appendix D.28) that the data from the transport output file and the data from the communication file are exactly the same! Therefore, although the model Delft2D-MOR gives the correct results, the program GPP is not plotting the data in the right manner. They reason the results of both files is plotted different in GPP is that the definition of the subtypes of the various parameters in the GPP-file 'filetype.gpp' differs for the communication file and the wave file and hence, interpolation takes place differently. Adjusting the file 'filetype.gpp' in such a way that both subtypes are consistent solves the problem. Interpreting the results when using the post-processing program GPP

only, must therefore be done with care. However, if one plots the data in a consistent manner (e.g. always using the same output files) sound qualitative statements can be made.

Conclusions

It is very useful to get more insight into the numerical procedure carried out by the model and the investigation described in this appendix is valuable for both the user and the makers of the model. Throughout this appendix two independent line of thoughts can be recognized. At first, the assumption was made that the asymmetrical problem could be solved completely. This yields the Backward method. But after a while the thought arose that maybe the problem cannot be solved completely, but that it is a consequence of the numerical procedure used by the model. This not only yields the Forward method, it also yields an investigation into how the numerical procedure is carried out. From then on, the objectives become determining the order of magnitude of the error (and its growth) and the consequences for the reliability of the numerical model. In short, conclusions which can be drawn from this research are:

- the asymmetry is the result of the propagation of the initial truncation error (caused by the discretization) throughout the model; this propagation is always in the positive y-direction;
- since discretisizing reality is inevitable when dealing with a numerical model the asymmetry in the results will always occur;
- the order of magnitude in which the results are asymmetrical is sufficiently small to make the model Delft2D-MOR a very useful tool for coastal engineering problems;
- the post processing program GPP is not plotting the obtained data correctly and hence interpreting the results must be done with care; however, sound qualitative statements can be made if the results are always plotted consistently.

It is further recommended to compare the order of magnitude of asymmetry with other numerical models by computing the same bathymetry with several numerical models. This may indicate that other numerical models are asymmetrical too and that the asymmetry problem is inextricably bound up with the necessity to discretizise nature when using numerical models.

It is also noted that GPP makes use of certain contour-classes to define the data in a clear way. Although the line of thought was present that these classes had to be defined each time one uses GPP (which is a rather labour-intensive job) it was found that it is possible to fix the contour-classes in a by the user defined way (in fact, this routine is simple and can be done in the GPP file 'routines.gpp', see also Appendix D.29). A useful recommen-

dations with respect to the definition of the contour classes might be to create an option in GPP which allows the program to define a range of data (e.g. creating a nearly infinite number of contour classes), rather than define several contour classes.

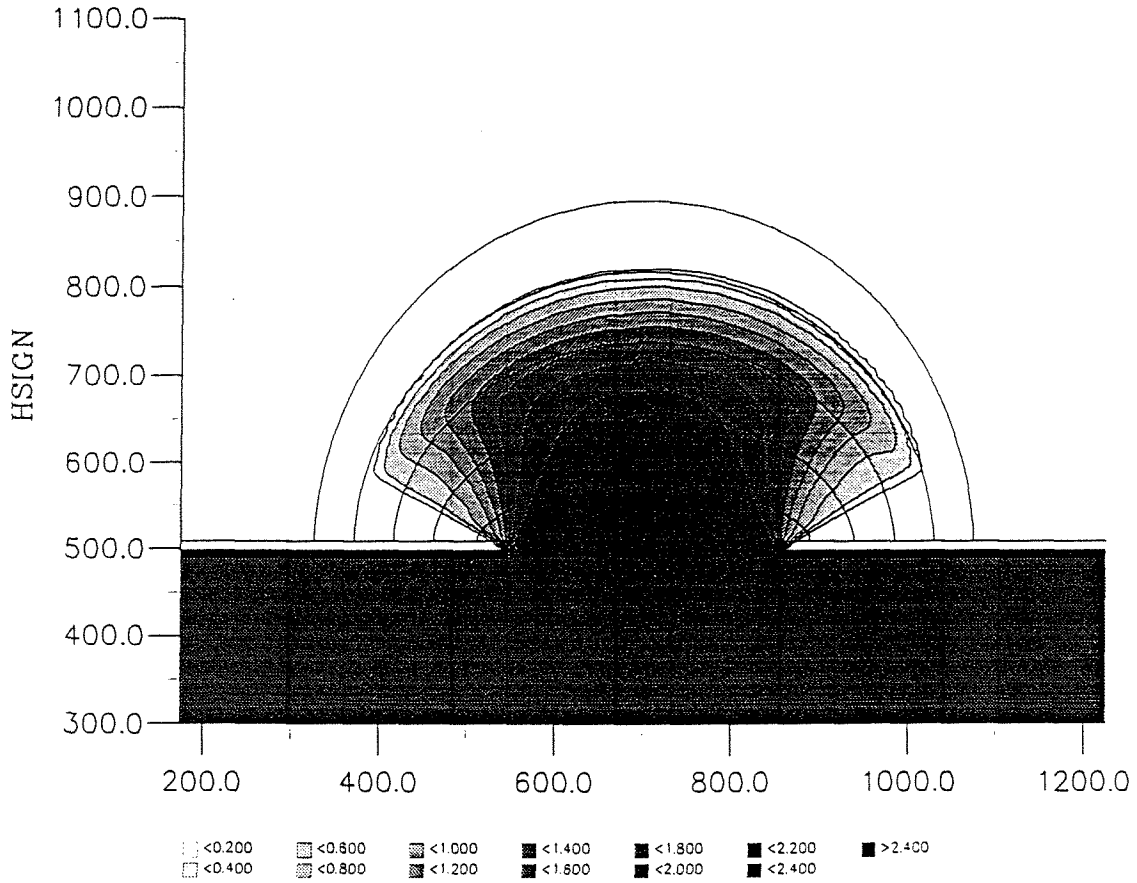

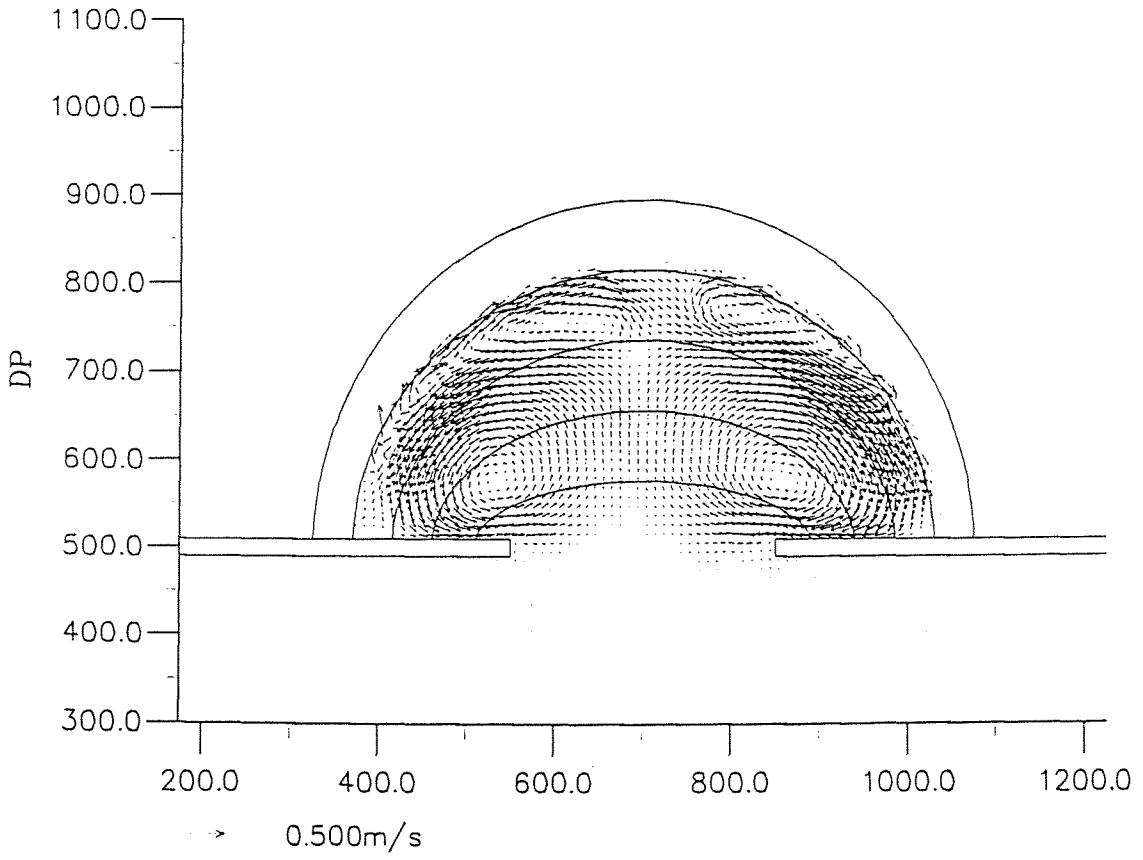

Upper graph: Hsig isolines (m) Lower graph: Flow velocity vectors (m/s) Depth contour interval is 2m	Delft3D–MOR	Appendix D.1
	Blankers' input	
DUT – EQUILIBRIUM BAYS	MaST–III	SASME

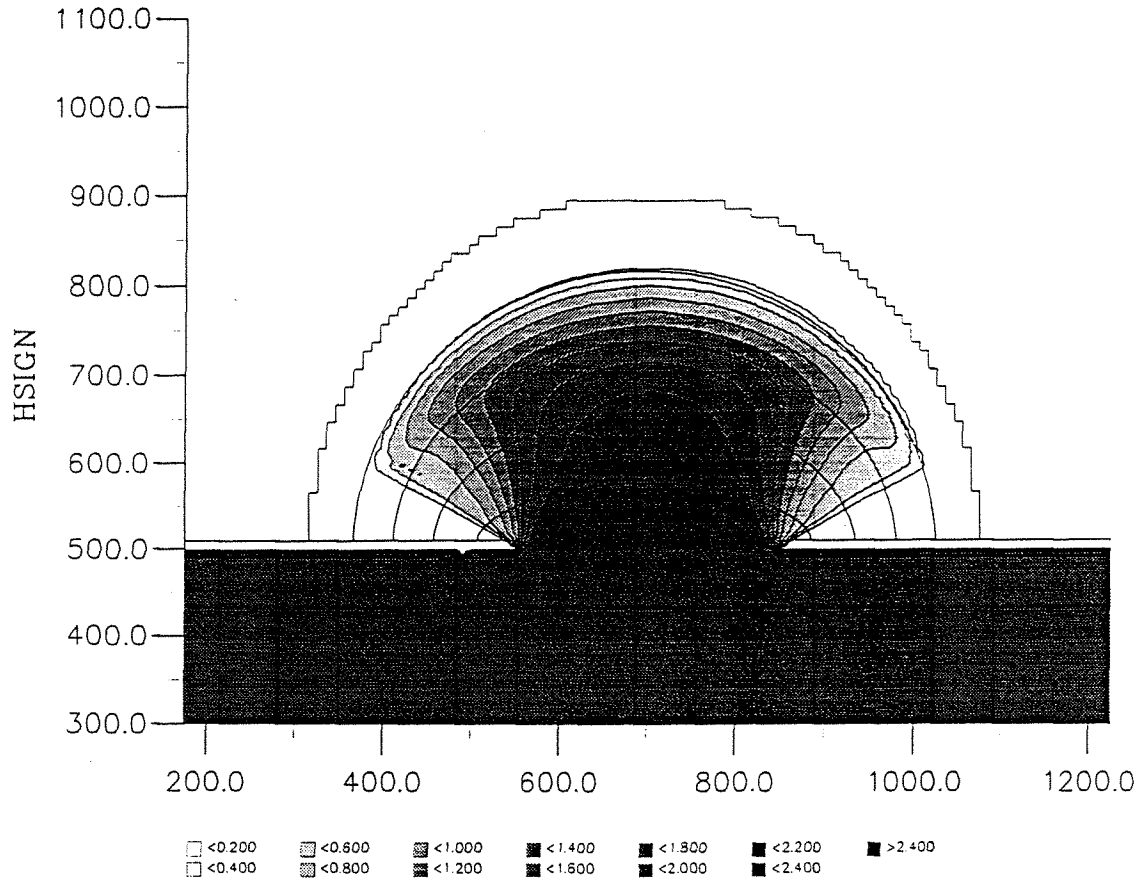

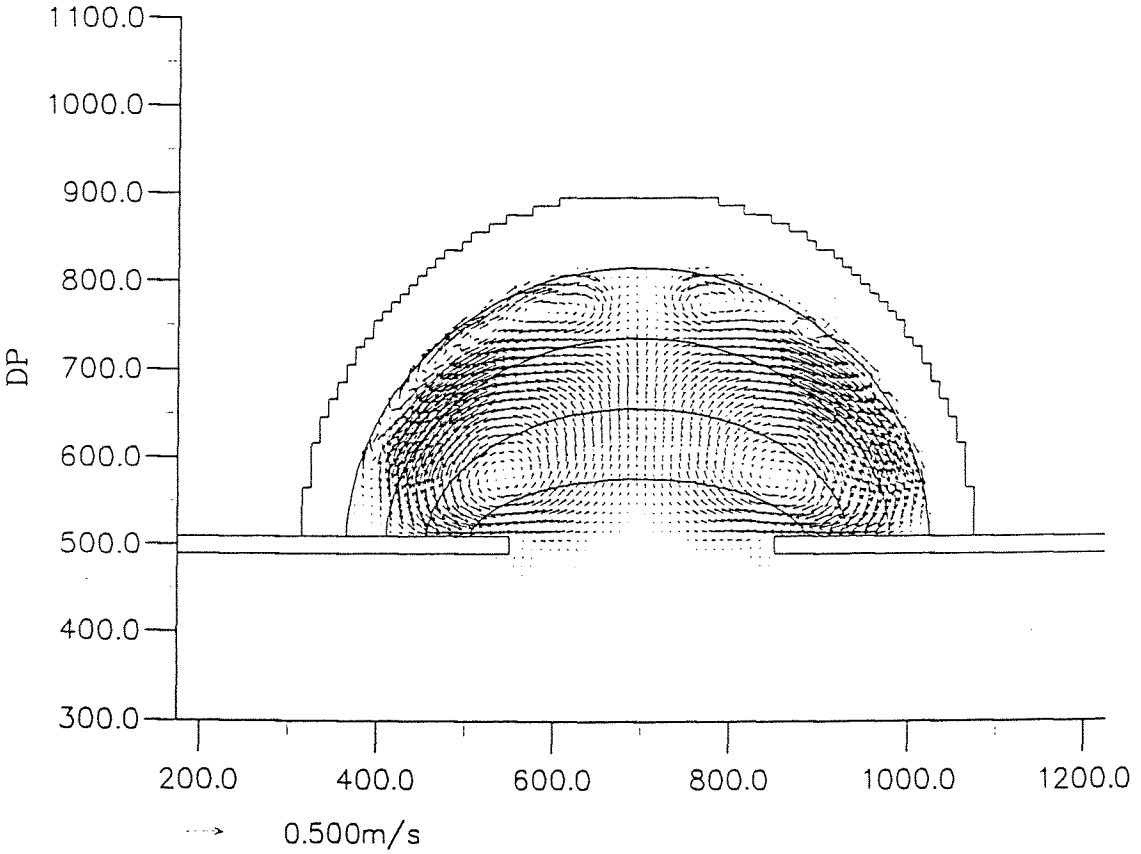

Upper graph: Hsig isolines (m) Lower graph: Flow velocity vectors (m/s) Depth contour interval is 2m	Delft3D–MOR	Appendix D.2
	Sweers' input	
DUT – EQUILIBRIUM BAYS	MaST–III	SASME

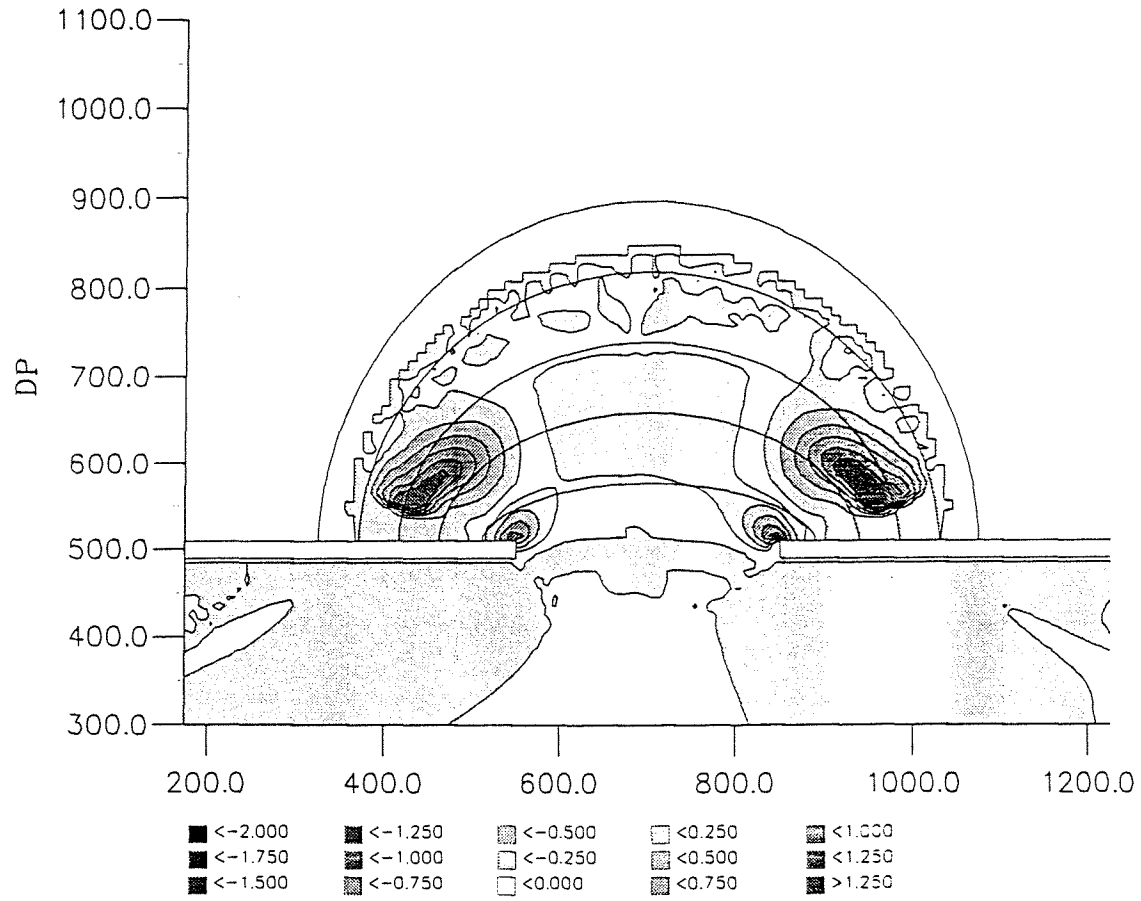

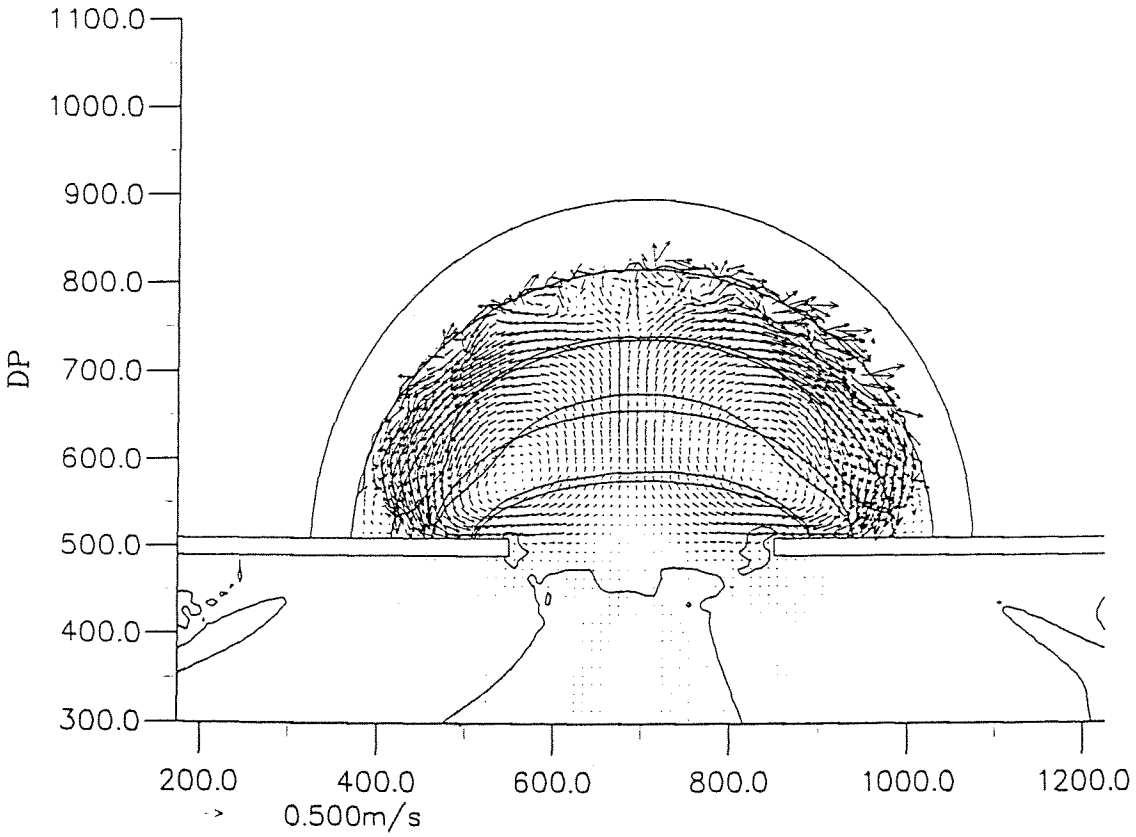

Upper graph: sedimentation and erosion (m) Lower graph: bathymetry after 7 days (m) Depth contour interval is 2m	Delft3D–MOR	Appendix D.3
	Blankers' input	
DUT – EQUILIBRIUM BAYS	MaST–III	SASME

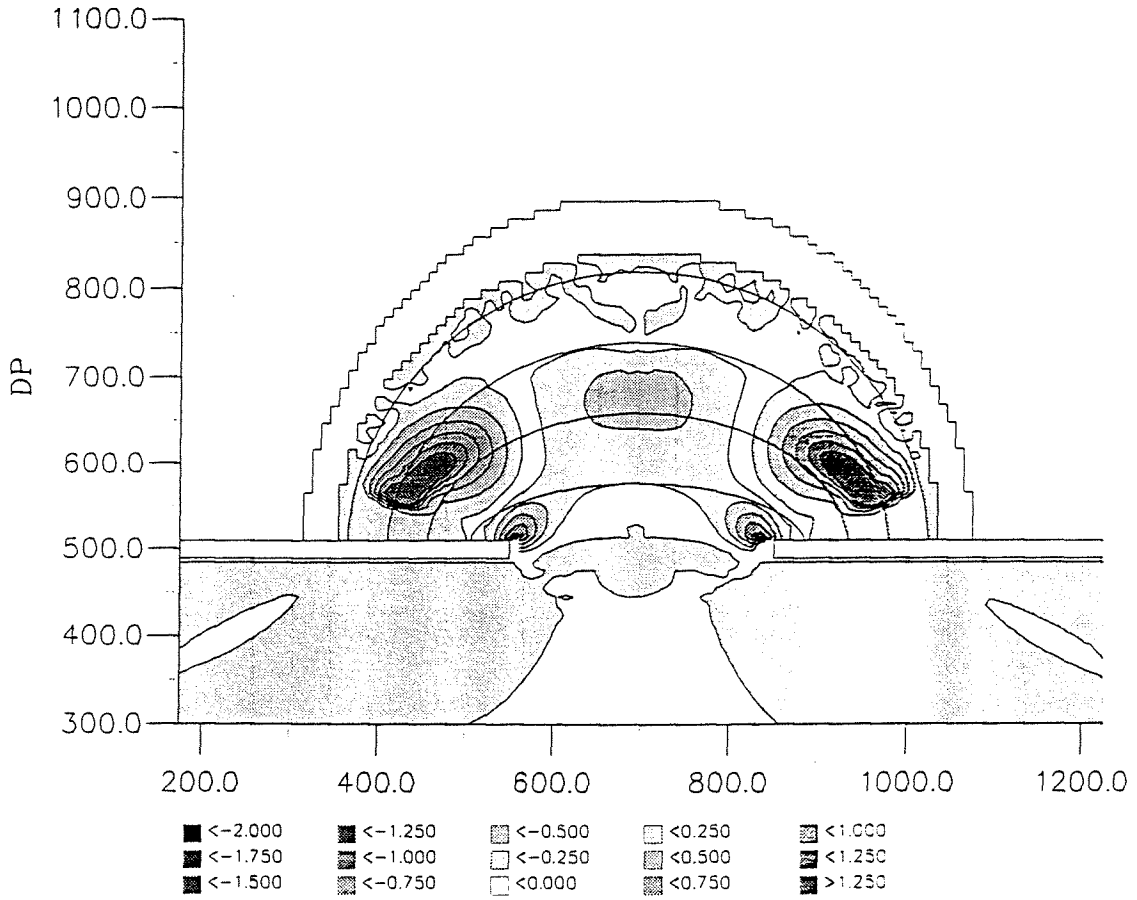

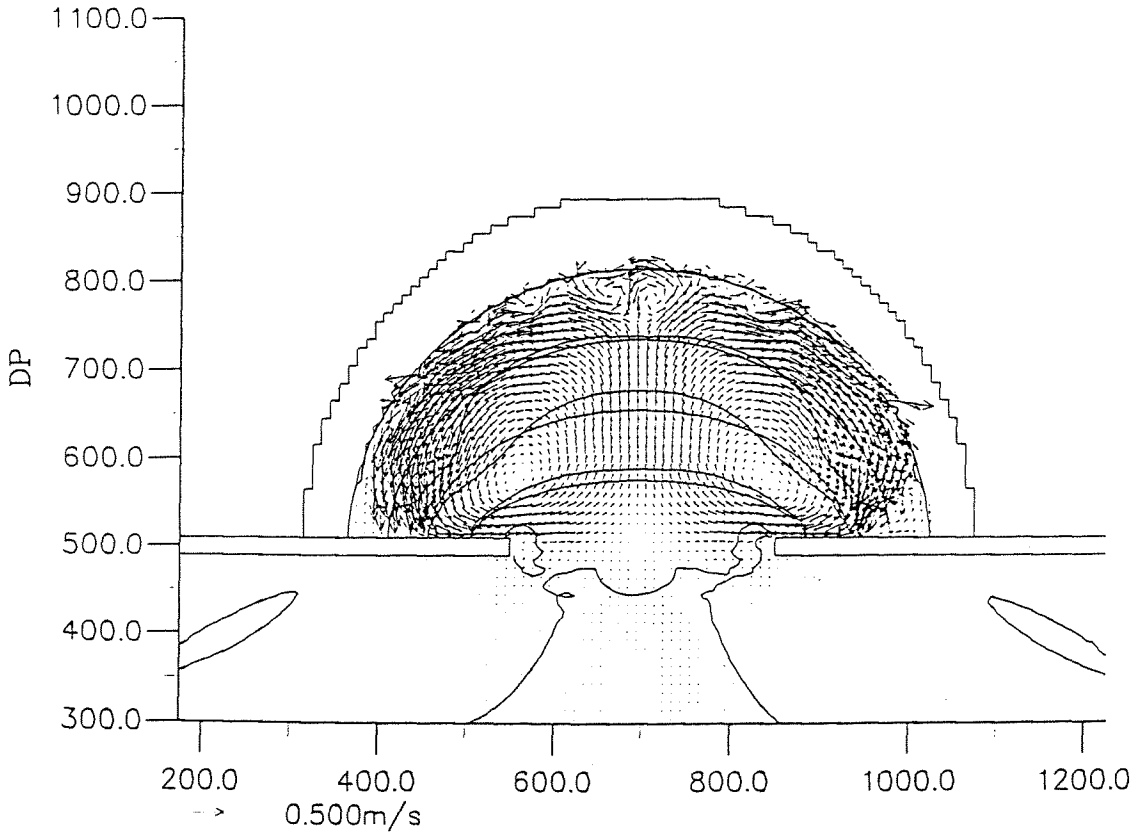

Upper graph: sedimentation and erosion (m) Lower graph: bathymetry after 7 days (m) Depth contour interval is 2m	Delft3D–MOR	Appendix D.4
	Sweers' input	
DUT – EQUILIBRIUM BAYS	MaST–III	SASME

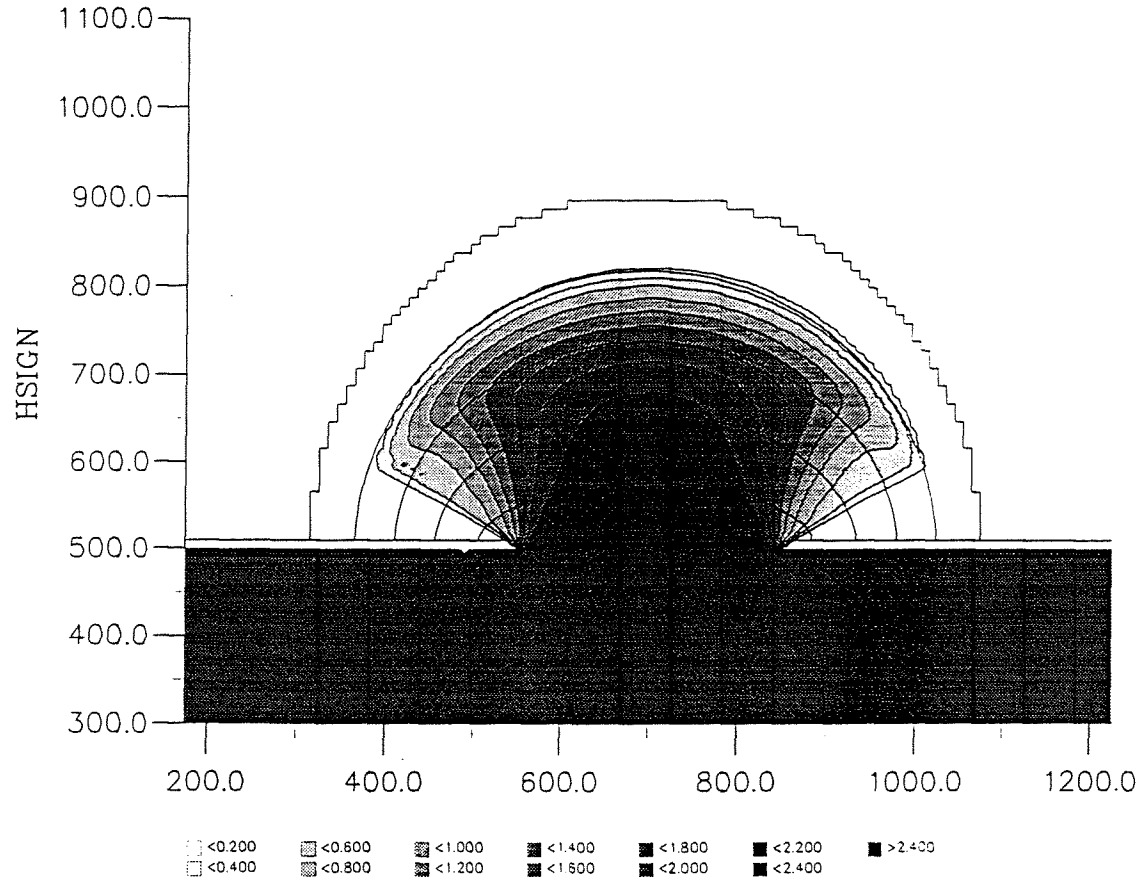

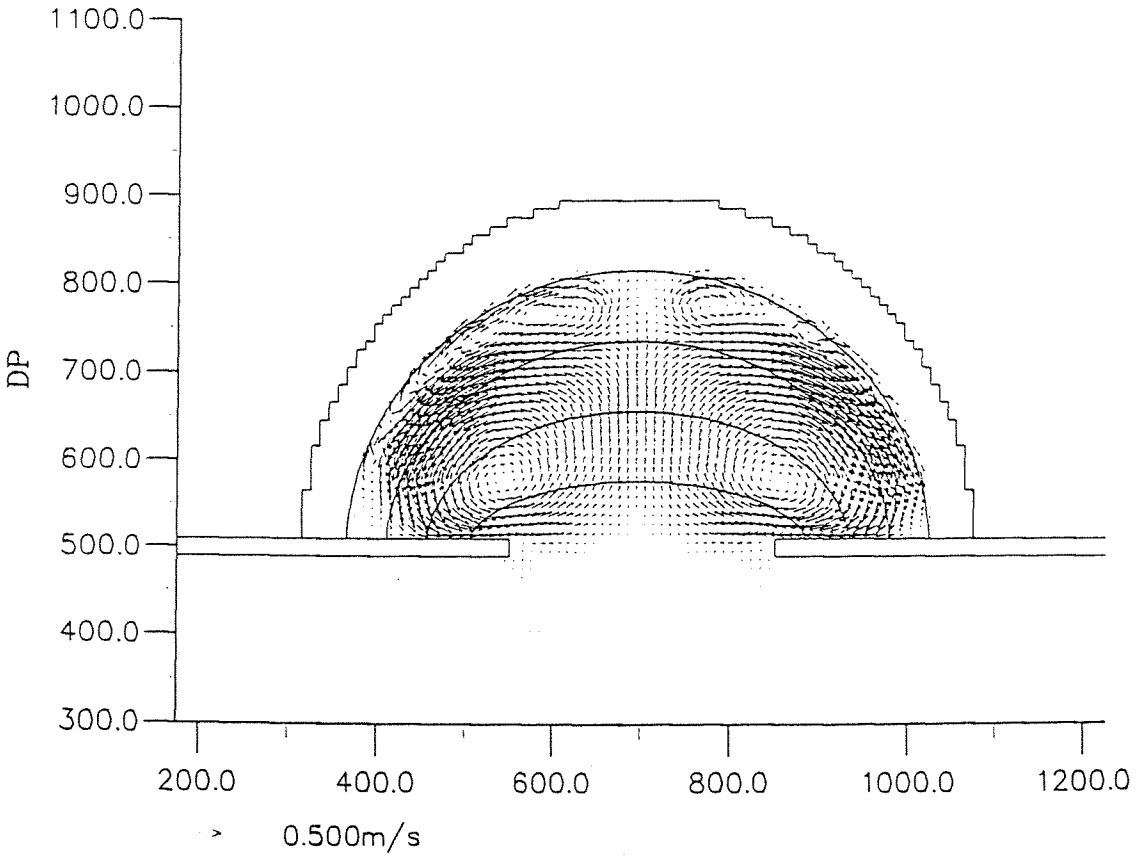

Upper graph: Hsig isolines (m) Lower graph: Flow velocity vectors (m/s) Depth contour interval is 2m	Delft3D–MOR	Appendix D.5
	Even number of cells	
DUT – EQUILIBRIUM BAYS	MaST–III	SASME

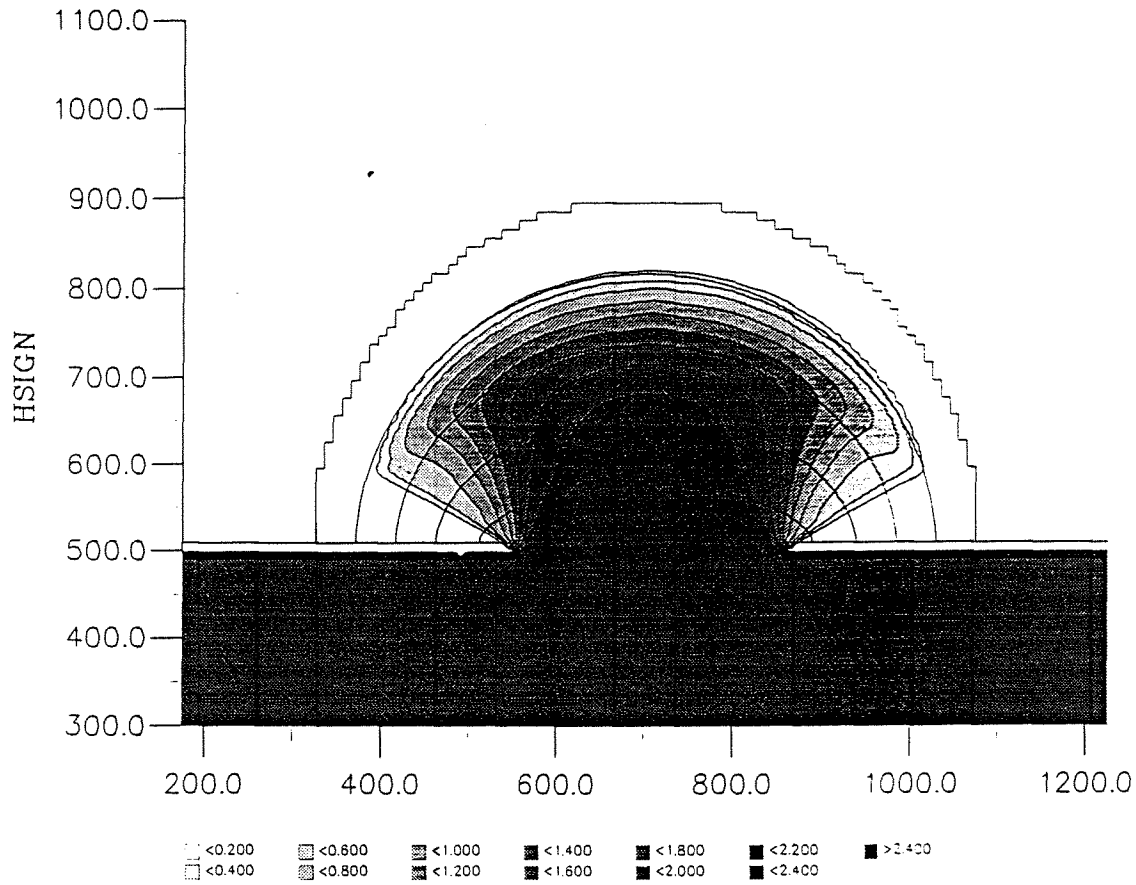

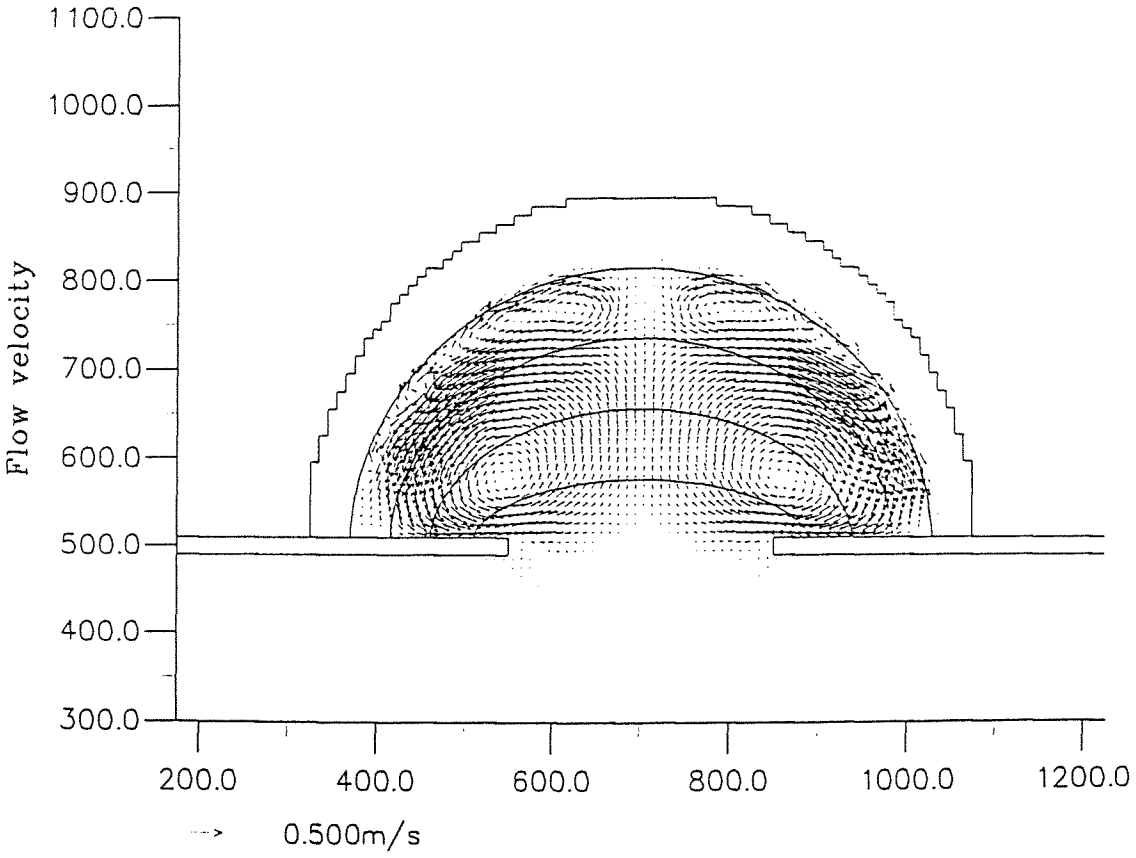

Upper graph: Hsig isolines (m) Lower graph: Flow velocity vectors (m/s) Depth contour interval is 2m	Delft3D–MOR	Appendix D.6
	Odd number of cells	
DUT – EQUILIBRIUM BAYS	MaST–III	SASME

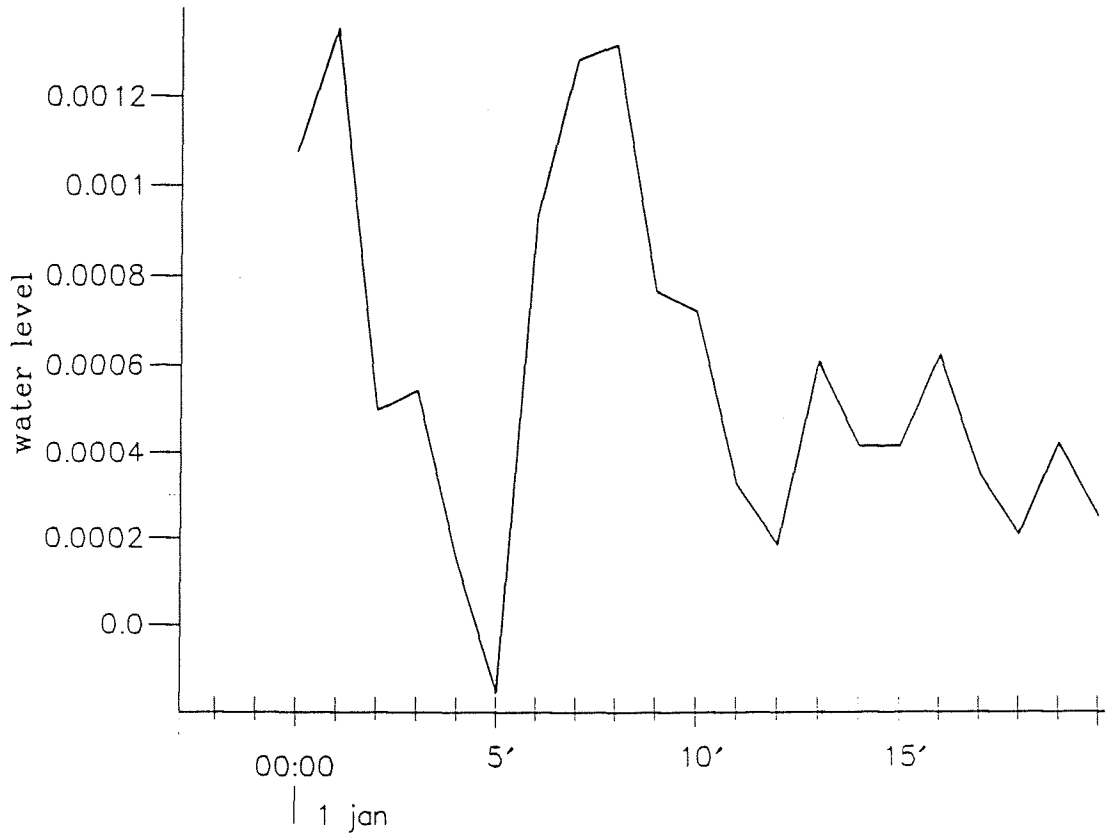

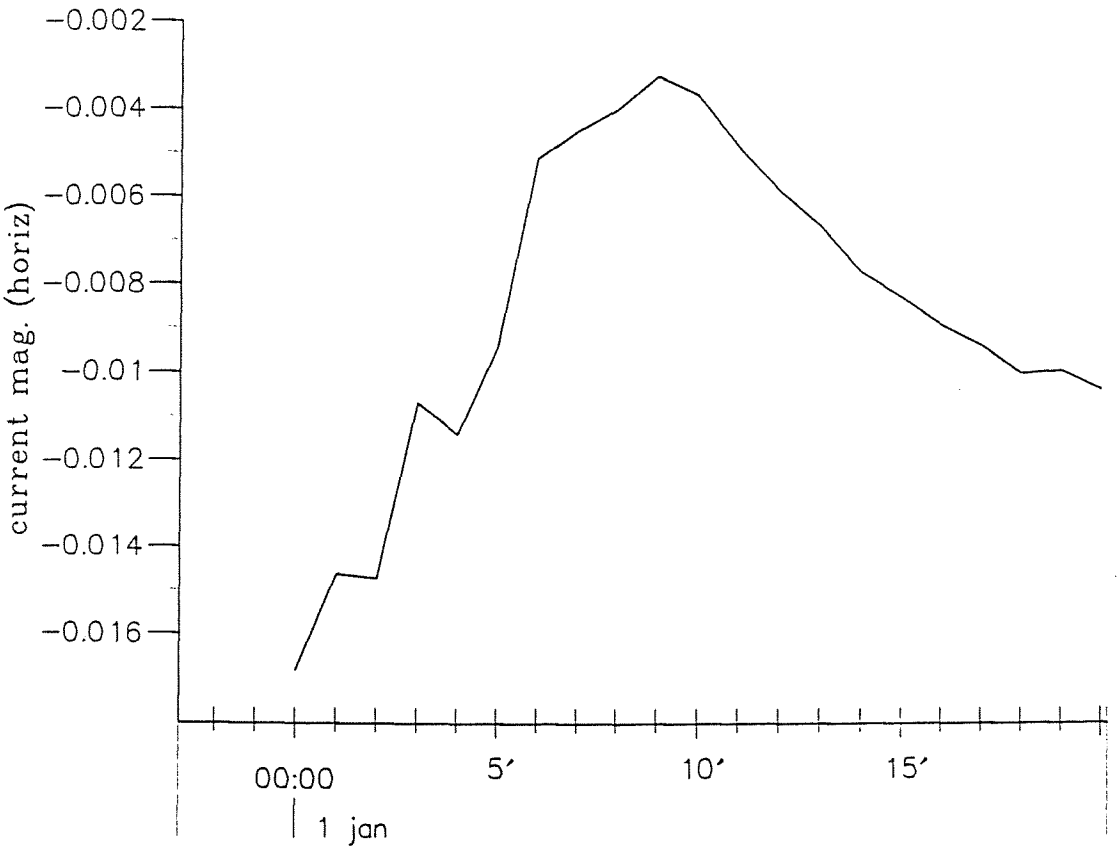

Comparison observation points Upper graph: Substracted water level (m) Lower graph: Substracted current magn. (m/s)	Delft3D–MOR	Appendix D.7
	Even number of cells	
DUT – EQUILIBRIUM BAYS	MaST–III	SASME

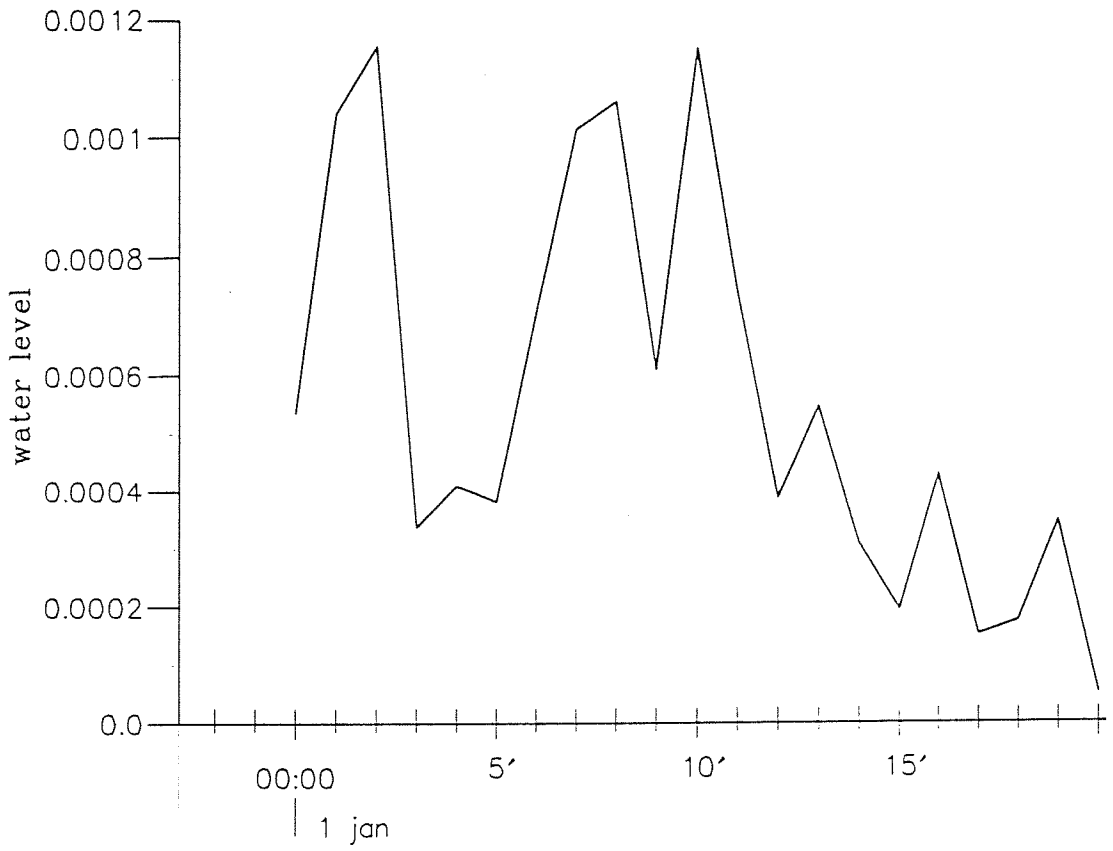

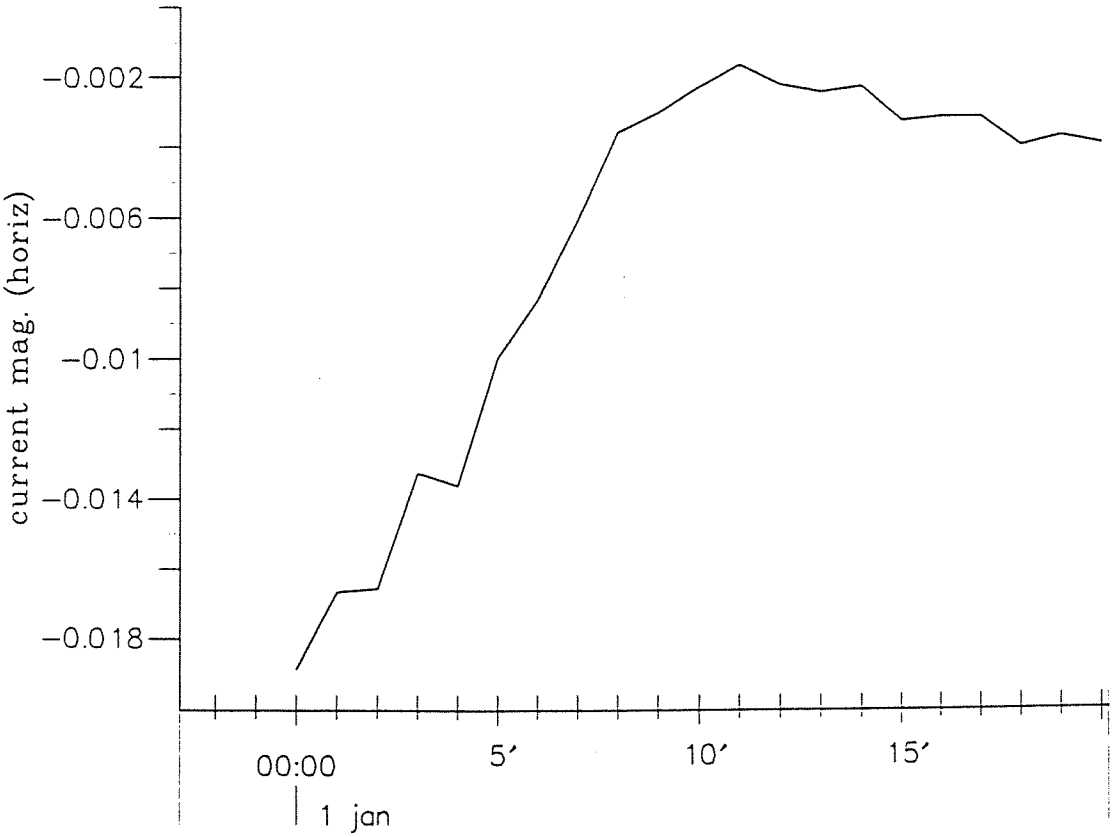

Comparison observation points Upper graph: Substracted water level (m) Lower graph: Substracted current magn. (m/s)	Delft3D–MOR	Appendix D.8
	Odd number of cells	
DUT – EQUILIBRIUM BAYS	MaST–III	SASME

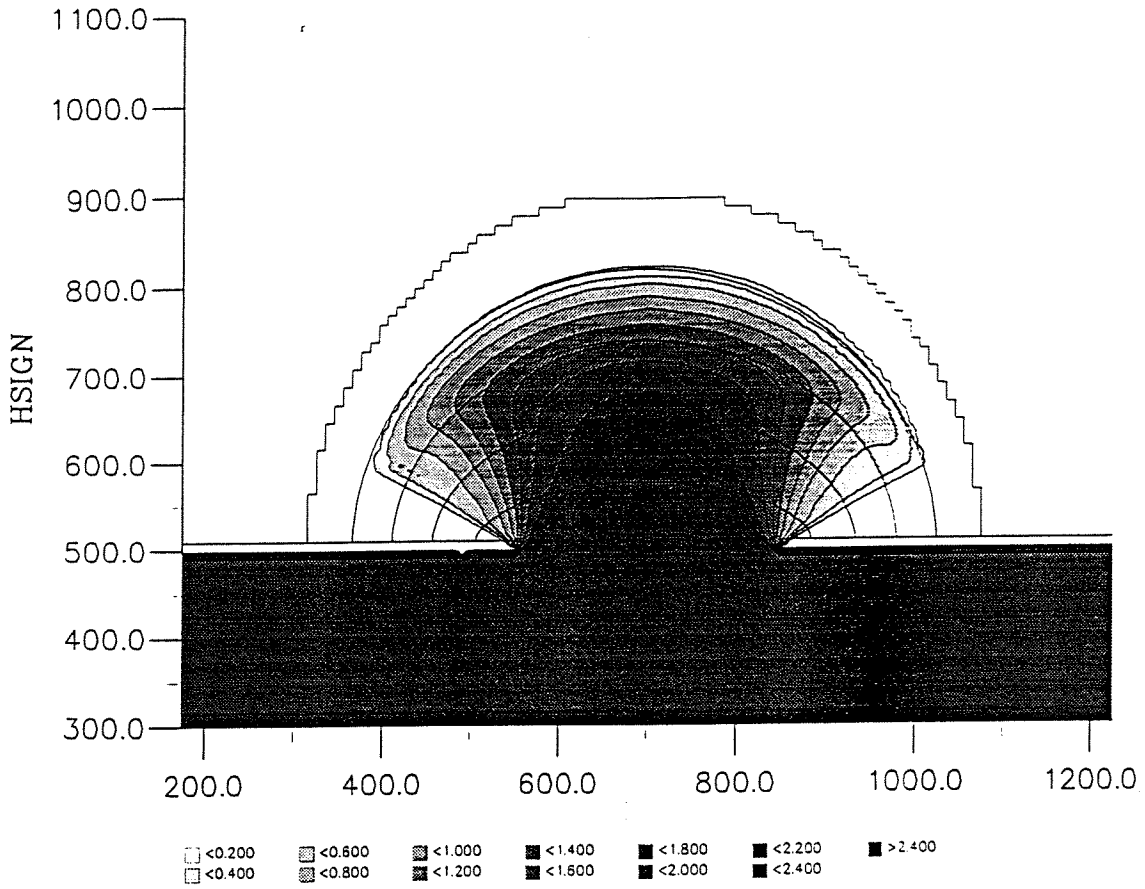

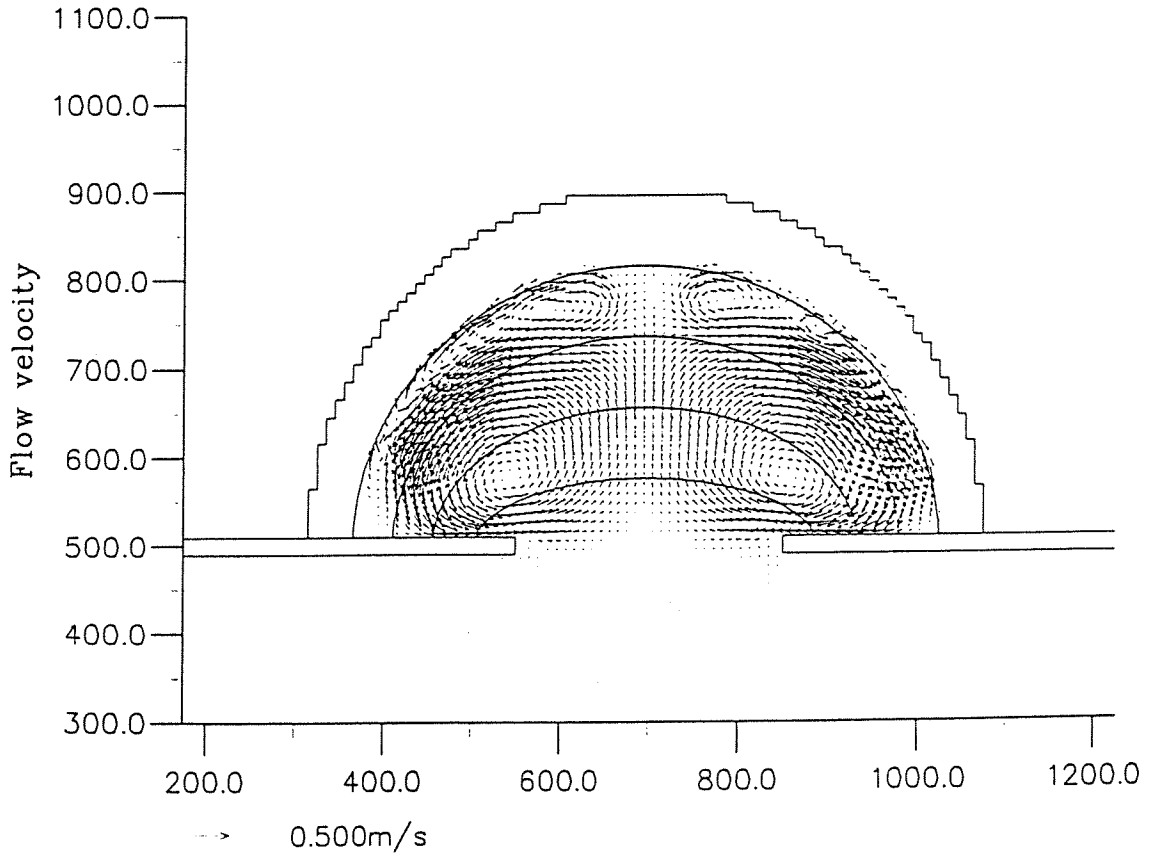

Upper graph: Hsig isolines (m) Lower graph: Flow velocity vectors (m/s) Depth contour interval is 2m	Delft3D–MOR	Appendix D.9
	Riemann boundary (zero)	
DUT – EQUILIBRIUM BAYS	MaST–III	SASME

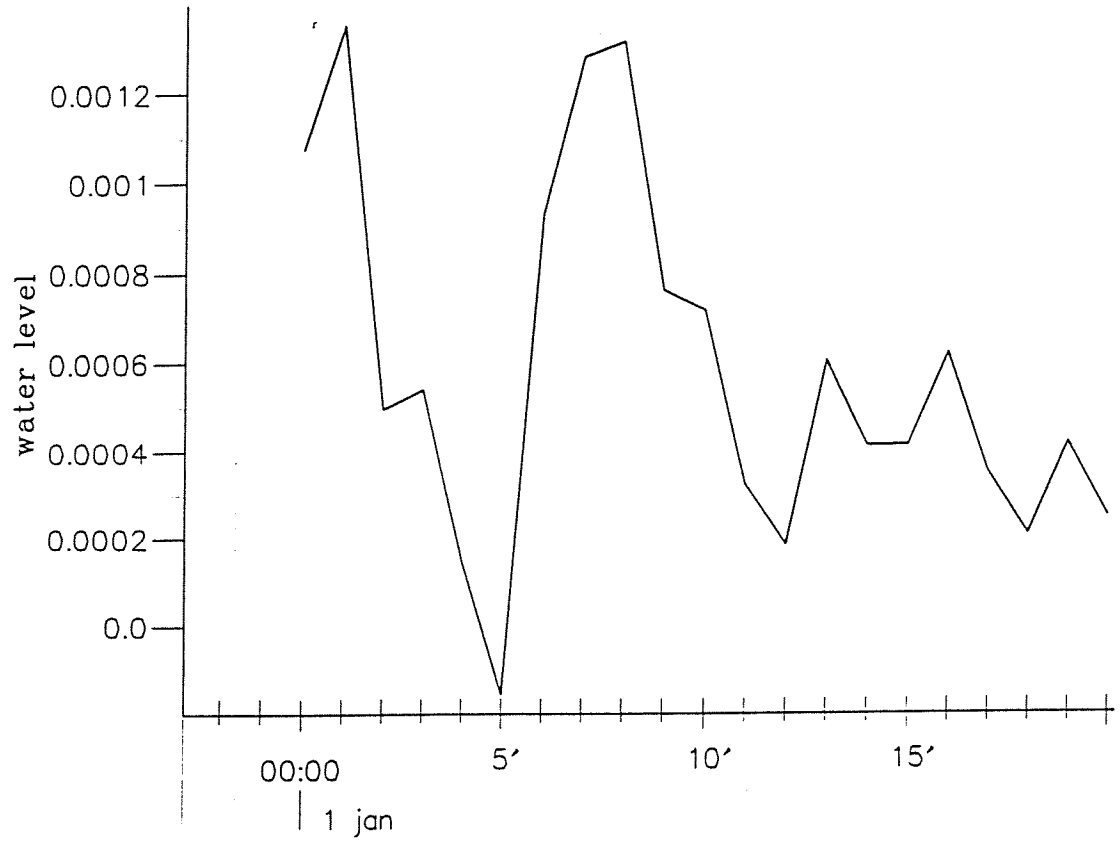

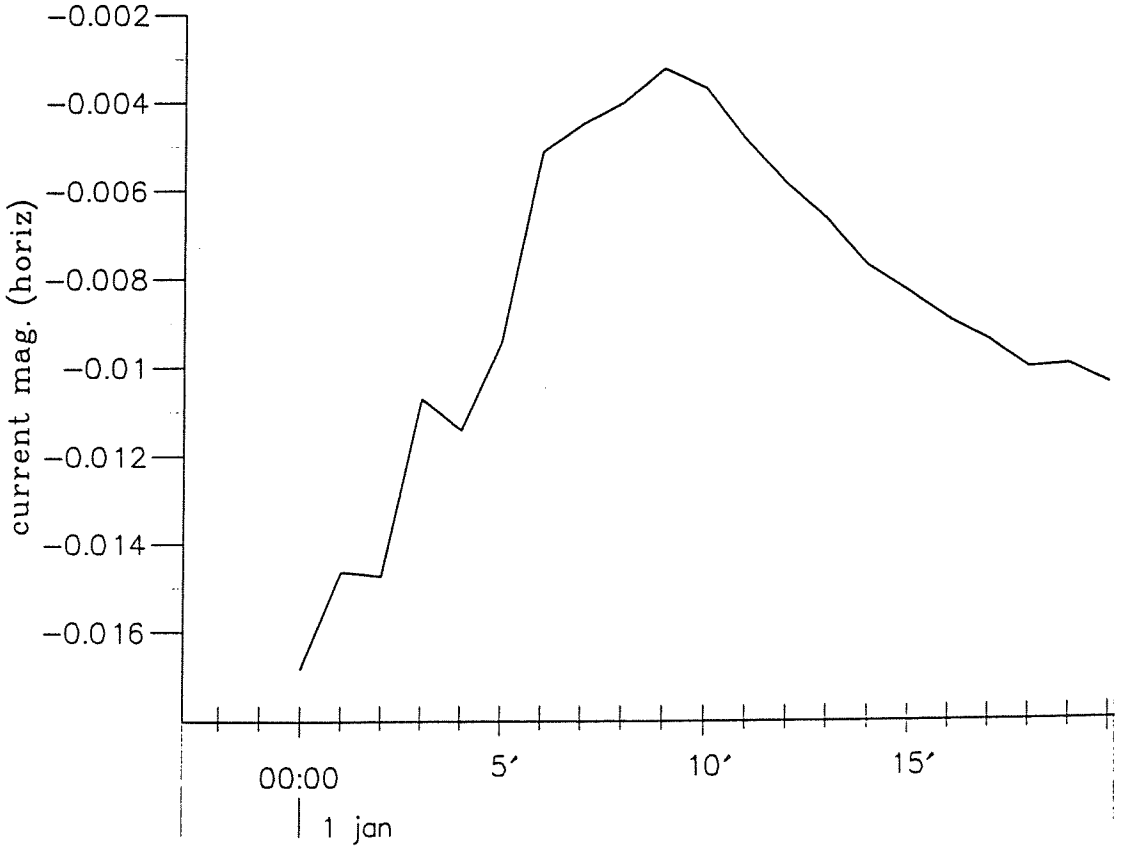

Comparison observation points Upper graph: Substracted water level (m) Lower graph: Substracted current magn. (m/s)	Delft3D–MOR	Appendix D.10
	Riemann boundary (zero)	
DUT – EQUILIBRIUM BAYS	MaST–III	SASME

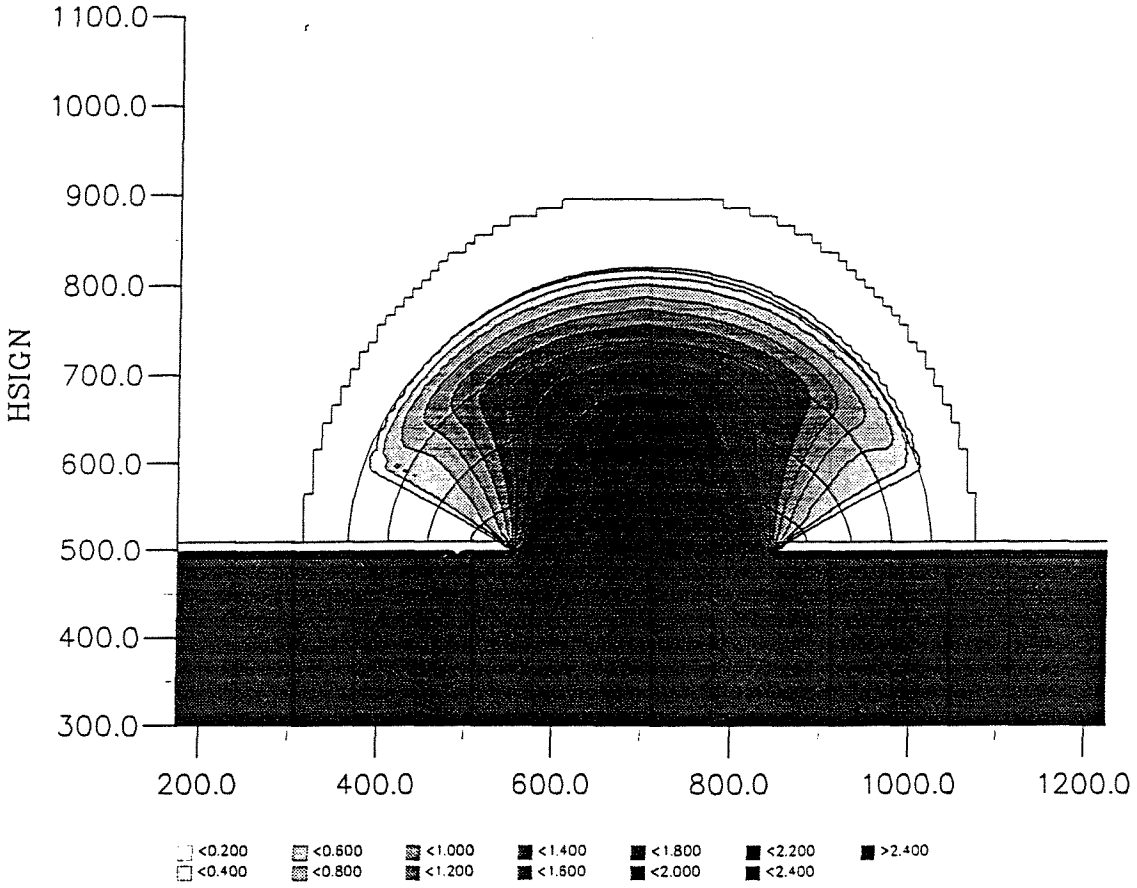

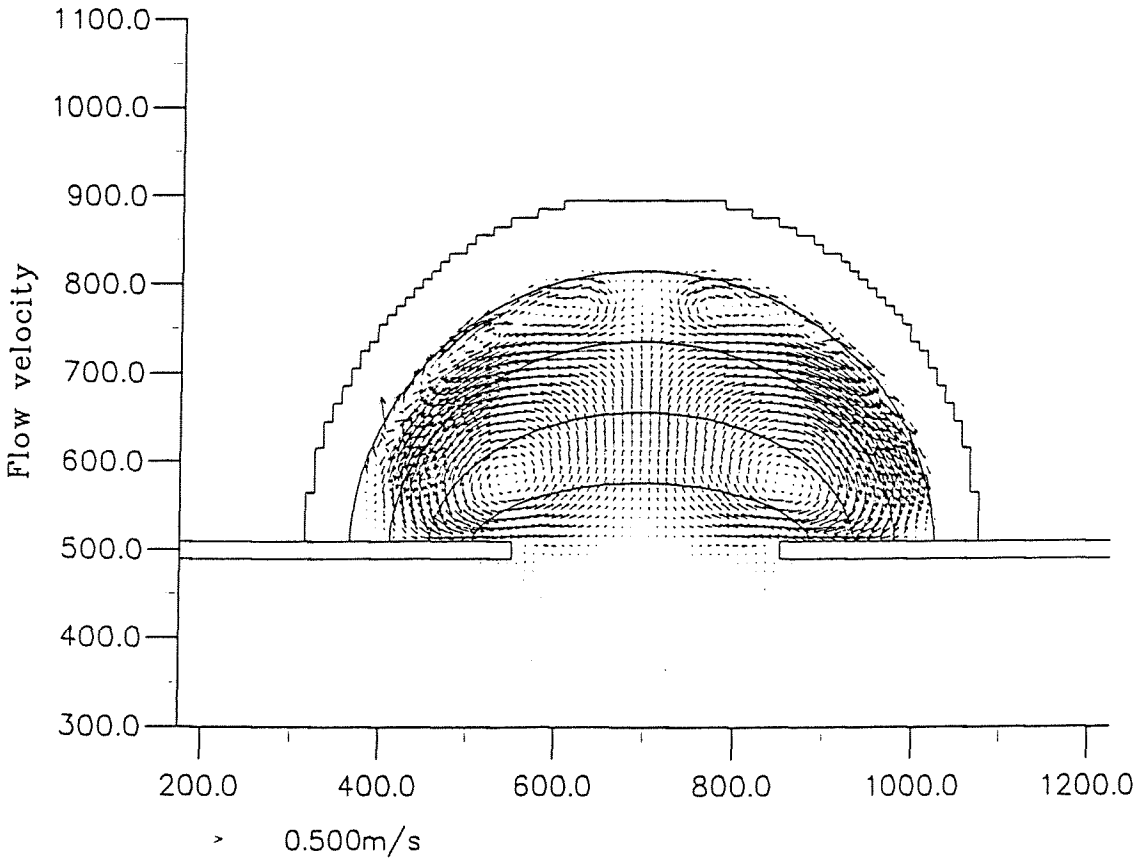

Upper graph: Hsig isolines (m) Lower graph: Flow velocity vectors (m/s) Depth contour interval is 2m	Delft3D–MOR	Appendix D.11
	Riemann boundary (non–zero)	
DUT – EQUILIBRIUM BAYS	MaST–III	SASME

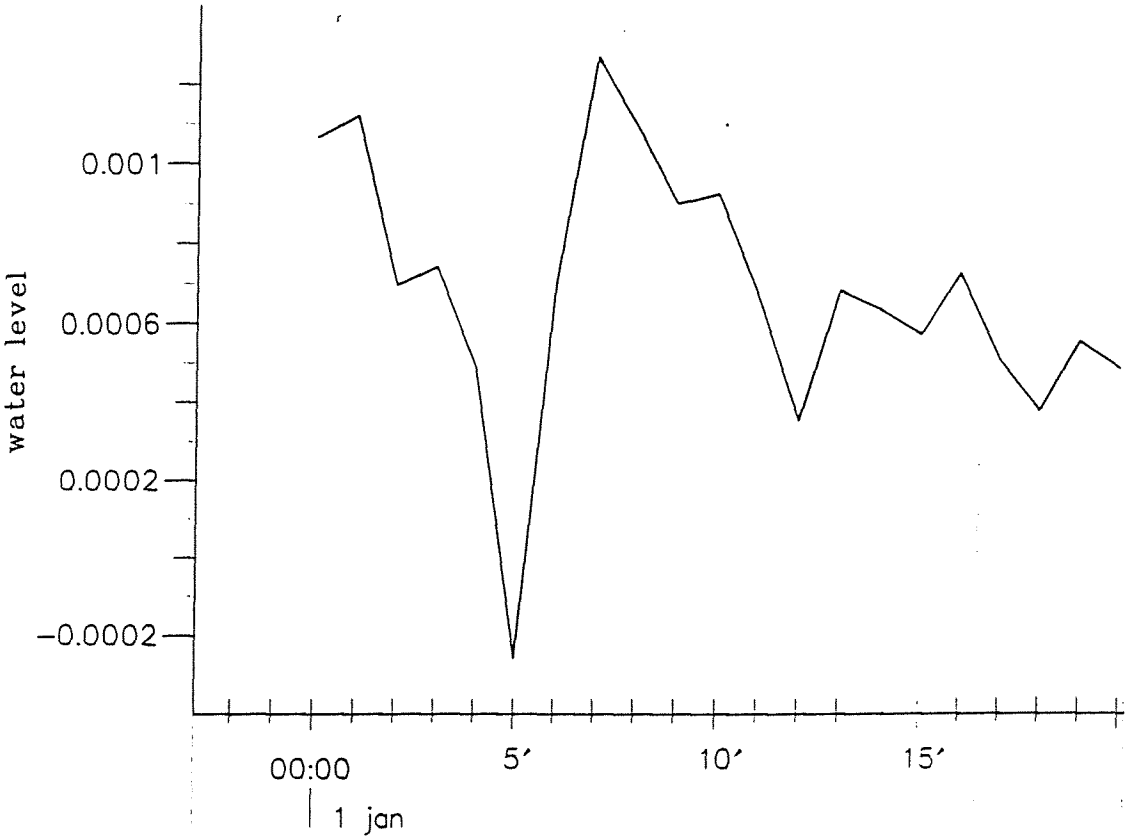

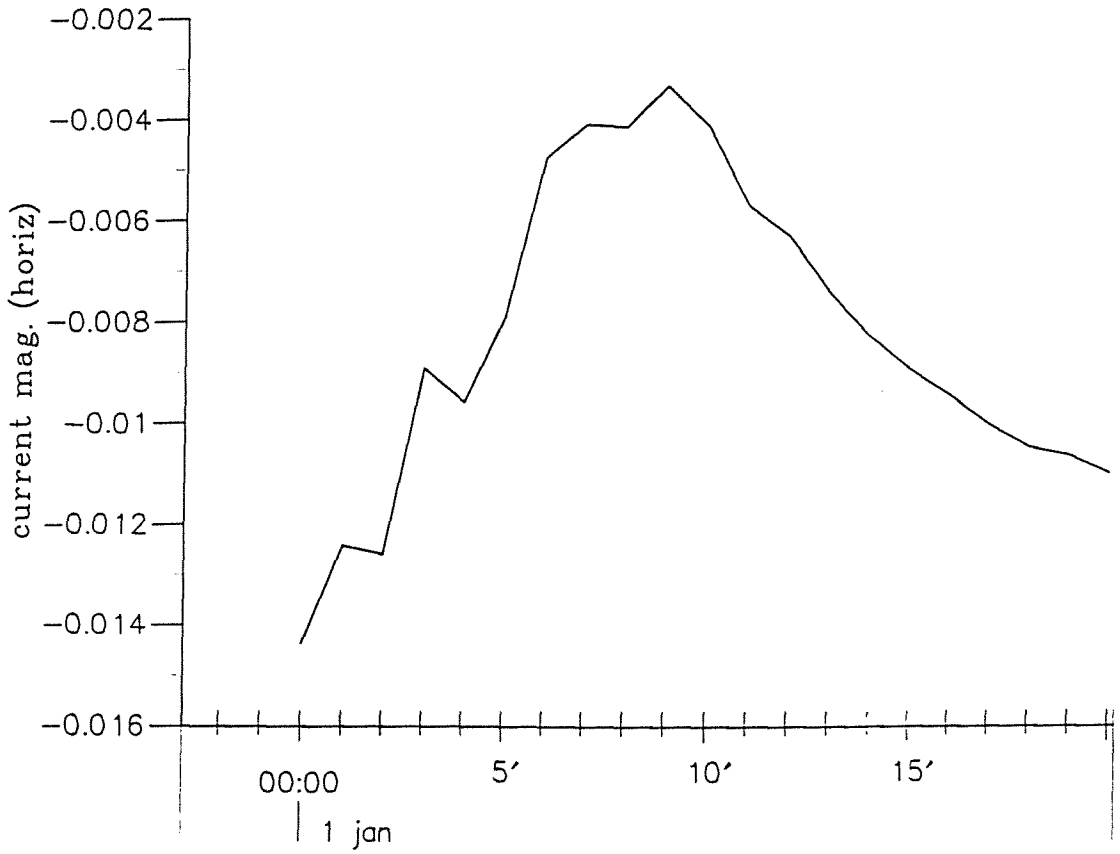

Comparison observation points Upper graph: Substracted water level (m) Lower graph: Substracted current magn. (m/s)	Delft3D–MOR	Appendix D.12
	Riemann boundary (non–zero)	
DUT – EQUILIBRIUM BAYS	MaST–III	SASME

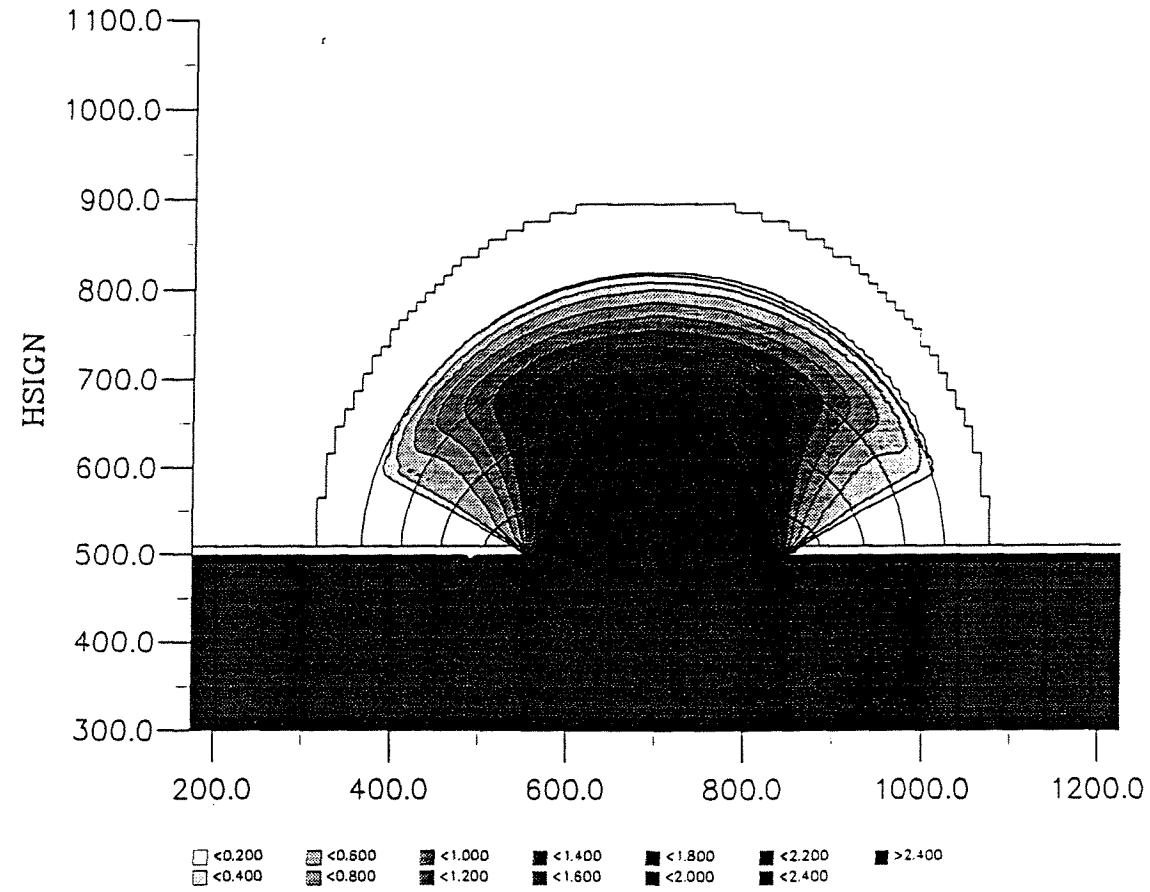

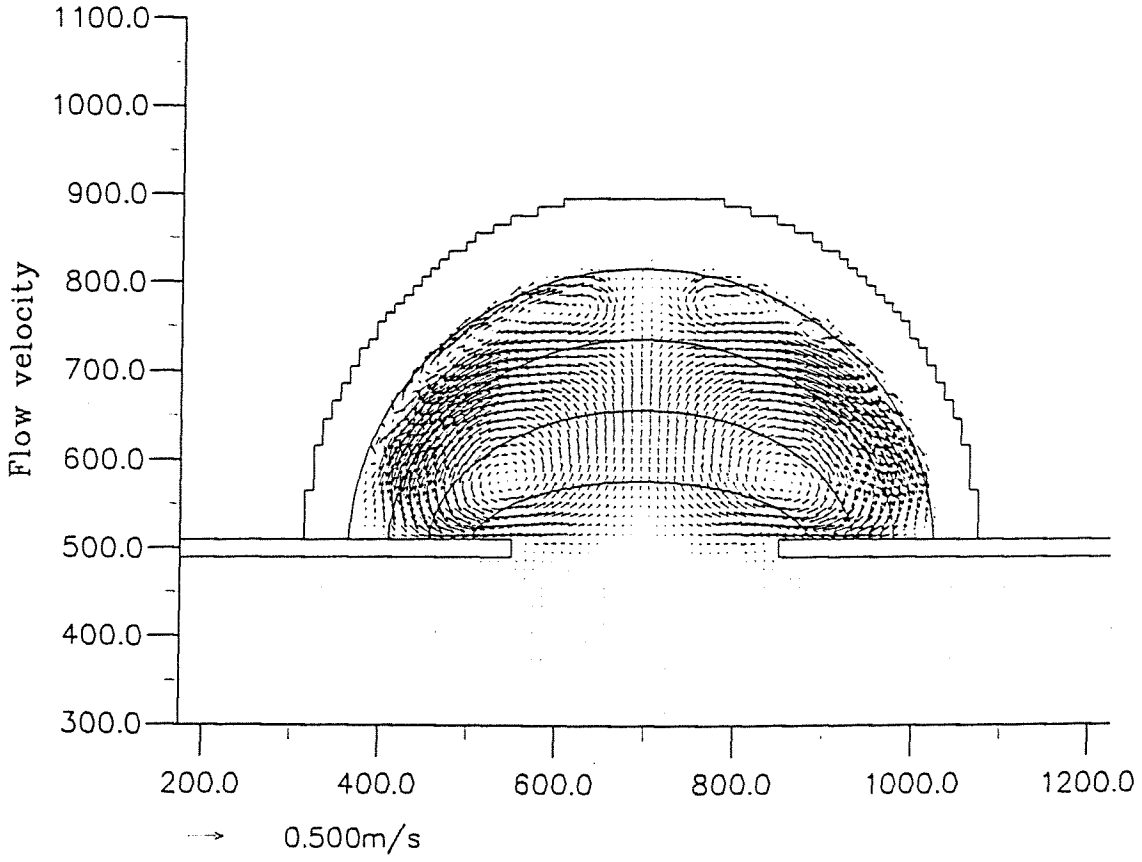

Upper graph: Hsig isolines (m) Lower graph: Flow velocity vectors (m/s) Depth contour interval is 2m	Delft3D–MOR	Appendix D.13
	Water level boundary (zero)	
DUT – EQUILIBRIUM BAYS	MaST–III	SASME

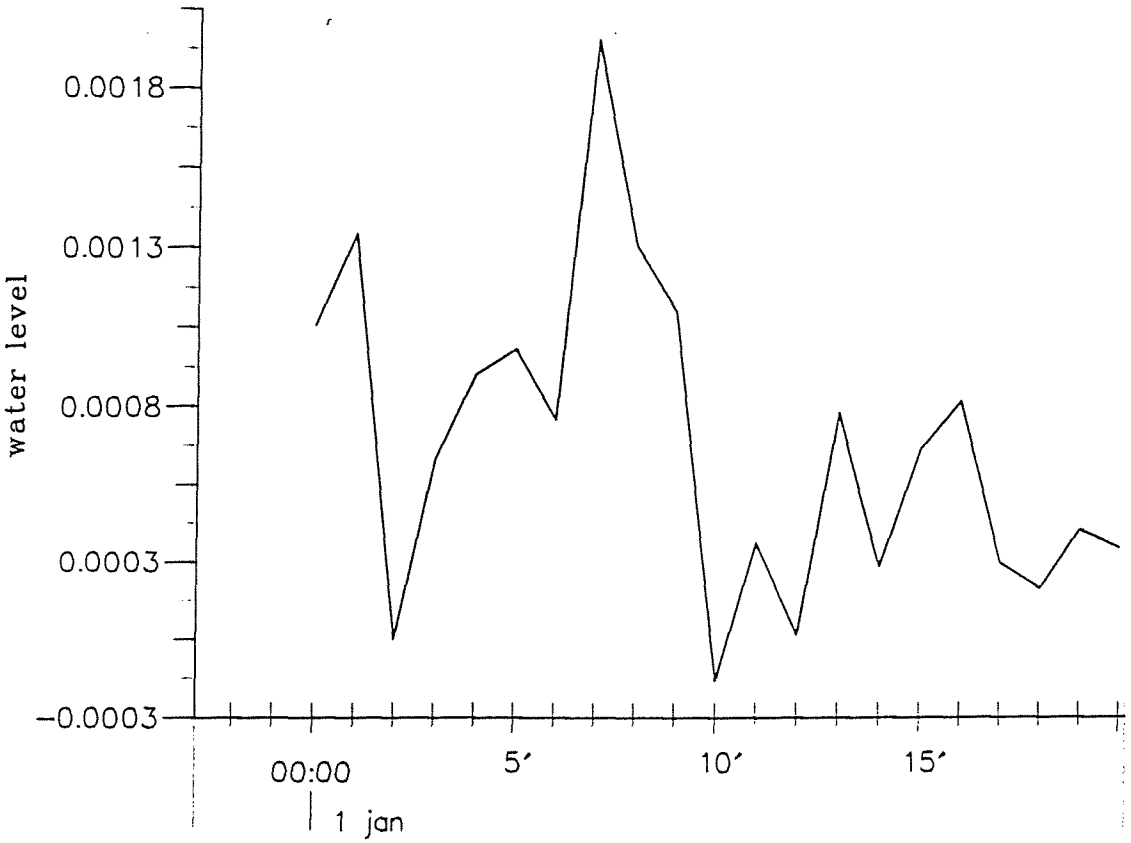

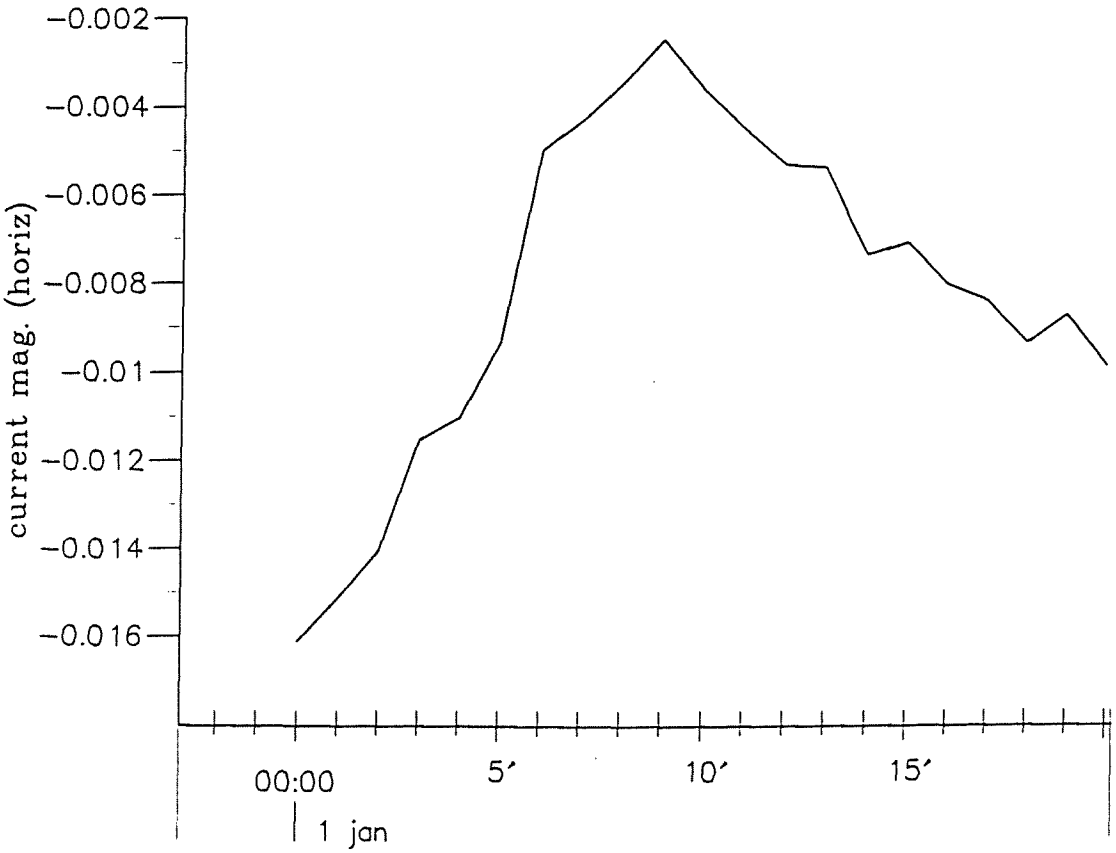

Comparison observation points Upper graph: Substracted water level (m) Lower graph: Substracted current magn. (m/s)	Delft3D-MOR	Appendix D.14
	Water level boundary (zero)	
DUT – EQUILIBRIUM BAYS	MaST-III	SASME

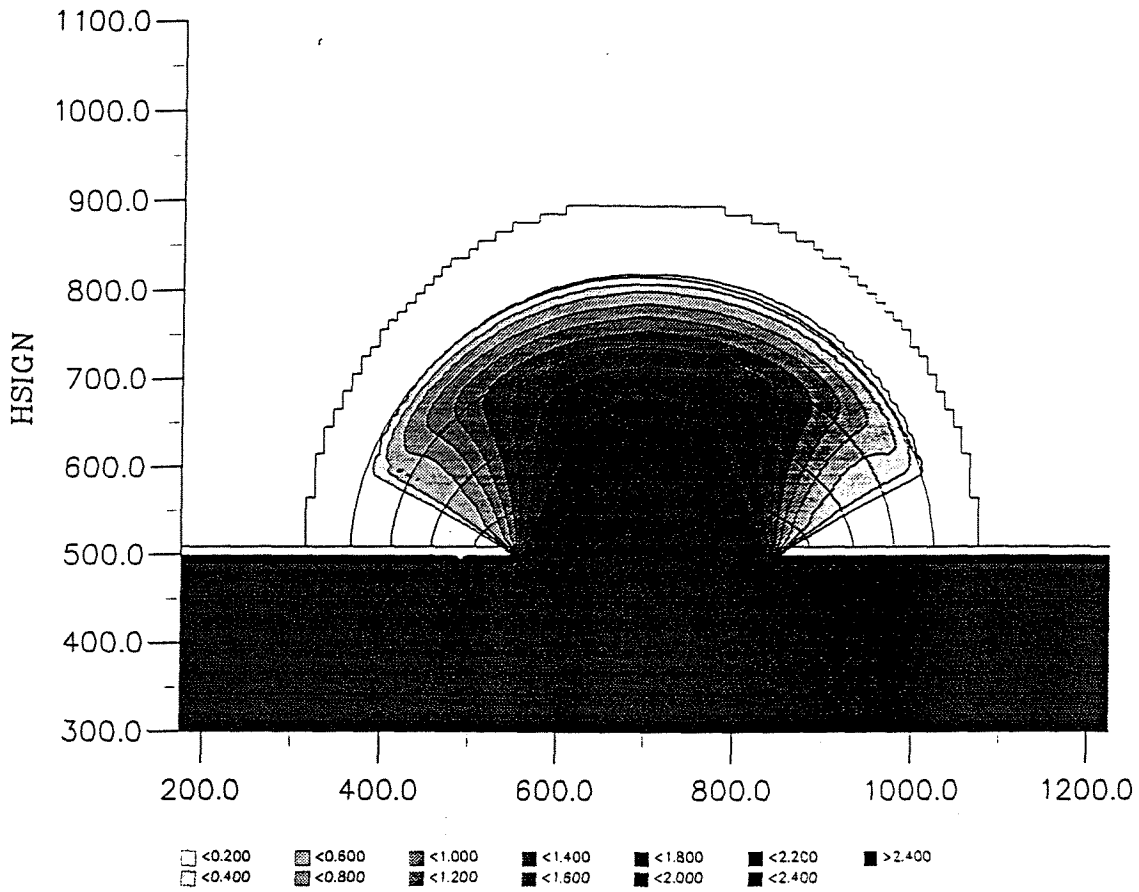

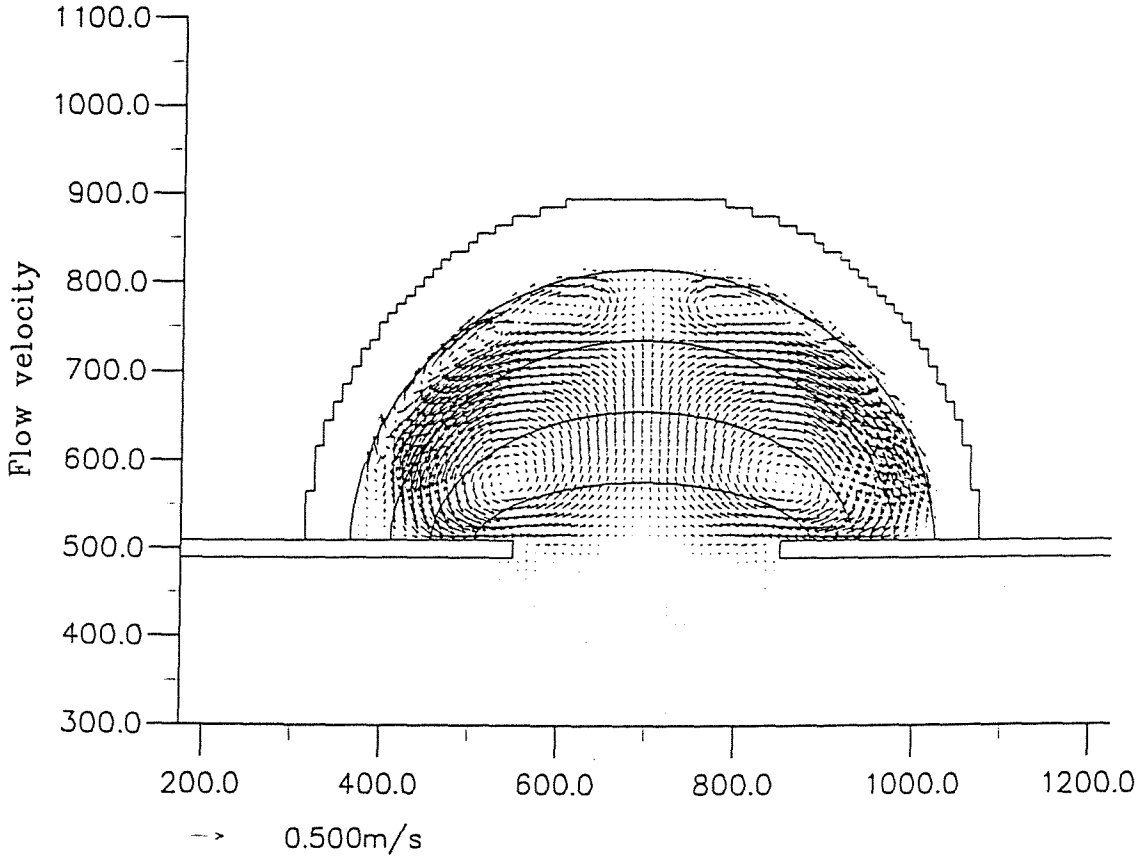

Upper graph: Hsig isolines (m) Lower graph: Flow velocity vectors (m/s) Depth contour interval is 2m	Delft3D–MOR	Appendix D.15
	Water level boundary (non–zero)	
DUT – EQUILIBRIUM BAYS	MaST–III	SASME

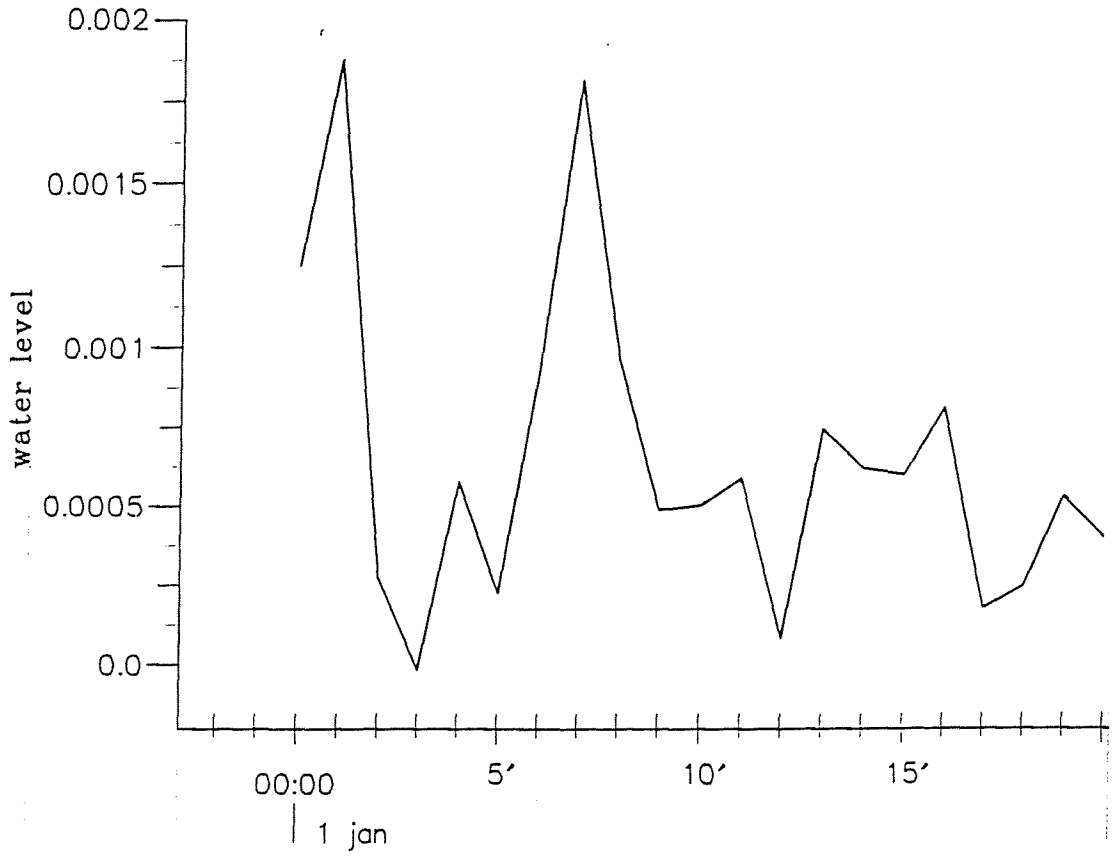

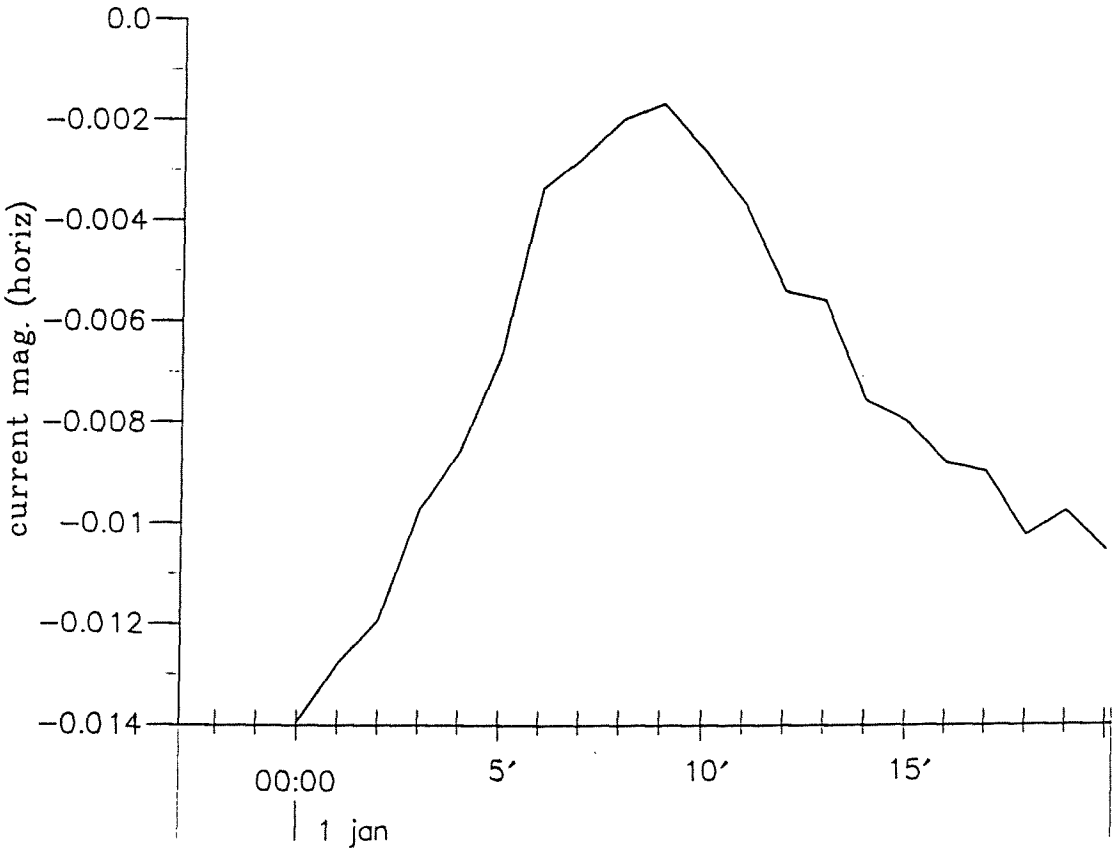

Comparison observation points Upper graph: Substracted water level (m) Lower graph: Substracted current magn. (m/s)	Delft3D–MOR	Appendix D.16
	Water level boundary (non–zero)	
DUT – EQUILIBRIUM BAYS	MaST–III	SASME

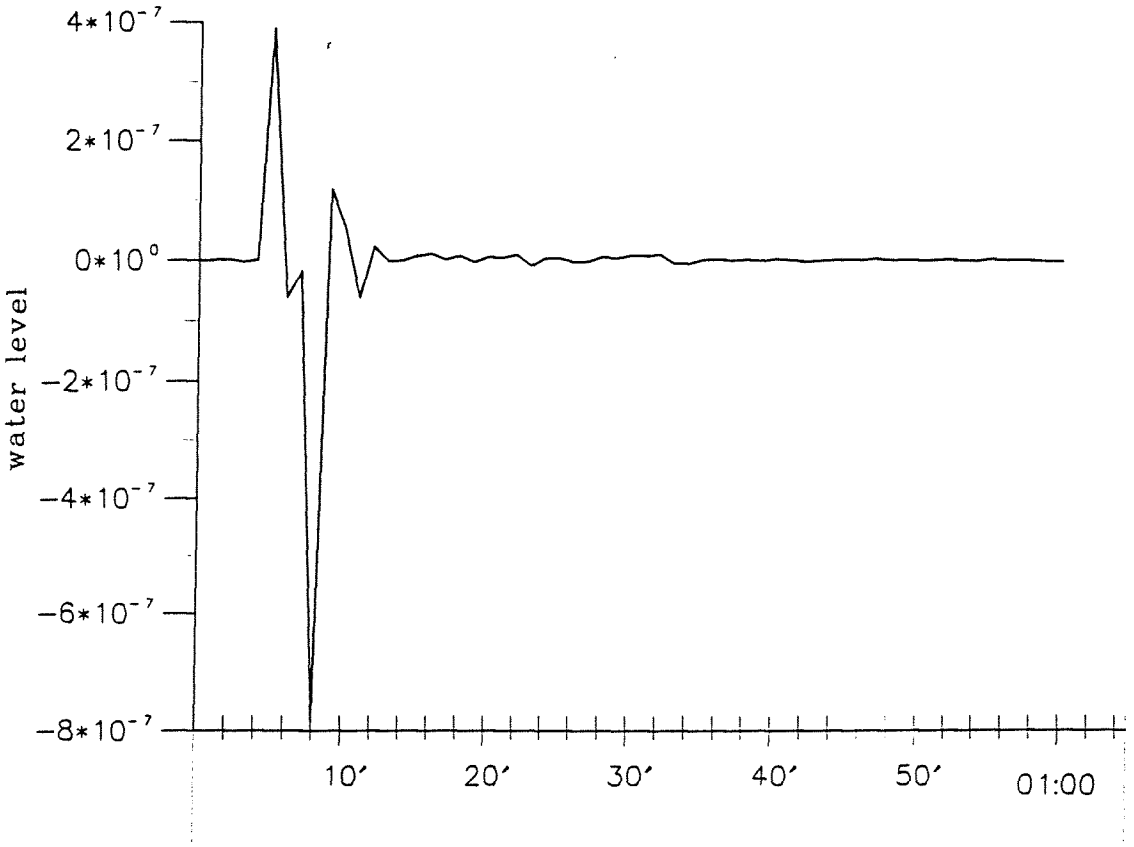

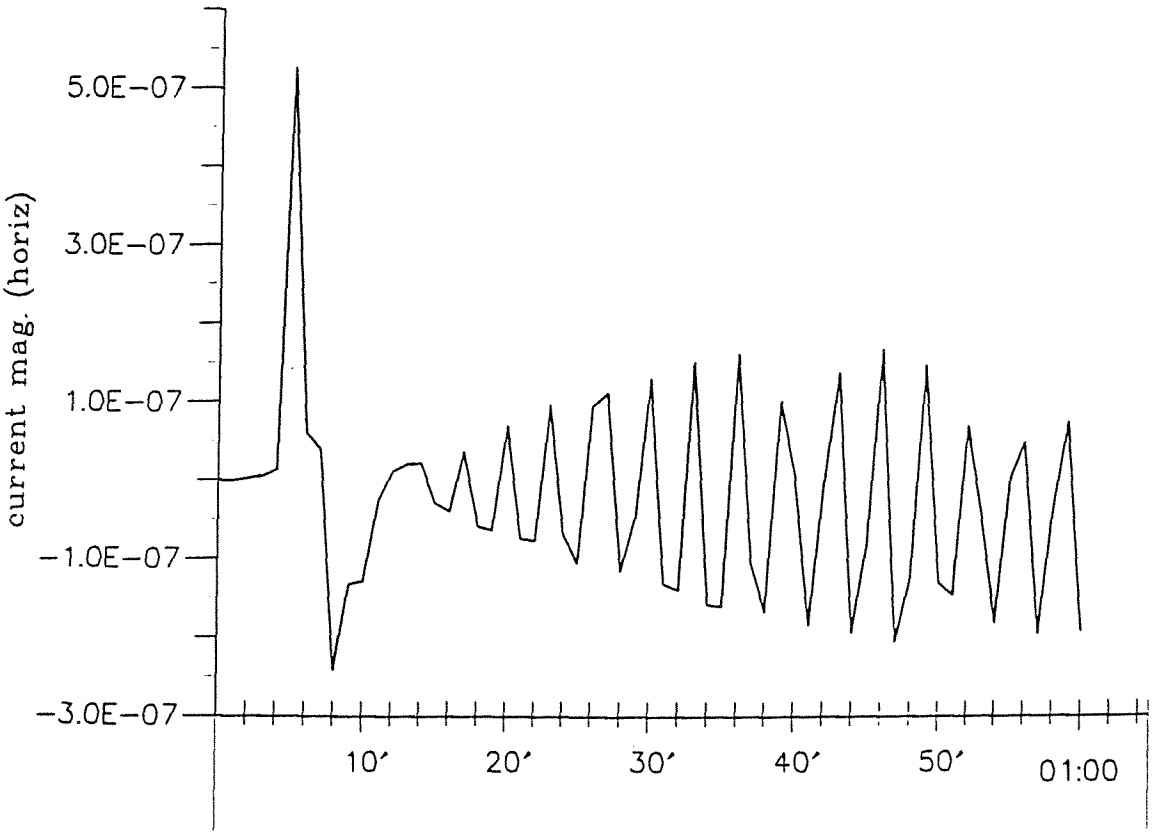

Comparison observation points Upper graph: Substracted water level (m) Lower graph: Substracted current magn. (m/s)	Delft3D–MOR	Appendix D.17
	Linear depth gradient	
DUT – EQUILIBRIUM BAYS	MaST–III	SASME

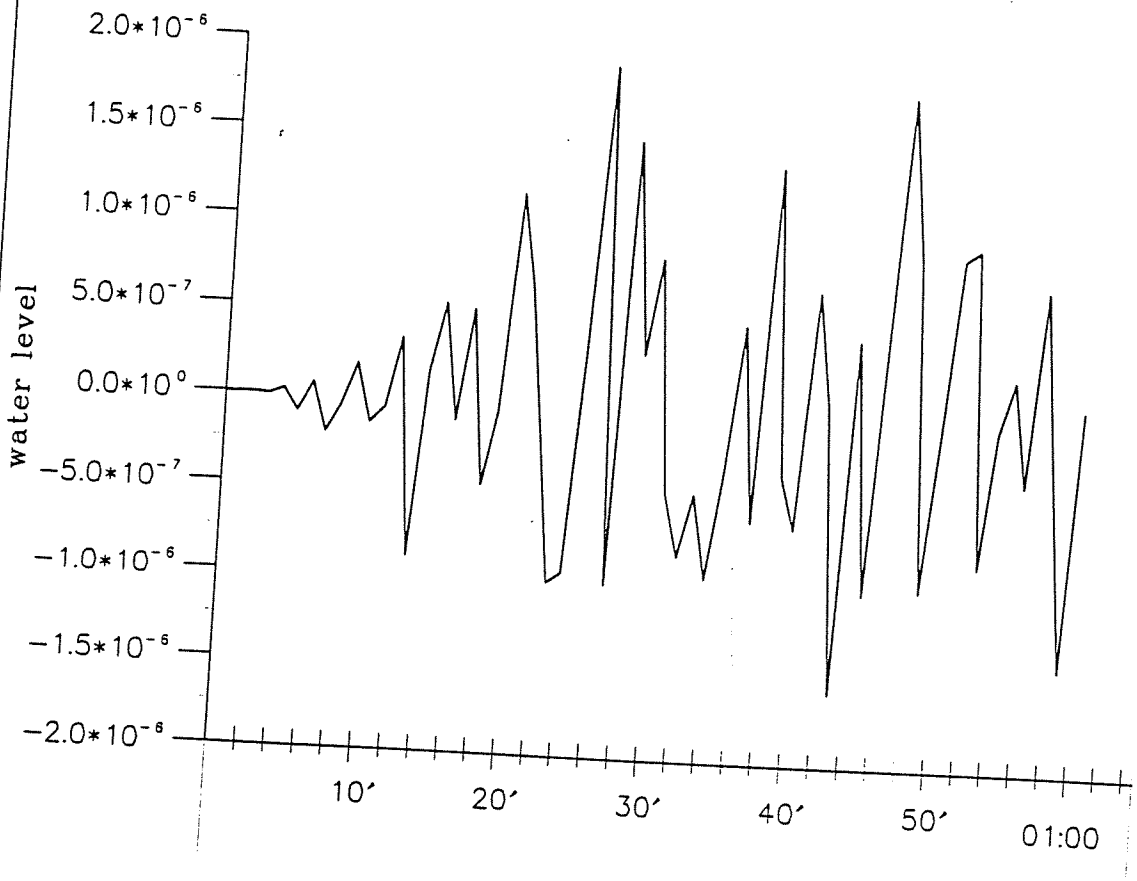

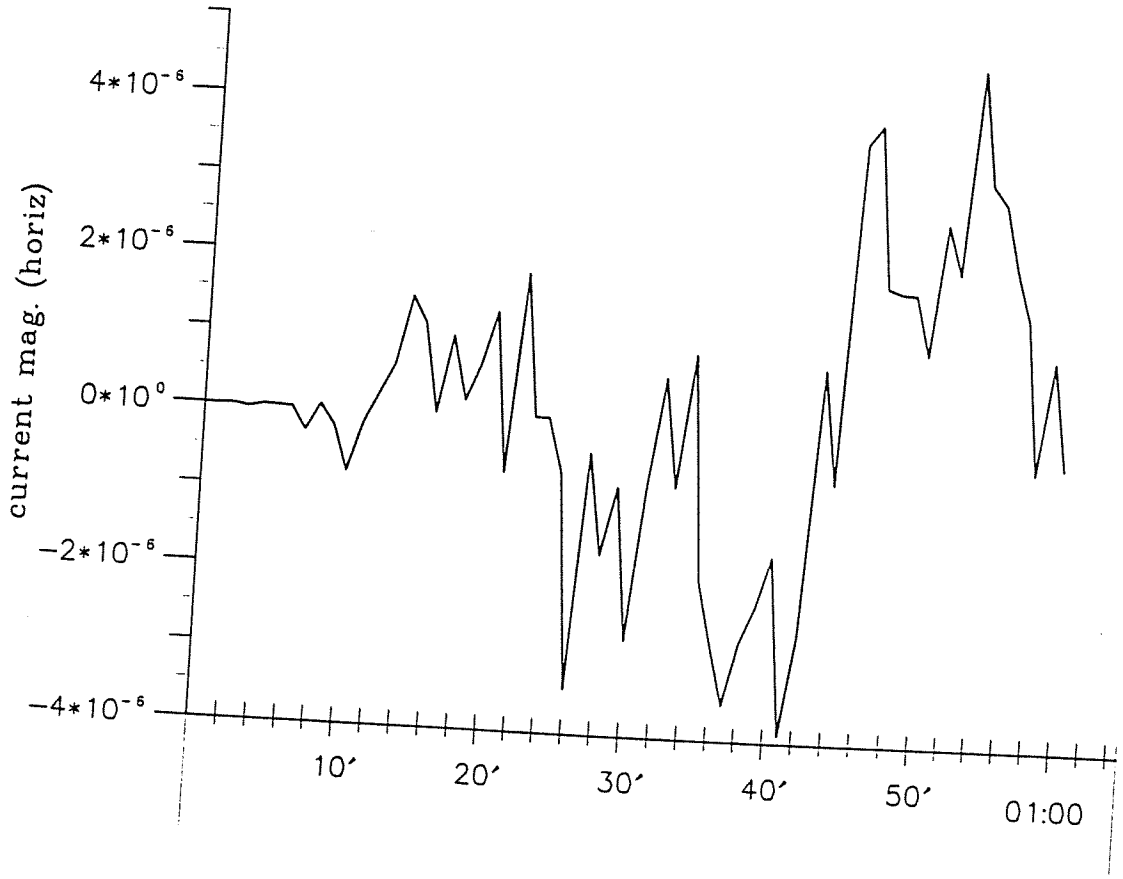

Comparison observation points
Upper graph: Substracted water level (m)
Lower graph: Substracted current magn. (m/s)

Delft3D–MOR	Appendix D.18
Flume calculation	
MaST–III	SASME

DUT – EQUILIBRIUM BAYS

Appendix D.19 - Water level

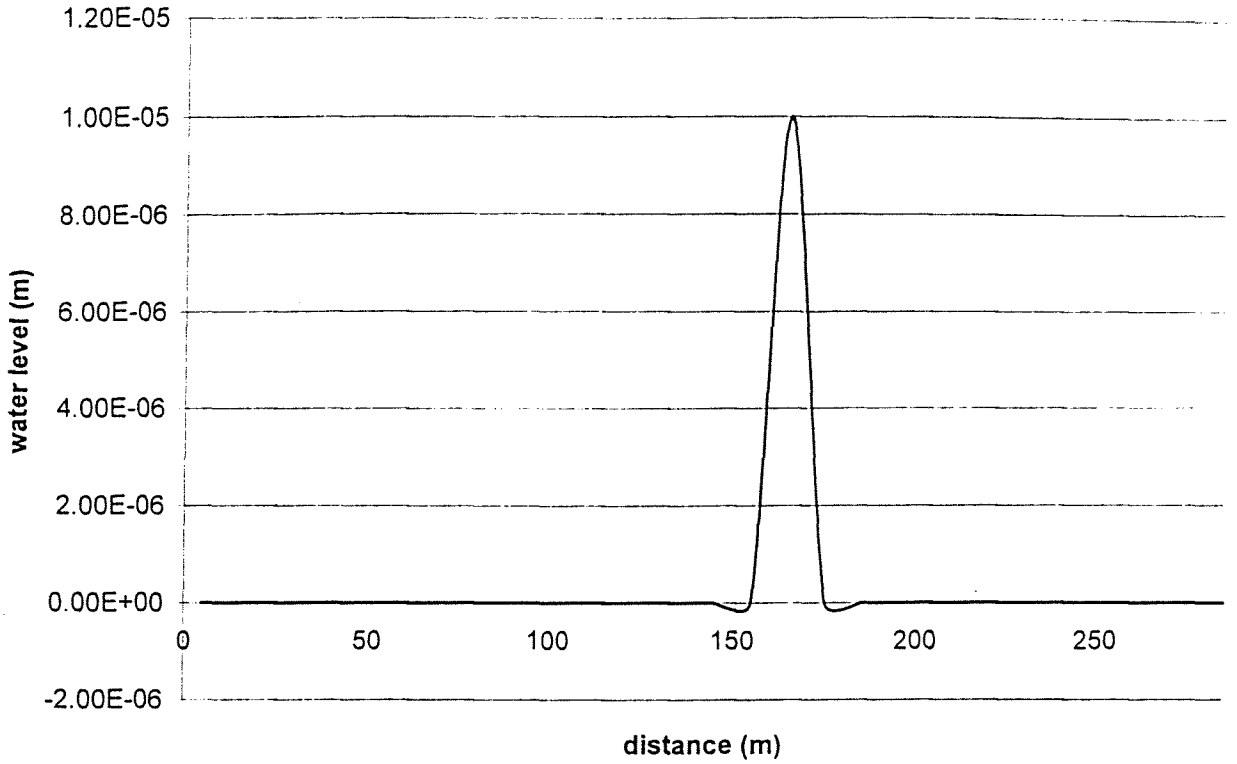

Discharge

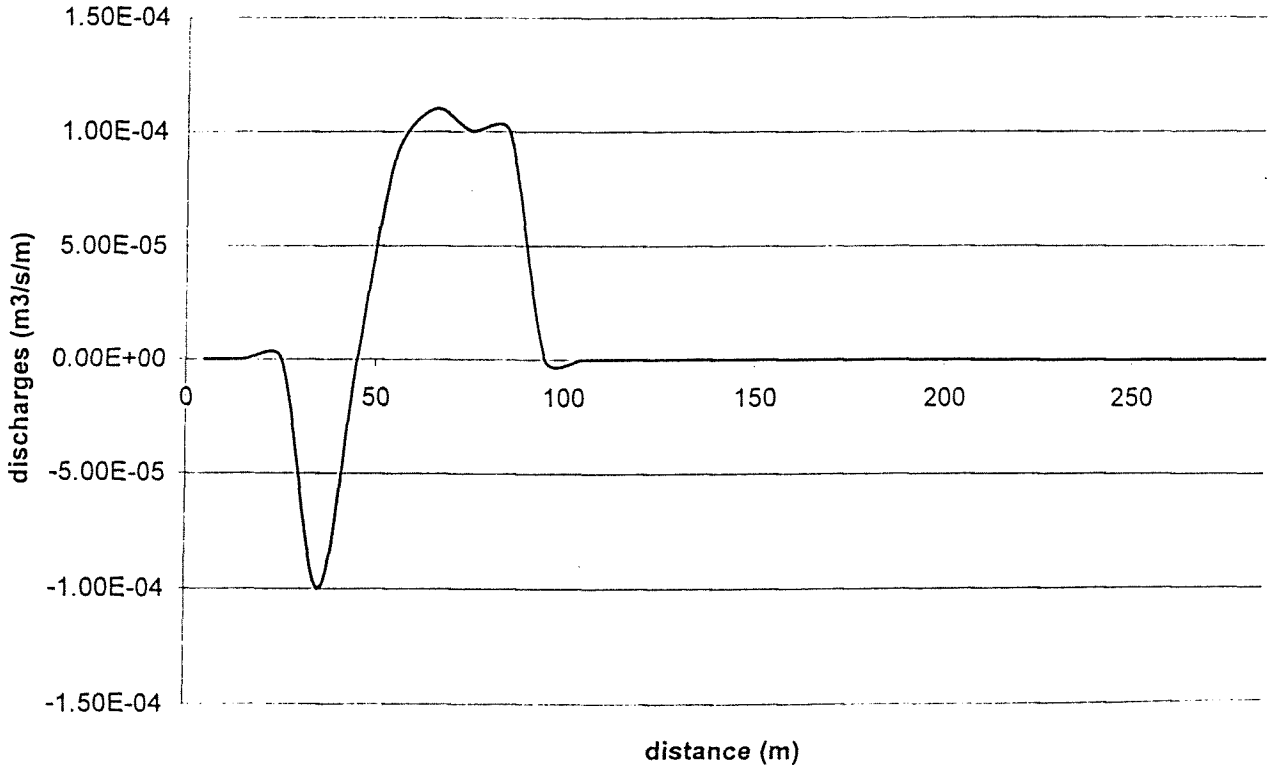

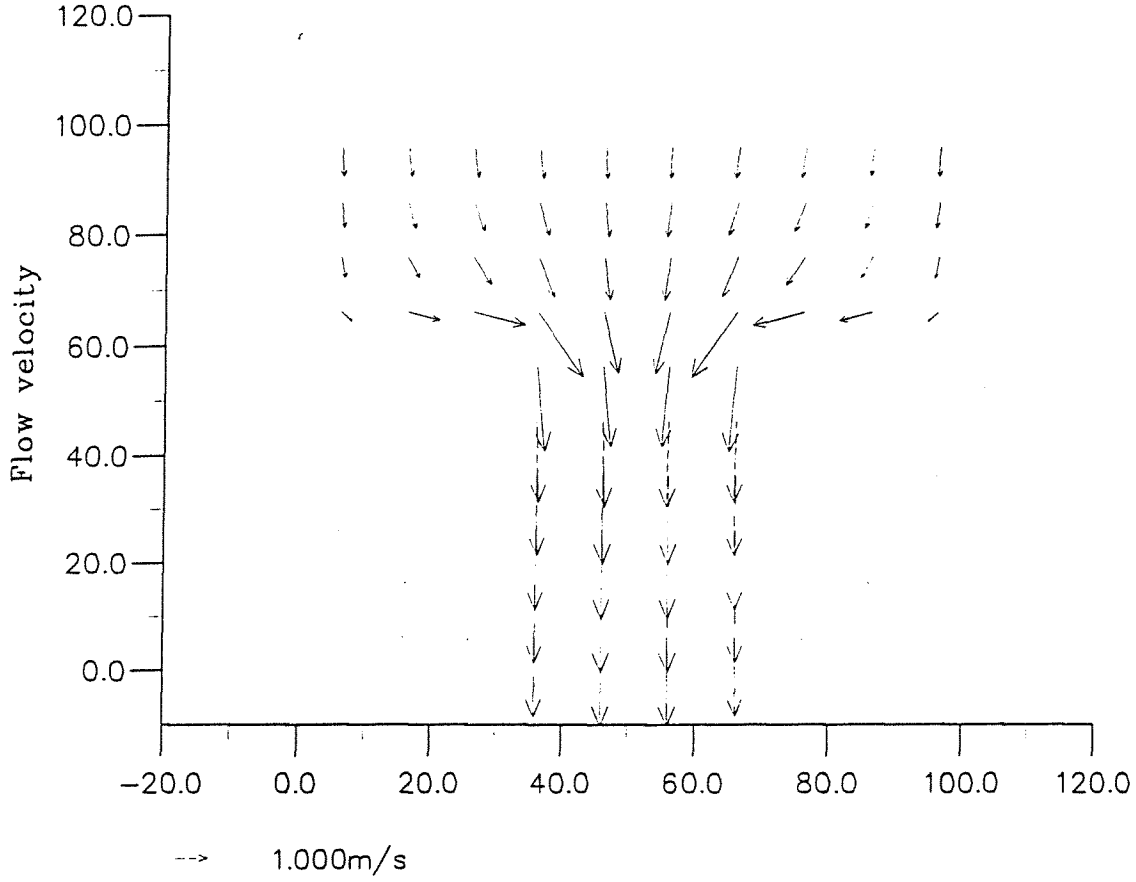

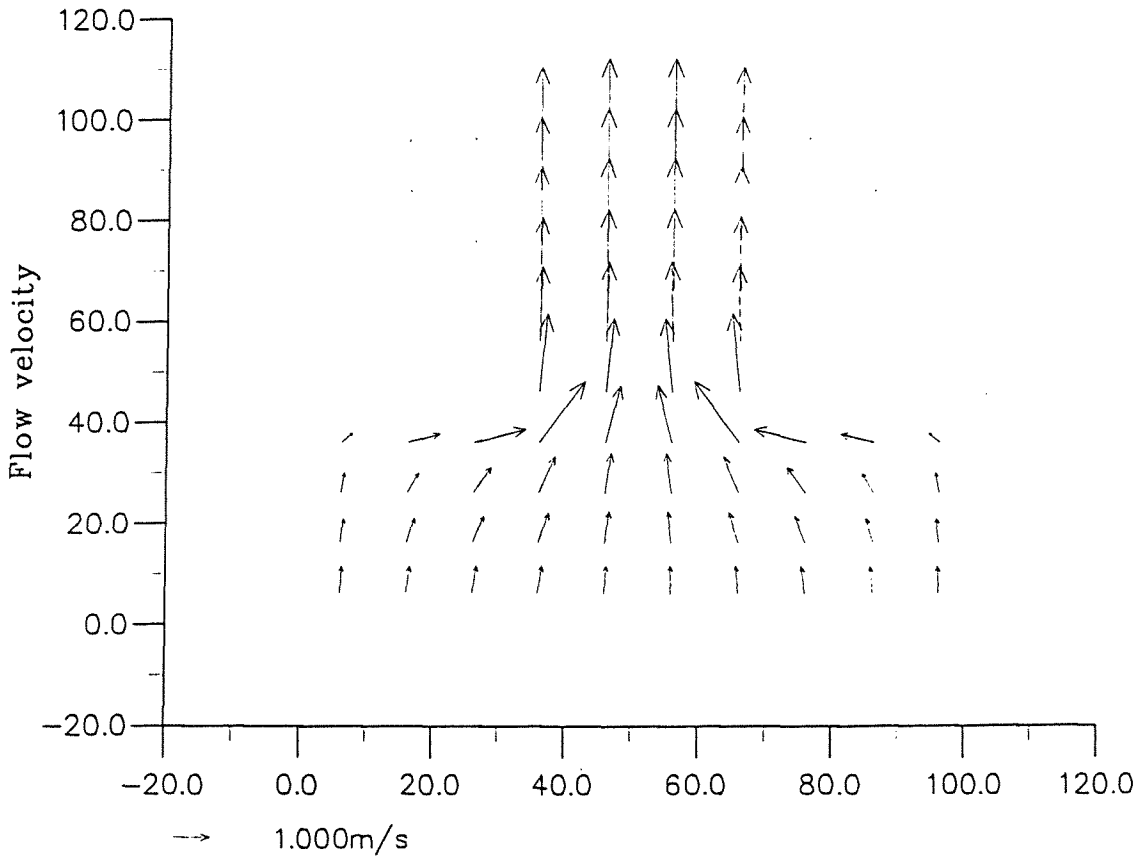

Upper graph: velocity boundary at the top Lower graph: velocity boundary at the bottom Depth contour interval is 2m	Delft3D–MOR	Appendix D.20
	Switching the boundaries	
DUT – EQUILIBRIUM BAYS	MaST–III	SASME

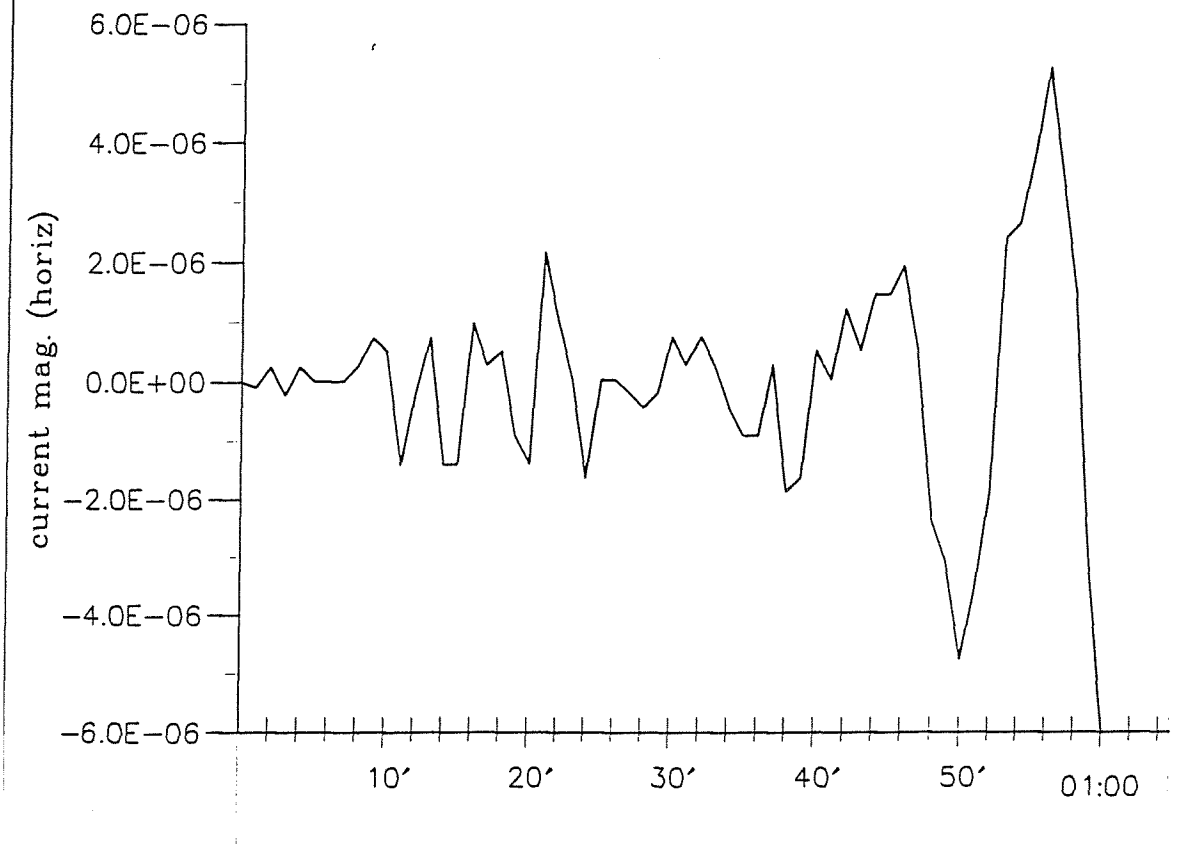

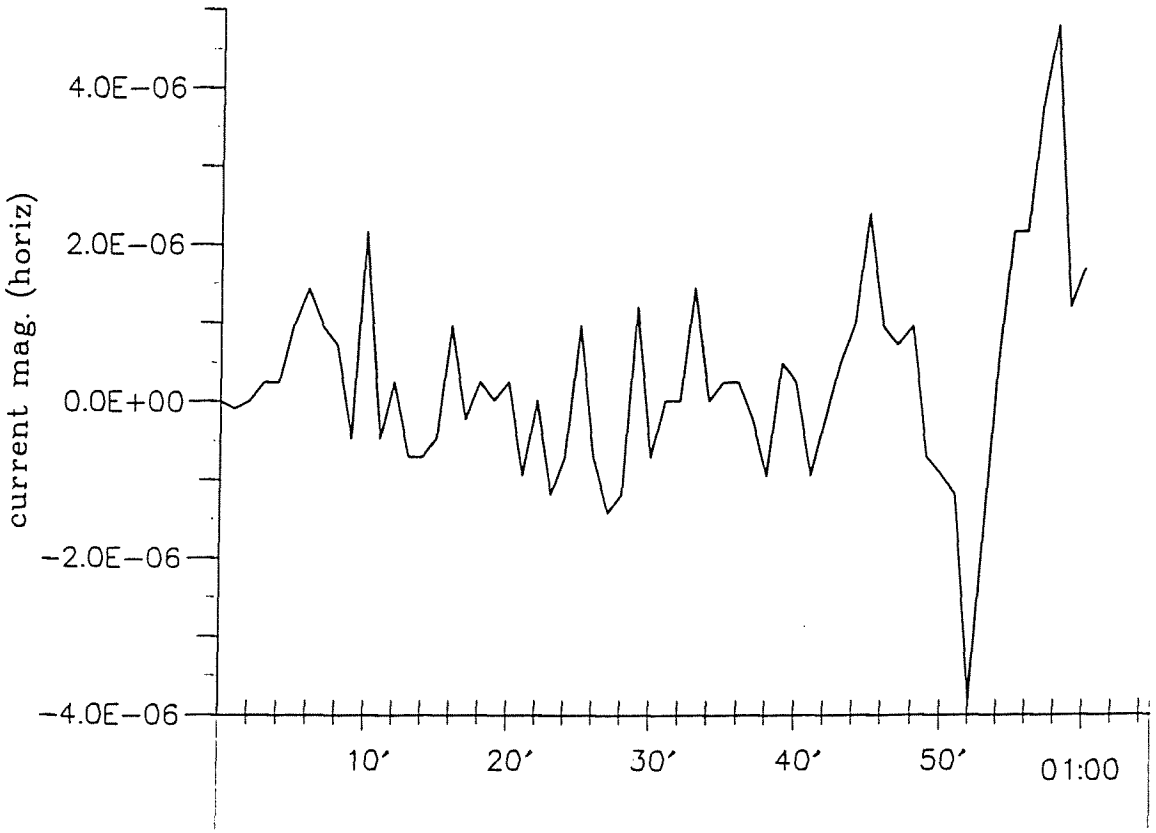

Comparison observation points Upper graph: Substracted current magnitude (U above) Lower graph: Substracted current magnitude (U below)	Delft3D−MOR	Appendix D.21
	Switching the boundaries	
DUT − EQUILIBRIUM BAYS	MaST−III	SASME

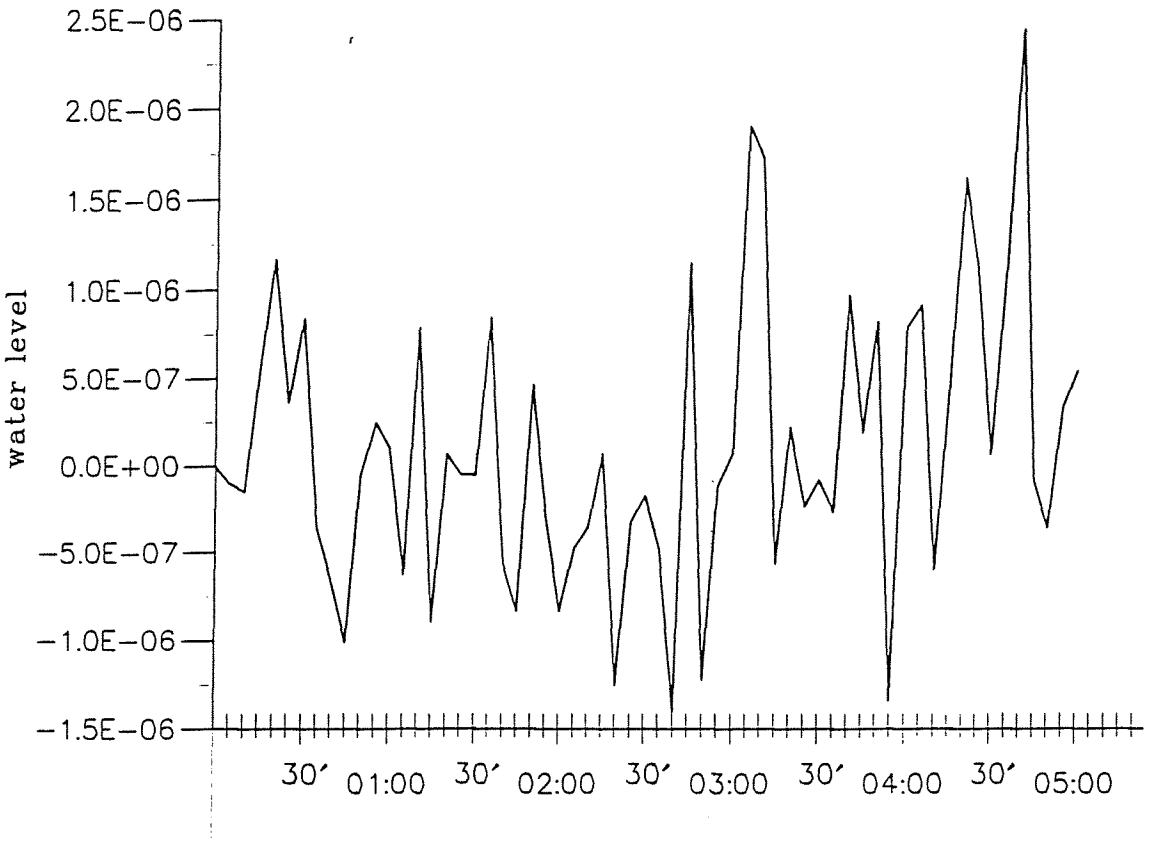

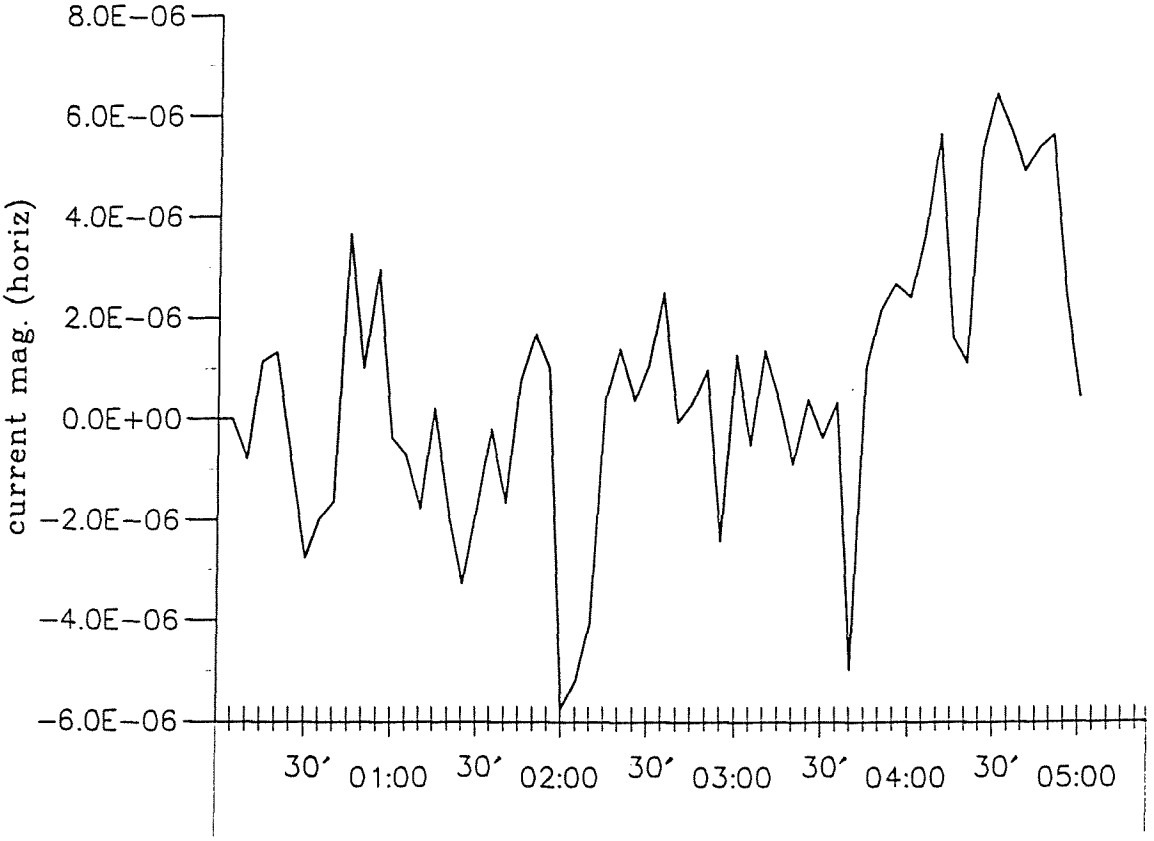

Comparison observation points Upper graph: Substracted water level (m) Lower graph: Substracted current magn. (m/s)	Delft3D–MOR	Appendix D.22
	Flume calculation (5 hrs)	
DUT – EQUILIBRIUM BAYS	MaST–III	SASME

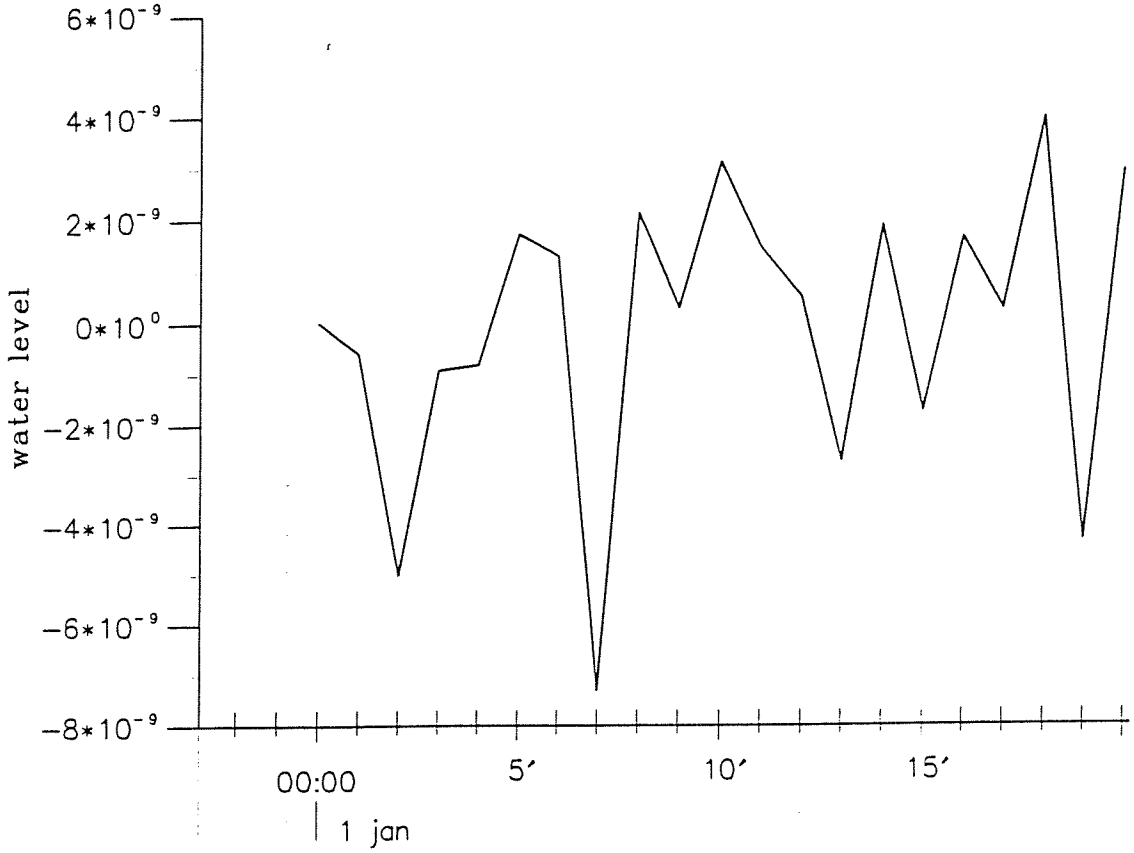

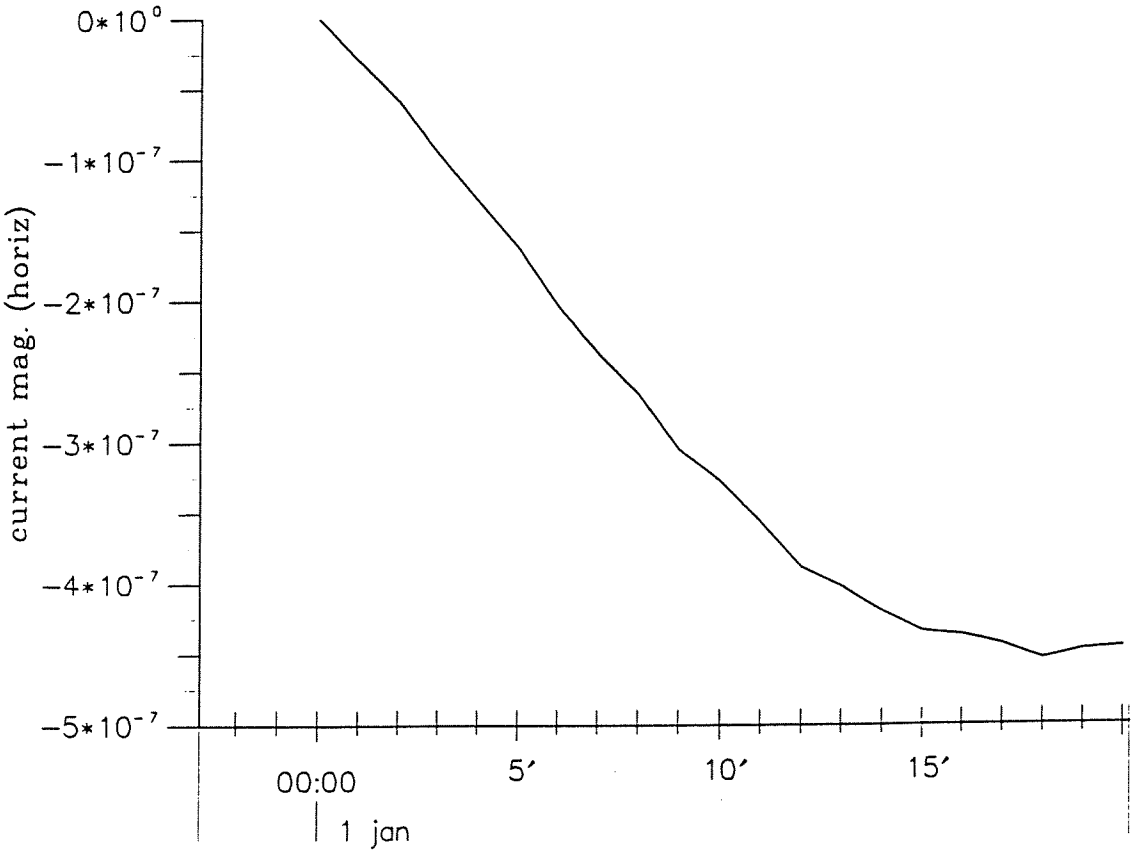

Comparison observation points Upper graph: Substracted water level (m) Lower graph: Substracted current magn. (m/s)	Delft3D–MOR	Appendix D.23
	Flow calculation	
DUT – EQUILIBRIUM BAYS	MaST–III	SASME

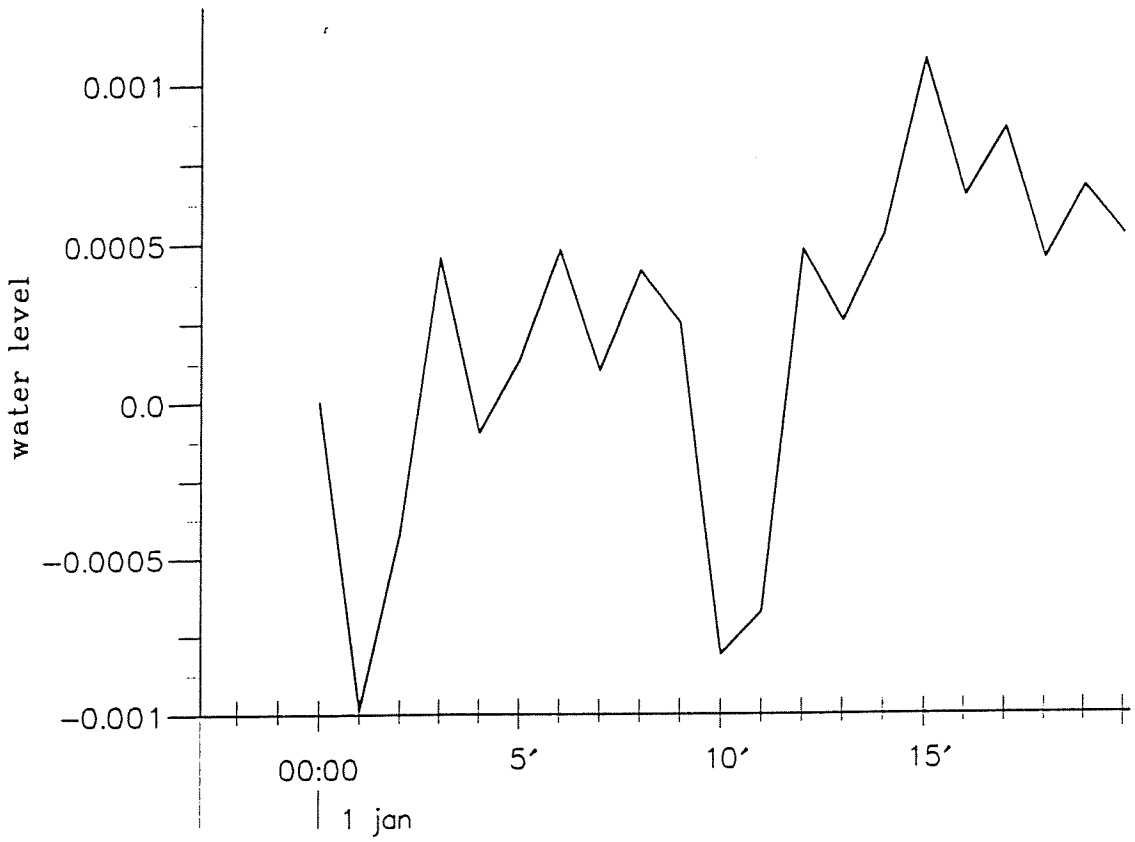

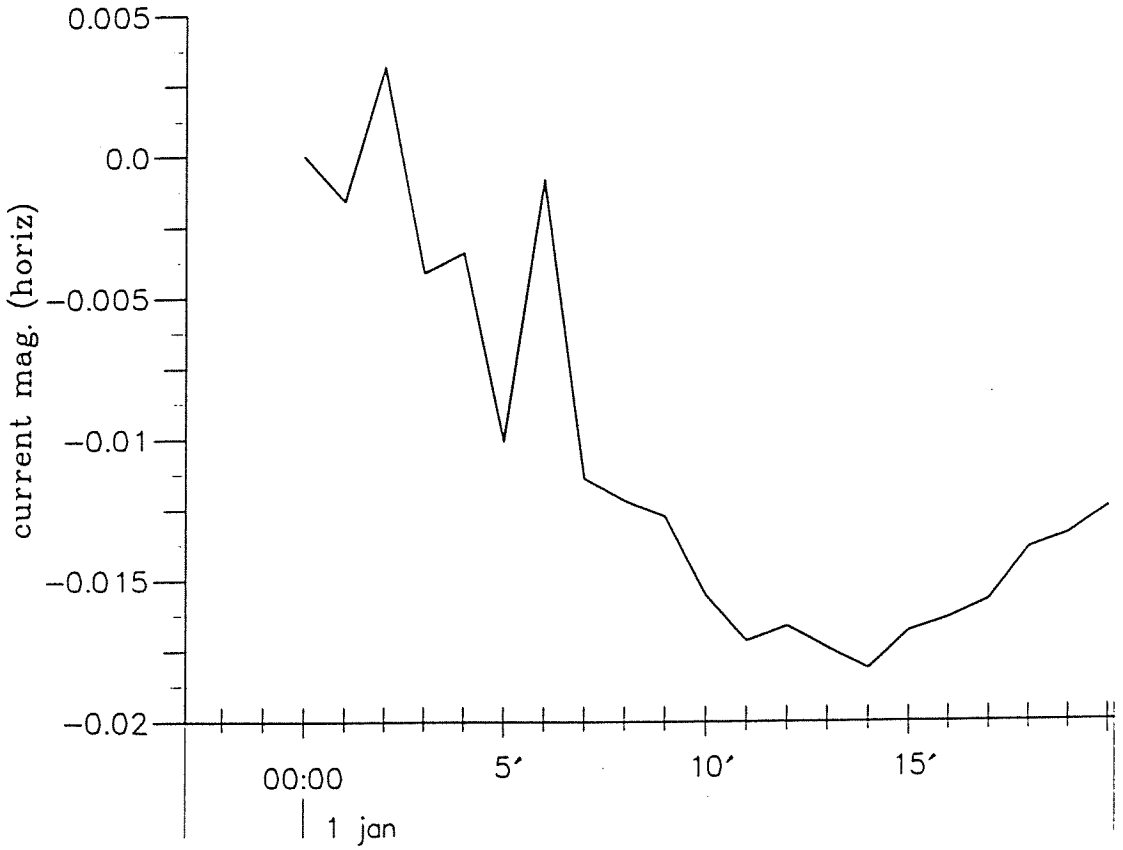

Comparison observation points Upper graph: Substracted water level (m) Lower graph: Substracted current magn. (m/s)	Delft3D–MOR	Appendix D.24
	Flow–Waves–Flow	
DUT – EQUILIBRIUM BAYS	MaST–III	SASME

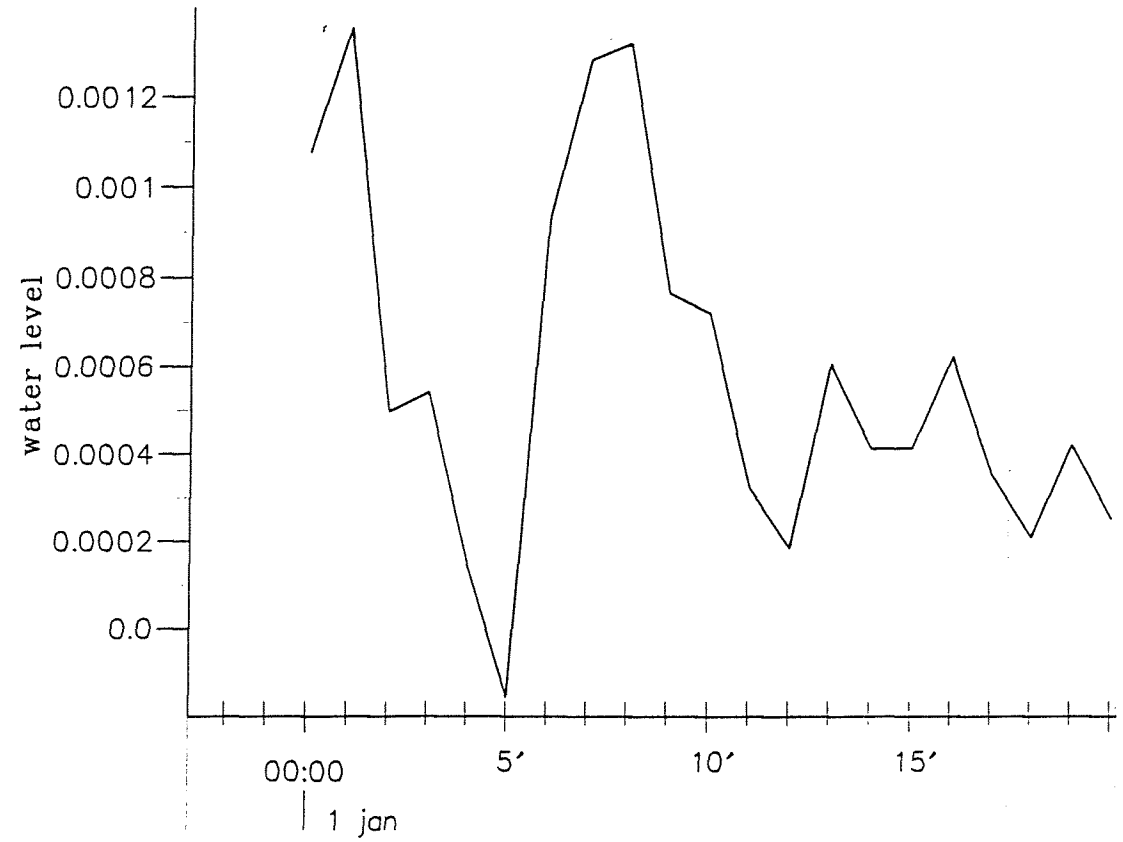

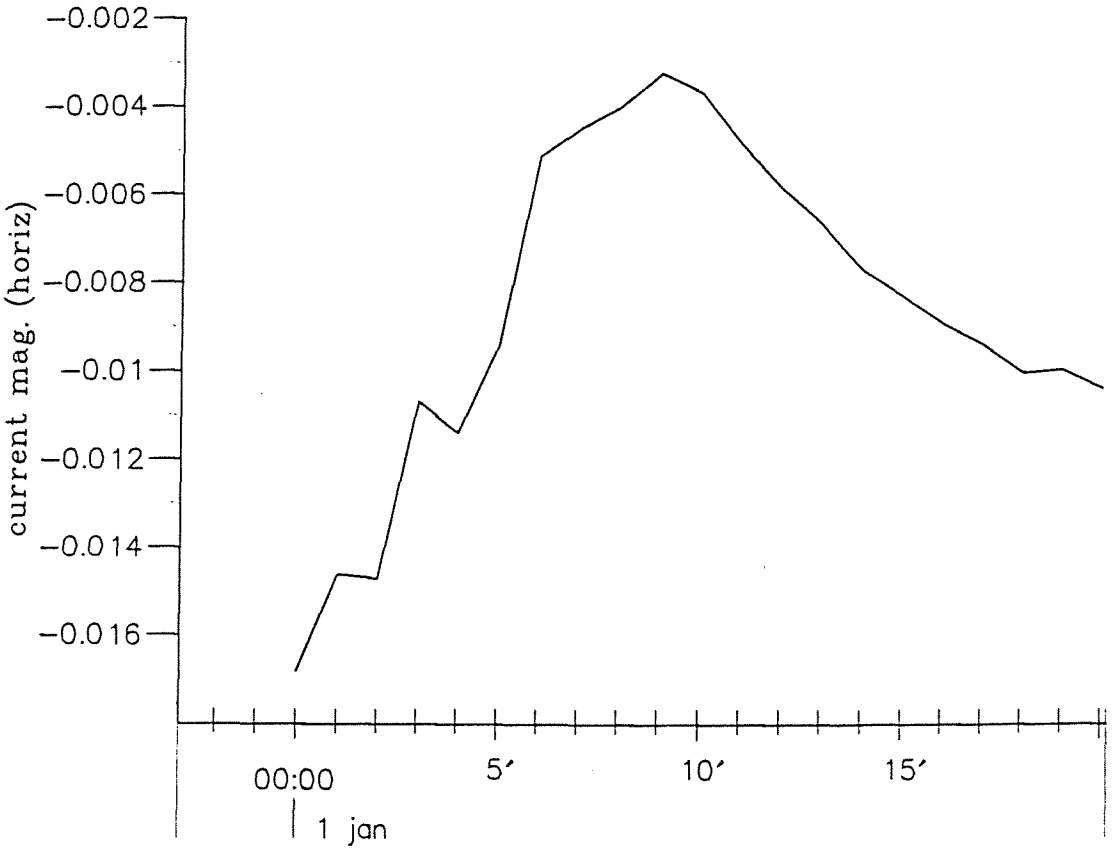

Comparison observation points Upper graph: Substracted water level (m) Lower graph: Substracted current magn. (m/s)	Delft3D–MOR	Appendix D.25
	Flow–Waves–Flow–Waves–Flow	
DUT – EQUILIBRIUM BAYS	MaST–III	SASME

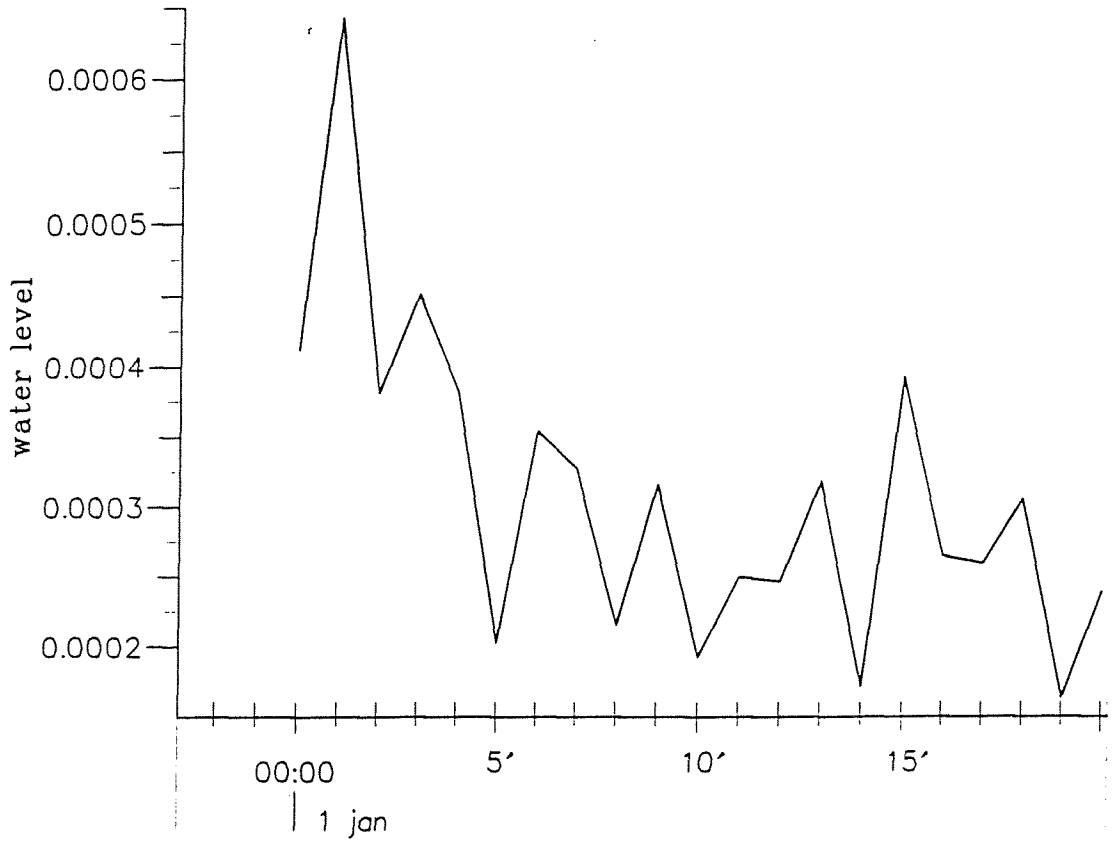

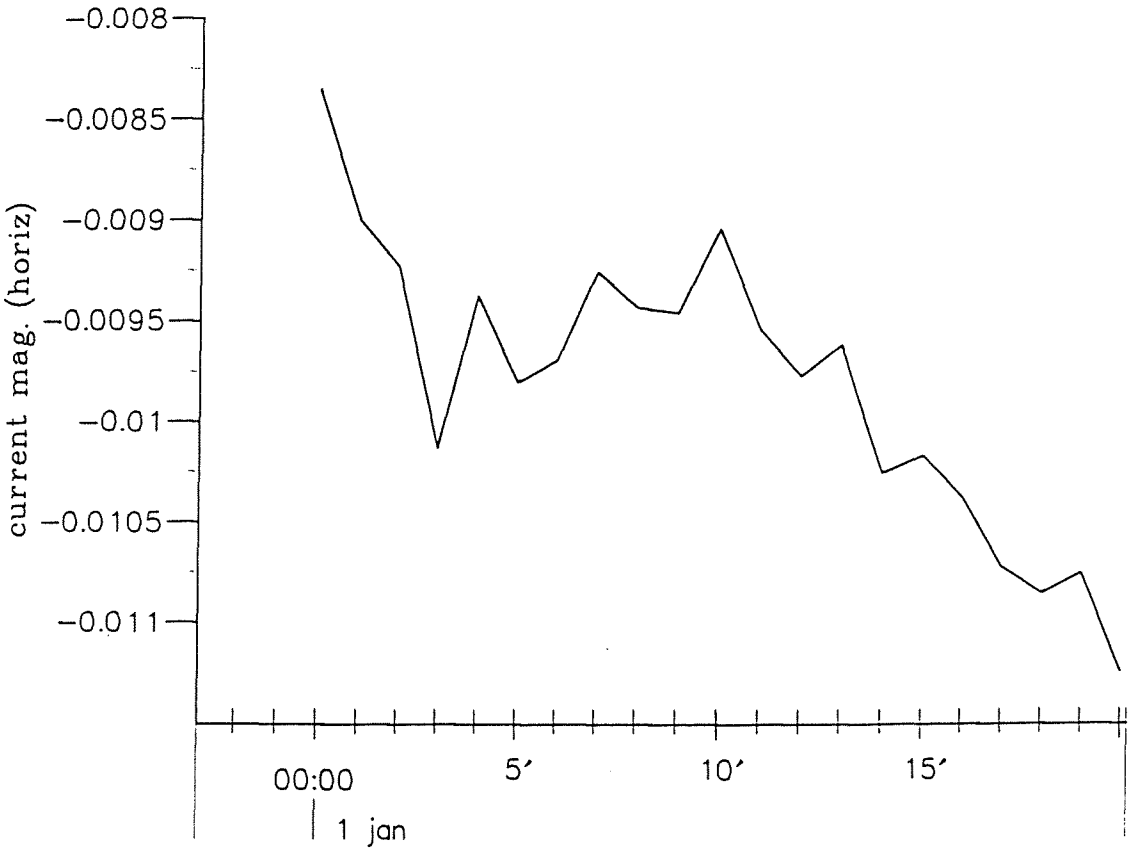

Comparison observation points Upper graph: Substracted water level (m) Lower graph: Substracted current magn. (m/s)	Delft3D–MOR	Appendix D.26
	F–W–F–W–F–W–F	
DUT – EQUILIBRIUM BAYS	MaST–III	SASME

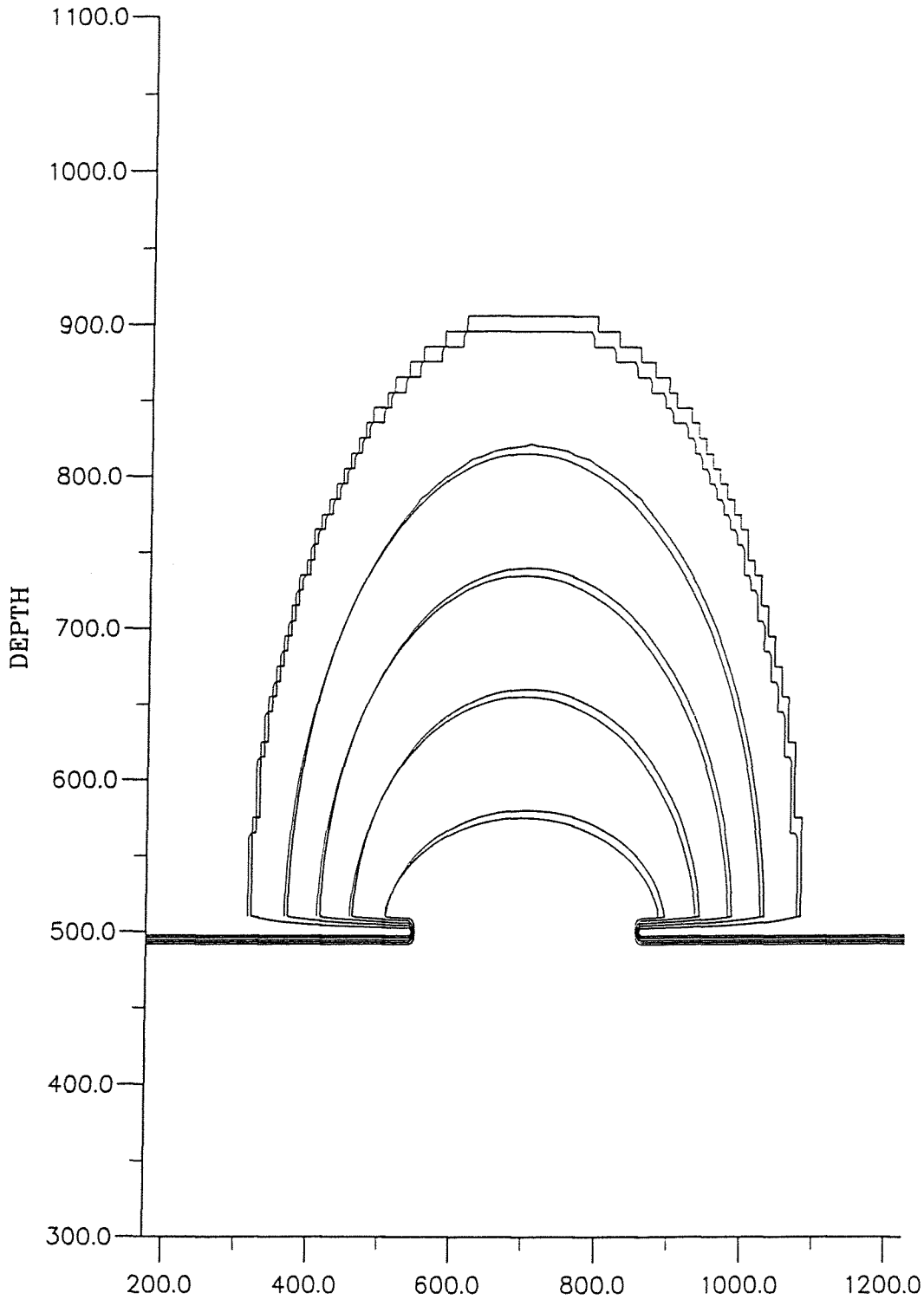

Initial bathymetry Depth contour interval is 2m Compared: comm. file (solid) & hwgxy. file (dashed)	Delft3D–MOR	Appendix D.27
	Asymmetrical plotting routine	
DUT – EQUILIBRIUM BAYS	MaST–III	SASME

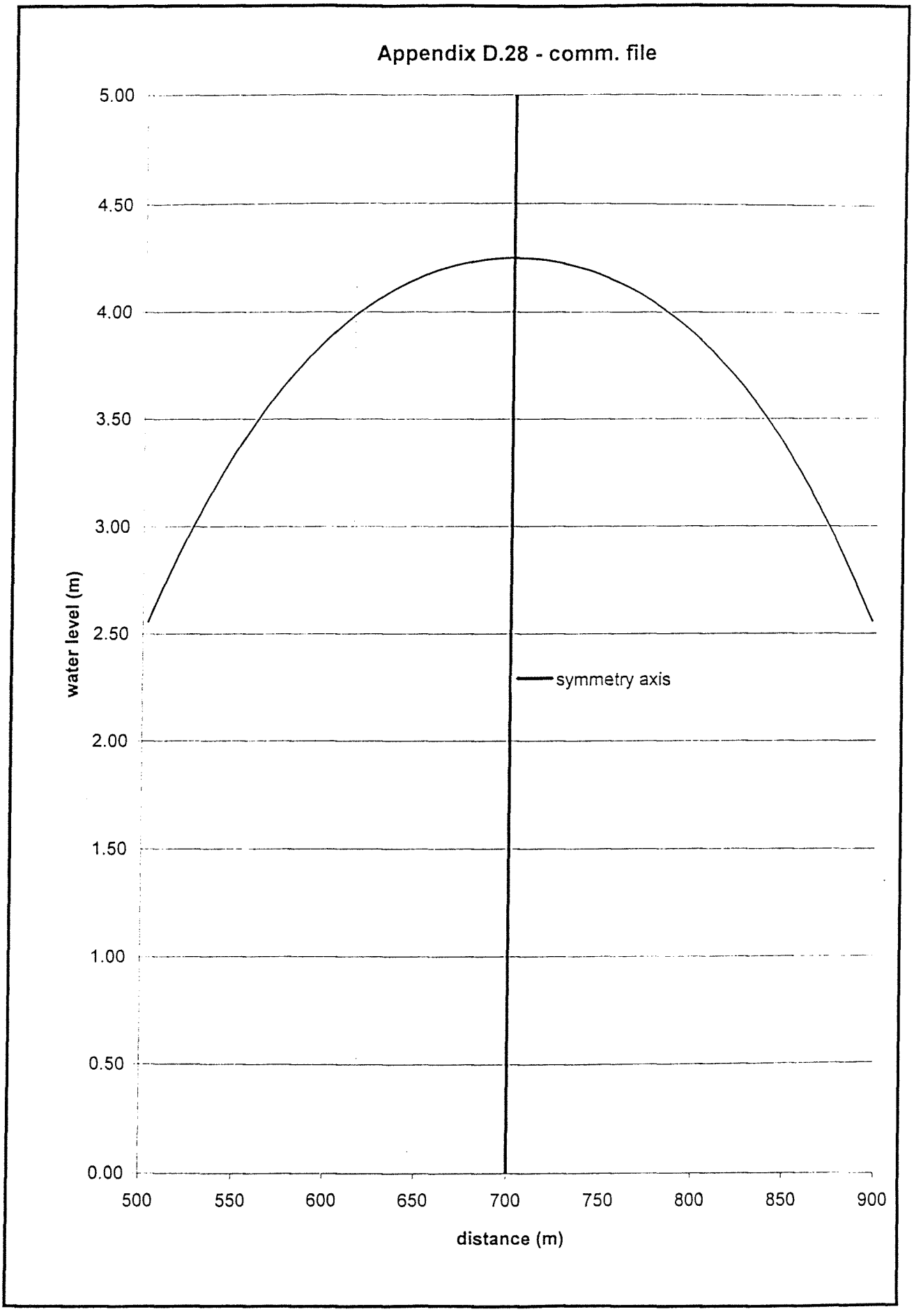
Appendix D.28 - comm. file
5.00
4.50
4.00
3.50
3.00
2.50
2.00
1.50
1.00
0.50
0.00
water level (m)
symmetry axis
500
550
600
650
700
750
800
850
900
distance (m)

Appendix D.29 – routines.gpp

```
plot-routine      'PlotIsolines'     'Hsig - isolines'
        no-topography
        accepts-datasets
                'MAP2D' 'SINGLE'
                'MAP2D' 'VALUE_AT_VERTEX'
        end-datasets
        options
                logical         'PlotAreaBord'   'Border around plotarea'   FALSE
                logical         'ColoredLines'   'Colored isolines'         FALSE
                classes-list    'ContourClasses' 'Contour classes'
                        values
                                0.2
                                0.4
                                0.6
                                0.8
                                1.0
                                1.2
                                1.4
                                1.6
                                1.8
                                2.0
                                2.2
                                2.4
                        end-values
                real            'ExtraMissVal'   'Extra missing value'      -999.0
                list            'TypeAxes'       'Axis type'                'Linear axes'
                        from
                                'Geographic axes'
                                'Linear axes'
                                'Polar axes'
                        end-values
        end-options
end-routine

plot-routine      'PlotIsolines'     'Dieptelijnen'
        no-topography
        accepts-datasets
                'MAP2D' 'SINGLE'
                'MAP2D' 'VALUE_AT_VERTEX'
        end-datasets
        options
                logical         'PlotAreaBord'   'Border around plotarea'   FALSE
                logical         'ColoredLines'   'Colored isolines'         FALSE
                classes-list    'ContourClasses' 'Contour classes'
                        values
                                -2
                                0
                                2
                                4
                                6
                                8
                        end-values
                real            'ExtraMissVal'   'Extra missing value'      -999.0
                list            'TypeAxes'       'Axis type'                'Linear axes'
                        from
                                'Geographic axes'
                                'Linear axes'
                                'Polar axes'
                        end-values
        end-options
end-routine
```

Appendix E.1 – Test cases

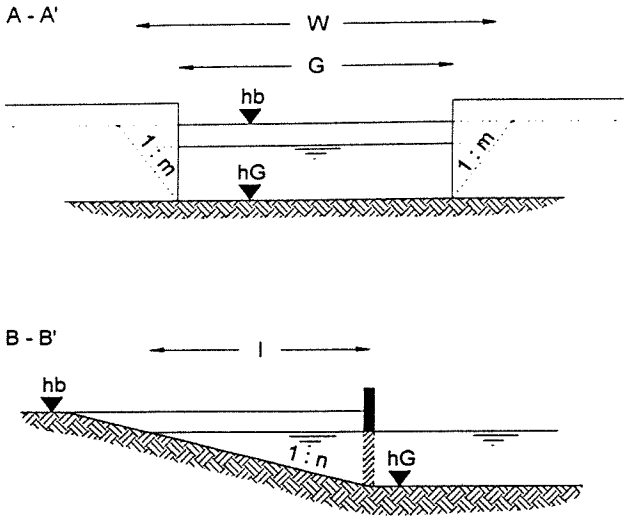

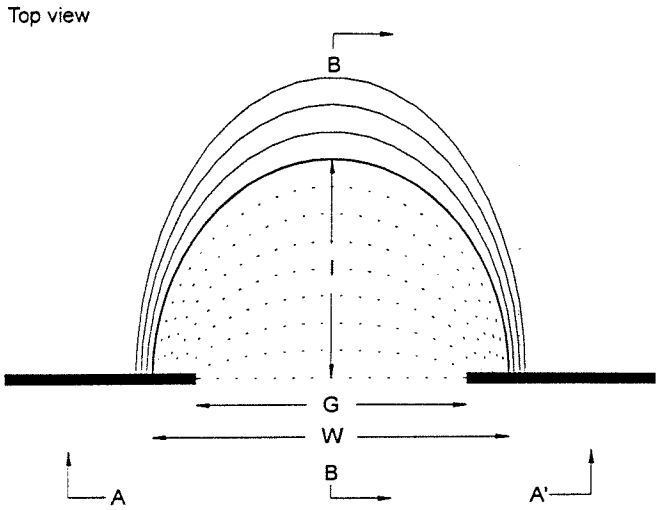

nr.		G (m)	W (m)	l (m)	m (-)	n (-)
1	a	100	660	200	35	25
	b	200	660	200	28.75	25
	c	300	660	200	22.5	25
	d	400	660	200	16.25	25
	e	500	660	200	10	25
2	a	100	660	240	35	30
	b	200	660	240	28.75	30
	c	300	660	240	22.5	30
	d	400	660	240	16.25	30
	e	500	660	240	10	30
3	a	100	660	280	35	35
	b	200	660	280	28.75	35
	c	300	660	280	22.5	35
	d	400	660	280	16.25	35
	e	500	660	280	10	35
4	a	100	660	320	35	40
	b	200	660	320	28.75	40
	c	300	660	320	22.5	40
	d	400	660	320	16.25	40
	e	500	660	320	10	40
5	a	100	660	360	35	45
	b	200	660	360	28.75	45
	c	300	660	360	22.5	45
	d	400	660	360	16.25	45
	e	500	660	360	10	45
6	a	100	660	400	35	50
	b	200	660	400	28.75	50
	c	300	660	400	22.5	50
	d	400	660	400	16.25	50
	e	500	660	400	10	50
7	a	100	660	440	35	55
	b	200	660	440	28.75	55
	c	300	660	440	22.5	55
	d	400	660	440	16.25	55
	e	500	660	440	10	55
8	a	100	660	480	35	60
	b	200	660	480	28.75	60
	c	300	660	480	22.5	60
	d	400	660	480	16.25	60
	e	500	660	480	10	60

G = width of gap
W = width behind breakwaters
l = identation
m = beach slope behind breakwater
n = beach slope in centre of bay

hb = height of beach
hG = depth in gap

Appendix E.2: Longshore velocities for a varying indentation

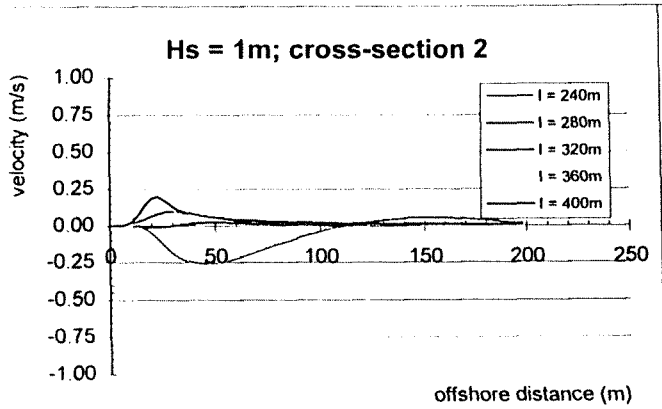

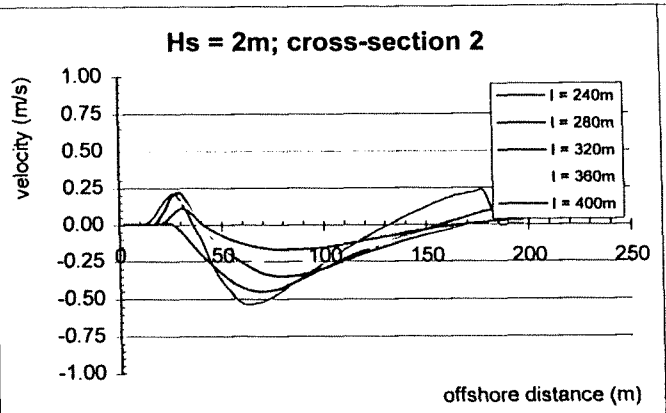

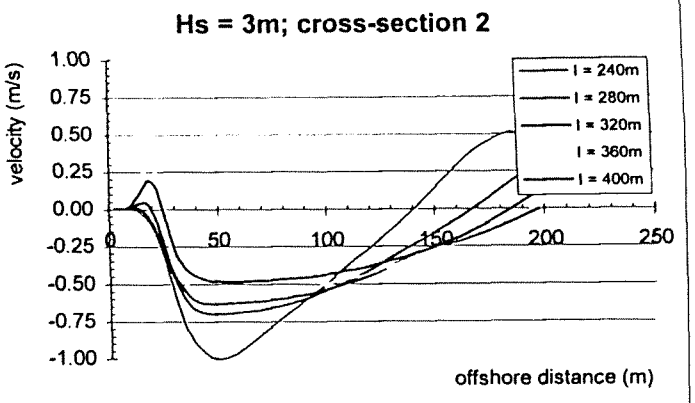

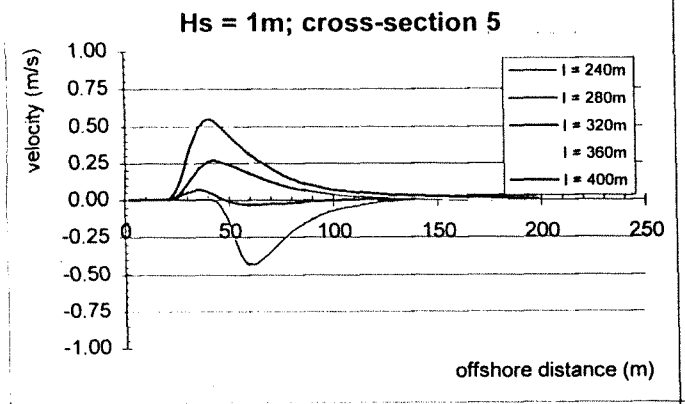

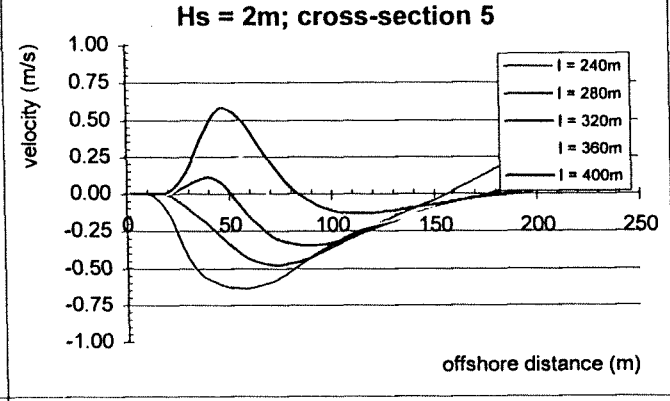

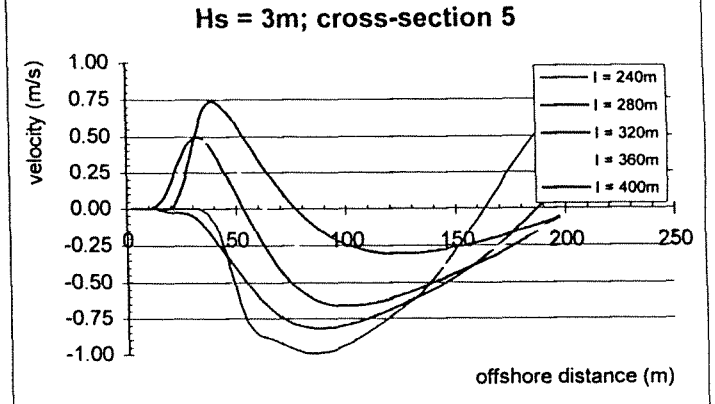

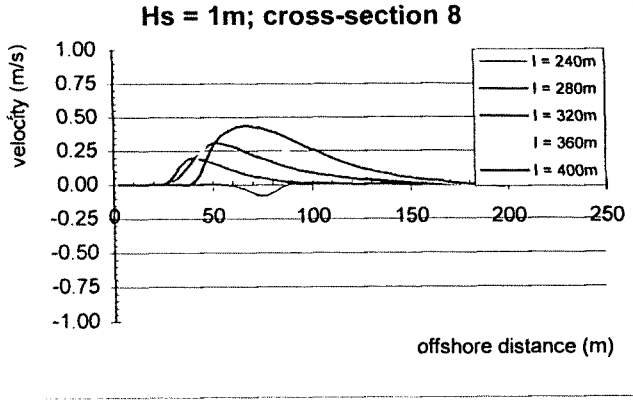

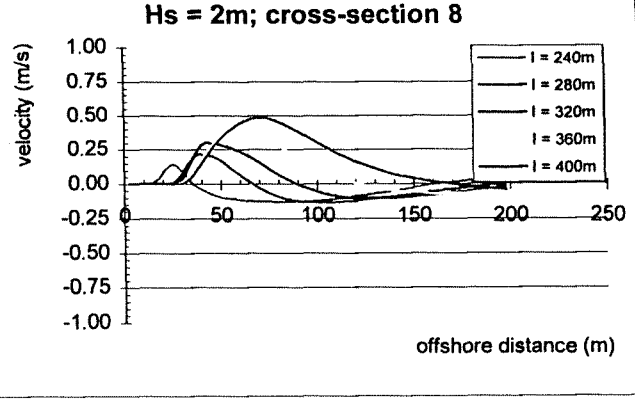

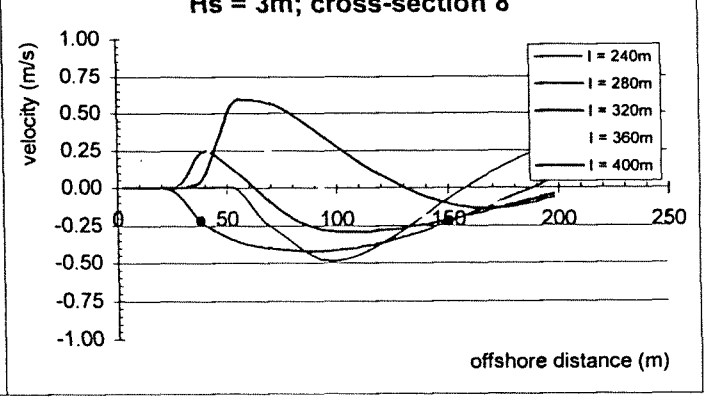

Appendix E.3: Longshore velocities for a varying gap width

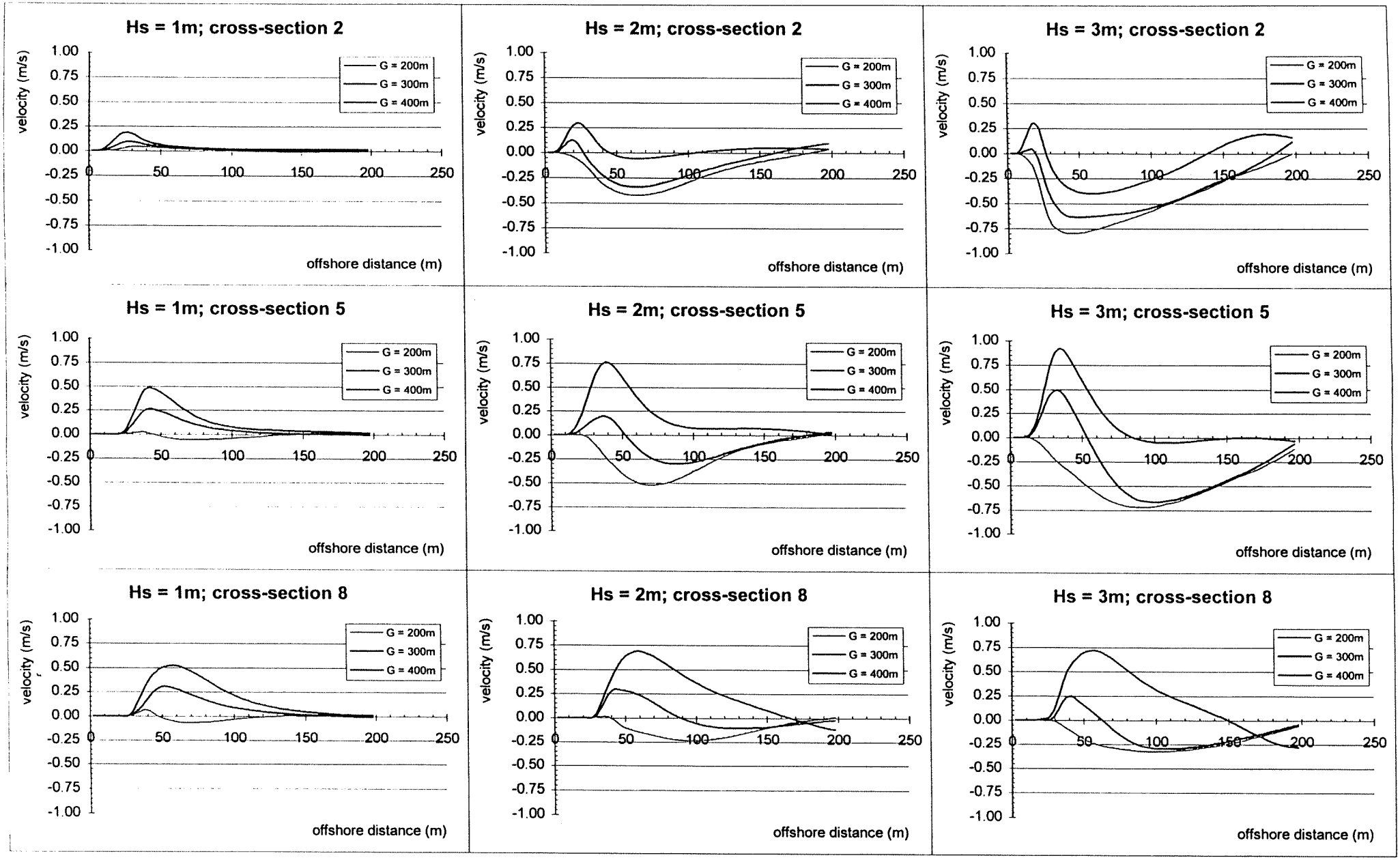

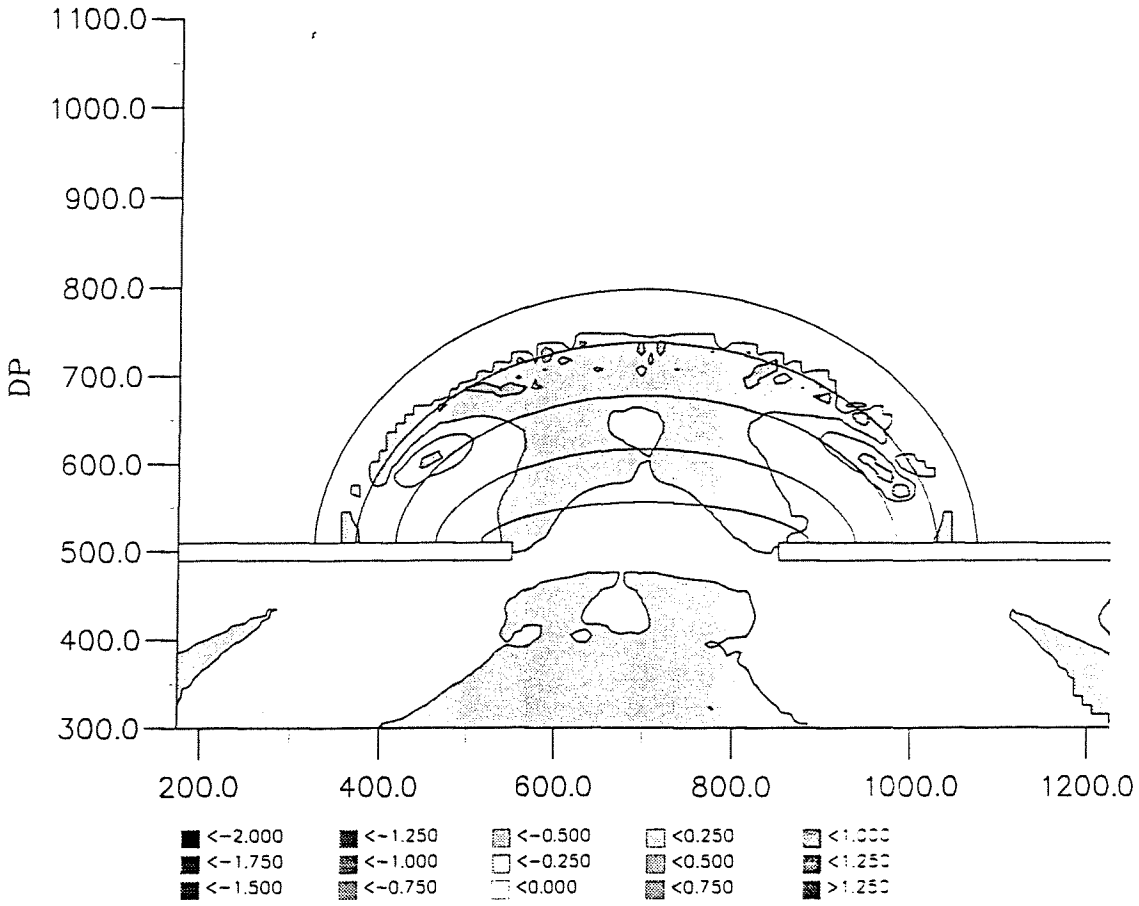

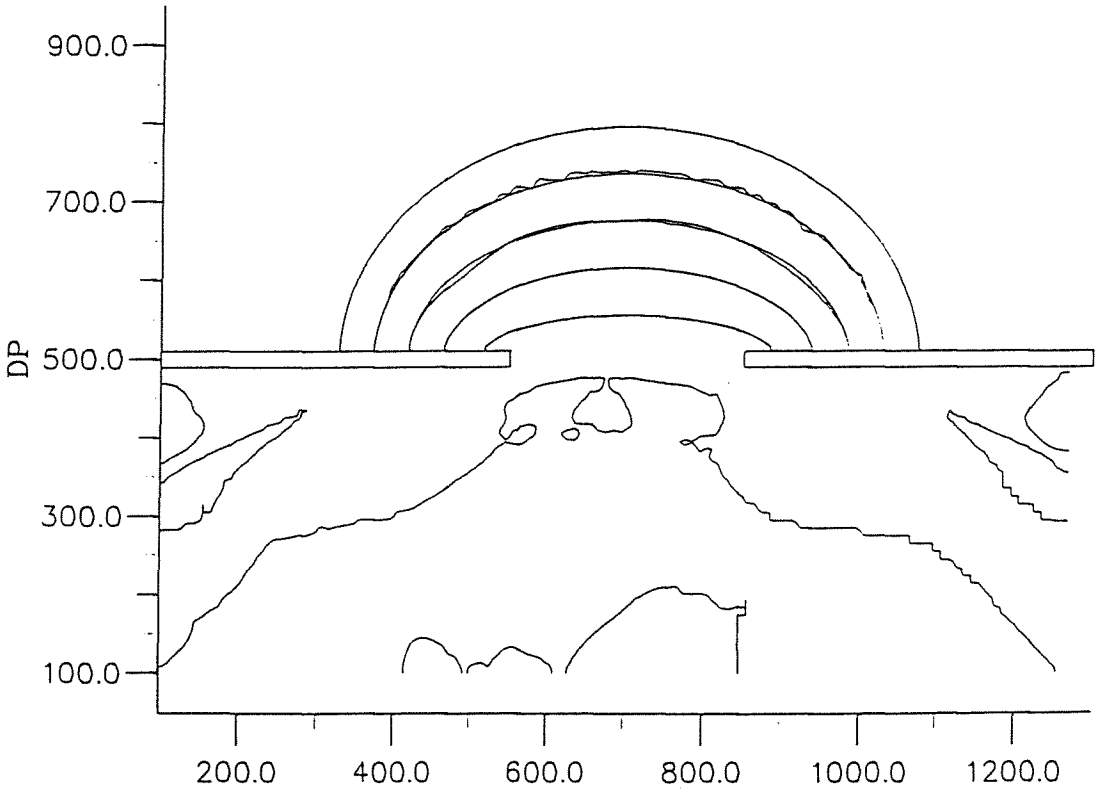

Upper graph: sedimentation and erosion (m) Lower graph: bathymetry after 7 days (m) Depth contour interval is 2m	Delft3D–MOR	Appendix E.4
	Bay 2c: Hs = 1m; d = 8m	
DUT – EQUILIBRIUM BAYS	MaST–III	SASME

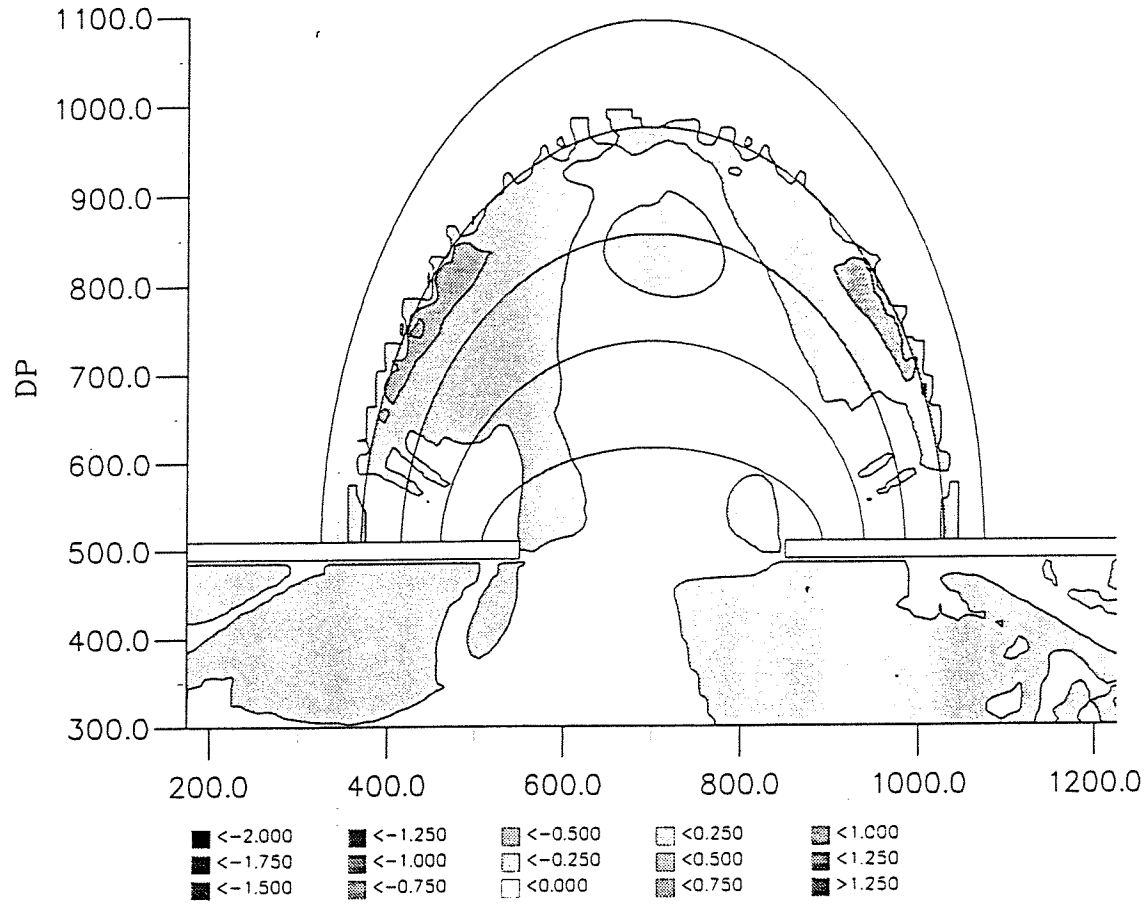

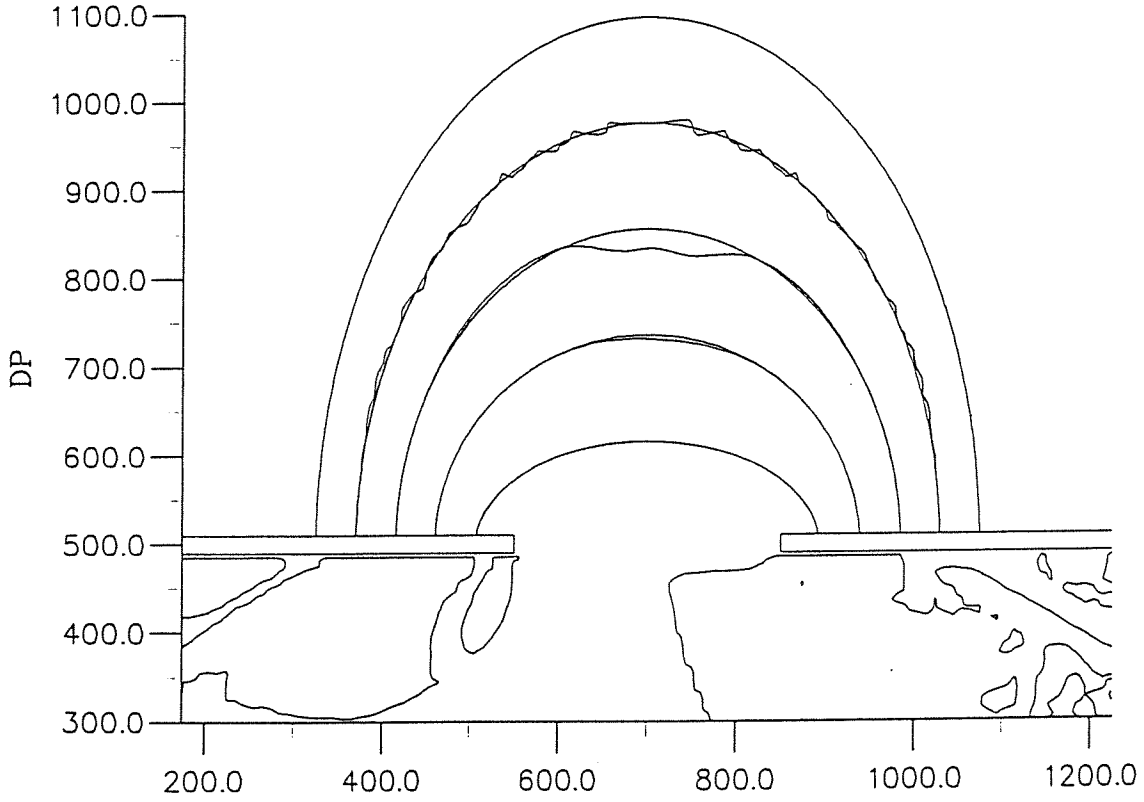

Upper graph: sedimentation and erosion (m) Lower graph: bathymetry after 7 days (m) Depth contour interval is 2m	Delft3D–MOR	Appendix E.5
	Bay 8c: Hs = 1m, d = 8m	
DUT – EQUILIBRIUM BAYS	MaST–III	SASME

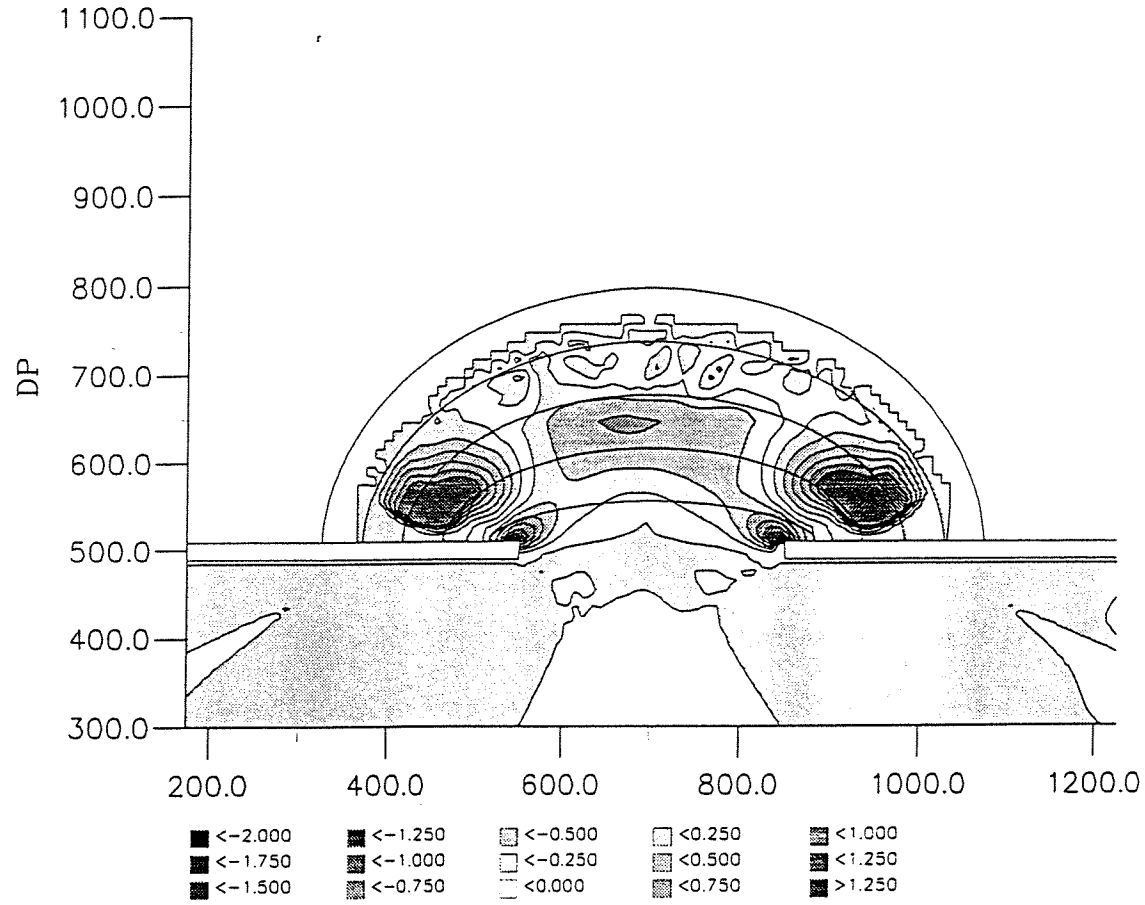

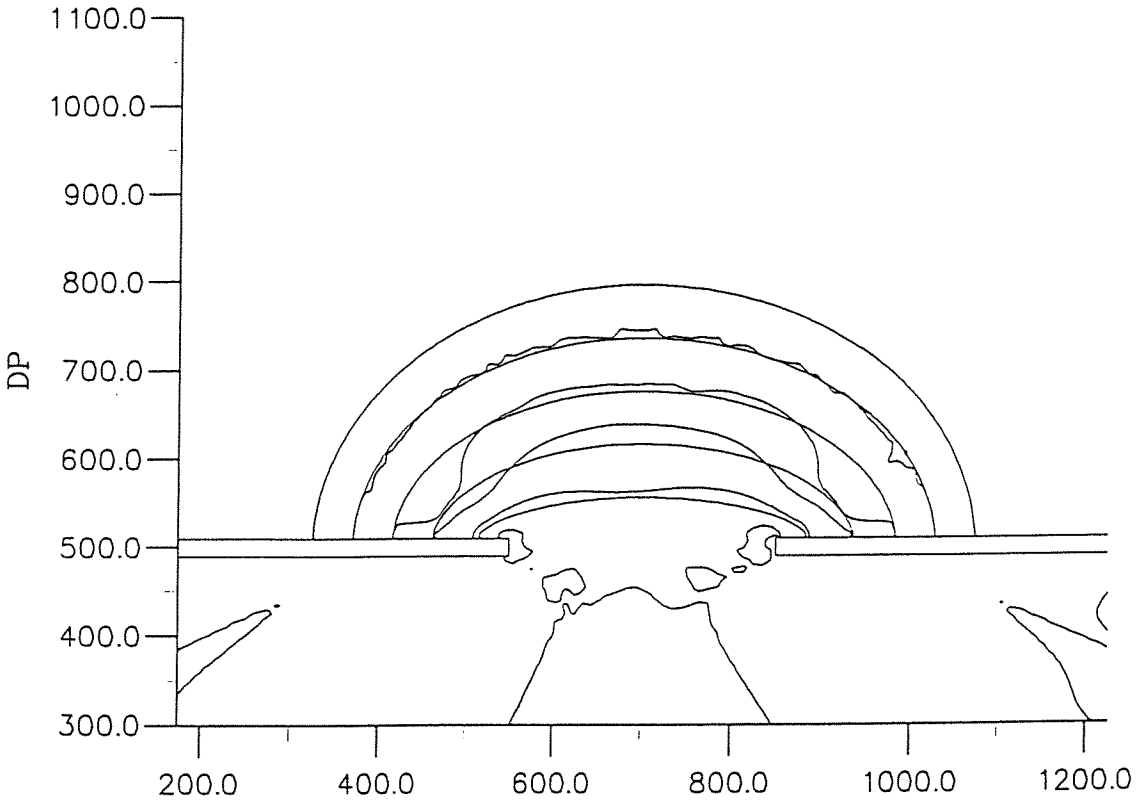

Upper graph: sedimentation and erosion (m) Lower graph: bathymetry after 7 days (m) Depth contour interval is 2m	Delft3D–MOR	Appendix E.6
	Bay 2c: Hs = 2m, d = 8m	
DUT – EQUILIBRIUM BAYS	MaST–III	SASME

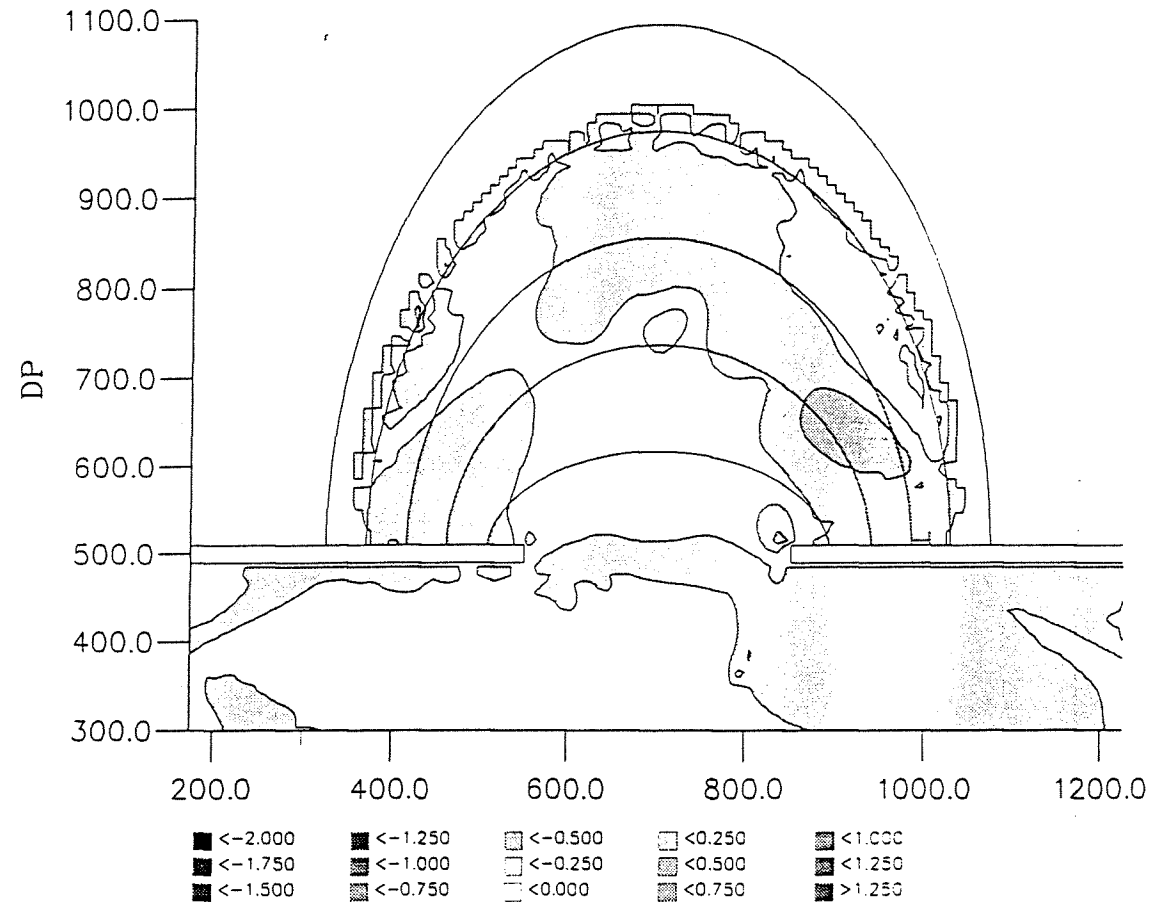

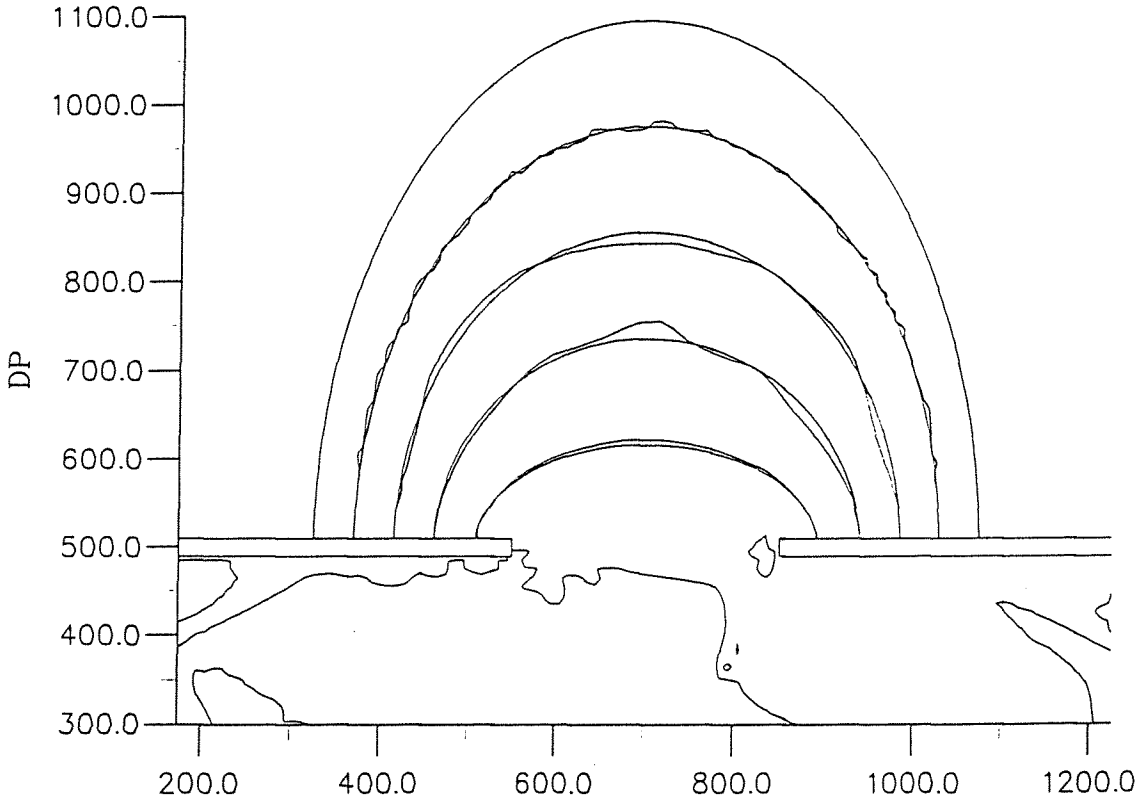

Upper graph: sedimentation and erosion (m) Lower graph: bathymetry after 7 days (m) Depth contour interval is 2m	Delft3D–MOR	Appendix E.7
	Bay 8c: Hs = 2m, d = 8m	
DUT – EQUILIBRIUM BAYS	MaST–III	SASME

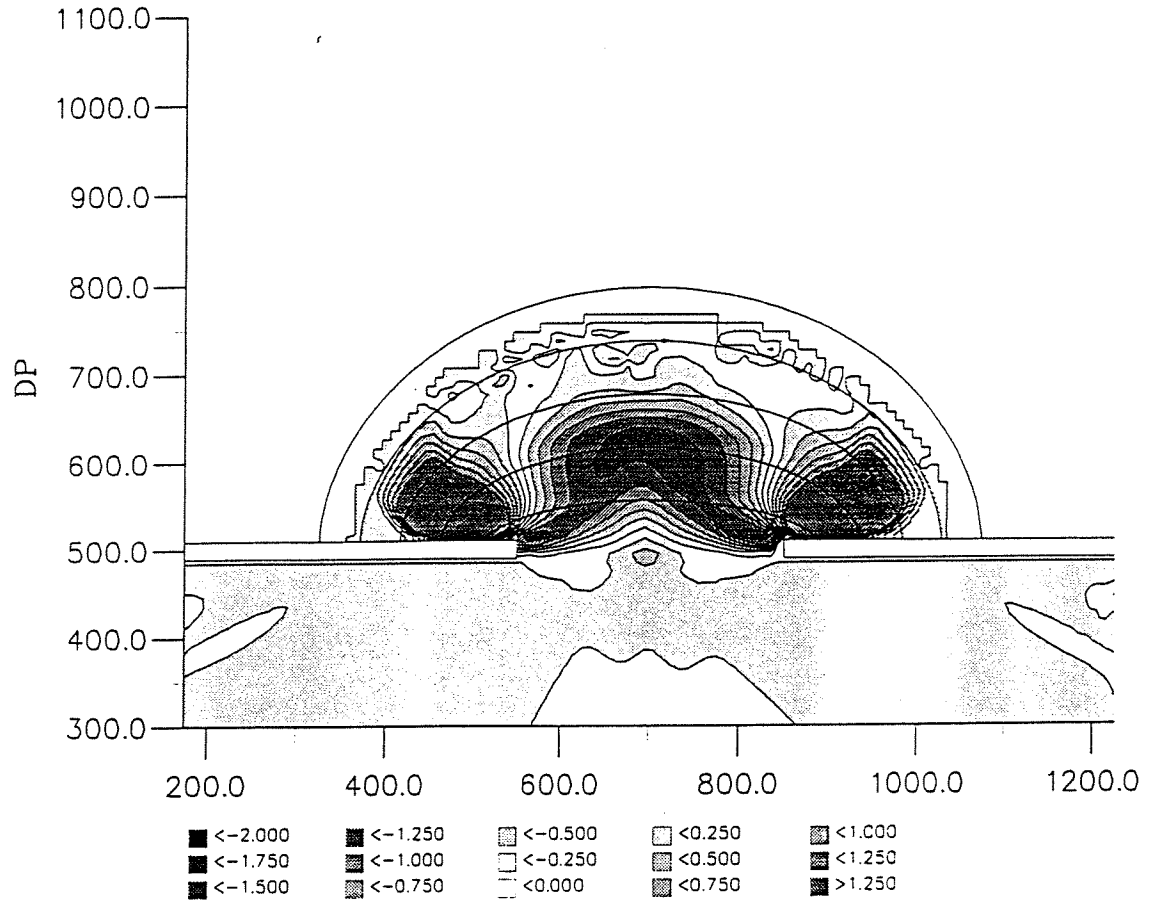

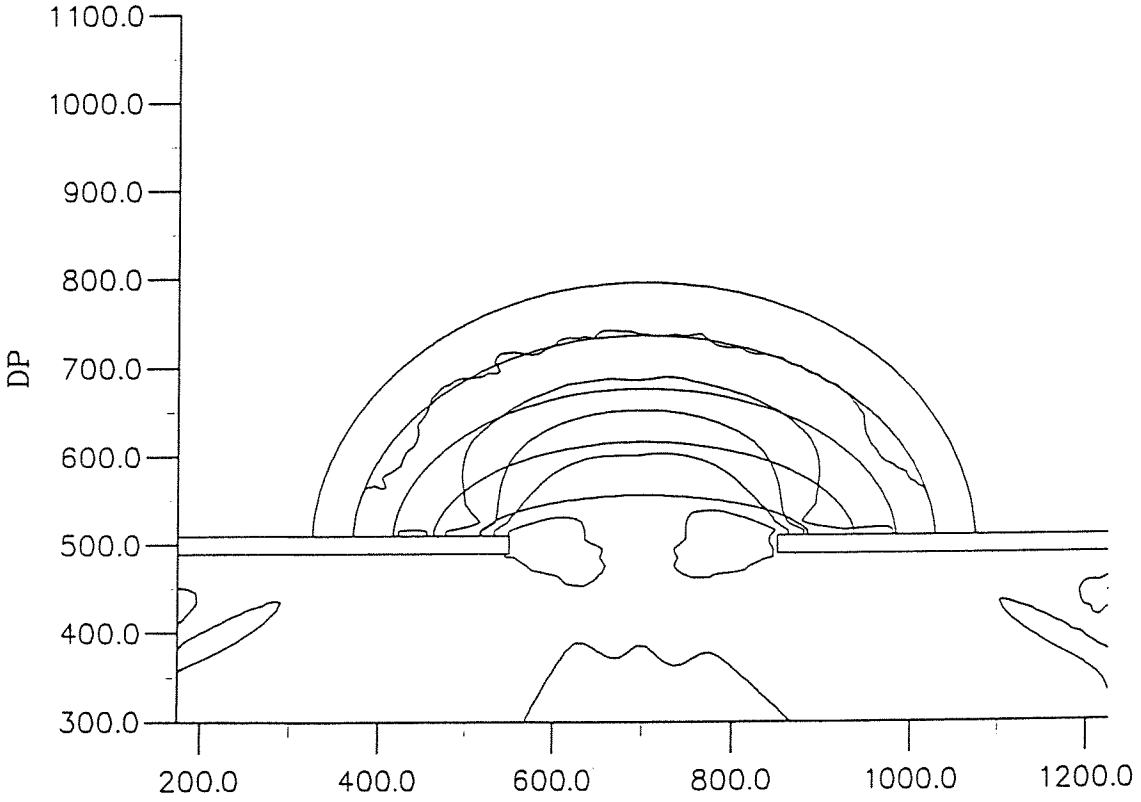

Upper graph: sedimentation and erosion (m) Lower graph: bathymetry after 7 days (m) Depth contour interval is 2m	Delft3D–MOR	Appendix E.8
	Bay 2c: Hs = 3m, d = 8m	
DUT – EQUILIBRIUM BAYS	MaST–III	SASME

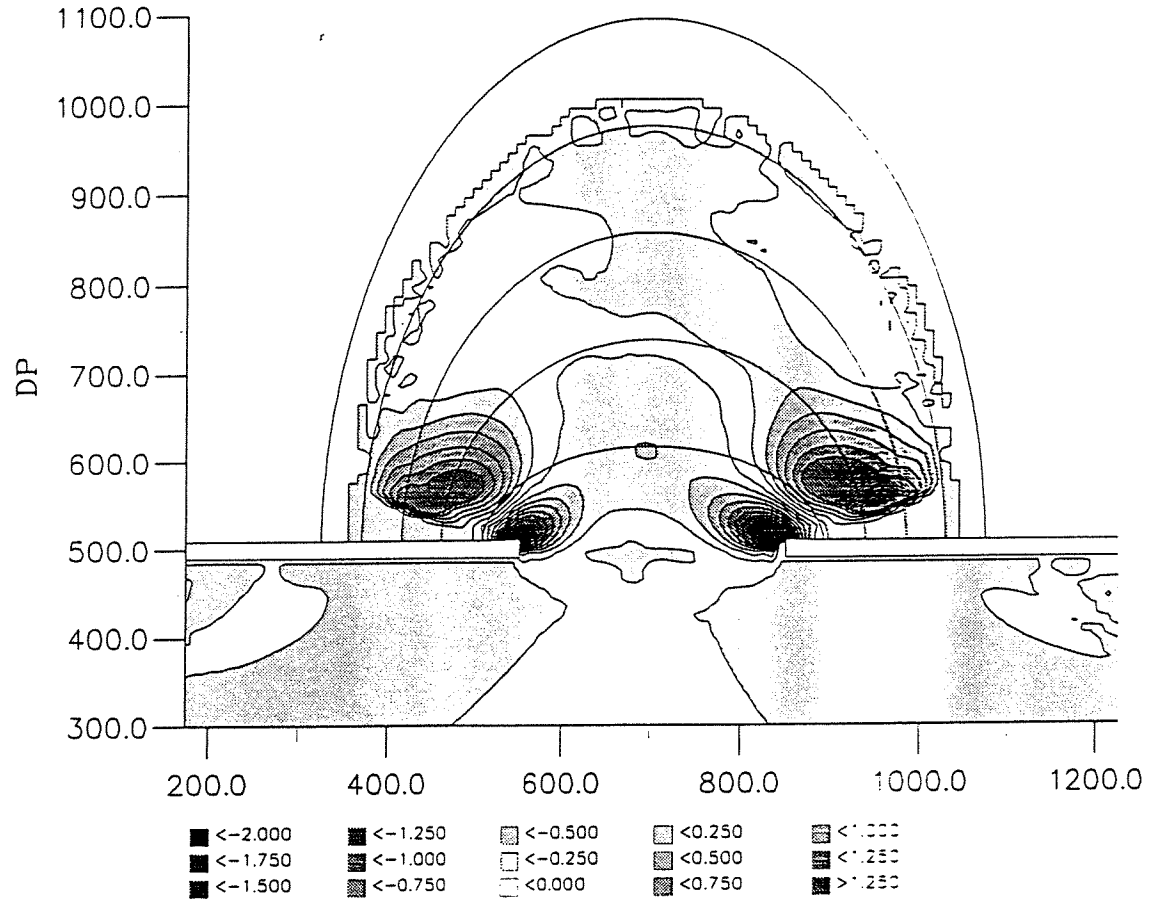

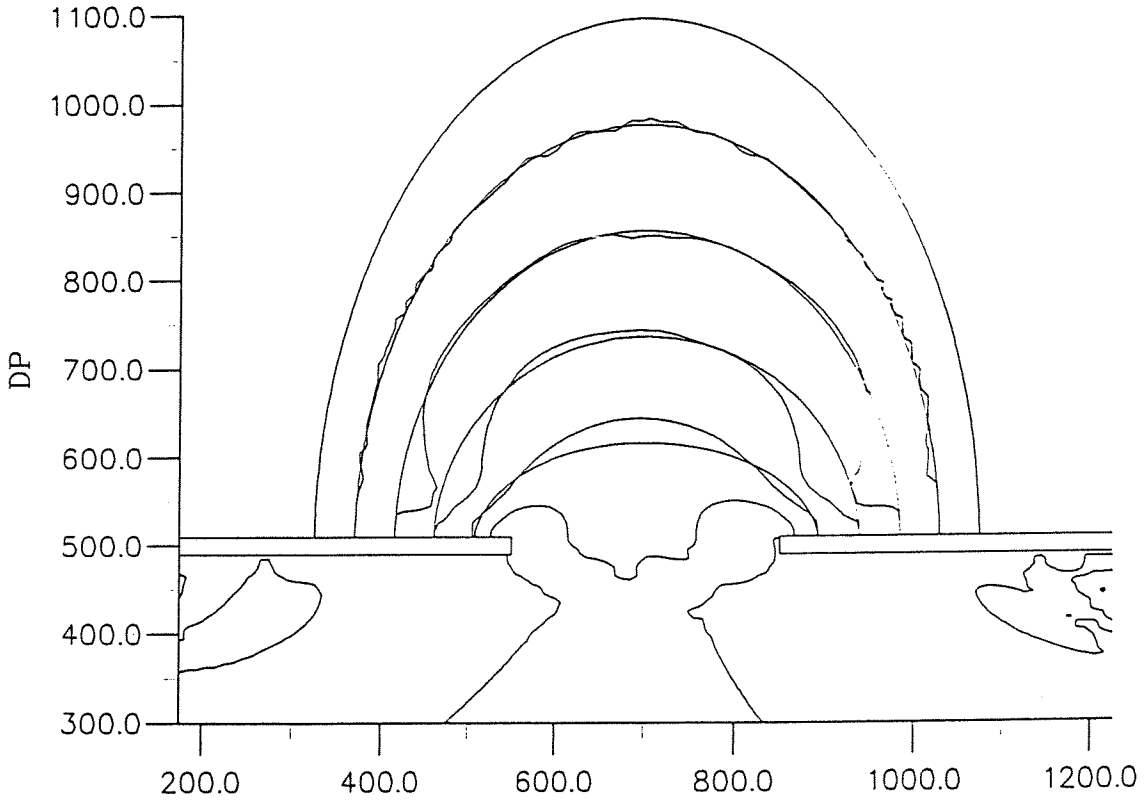

Upper graph: sedimentation and erosion (m) Lower graph: bathymetry after 7 days (m) Depth contour interval is 2m	Delft3D–MOR	Appendix E.9
	Bay 8c: Hs = 3m, d = 8m	
DUT – EQUILIBRIUM BAYS	MaST–III	SASME

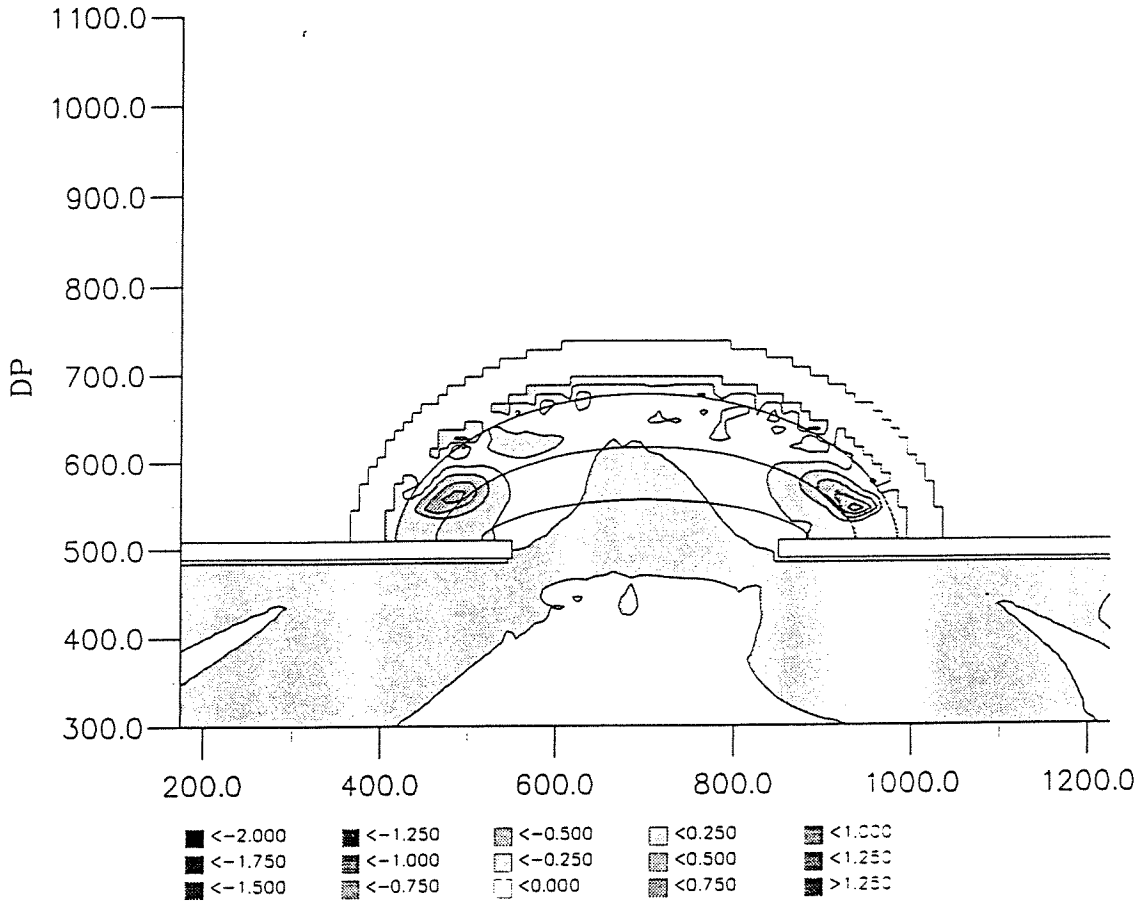

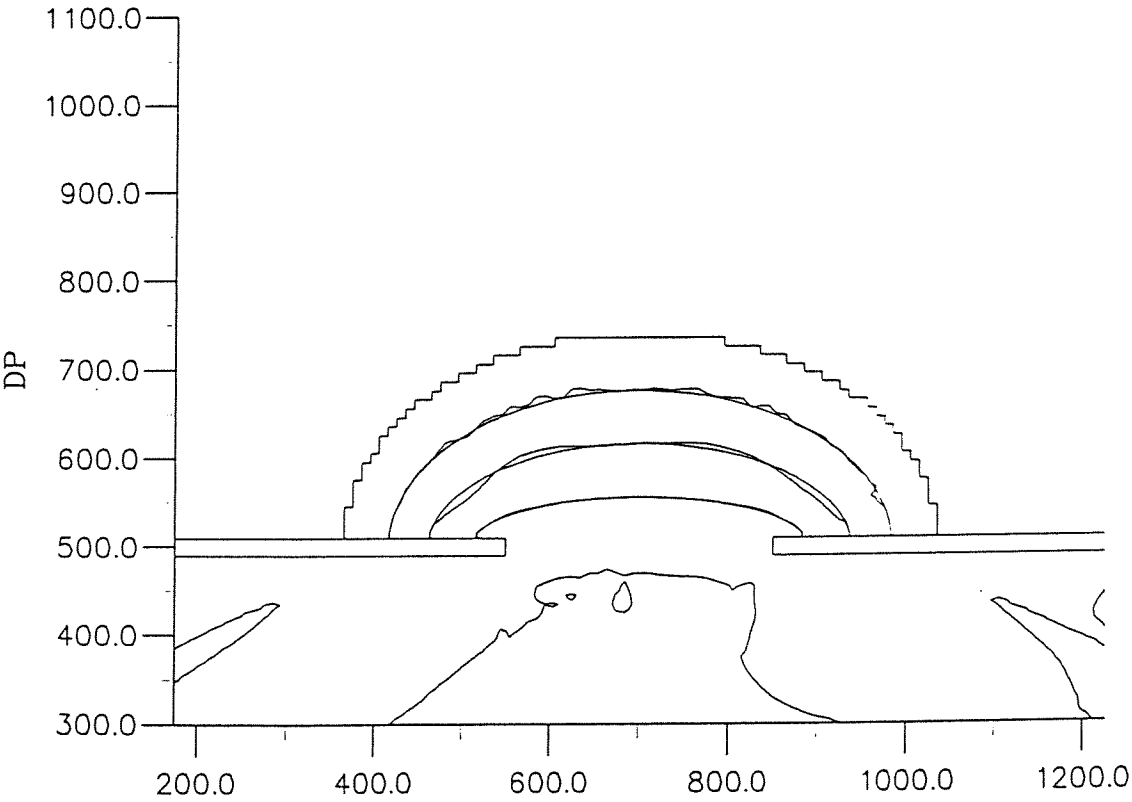

Upper graph: sedimentation and erosion (m) Lower graph: bathymetry after 7 days (m) Depth contour interval is 2m	Delft3D–MOR	Appendix E.10
	Bay 2c: Hs = 1m, d = 6m	
DUT – EQUILIBRIUM BAYS	MaST–III	SASME

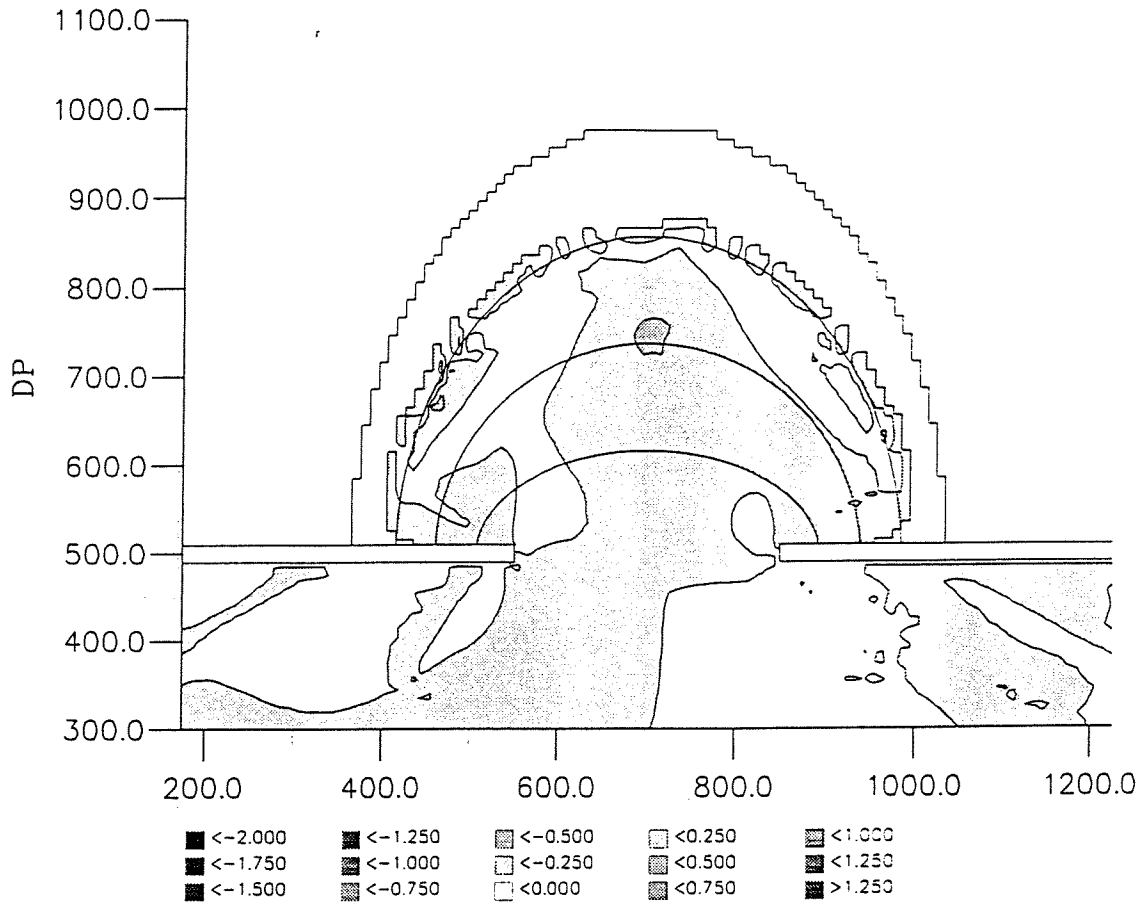

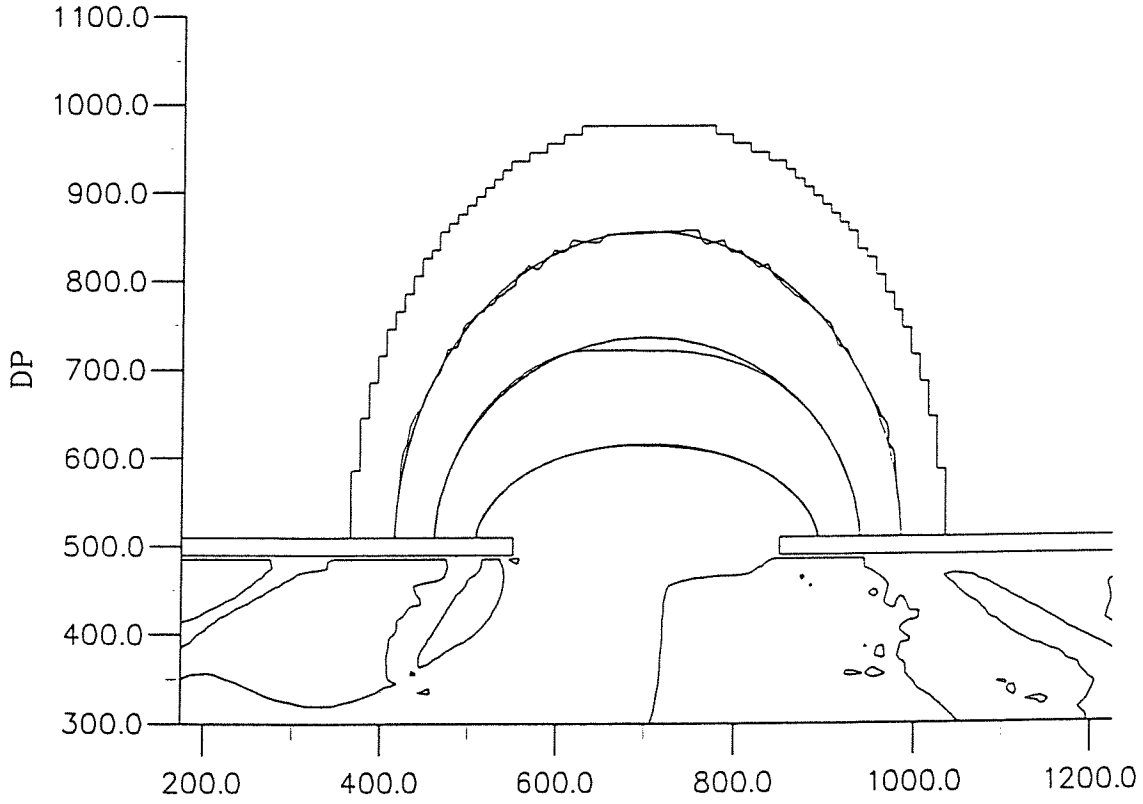

Upper graph: sedimentation and erosion (m) Lower graph: bathymetry after 7 days (m) Depth contour interval is 2m	Delft3D–MOR	Appendix E.11
	Bay 8c: Hs = 1m, d = 6m	
DUT – EQUILIBRIUM BAYS	MaST–III	SASME

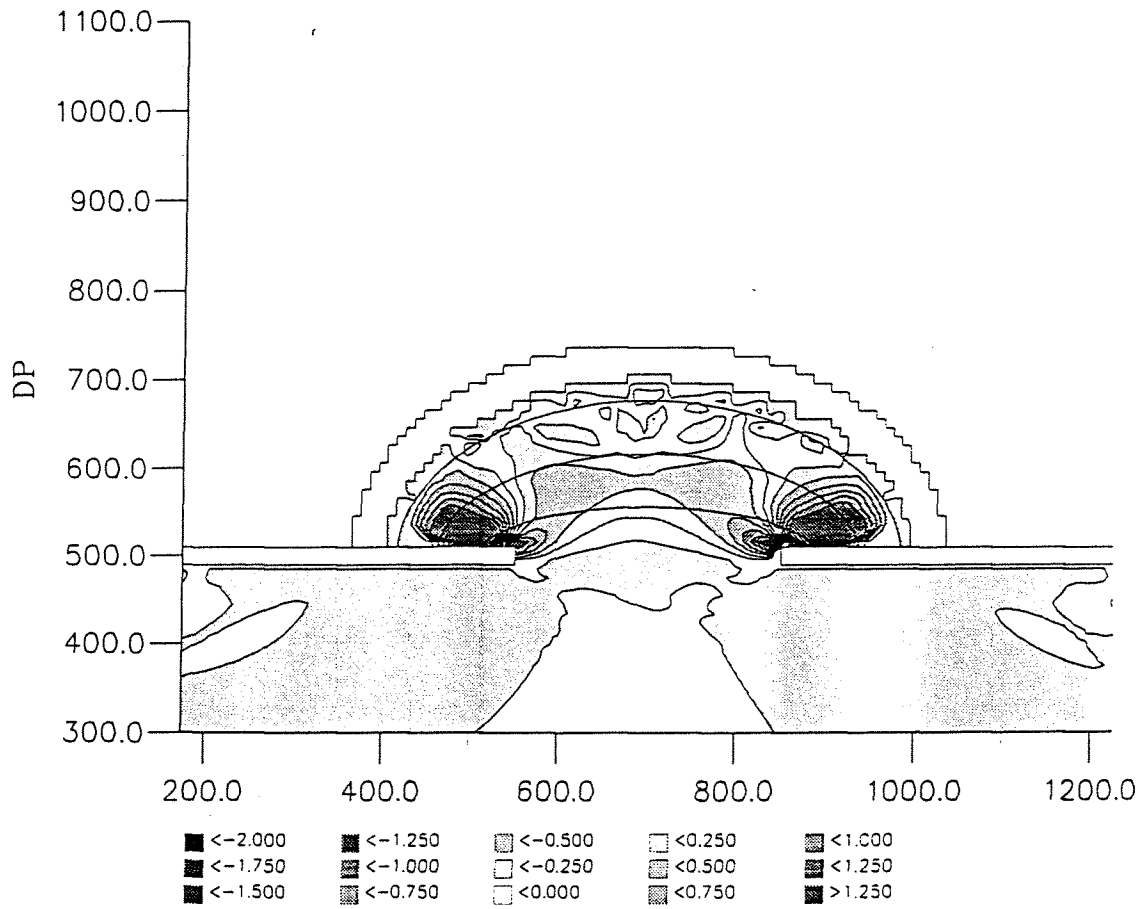

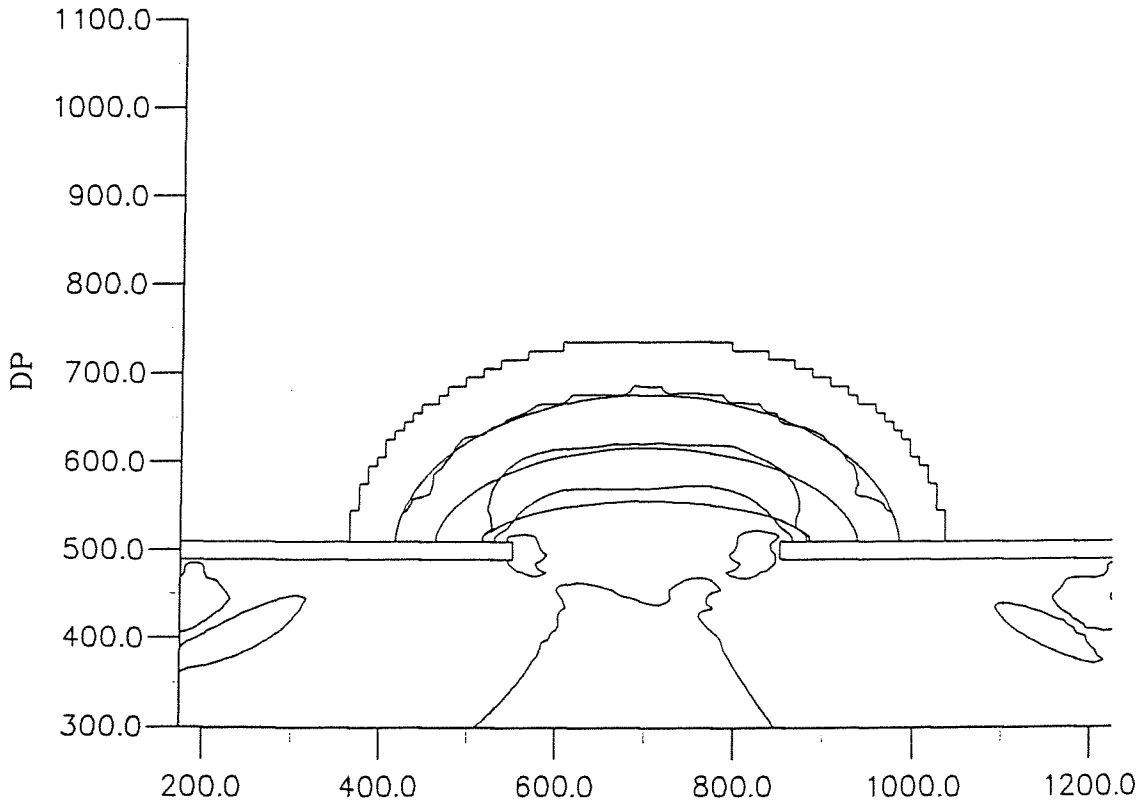

Upper graph: sedimentation and erosion (m) Lower graph: bathymetry after 7 days (m) Depth contour interval is 2m	Delft3D–MOR	Appendix E.12
	Bay 2c: Hs = 2m, d = 6m	
DUT – EQUILIBRIUM BAYS	MaST–III	SASME

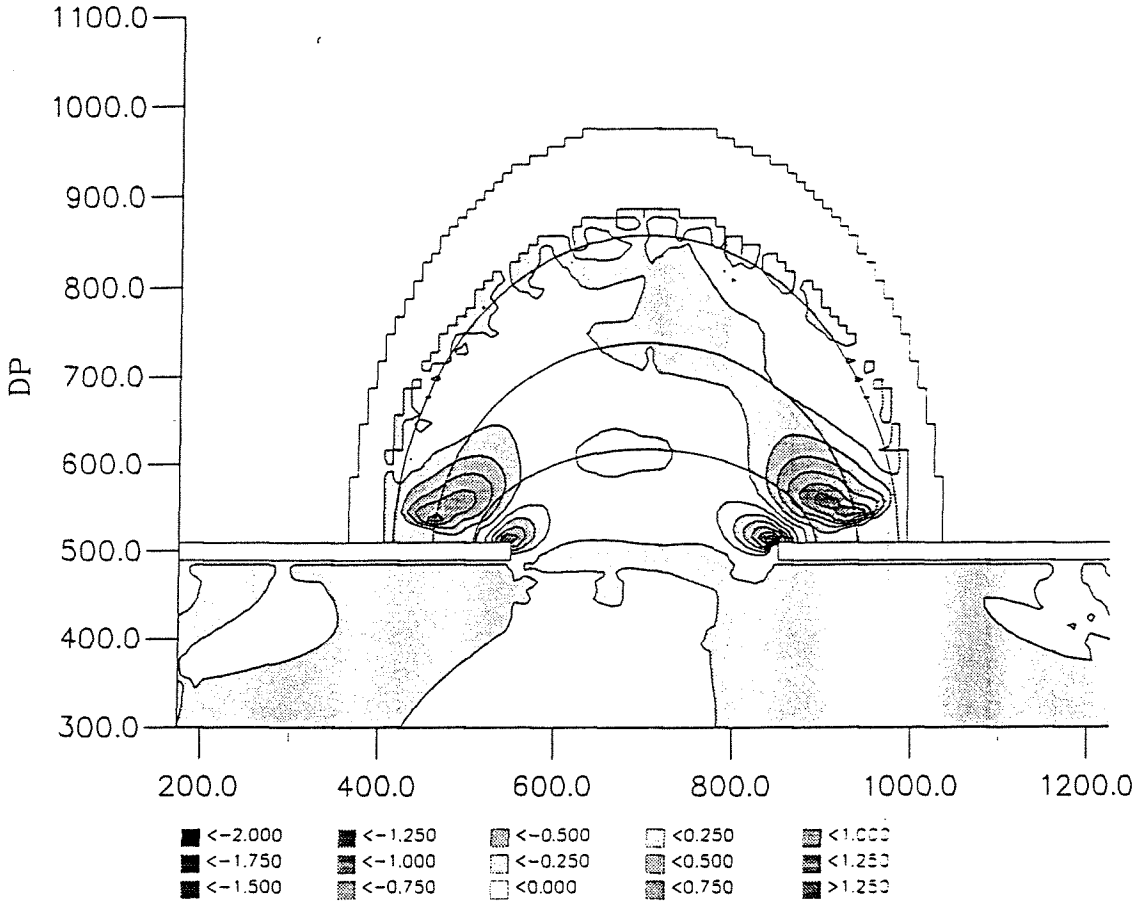

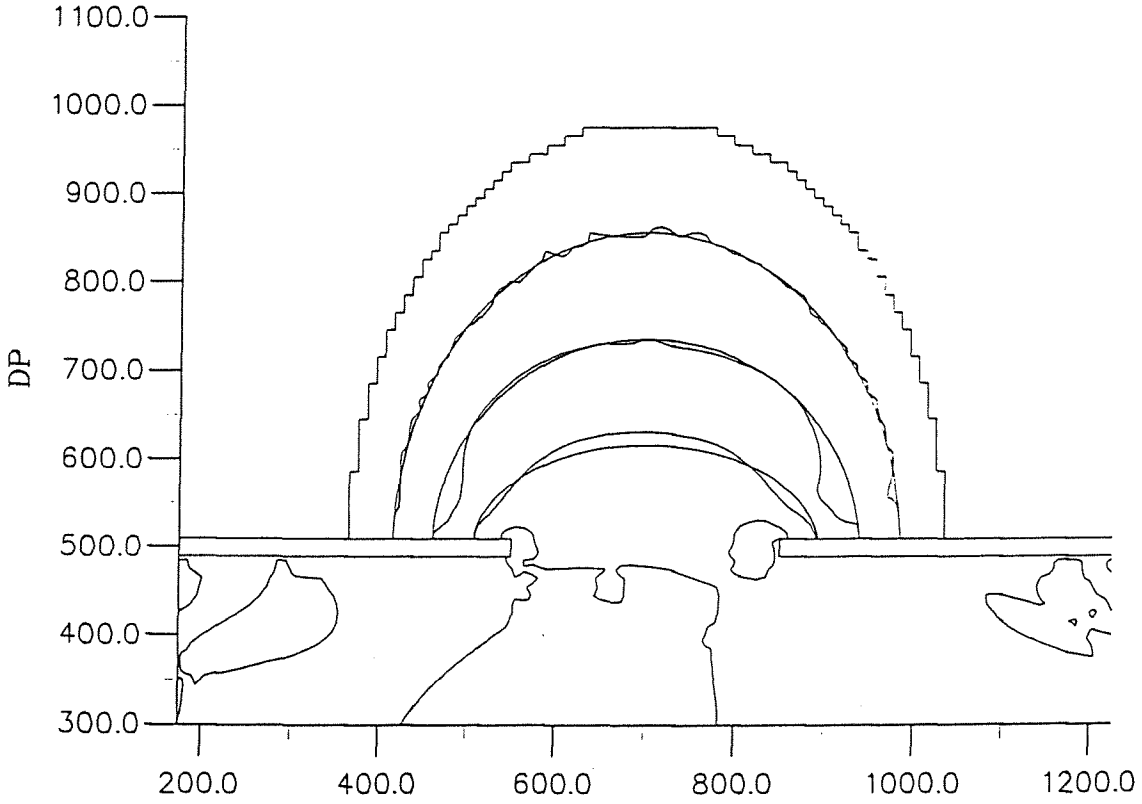

Upper graph: sedimentation and erosion (m) Lower graph: bathymetry after 7 days (m) Depth contour interval is 2m	Delft3D–MOR	Appendix E.13
	Bay 8c: Hs = 2m, d = 6m	
DUT – EQUILIBRIUM BAYS	MaST–III	SASME

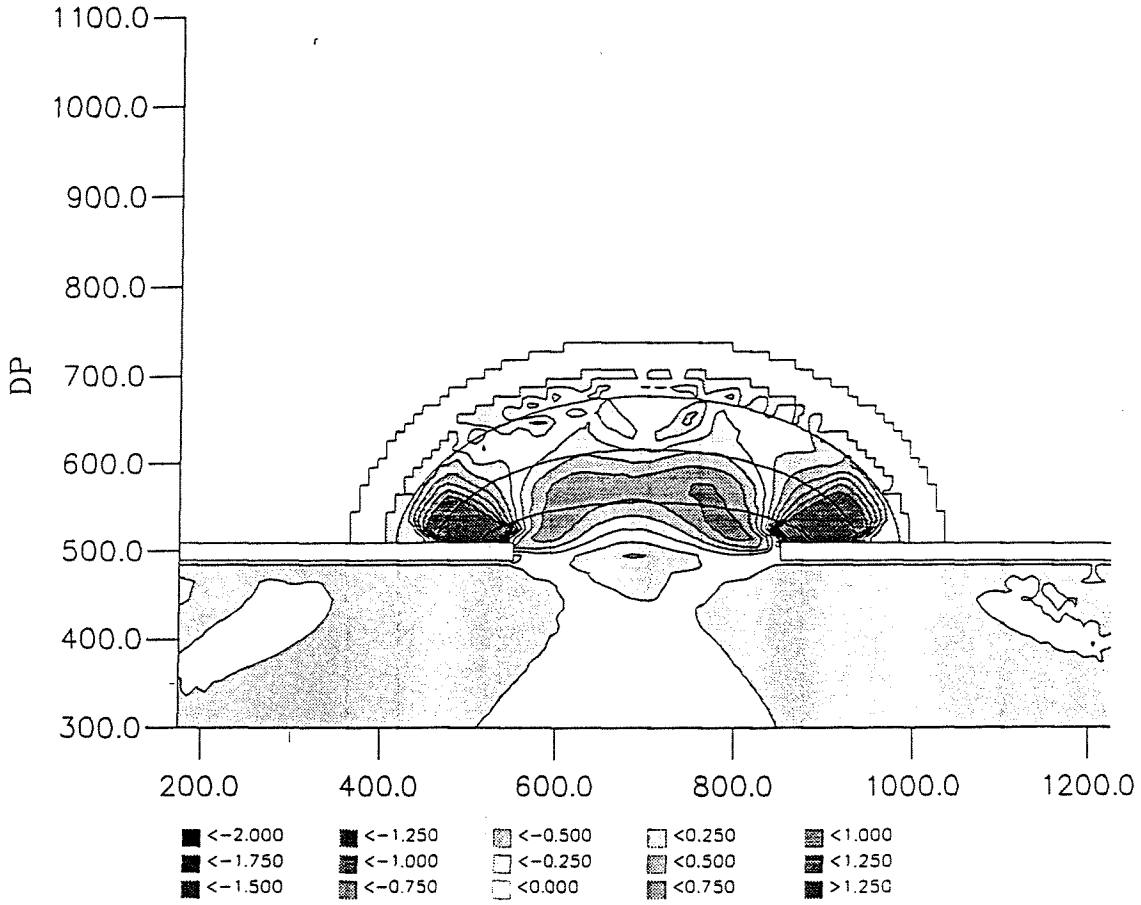

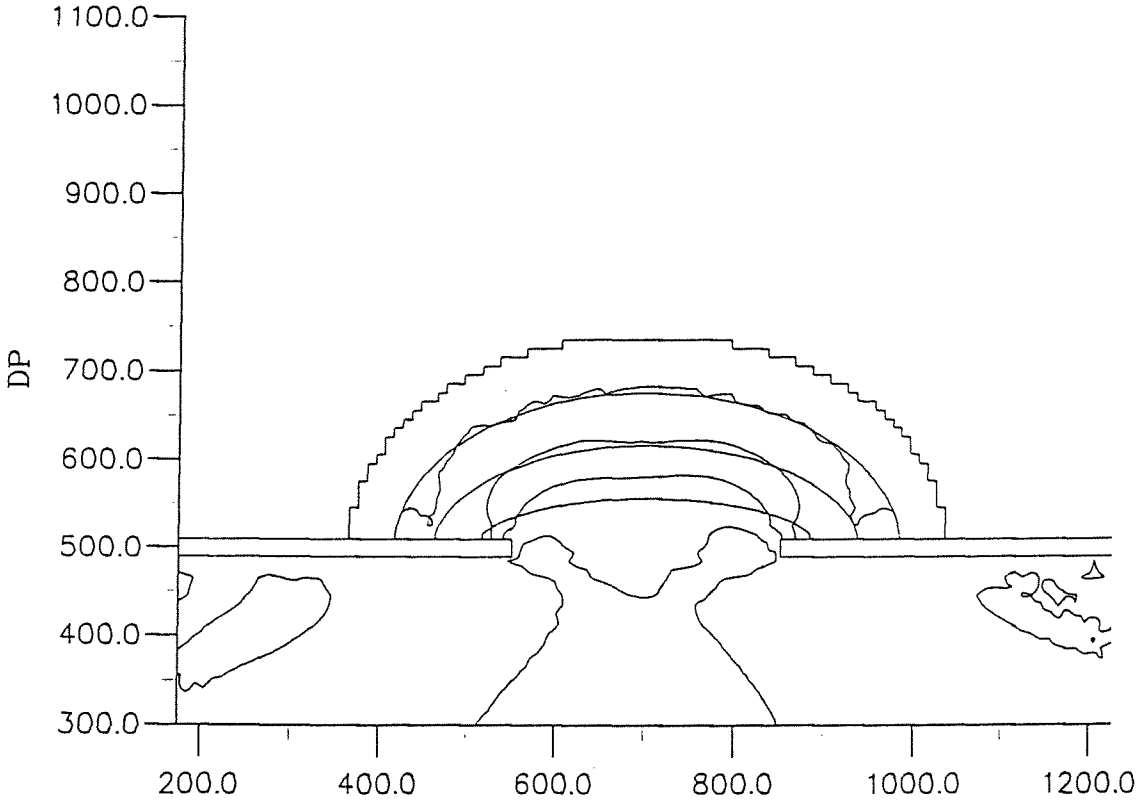

Upper graph: sedimentation and erosion (m) Lower graph: bathymetry after 7 days (m) Depth contour interval is 2m	Delft3D–MOR	Appendix E.14
	Bay 2c: Hs = 3m, d = 6m	
DUT – EQUILIBRIUM BAYS	MaST–III	SASME

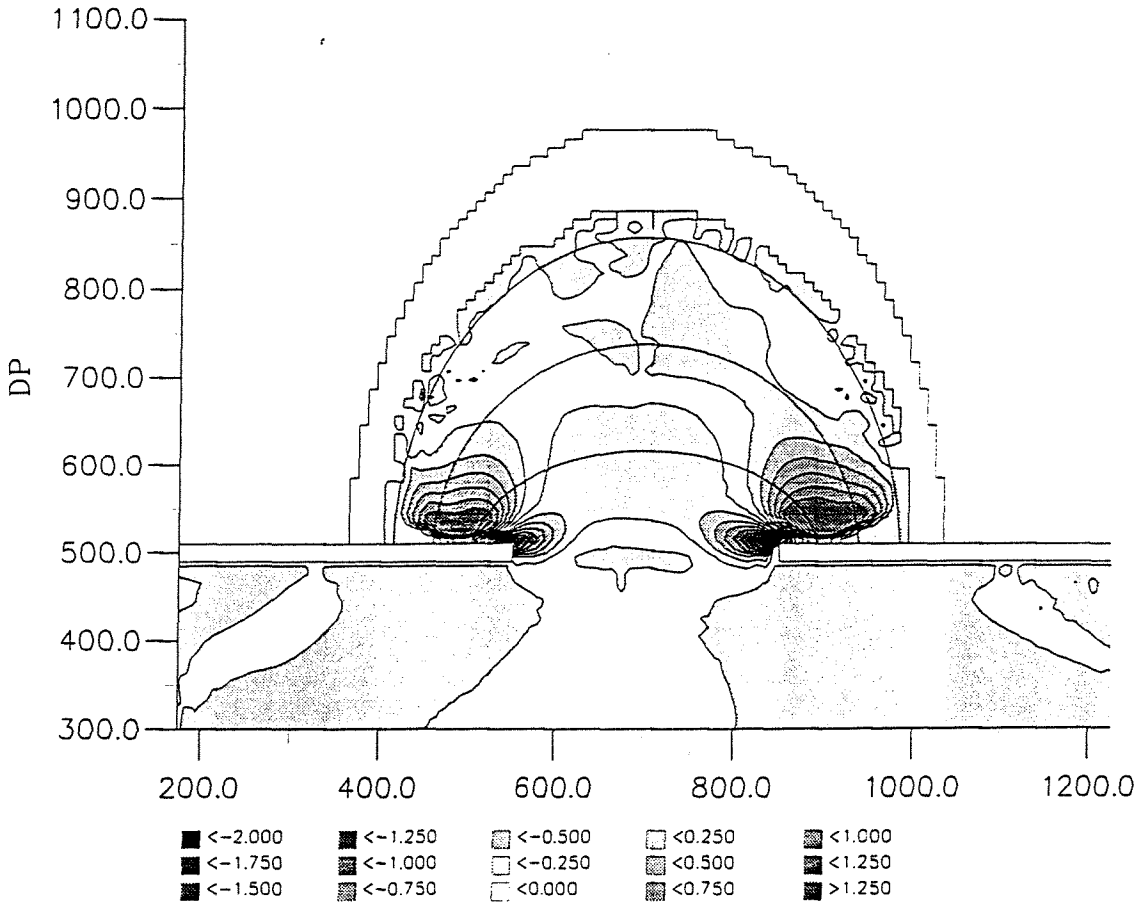

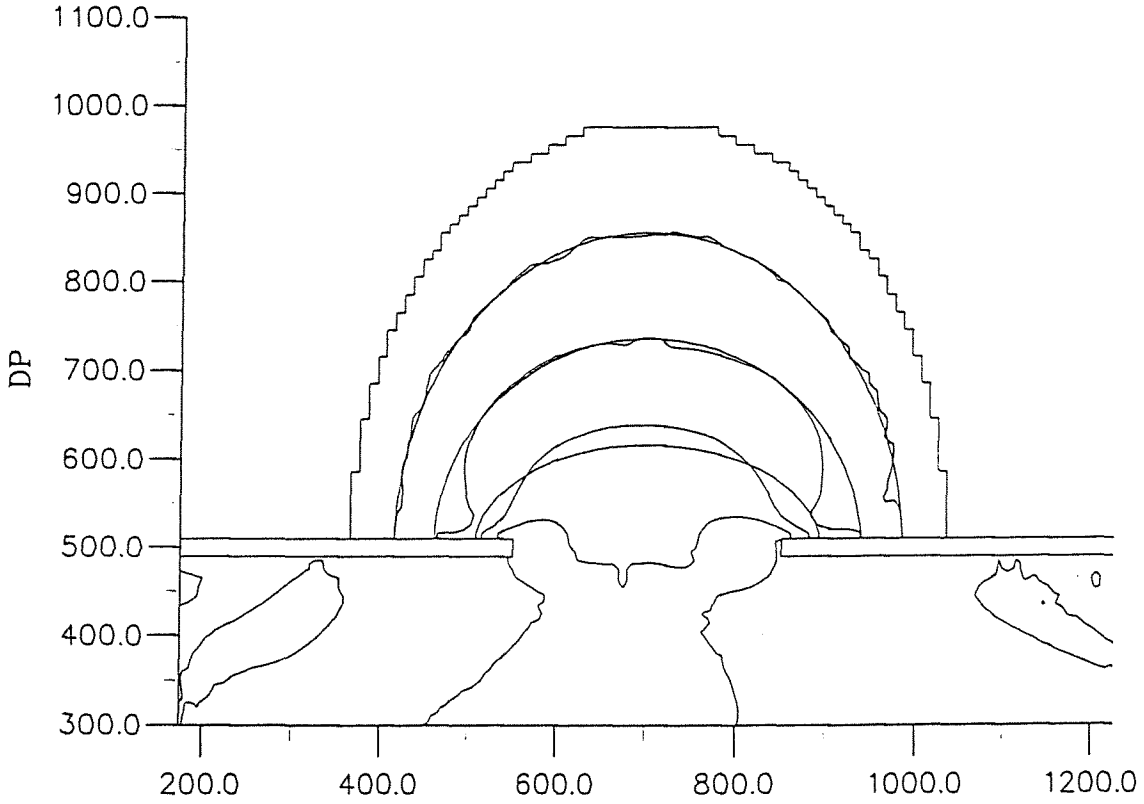

Upper graph: sedimentation and erosion (m) Lower graph: bathymetry after 7 days (m) Depth contour interval is 2m	Delft3D–MOR	Appendix E.15
	Bay 8c: Hs = 3m, d = 6m	
DUT – EQUILIBRIUM BAYS	MaST–III	SASME

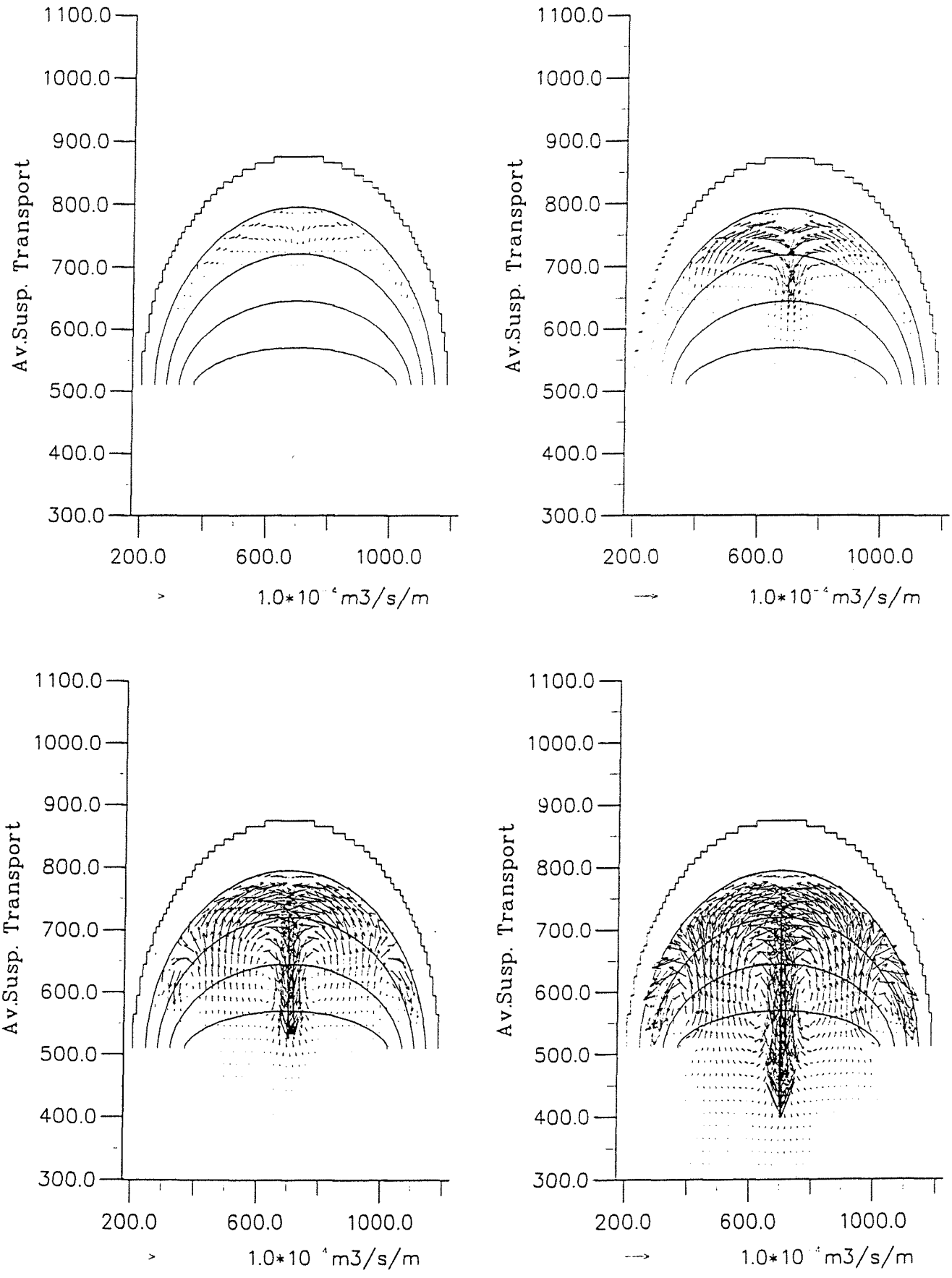

Upper graphs: Hsig = 0.5 m & Hsig = 1 m
Lower graphs: Hsig = 1.5 m & Hsig = 2 m
Depth contour interval is 2m

Delft3D–MOR	Appendix E.16
Suspended sediment transport	
MaST–III	SASME

Delft University of Technology

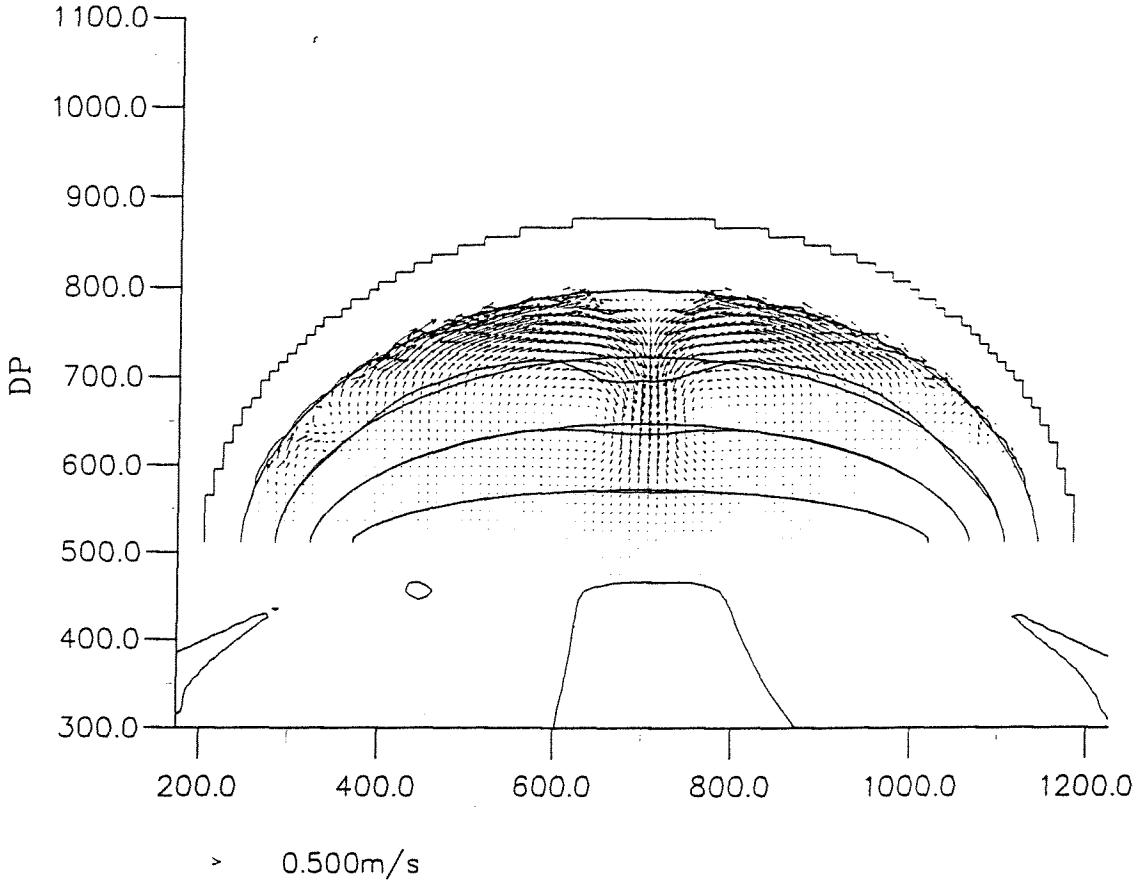

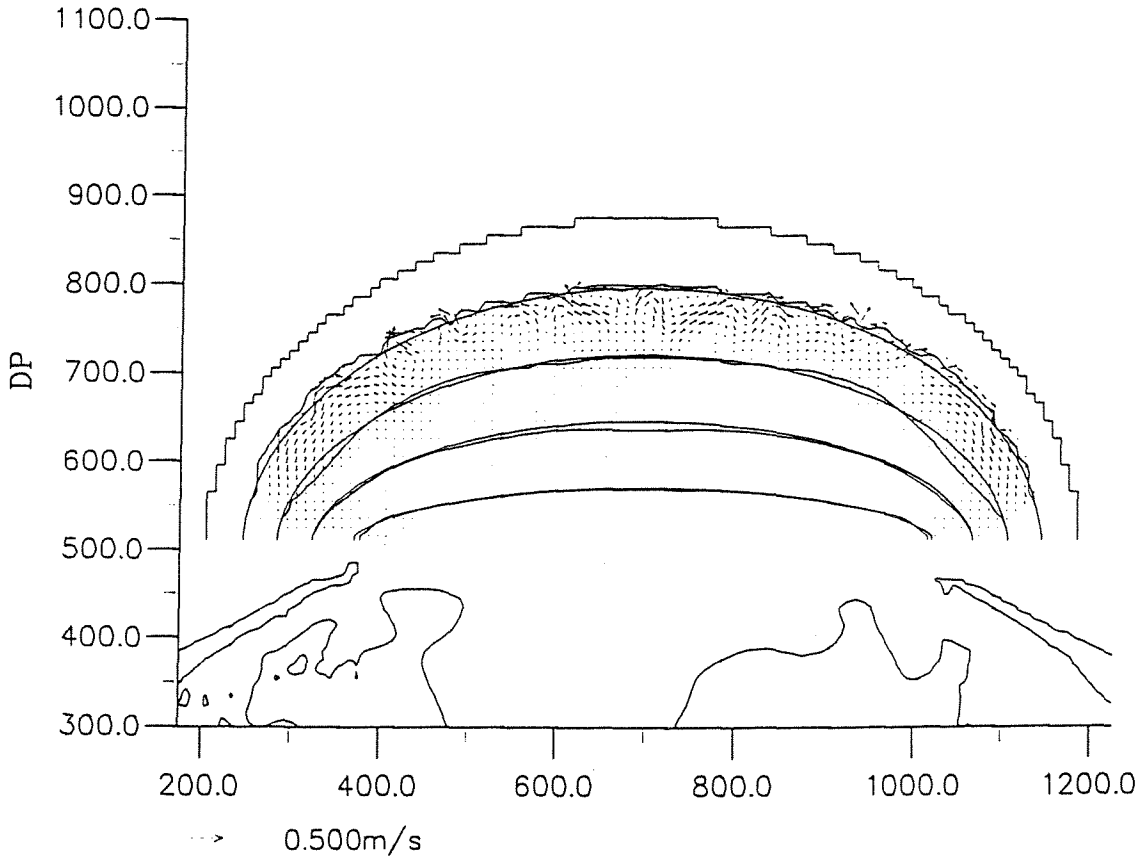

Upper graph: bathymetry after 7 days & initial flow Lower graph: bathymetry & flow vectors after 30 days Depth contour interval is 2m	Delft3D–MOR	Appendix E.17
	Hsig = 1 m; Tp = 5 s	
DUT – EQUILIBRIUM BAYS	MaST–III	SASME